

Identification of Phenotypically Modulated SMCs within Atherosclerotic Lesions and the
Role of Pluripotency Factors, KLF4 and OCT4, in their Modulation

Laura Susan Shankman
Arlington, Virginia

Bachelor of Science, Biological Sciences, University of Delaware, May 2007
Master of Science, Physiology, University of Virginia, December 2009

A Dissertation presented to the Graduate Faculty
of the University of Virginia in Candidacy for the Degree of
Doctor of Philosophy

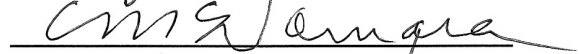
Department of Molecular Physiology and Biological Physics

University of Virginia
May 2014

Dr. Gary Owens



Dr. Coleen McNamara



Dr. Norbert Leitinger



Dr. Brant Isakson



Dr. Timothy Bender



Abstract

Cardiovascular disease is the leading cause of death in developed countries, and there is compelling evidence that the majority of these fatalities are secondary to rupture of unstable atherosclerotic plaques. However, the mechanisms that control plaque stability are poorly understood, although it is widely believed that plaques having a decreased ratio of cells positive for smooth muscle cell (SMCs) markers such as ACTA2 relative to macrophage markers are more likely to rupture with consequent clinical sequelae. While several studies have shown that SMCs can undergo phenotypic modulation into an inflammatory or macrophage-like state *in vitro*, there is no direct evidence this occurs *in vivo* or that the process is functionally important in the pathogenesis of atherosclerosis.

Studies within this dissertation are focused on identifying phenotypically modulated SMCs within atherosclerotic lesions using a newly developed conditional SMC specific lineage tracing mouse model, and a novel method that allows for the visualization of histone modifications of single genomic loci with single-cell resolution in formaldehyde-fixed paraffin-embedded tissue sections. Results show that dimethylation of lysine 4 of histone H3 (H3K4me₂) at the *MYH11* locus is restricted to the smooth muscle cell (SMC) lineage in human and mouse tissue sections and that the mark persists even in phenotypically modulated SMC in atherosclerotic lesions that show no detectable expression of SMC marker genes. We also show that traditional methods for staining and detecting SMCs are unable to detect $\geq 80\%$ of SMC-derived cells within advanced

atherosclerotic lesions of *ApoE*^{-/-} mice following 18 weeks of Western diet feeding. Remarkably, nearly a quarter of macrophages identified by markers such as LGALS3 are of SMC- and not myeloid origin as has been assumed in previous studies in the field. Moreover, using our novel single cell epigenetic assay we provide evidence that a population of SMC-derived cells within advanced human coronary artery atherosclerotic lesions also express the macrophage marker CD68.

We also demonstrate that pluripotency factors krüppel-like factor 4 (*Klf4*) and octamer binding factor 4 (*Oct4*) play critical, albeit distinct roles in regulating SMC phenotypic switching. SMC specific knock out (KO) of *Oct4* in *ApoE*^{-/-} mice fed a high fat Western diet for 18 weeks resulted in a significant reduction in phenotypically modulated SMCs within atherosclerotic lesions but resulted in lesions that were larger but less stable. In contrast, SMC specific knock out (KO) of *Klf4* in *ApoE*^{-/-} mice fed a high fat Western diet for 18 weeks showed no significant change in the number of phenotypically modulated SMC within the plaque but was associated with decreased lesion size and multiple changes consistent with increased plaque stability.

Taken together, results demonstrate that the contribution of SMCs to atherosclerotic lesion size and stability has been greatly underestimated by previous studies in the field. Moreover, studies are the first to provide direct evidence that changes in SMC phenotypic switching can exert dominant effects on the size, cellular composition, and stability of advanced atherosclerotic

plaques, and indicate that regulating SMC phenotypic states should be investigated as a potential therapeutic target to help stabilize atherosclerotic plaques to reduce possible clinical sequelae including plaque rupture, myocardial infarction, and/or stroke.

Acknowledgements

I am so thankful for the opportunity to have been able to work with and alongside so many talented researchers during my time in graduate school. Without them, this work would not have been possible. I first have to thank my mentor, Dr. Gary Owens, for allowing me to be a part of his team and teaching me how to excel in an increasingly competitive field. Thank you for believing in my theories and supporting me, financially and intellectually. Thanks to all the technical and administrative staff in the lab including Rupande Tripathi, Mary McCanna, Tiana Wyatt, Liz Greene, John Sanders, Missy Bevard, Barbara Spangler, and Wendy Burton for all your assistance and helping to make everything in the lab run smoothly. Special thanks to Liz Greene, Missy Bevard, and Mary McCanna for being there for me when I was in need and providing an emotional support system in the laboratory. I would like to thank Matt Alexander for always answering my questions and guiding me through my first years in the lab, and post-docs Olga Cherepanova, Delphine Gomez, and Anh Nyguen for helping me to the finish line. Also, thanks to all the undergraduate students, graduate students and post-docs, past and present, for making the lab environment a wonderfully collegial and exciting place to learn and labor together. Thanks to my Ph.D. committee members Norbert Leitinger, Coleen McNamara, Brant Isakson, and Tim Bender for their guidance and encouragement along the way.

I would like to thank my parents, Teresa and Jack Shankman, who have always supported my academic endeavors. Thank you to the ladies of the Phoenix Dance Studio who provided an amazing outlet for stress and an endless source of love and support over the last six years. Finally, I thank my sister, Sarah Swinehart, for always pushing me to excel in **all** aspects of my life and for being an excellent role model. I dedicate this dissertation to her.

Table of Contents

Abstract	ii
Acknowledgements	v
Table of Contents	vii
List of Abbreviations	xii
List of Figures	xiv
List of Tables	xxii
 Chapter 1:	
Introduction	1
Public Health Burden of Atherosclerosis.....	2
Smooth Muscle Cell Identification in Atherosclerosis.....	2
<i>How a Smooth Muscle Cell is identified</i>	2
<i>Smooth Muscle Cell Lineage Tracing Models</i>	4
<i>A Case of Mistaken Identity</i>	6
Smooth Muscle Cell Phenotypic Modulation in Atherosclerosis.....	8
The Accepted Dogma of Atherosclerotic Plaque Formation and Assessment of Plaque Stability.....	12
<i>Pathophysiology of Atherosclerotic Plaque Formation</i>	13
<i>Indices of plaque stability</i>	15
KLF4 Signaling and Smooth Muscle Cells Phenotypic Modulation.....	18

Focus of Dissertation	21
-----------------------------	----

Chapter 2:

Detection of histone modifications at specific gene loci in single cells in histological sections	29
--	-----------

Abstract.....	30
---------------	----

Introduction	31
--------------------	----

Materials and Methods.....	34
----------------------------	----

Results.....	40
--------------	----

Discussion	47
------------------	----

Chapter 3:

Transition of smooth muscle cells to a macrophage-like state within advanced atherosclerotic lesions plays a key role in regulating indices of plaque stability and is regulated by Krüppel-like factor 4	100
--	------------

Abstract.....	101
---------------	-----

Introduction	103
--------------------	-----

Materials and Methods.....	107
----------------------------	-----

Results.....	114
--------------	-----

Discussion	126
------------------	-----

Chapter 4:

The pluripotency factor Oct4 modulates blood vessel remodeling in atherosclerotic lesions	176
Abstract.....	177
Introduction	179
Materials and Methods.....	181
Results.....	190
Discussion	199
 Chapter 5:	
Conclusions and Future Directions	241
Development and uses of ISH-PLA in disease state models	243
Smooth muscle cell lineage tracing and atherosclerosis	244
Pluripotency factors KLF4 and OCT4 regulate SMC phenotypic modulation and differentially affect atherosclerotic plaque size and indices of plaque stability	245
Smooth muscle cells as a therapeutic target	246
Future Directions	247

<i>Do macrophages from SMC origins possess different functions than macrophages of hematopoietic origins?.....</i>	<i>248</i>
<i>How does KLF4 regulate the phenotypic modulation of SMCs to a macrophage-like state, and how might this transition effect plaque size/stability?.....</i>	<i>250</i>
<i>Studies revealed that 86% of SMCs within atherosclerotic lesions of 18 week Western diet fed animals are undetectable by ACTA2, but only 23% of these cells were identified as macrophage-like. What is phenotypic state of the other ~60% and how are they affecting atherosclerotic plaque stability?</i>	<i>252</i>
<i>Other cells in the intima (Figure 13) also expressed OCT4 after Western diet treatment (in the SMC Oct4 KO mouse). What are those cells and how are they contributing to lesion development?</i>	<i>255</i>
<i>Earlier loss of KLF4 was shown to dramatically reduce the instance of SMC derived macrophages (Figure 10). What is the role of OCT4 in SMC phenotypic switching to a macrophage-like state?</i>	<i>256</i>
<i>How frequent are SMC derived macrophages within human lesions? Are SMC derived macrophages more common in human lesions that have high indices of plaque instability?.....</i>	<i>257</i>
<i>Does acute pharmacological treatment inhibiting KLF4 also result in reduced lesion? What about overexpression of OCT4?.....</i>	<i>258</i>

Does the H3K4dime mark on the Myh11 promoter confer SMC lineage memory? If so, can removal of the H3K4dime mark on the Myh11 promoter make SMCs “forget” to re-differentiate? Can addition of the H3K4dime mark on the Myh11 promoter of other cell types cause them to differentiate into SMCs?..... 260

At what point in development do SMCs acquire the H3K4dime mark?..... 264

Chapter 6:

References 278

List of Abbreviations

ACTA2, smooth muscle alpha actin

ApoE, apolipoprotein E

BCA, brachiocephalic artery

ChIP, Chromatin ImmunoPrecipitation

CNN1, calponin-1

CVD, Cardiovascular Disease

DAB, 3,3'-Diaminobenzidine

DAPI, 4',6-diamidino-2-phenylindole

EEL, external elastic lamina

IEL, internal elastic lamina

iNOS, inducible nitric oxide synthase

ISH, in situ hybridization

KLF4, Krüppel-like factor 4

KO, Knock Out

LacZ, beta-galactosidase

LDL, low density lipoprotein

LDLR, low density lipoprotein receptor

LGALS3, Lectin Galactoside-Binding Soluble 3 (mac-2)

MCP-1, monocyte chemoattractant protein 1

MMP, matrix metalloproteinase

MYH11, smooth muscle myosin heavy chain 11

NF κ B, nuclear factor kappa B

OCT4, octamer-binding transcription factor 4

PDGF, platelet-derived growth factor

PLA, proximity ligation assay

POVPC, 1-palmytoyl-2-(5-oxovaleroyl)-sn-glycero-3-phosphocholine

RBC, red blood cell

RT-PCR, real-time polymerase chain reaction

SEM, standard error of the mean

SMC, smooth muscle cell

TAGLN, Smooth muscle 22 alpha

TGF β , transforming growth factor beta

TLR, toll-like receptor

TNF α , tumor necrosis factor alpha

VCAM-1, vascular cell adhesion molecule 1

WD, Western Diet

List of Figures

Chapter 1:

Figure 1: Mutation of the G/C repressor region of the Tagln promoter enables visualization of phenotypically modulated SMCs in models of vascular injury and atherosclerosis. 25

Figure 2: Smooth muscle cells and macrophages are capable of up-regulating marker genes of the other cell type..... 27

Chapter 2:

Figure 3: ISH-PLA: a new method of detection of histone modifications at a single genomic locus in tissue sections..... 51

Figure 4: Validation of ISH-PLA using SMC lineage tracing mouse model..... 53

Figure 5: Visualization of H3K4dime on the MYH11 promoter in SMCs in situ in histological sections of human carotid arteries. 55

Figure 6: H3K4dime on the MYH11 promoter persists during phenotypic switching in vivo in SMC lineage tracing mice developing atherosclerosis. 57

Figure 7: Identification of epigenetic regulation of phenotypically modulated SMCs within human coronary atherosclerotic lesions by ISH/PLA. 59

Supplemental Figure 1: Compatibility between PLA and chromatin structure. ... 61

Supplemental Figure 2: Pepsin treatment does not affect H3K4dime staining in tissue sections. 63

Supplemental Figure 3: Mapping of H3K4dime enrichment on the MYH11 promoter.	65
Supplemental Figure 4: Y chromosome FISH in male patient tissue sections....	67
Supplemental Figure 5: Assessment of H3K4dime enrichment at MYH11 promoter in various cultured cell lines.....	69
Supplemental Figure 6: Assessment of eYFP expression in Myh11-CreERT2 ROSA26 STOP flox eYFP ^{+/+} and eYFP ^{-/-} mice.	71
Supplemental Figure 7: Quantification of ISH-PLA efficiency.....	79
Supplemental Figure 8: CDH5 H3K4dime PLA in human and mouse tissue sections.....	83
Supplemental Figure 9: TagIn H4ac PLA in mouse tissue sections.....	87
Supplemental Figure 10: MYH11 H3K4dime ISH-PLA assay in FFPE human carotid arteries.....	91
Supplemental Figure 11: MYH11 H3K4dime ISH-PLA assay in FFPE human brain sections.....	93
Supplemental Figure 12: Immunofluorescent staining of SMC marker proteins in healthy and atherosclerotic human carotids.....	95
Supplemental Figure 13: MYH11 H4ac PLA in human atherosclerotic vessel tissue sections.	97

Chapter 3:

Figure 8: Multiple SMC lineage tracing methods provide evidence for large populations of phenotypically modulated SMCs within braciocephalic

arteries (BCA) of 18 Week WD fed SMC eYFP ^{+/+} Apoe ^{-/-} mice some of which have activated multiple markers of macrophages.....	131
Figure 9: Evidence that SMCs within advanced human coronary artery lesions express the macrophage marker CD68.	134
Figure 10: SMC specific Klf4 conditional knockout in Apoe ^{-/-} mice fed a high fat diet for 18 weeks resulted in decreased lesion size and increased indices of plaque stability.	136
Figure 11: Global conditional knockout of one Klf4 allele increased indices of plaque stability.	138
Figure 12: KLF4 is upregulated in SMCs during atherosclerosis, binds to the promoters of SM marker genes, and loss of KLF4 diminishes LGALS3 expression.	140
Supplemental Figure 14: SMC lineage tracing mice exhibit recombination exclusively in the SMCs of tamoxifen treated SMC eYFP ^{+/+} mice.....	144
Supplemental Figure 15: Recombination of the ROSA STOP eYFP locus is not present in cells within the blood or bone marrow of tamoxifen treated SMC eYFP mice, but is abundant in freshly dissociated cell preparations from the aorta.....	146
Supplemental Figure 16: Absence of spontaneous recombination of the ROSA STOP eYFP locus or appearance of circulating eYFP ⁺ cells following long term Western diet feeding.....	148

Supplemental Figure 17: SMC lineage tracing studies provide evidence for large populations of phenotypically modulated SMCs within braciocephalic arteries (BCA) of 18 Week Western diet fed SMC eYFP ^{+/+} Apoe ^{-/-} mice that cannot be identified using conventional SMC marker genes including some of which have activated multiple markers of macrophages.	150
Supplemental Figure 18: Mouse macrophages do not acquire the H3K4dime mark on the Myh11 promoter when treated with the oxidized phospholipid POVPC.	152
Supplemental Figure 19: Combinatorial epigenetic SMC and Y chromosome lineage tracing analyses of cross gender heart transplant samples provides further evidence for SMC-derived macrophage-like samples in advanced atherosclerotic lesions of human coronary artery samples....	154
Supplemental Figure 20: Tamoxifen treatment between 6-8 weeks of age induced high efficiency SMC-specific recombination of the floxed Klf4 gene locus.	156
Supplemental Figure 21: Smooth muscle cell specific KLF4 knockout SMC eYFP ^{+/+} Apoe ^{-/-} mice exhibited marked changes in the cellular composition of plaques.	158
Supplemental Figure 22: SMC specific KLF4 knockout decreases lesion size without affecting overall body weight or cholesterol levels.....	160
Supplemental Figure 23: Confirmation of global conditional knockout of one Klf4 allele as assessed by PCR and immunohistochemical analysis.	162

Supplemental Figure 24: Global conditional knockout of one Klf4 allele does not affect overall body weight or cholesterol levels.....	164
Supplemental Figure 25: Global conditional knockout of one Klf4 allele decreased cellular proliferation and apoptosis.....	166
Supplemental Figure 26: KLF4 binds to the Tagln promoter in response to Western diet treatment is dependent on the GC repressor element.	168
Supplemental Figure 27: Cultured aortic SMCs from SMC YFP ^{+/+} ApoE ^{-/-} mice are 98% pure by flow cytometry.....	170
Supplemental Figure 28: Pure aortic SMCs from SMC YFP ^{+/+} Klf4 Δ/Δ mice do not express KLF4 when exposed to water soluble cholesterol.	172
Chapter 4:	
Figure 13: SMC-specific conditional KO of the pluripotency gene Oct4 was associated with an increased size of lesions, as well as a marked reduction in phenotypically modified SMC within the atherosclerotic lesions of 18 weeks Western diet fed ApoE KO mice.....	200
Figure 14: Role of the pluripotency factor Oct4 in regulating SMC proliferation, migration and apoptosis.....	203
Figure 15: SMC-specific conditional KO of the pluripotency gene Oct4 increased multiple indices of atherosclerotic plaque instability.....	206
Figure 16: Activation of Oct4 in SMC was dependent on Klf4 and Hif1 α	208
Supplemental Figure 29: Oct4 is recombined specifically in SMC rich tissues of Oct4 Δ/Δ ApoE ^{-/-} versus Oct4 ^{WT/WT} ApoE ^{-/-} mice.	211

Supplemental Figure 30: Genetic knockout of Oct4 did not significantly change metabolic parameters in Oct4 ^{Δ/Δ} ApoE ^{-/-} versus Oct4 ^{WT/WT} ApoE ^{-/-} mice fed a Western diet.....	213
Supplemental Figure 31: SMC-specific conditional KO of the pluripotency gene Oct4 increased atherosclerotic lesion size in brachiocephalic arteries. .	215
Supplemental Figure 32: SMC-specific conditional KO of the pluripotency gene Oct4 did not change overall Lgals3 (Mac2) staining or Acta2 (SM α-actin) staining of brachiocephalic lesions.	217
Supplemental Figure 33: Oct4 protein levels were markedly induced within cells of the tunica media and atherosclerotic lesions of the human atherosclerotic lesion.	219
Supplemental Figure 34: SMC-specific conditional KO of the pluripotency gene Oct4 accelerated neointima formation and tunica media following carotid artery ligation-induced vascular injury.....	221
Supplemental Figure 35: Genetic loss of Oct4 in SMCs decreased non-SMC apoptosis.	223
Supplemental Figure 36: SMC specific KO of Oct4 has no significant effect on cellular proliferation in atherosclerotic lesions.....	225
Supplemental Figure 37: Oct4 KO increases cellular proliferation in vitro in baseline conditions which is ameliorated during treatment with POVPC.	227

Supplemental Figure 38: Lentiviral-induced overexpression of the pluripotency factor Oct4 induced increased migration, but reduced proliferation of cultured SMC.	229
Supplemental Figure 39: Expression of the extracellular matrix-dependent genes was abolished in Oct4 ^{Δ/Δ} SMC.	231
Supplemental Figure 40: SMC specific KO of Oct4 does not affect overall lipid accumulation as quantified by Oil Red O positive staining lesion area. .	233
Supplemental Figure 41: SMC-specific conditional KO of the pluripotency gene Oct4 did not alter total lesion collagen content.	235
Supplemental Figure 42: Schematic of the sequence of 1.5 kb mouse promoter region of the Pou5f1 gene.	237
Chapter 5:	
Figure 17. Schematic of KLF4 and OCT4 function in SMC phenotypic switching in response to vascular injury and atherosclerosis.	266
Figure 18. Oct4 is up-regulated in SMCs in the context of Western diet feeding.	268
Figure 19. YFP+ cells from aortas of 18 week western diet fed SMC lineage tracing mice express multiple markers of mesenchymal stem cells (MSC).	270
Figure 20. OCT4 activates Lgals3 in response to POVPC treatment and exhibits increased phagocytosis of red blood cells in response to cholesterol loading treatment.	272

Figure 21. A Novel Myocardin-LSD1 fusion protein selectively demethylates H3K4me2 at SMC specific gene promoters.	274
Figure 22. H3K4dime is acquired on the MYH11 promoter before the expression of SMC marker genes.	276

List of Tables**Chapter 2:****Supplemental Table 1:** Primer table.....99**Chapter 3:****Table 1:** Cellular composition of 18 week Western diet SMC eYFP^{+/+} *Apoe*^{-/-} mice.....142**Supplemental Table 2:** Quantification of immunofluorescent stained slides from 18 week WD fed SMC eYFP^{+/+} *Apoe*^{-/-} mouse lesions reveal new SMC populations.....174**Chapter 4:****Supplemental Table 3:** Primers used for quantitative real time RT-PCR and site-direct mutagenesis.....239

Chapter 1: Introduction

Public Health Burden of Atherosclerosis

Atherosclerosis is a chronic disease of elastic and muscular arteries that involves formation of plaques that can restrict blood flow to dependent tissues^{1, 2}. Rupture of these plaques can lead to clinical sequelae including myocardial infarction, and stroke. Although the incidence of cardiovascular disease (CVD) has declined between 2000 and 2010, probably from the widespread use of statins, CVD still accounts for approximately one in every three deaths in the United States³, and one in five deaths worldwide⁴. Despite the success of statins in reducing circulating cholesterol levels, the incidence of CVD remains high. Moreover, there has been a profound increase in obesity and early onset type II diabetes in the USA and worldwide. Since obesity and diabetes are unequivocally linked to the accelerated development of atherosclerosis, it is expected that the incidence of atherosclerotic disease and its clinical consequences will increase dramatically in the coming decades. Therefore it is critically important to discover molecular and cellular mechanisms responsible for the development of atherosclerosis in order to better prevent and treat the disease and its clinical complications.

Smooth Muscle Cell Identification in Atherosclerosis

How a Smooth Muscle Cell is identified

Smooth muscle cells are believed to play an important role in atherosclerotic plaque development and progression, however due to limitations

that will be discussed here, their full contribution to plaque development has not yet been assessed⁵. One of the main dogmas in the field today is that SMC migration into the intima where they are believed to lay down extracellular matrix, is the hallmark of the transition from fatty streak to a more advanced plaque⁶.

In order to enter the intima SMCs must first undergo a process known as phenotypic modulation, also referred to as phenotypic switching⁵. During phenotypic modulation, SMCs down-regulate contractile/cytoskeletal proteins, such as, smooth muscle (SM) myosin heavy chain (SMMHC, MYH11)⁷, SM 22 alpha (SM22 α , TAGLN)⁸, SM alpha actin (SM α -actin, ACTA2)^{9, 10}, and h1-calponin (CNN1)⁸, which are used in their fully differentiated/contractile state to regulate vascular tone⁵. The phenotypically modulated SMCs that enter the intima are then believed to undertake new functional roles within the vessel wall, likely as a means of vascular repair to restore homeostasis⁵. A major question remains is how does one identify the functions of a phenotypically modulated SMC within the lesion, if in order to get there that SMC down-regulated all of its lineage/differentiation marker genes? Unfortunately, the answer to this question is we have little to no idea what is happening *in vivo* to phenotypically modulated SMCs, and the majority of 'facts' in the field, are based on *in vitro* cell culture studies.

Smooth Muscle Cell Lineage Tracing Models

Depending on the degree of phenotypic modulation, SMCs may lose expression of their marker genes all together and can only be identified by the structure of the cell, the rough endoplasmic reticulum (RER) and the “presence of groups of micropinocytotic vesicles, basement membranes, and residual thick filaments” via electron microscopy⁶. Due to the loss of SMC marker genes during the process of phenotypic switching, it is critical in the field to optimize and utilize rigorous SMC lineage tracing in order to properly describe phenotypic transitions of SMCs *in vivo* in order to assess their contribution to vascular injury and repair.

While transgenic lacZ mouse models driven by SM marker gene promoters^{10, 11} have helped the field identify the normal function of SMCs in vascular development, they cannot assist with SMC lineage tracing since they are also subject to down-regulation during phenotypic modulation. Smooth muscle cell constitutive Cre mice, such as the *Tagln-cre ROSA26 lacZ* mouse, also cannot be used for lineage tracing, since many SMC marker genes are transiently activated in other cell types during development, such as cardiac^{12, 13} and skeletal muscle cells¹³. The *Tagln G/C-mut lacZ* mouse was one of the first promising SMC lineage tracing mouse models that lead to the *in vivo* identification of phenotypically modulated SMCs after vascular injury¹¹ and Western diet treatment¹⁴ (Figure 1).

However, there are several limitations of the *Tagln G/C-mut lacZ* mice that prevent rigorous SMC lineage tracing. First, TAGLN is not SMC specific. Several

studies have shown that not only is TAGLN transiently expressed during embryogenesis¹², but can also be expressed by hematopoietic derived cells under atherosclerotic conditions^{15, 16}. Second, the *Tagln G/C-mut lacZ* mouse is not conditionally regulated and therefore might be subject to down-regulation in response to environmental cues, leading to an underestimation of the contribution of phenotypically modulated SMCs to wound repair and atherosclerosis development. This same issue may lead to non-SMCs activating the gene and being falsely identified as a SMC. Thirdly, the *lacZ* gene used in the creation of these transgenic mice is from *E. coli* and encodes for a β -galactosidase is hardier to pH changes than the mammalian gene product. In *in vivo* models of atherosclerosis the endogenous β -galactosidase is highly up-regulated due to increases in metabolism which can cause background staining in 4-bromo-5-chloro-3-indoyl-beta-D-galactopyranoside (X-gal) staining mediated detection of β -galactosidase and make antibody mediated detection of the *E. coli* β -galactosidase from the endogenous protein impossible¹⁷.

More recently researchers are beginning to use SMC lineage tracing models based on *Myh11* expression, the most specific SMC marker known to date. One such paper used a non-inducible *Myh11^{Cre/GFP} ROSA26 eGFP* mouse model to lineage trace SMCs after vascular injury¹⁸. At five days post injury they report no eGFP positive cells in the media or intima of the injured vessel and conclude that SMC progenitors are not the source of cells within the neointima, rather, neointimal cells are derived from a small population of multipotent

vascular stem cells (MVSCs)¹⁸. However, there are many technical flaws and inconsistencies with the rest of the vascular biology field as outlined by Nguyen *et al.*¹⁹. First, results from our lab report that 7 days post wire injury in a *Tagln G/C-mut lacZ* mouse reveal that almost 100% of the newly formed intima is SMC derived¹¹. Since several caveats to the *Tagln G/C-mut lacZ* model system are listed above it was really work by Drs. Weiser-Evans and Miano using a tamoxifen inducible conditional SMC lineage tracing system (*Myh11-CreER^{T2} ROSA26 flox Stop-lacZ*) showing SMCs within the media proliferating and entering the neointima 7 days after wire injury^{19, 20} that discredit the work presented by Tang *et al.*¹⁸. Indeed the *Myh11-CreER^{T2}* mouse developed by Wirth *et al.*²¹ may prove to be the best lineage tracing model of SMCs. *Myh11-CreER^{T2}* mice crossed to a reporter mouse such as, ROSA26 floxed Stop lacZ or ROSA26 floxed Stop eGFP demonstrate conditional labeling of fully mature SMCs at the time of tamoxifen injection²¹. Since the Cre excision is permanent, all progeny of the labeled cells will also be labeled, but without continuous tamoxifen treatment, no additional cells will activate the lineage mark.

A Case of Mistaken Identity

Controversy over the source of intimal SMCs in atherosclerotic lesions led to the discovery that a subset of hematopoietic derived cells can express SMC marker genes during the development of atherosclerosis *in vivo*¹⁶. While it is unclear whether or not a subset of hematopoietic cells become SMCs^{22, 23}, Iwata

*et al.*¹⁶ showed convincing data using a GFP⁺ → GFP⁻ mouse bone marrow transplant (BMT) experiment, that hematopoietic derived cells can express a repertoire of SMC marker genes four weeks after wire injury (Figure 2a). Interestingly, while ACTA2 and TAGLN were both upregulated in GFP⁺ (bone marrow derived) cells, Iwata *et al.* saw no evidence of GFP⁺ MYH11⁺ cells¹⁶ confirming that MYH11 remains the most specific SMC marker. Additional experiments transplanting *Myh11-Cre ROSA lacZ* bone marrow into a wild type recipient also failed to show evidence of bone marrow derived cells expressing MYH11 (by detection of lacZ)¹⁶. Supporting this finding, Caplice *et al.*²⁴ found evidence that approximately 10% of ACTA2⁺ cells in human coronary artery lesions were of myeloid and not SMC origin based on Y-chromosome FISH analysis of atherosclerotic lesions from patients who had undergone a cross gender BMT. The expression of SMC marker genes in hematopoietic derived cells may be mediated at least in part through TGF- β signaling²⁵, also described to be involved in ACTA2 induction in endothelial cells and fibroblasts^{26, 27}, as well as critical to SMC differentiation^{28, 29}.

While the evidence of hematopoietic cells expressing markers of SMC phenotypes has been well characterized, less is known about the ability of SMCs to up-regulate markers of hematopoietic lineage *in vivo*, in part due to the lack of an ideal SMC lineage tracing model system. Due to the ability of both hematopoietic and SMC lineages to down-regulate their traditional marker genes, and express markers of the other cell type, there is controversy over the true cell

origins of immunohistochemically stained ACTA2 and CD68 positive cells in atherosclerotic lesions³⁰.

As eloquently stated in a review by Owens *et al.*⁵ “one of the major deficiencies in studies investigating the role of the SMC phenotypic switching in vascular disease has been the failure of most studies to adequately distinguish ‘differentiation markers’ that serve as indices of the relative state of differentiation of the SMC versus ‘lineage markers’ that can serve to identify SMCs to the exclusion of all other cell types.” This issue is highlighted by a recent article by Allahverdian *et al.* where foam cells are determined to be of SMC origin based on ACTA2 staining³¹, despite almost a decade of evidence that multiple cell lineages, including hematopoietic derived cells, are capable of expressing ACTA2. Only through rigorous SMC lineage tracing models will the field be able to assess the true contribution of phenotypically modulated SMCs in vascular disease.

Smooth Muscle Cell Phenotypic Modulation in Atherosclerosis

Despite the limitations listed above, many researchers have established putative functions of SMCs within atherosclerotic lesions through the use of *in vitro* cell culture, and genetic KO mouse models. Although, it is important to remember that the specificity of SMC driven genetic KO models is up for question depending on what promoter was utilized to generate the KO. One of the main functions of SMCs within the lesion is believed to be collagen and

extracellular matrix production. Of all the cell types present in atheromas, SMCs are thought to be the major source of collagen production, and while collagen can comprise as much as 60% of the lesion, leading to stenosis, collagen deficiency can lead to unstable atheromas³². Based on experiments where *Tagln* expressing cells within long-term Western diet fed mice were induced to undergo low levels of apoptosis, collagen content was greatly reduced and dis-organized, suggesting that loss of SMCs within atherosclerotic lesions causes plaque destabilization, in part through their ability to produce collagen³³.

However, not all of the functions of SMCs within the atherosclerotic lesion are known. During the development of atherosclerosis, SMCs can be exposed to a milieu of factors that could potentially cause SMC phenotypic switching. Of the factors studied, only a handful can consistently down-regulate multiple SMC contractile proteins and induce phenotypic modulation, although the list is continually expanding as more research on phenotypically modulated SMCs is completed. These include the platelet derived growth factors PDGF-BB^{34, 35}, PDGF-DD^{36, 37}, and epidermal growth factor (EGF)³⁸, the lipids lysophosphatidic acid (LPA)³⁹, and oxidized phospholipids including 1-palmytoyl-2-(5-oxovaleroyl)-sn-glycero-3-phosphocholine (POVPC)⁴⁰, cyclodextrin-coupled cholesterol⁴¹, and the inflammatory cytokine interleukin-1beta (IL-1 β)⁴². In addition to inhibiting SMC marker gene expression, these factors also promoted SMC proliferation, migration, collagen production, and inflammatory cytokine gene expression. *In vitro* experiments using these factors to induce phenotypic switching have

revealed several tentative classifications and functions for potential SMC phenotypic states including: 1) contractile state, 2) synthetic state, 3) inflammatory state³⁶, 4) chondrocyte-like state^{43, 44}, and 5) macrophage-like state⁴¹. The **contractile state**, or fully differentiated, SMC phenotype in large blood vessels is defined by its expression of the contractile/cytoskeletal proteins listed above; a specific repertoire of ion channels; low rates of proliferation and extracellular matrix production; and minimal migration⁴⁵. The combination of these factors allows SMCs to perform their normal contractile functions in order to maintain proper vascular tone. The next SMC phenotype to be discovered was the **synthetic state** SMC, a term coined for an increase in synthetic organelles such as Golgi and rough endoplasmic reticulum⁴⁵. Originally the term “synthetic state SMC” was used for any SMC that had down-regulated a subset of the SMC marker genes that are used to identify a contractile state SMC. For example, studies in porcine models attempted to categorize SMCs based on the expression patterns of the SMC marker genes expressed within the media⁴⁶, where they concluded that at least four unique SMC phenotypes existed and may contribute to the development of vascular disease in different capacities. However, as time went on, the study of synthetic state SMCs was expanded to describe not only a change in SMC marker gene expression, but also a concurrent gain-of-function, such as increased cellular proliferation, migration, or extracellular matrix production. PDGF-BB was one of the first factors identified that could initiate reversible SMC phenotypic switching to a synthetic state,

causing simultaneous increase in cellular proliferation and decrease in ACTA2 expression³⁴. More recently, PDGF-DD, a growth factor released by endothelial cells exposed to disrupted flow patterns that signals through the PDGF- β R, was also indicated as an agonist of SMC phenotypic modulation to a synthetic state in *in vitro* SMC cell culture models³⁷.

With the growing body of work describing the synthetic state SMC, researchers began to postulate that there exist more than two types of SMC phenotypes, and that SMCs may be so plastic that it is impossible to categorize them into distinct phenotypes^{5, 45-47}. Nevertheless, using microarray data from SMCs treated with IL-1 β (reported to increase pro-inflammatory genes in vascular SMCs^{42, 48-51}) or PDGF-DD³⁷ Alexander *et al.* distinguished a putative third SMC phenotypic state herein referred to as the **inflammatory state SMC**³⁶. His work revealed that, while there was a cohort of genes up-regulated and down-regulated by both factors, the majority of the gene expression changes were different between the two groups. In particular, it was discovered that IL-1 β mediated SMC phenotypic switching was regulated by NF- κ B signaling, but PDGF-DD signaling was NF- κ B independent³⁶.

In addition, researchers have proposed that SMCs can become both **chondrocyte-like**^{43, 44} and **macrophage-like**⁴¹, although it is unclear whether or not these two states are encompassed by the synthetic state or inflammatory state phenotypes proposed by Alexander *et al.*³⁶. After ten days of treatment with beta-glycerophosphate, an organic phosphate donor, bovine aortic SMCs

decreased their SMC marker gene expression and induced expression of *Cbfa1*, a transcriptional regulator of osteochondrocytic genes including osteopontin, and alkaline phosphatase⁴⁴. These cells were also noted to accumulate extracellular calcium phosphate mineral deposit, furthering the argument that SMCs can become osteochondrocyte-like⁴⁴. Smooth muscle cell derived macrophage-like cells were identified after three days of treatment with methyl β -cyclodextran coupled cholesterol⁴¹. These primary mouse aortic SMCs down-regulated their contractile marker genes and had increased expression of multiple macrophage markers including CD68 and LGALS3 (MAC2) (Figure 2b) in addition to increased phagocytosis of latex beads⁴¹. While some evidence of chondrocyte-like⁴³ and macrophage-like^{52, 53} SMCs *in vivo* exists, there has been no definitely lineage tracing that can conclusively state that SMCs give rise to any of the aforementioned phenotypic states.

The Accepted Dogma of Atherosclerotic Plaque Formation and Assessment of Plaque Stability

In order to understand the significance of properly identifying phenotypically modulated SMCs within atherosclerotic lesions, especially the importance of identifying a phenotypically modulated SMC versus a macrophage, it is essential to understand the current dogma about the development of atherosclerosis and how to assess plaque stability.

Pathophysiology of Atherosclerotic Plaque Formation

Atherosclerosis is a chronic inflammatory disease of the arteries that is defined by the accumulation of lipids, extracellular matrix, and an accrual of SMCs and immune cells within the subendothelium of arterial walls². The onset of atherosclerosis begins with lipoprotein deposition in the subendothelial matrix². Changes in hemodynamic shear stress due to the inherent branching nature of the vascular tree can create regions of temporal oscillations that disrupt the endothelium, increasing the incidence of low density lipoprotein (LDL) deposition, and making curvatures and branch points of the vasculature more prone to atherosclerosis^{54, 55}. The shear stress at these locations also makes them more prone to rupture later in disease development⁵⁶, therefore lesions at these locations have been the focus for studying atherosclerotic disease, development, and downstream clinical sequelae.

The second stage of atherosclerosis formation is the development of the fatty streak. Accumulated LDL within the subendothelial space aggregates and becomes oxidized when interacting with reactive oxygen species, which leads to endothelial cell inflammation^{55, 57}. Endothelial pro-inflammatory signaling recruits circulating monocytes and causes them to penetrate into the subendothelium space where they differentiate into macrophages and uptake the oxidized lipids. The hallmark of a fatty streak is the presence of foam cells, macrophages that have become engorged with lipids, within the vessel wall. However, fatty streaks

are not considered clinically significant as they are routinely noted in infants and are believed to be capable of complete regression⁶.

More advanced lesions are defined by the proliferation and migration of SMCs from the medial layer into the atheroma⁵⁷, as been assessed by [³H] thymidine radiolabeling and careful examination of immunohistochemical stains for SMC marker genes^{46, 47}. These intimal SMCs secrete large amounts of extracellular matrix, particularly collagens type I and III, and are believed to be the contributors to the fibrous buildup within the plaque^{32, 57}. Next, the development of a large lipid-laden necrotic core, marks the transition from a clinically silent atherosclerotic event to an advanced atherosclerotic lesion^{57, 58}.

Advanced atherosclerotic lesions are associated with an increased risk for clinical complications ranging from a gradual decrease in blood flow that can cause angina, to complete vessel occlusion that can have catastrophic clinical consequences including myocardial infarction, stroke, and death. These clinical complications arise through two primary mechanisms: 1) narrowing of the vessel lumen due to atherosclerotic plaque growth with inadequate outward vessel remodeling, and 2) plaque destabilization leading to rupture and occlusive thrombus formation^{59, 60}. Of the two mechanisms, plaque rupture events have been more closely linked to acute ischemic syndromes⁶¹, mostly due to the thrombogenic nature of the lipid laden necrotic core⁶². Therefore, during rupture events, the necrotic core is exposed leading to platelet adhesion, aggregation, and occlusive thrombus formation⁶¹.

Indices of plaque stability

Careful autopsy studies of fatal occlusive thrombi revealed that 70-80% were associated with rupture of the atherosclerotic plaque fibrous caps⁶³⁻⁶⁵. Given that plaque rupture accounts for the majority of acute ischemic syndromes, understanding the defining features of an unstable atheroma is paramount to discovering methods to improve plaque stability. Histopathological studies in humans have revealed that ruptured plaques exhibit distinctive cellular and morphological characteristics relative to stable plaques.

The most highly correlated index of plaque instability with plaque rupture is a thin, inflamed fibrous cap in conjunction with a large lipid laden necrotic core^{57, 59, 60, 63, 66}. In particular, Davies *et al.* quantified the ratio of ACTA2 positive staining cells (SMCs) to CD68 positive staining cells (macrophages) in human lesions that either had experienced a thrombotic event or not and found that the thrombotic lesions had a decreased ACTA2/CD68 ratio compared to the lesions that had not undergone a thrombotic event⁶⁷. While mentioned earlier in the Introduction, I would like to reiterate that the use of ACTA2 and CD68 is not an accurate examination of the contribution of SMCs and macrophages to the atherosclerotic plaque, but rather biomarkers of plaque characteristics. The ACTA2/CD68 ratio is believed to be important, in part due to the associated functions of cells expressing these markers.

As mentioned previously, monocytes are recruited to the atherosclerotic lesion in response to inflammatory signaling. Here, they differentiate into

macrophages, phagocytize oxidized lipoproteins, apoptotic cells, and apoptotic bodies. They are also noted to release matrix metalloproteinases (MMPs)⁶⁶. However, in the context of chronic atherosclerosis, cells expressing macrophage markers will signal for additional macrophages to enter the lesion as they become overwhelmed by oxidized phospholipids and initiate apoptosis, releasing esterified cholesterol into the growing necrotic core^{55, 58, 66}. In response, SMCs proliferate to surround the necrotic core and release extracellular matrix proteins, such as, proteoglycans and collagen fibrils covering the lipid laden necrotic core and therefore stabilizing the atheroma⁵⁵.

Thrombotic events do not always result in clinical symptoms, in fact, autopsies of individuals whom died of non-cardiac related causes revealed that as many as 8% of the individuals had had a recent thrombotic event⁶⁸. In addition, Davies *et al.* has found that almost half of individuals whom have had a fatal thrombotic event also had evidence of previous events (mural intraluminal coronary thrombi)⁶⁸. Therefore the majority of the following indices used to identify a plaque as stable or unstable focus on identifying whether or not a plaque has had a rupture event in the past.

Intraplaque hemorrhage is the major indicator of a prior rupture event and can arise through multiple mechanisms including: 1) a resolved plaque fissure event 2) a resolved rupture event, and 3) neovascularization of the intima from the vasa vasorum⁶⁹. All of these events are evident and can be identified by the presence of red blood cells and fibrin depositions within the lumen. Although not

as accurate, evidence of intraplaque hemorrhage can also be identified in patients using intravascular ultrasound and angioscopy^{70, 71}.

Also correlated to an increase in incidence of plaque rupture are plaque calcification and collagen content. While a strong predictor of future plaque rupture events, calcification within the plaque is not a determining factor for a given plaque to be unstable⁷², nor does calcification seem to modify the mechanical stability of the plaque⁷³. Cardiac pathologists have noted that spotty calcification rather than dense calcification seems to incur more risk, and may be due to localized apoptosis, but have yet to make a direct link between calcium deposits and plaque rupture^{69, 74}. Opposite to calcification, histological sections revealed a decrease in plaque collagen content associated with ruptured versus non-ruptured plaques^{75, 76}, and clinical intervention with Pravastatin increased intimal collagen content while simultaneously decreasing other indices of plaque instability, suggesting collagen might be correlated with increased plaque stability^{75, 77}.

Taken together, these findings have established a set of morphological and cellular characteristics that define a plaque as 'vulnerable' and make them prone to rupture, thereby leading to acute coronary syndromes⁷⁸. As stated prior, the majority of these insights came from pathophysiological data from plaques that had either ruptured or remained intact at the time of autopsy. In order to better understand the cellular and molecular mechanisms behind these indices of plaque stability researchers have turned to genetically modified mouse models

such as hypercholesterolemic apolipoprotein E (ApoE)-deficient and low density lipoprotein receptor (LDLR)-deficient mice^{55, 79-81}. Although lesions from murine models of atherosclerosis do not regularly undergo plaque rupture without mechanical intervention, they largely recapitulate the stages of plaque formation found in humans including the presence of necrotic cores and fibrous caps, macrophage infiltration (as assessed by LGALS3 staining), SMC accumulation (as assessed by ACTA2 staining), collagen deposition, and intraplaque hemorrhage^{80, 82, 83}. The presence of these features of advanced atherosclerosis in murine models thus permits genetic or pharmacological testing of the roles of individual molecular factors in regulating processes leading to the development of these features⁸⁴.

KLF4 Signaling and Smooth Muscle Cells Phenotypic Modulation

As described above, SMCs and phenotypically modulated SMCs are believed to be critical to the development of atherosclerosis and plaque stability. In order to assess how the various SMC phenotypic states may differentially contribute to atherosclerosis development, we must first understand the mechanisms behind SMC phenotypic switching. While many pathways including NF- κ B signaling³⁶ have been indicated in the regulation of SMC phenotypic switching, the focus of this dissertation will be on the role of the induced pluripotency transcription factors, such as, krüppel-like factor 4 (KLF4, or GKLF), and octamer binding protein (OCT4, or POU5F1), in SMC phenotypic switching.

KLF4 was first discovered to play a role in SMC contractile gene expression when investigating mechanisms of transforming growth factor β (TGF β) induced SMC differentiation^{28, 85}. Mutation of a TGF- β control element (TCE)²⁹ in the *Tagln* gene promoter abolished TAGLN expression in *Tagln* TCE mutant-lacZ transgenic mice²⁸. A yeast-one hybrid screen for binding partners to the TCE element revealed KLF4 as a potent binder to the TCE element²⁸. However, further studies showed that KLF4 did not directly bind to the TCE element, instead, KLF4 binds to a G/C repressor region of the gene promoter and functions in opposition to TGF- β dependent, TCE mediated *Tagln* and *Acta2* induction^{86, 87}. Consistent with this finding, studies show that KLF4 is not present in differentiated SMCs, but up-regulated in de-differentiated, phenotypically modulated SMC after models of vascular injury and atherosclerosis^{28, 88, 89}.

From this finding it was postulated that KLF4 might be a key regulator of SMC phenotypic switching. Indeed, KLF4 has been found to inhibit serum response factor (SRF) binding to CArG boxes within SM promoter genes, thereby reducing myocardin-mediated SM marker gene activation⁹⁰ (myocardin has been identified as a master regulator of SMC marker gene expression⁹¹⁻⁹⁴). KLF4 was also rapidly up-regulated *in vitro* in response to PDGF BB⁸⁶, POVPC^{40, 95}, as well as *in vivo* in response to vascular injury⁹⁰. Furthermore, total conditional knockout of KLF4 caused a transient delay in SMC marker gene down-regulation after carotid ligation injury⁸⁹, and siRNA knockdown significantly inhibited suppression of SMC marker genes and collagen type VIII after application of POVPC within

pluronic gel to the rat carotid artery⁸⁸. However, siRNA knockdown of KLF4 was only able to partially reduce PDGF-BB mediated SMC marker gene down-regulation, indicating that KLF4 is not the only regulator of SMC phenotypic switching⁸⁷. Down-regulation of SMC marker genes by KLF4 following vascular injury, POVPC treatment, and PDGF-BB treatment was later shown to be mediated through KLF4 binding to G/C repressor elements present in the promoters of many SMC marker genes⁸⁷.

Interestingly, after the discovery of the importance of KLF4 in transitioning SMCs from a more differentiated contractile phenotype to a less differentiated phenotype, KLF4 was revealed as one of several transcription factors including OCT4, SOX2, c-MYC, and lin28 responsible for inducing pluripotency from a differentiated cell type to a pluripotential stem (iPS) cell^{96, 97}. Of these transcription factors, OCT4 was the only one that was sufficient for cell reprogramming⁹⁸, but convincing data has not been published that identifies OCT4 expression in somatic cells⁹⁹. Given our findings about KLF4 regulating SMC phenotypic transition, we are excited to investigate the potential role of OCT4 in SMC phenotypic transition since no studies to date have investigated the role of other pluripotency factors on SMC phenotypic switching.

Focus of Dissertation

The overall goal of the projects within this dissertation was to accurately identify phenotypically modulated SMCs within atherosclerotic lesions and determine their role in advanced atherosclerosis. One of the main indices of an unstable atheroma is the presence of a thin, SMC poor, fibrous cap, and a large foam cell rich necrotic core⁶⁷ as identified using ACTA2 as a marker for SMCs and CD68 as a marker for macrophages. However, as summarized earlier in this chapter, there are major ambiguities regarding the accurate contribution of each cell type to lesion progression^{1, 55}. Of particular interest are the studies showing that SMCs and macrophages are capable of down-regulating lineage specific marker genes typically used to identify each respective cell type^{8-10, 100-107}; and studies in cultured cells showing that both cell types are capable of expressing “definitive” markers of the other cell type under conditions likely to exist within atherosclerotic lesions (reviewed in Gomez and Owens³⁰). Several studies analyzing the human coronary artery plaques have also shown a population of cells that express both ACTA2 and CD68^{31, 52}, which raises questions about the true origin of these cells. Due to this controversy, the particular focus of this dissertation was to determine whether or not SMCs phenotypically modulate into a macrophage-like state, and whether these cells play a role in lesion stability. ***We hypothesized that a population of previously unidentified phenotypically modulated SMCs take on characteristics of macrophages within atherosclerotic lesion. We also hypothesized that the pluripotency***

factors regulating somatic cell reprogramming, such as, KLF4 and OCT4, also regulated the transition of differentiated SMCs to a more plastic state in the context of atherosclerosis.

Studies within **Chaper 2** outline the development of a novel method for detecting histone modifications at specific gene loci in single cells in histological sections. Through the use of *in situ* hybridization (ISH) of a biotinylated probe to the *MYH11* promoter and a proximity ligation assay (PLA), this method was able to detect the histone modification H3K4dime on the *MYH11* promoter in SMCs (ISH-PLA method). Previous work in the Owens lab showed this mark to be specific to SMCs and resistant to down-regulation upon treatment with SMC phenotypic modulation factor PDGF-BB¹⁰⁸. ISH-PLA for H3K4dime on the *Myh11* promoter was confirmed using a SMC specific lineage tracing mouse model, *Myh11-CreER^{T2} ROSA floxed STOP eYFP Apoe^{-/-}* (SMC YFP^{+/+} *Apoe^{-/-}*). Importantly, this model is conditionally activated through an ER^{T2}-Cre system creating a permanent lineage tag of mature SMCs that were expressing MYH11 during the tamoxifen treatment period, and all of their subsequent progeny. Western diet treatment of SMC YFP^{+/+} *Apoe^{-/-}* mice for 18 weeks consistently shows phenotypically modulated SMCs (eYFP^{+/+}/ACTA2⁻) within the intima. Therefore, further experiments were conducted in these mice to validate that the H3K4dime mark on the *Myh11* promoter was specific to SMCs and that this assay can be used to lineage trace SMCs in mice and humans, even after phenotypic modulation.

Studies in **Chapter 3** provide the most rigorous analysis of phenotypically modulated SMCs within advanced atherosclerotic plaques to date and show that genetic depletion of pluripotency factor KLF4 specifically in SMCs creates smaller, more stable atherosclerotic lesions. Results also show for the first time *in vivo* definitive proof of SMC derived macrophage-like cells within atherosclerotic lesions of mice and humans, and the dependence of KLF4 in their derivation. These studies are extended to show that global heterozygous KO of KLF4 also results in decreased lesion size and indices of stability in a nearly identical fashion as the SMC specific KLF4 KO suggesting that the main function of KLF4 in determining lesion size and stability is through its actions on SMCs.

While KLF4 was shown to play an important role in SMC phenotypic switching to a macrophage-like state, there were no significant changes in the total number of phenotypically modulated SMCs within the lesions of the SMC specific *Klf4* KO mice. Based on studies showing that KLF4 was one of four factors used to induce pluripotency in fibroblasts⁹⁷, but OCT4 alone was sufficient to induce pluripotency¹⁰⁹, we hypothesized that OCT4 was required for SMC phenotypic switching. To answer this question **Chapter 4** focuses on the expression of OCT4 within SMCs and its role of blood vessel remodeling. Herein OCT4 was found to be expressed in SMCs after vascular injury and Western diet induced atherosclerosis in mice. SMC selective KO of *Oct4* resulted in larger, less stable atherosclerotic lesions that were characterized by a 50% reduction in phenotypically modulated SMCs. Upon further investigation it was revealed that

Oct4 KO in SMCs impaired the ability of SMCs to down-regulate their SMC marker genes and initiate migration, in part through diminished MMP3 and MMP13 activity. Analysis of the *Oct4* promoter revealed putative KLF4 and HIF1 binding sites that when mutated lead to impaired *Oct4* induction after exposure to POVPC. Therefore KLF4 and HIF1 binding to the *Oct4* promoter may be the mechanism behind OCT4 expression in phenotypically modulated SMCs. Finally, **Chapter 5** concludes with future directions based on this work and preliminary data from other experiments.

Figure 1: Mutation of the G/C repressor region of the *Tagln* promoter enables visualization of phenotypically modulated SMCs in models of vascular injury and atherosclerosis.

β -Gal staining of mouse carotid arteries from *Tagln* LacZ (a, c), and *Tagln* G/C mut LacZ (b, d) transgenic mice 7 days after injury (c, d) or in uninjured controls (a, b). Arrows denote the internal elastic lamina and the arrowheads denote the external elastic lamina. β -Gal staining of mouse arteries from *Tagln* LacZ *ApoE*^{-/-} (e-i) and *Tagln* G/C mut LacZ *ApoE*^{-/-} (j-n). Mice were fed a Western diet for 18 weeks. e and j represent staining of the intact aortic tree. f and k represent nonatherosclerotic regions of the thoracic aorta as denoted in e and j. g and l represent atherosclerotic lesion cross-sections from the aortic arch as denoted in e and j. h and m and i and n represent high-magnification images of the lesion shoulder and medial vessel wall below the lesion in g and l, respectively. Arrowheads denote the internal elastic lamina.

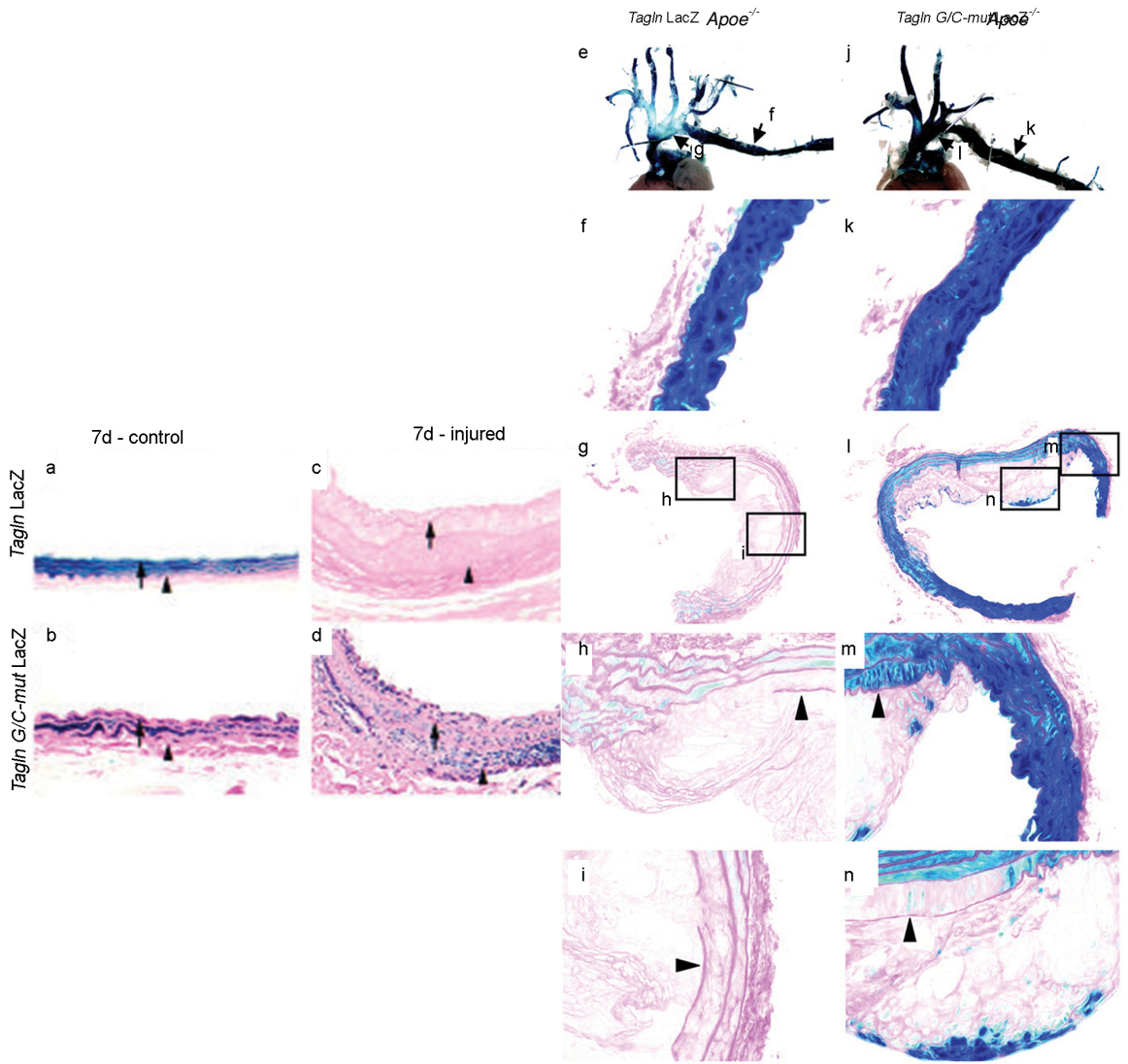
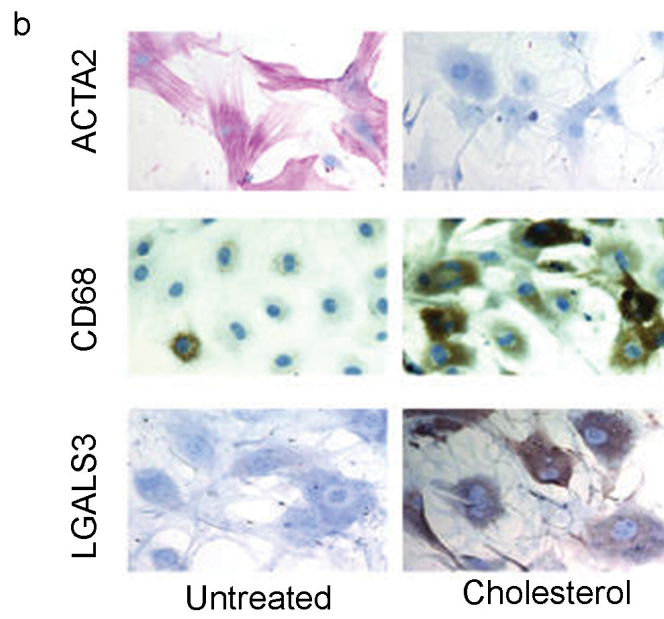
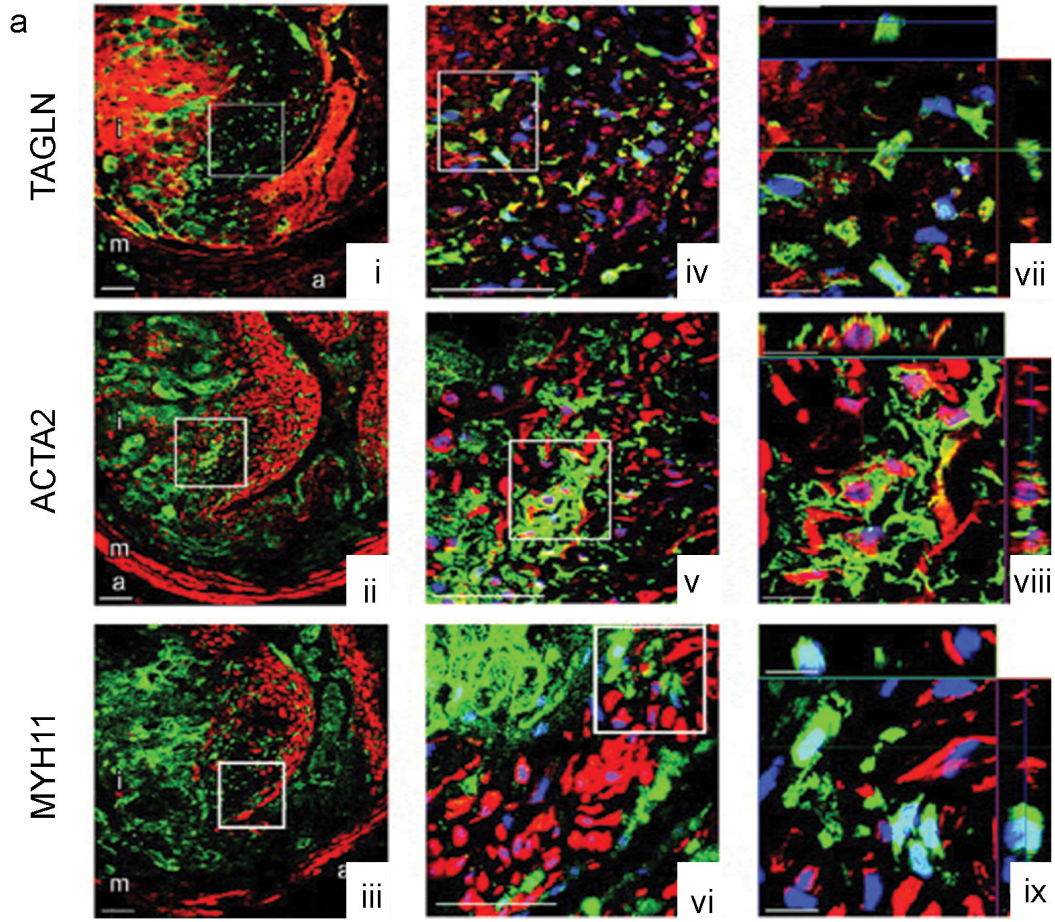


Figure 2: Smooth muscle cells and macrophages are capable of up-regulating marker genes of the other cell type.

Adapted from Rong *et al.*⁴¹ and Iwata *et al.*¹⁶ (a) M β CD-cholesterol treatment of primary cultured mouse SMCs for 72 hours down-regulated SMC marker gene ACTA2 and up-regulated macrophage marker genes, CD68 and LGALS3. (b) Bone marrow transplant of eGFP bone marrow into an eGFP negative recipient mouse that underwent wire injury. Staining four weeks after wire injury for TAGLN (i, iv, vii), ACTA2 (ii, v, vii), and MYH11 (iii, vi, ix).



**Chapter 2: Detection of histone modifications at specific gene loci in single
cells in histological sections**

Authors: Delphine Gomez, Laura S Shankman, Anh T Nguyen, and
Gary K Owens

Adapted from *Nature Methods* Article

Abstract

Chromatin immunoprecipitation assays have contributed greatly to our understanding of the role of histone modifications in gene regulation. However, they do not permit analysis with single-cell resolution, thus confounding analyses of heterogeneous cell populations. Here we present a method that permits visualization of histone modifications of single genomic loci with single-cell resolution in formaldehyde-fixed paraffin-embedded tissue sections based on combined use of *in situ* hybridization and proximity ligation assays. We show that dimethylation of lysine 4 of histone H3 (H3K4me2) at the *MYH11* locus is restricted to the smooth muscle cell (SMC) lineage in human and mouse tissue sections and that the mark persists even in phenotypically modulated SMC in atherosclerotic lesions that show no detectable expression of SMC marker genes. This methodology has promise for broad applications in the study of epigenetic mechanisms in complex multicellular tissues in development and disease.

Introduction

Epigenetics is defined as a heritable code other than the genomic sequence and include histone post-translational modifications, DNA methylation and ATP-dependent chromatin remodeling¹¹⁰⁻¹¹². Differentiation from embryonic stem cells (ESCs) to multiple differentiated cell types requires establishment of spatiotemporal expression of gene patterns^{113, 114}. As one example out of many¹¹⁵⁻¹¹⁸, we have previously shown that a SMC-specific epigenetic repertoire of histone modifications are acquired during development of SMC from ESC, including H3K4dime of SMC marker genes such as *ACTA2* and *MYH11*, the latter being the most specific marker of SMC lineage^{106, 108, 119}. Importantly, results show that H3K4dime of these genes is restricted to SMCs and absent in non-SMCs. Moreover, H3K4dime enrichment of these genes persists when cultured SMCs are induced to undergo phenotypic switching to a less differentiated state¹⁰⁸, a process dependent on activation of the ESC pluripotency factor KLF4 both *in vivo*⁸⁷ and in cultured cells¹⁰⁸. These results suggest that H3K4dime of the *MYH11* and other SMC marker gene loci represent stable epigenetic markers of SMC lineage. However, a major limitation in studies thus far is that data are derived nearly exclusively from studies in cultured SMC which are poorly differentiated since cell culture systems do not recapitulate complex environmental cues that regulate SMC differentiation *in vivo*^{5, 120} under normal as well as in pathological conditions. Moreover, it is impossible to obtain chromatin exclusively derived from SMCs from tissue sources, since all SMC-containing

tissues contain multiple other cell types. Conversely, all “non-SMC” tissues contain large numbers of SMCs since all tissues are vascularized. As such, conventional ChIP^{121, 122} analyses cannot be used to rigorously test if H3K4dime of SMC gene loci are an exclusive epigenetic signature of SMC lineage *in vivo*. Indeed, a major general limitation of ChIP assays is that they do not permit analysis of histone modifications at a given gene locus within individual cells thus confounding interpretation of analyses of heterogeneous cell populations, and precluding direct assessment of the role of specific histone modifications within individual cell types within complex multicellular tissues including disease specimens. For example, ChIP analyses on a tumor biopsy or atherosclerotic tissue specimen, represents a composite signal derived from the many different cell types present within that tissue sample. Although one may perform ChIP assays on a given cell population obtained by cell sorting, such analyses of course results in loss of critical information regarding the spatial orientation of cells within tissues, and may be subject to epigenetic changes that occur during the tissue dissociation and/or the sorting procedures.

Here, we describe a new method that permits visualization of histone modifications at a single genomic locus in human and mouse formalin-fixed paraffin-embedded tissue sections that is an equivalent of a “single-cell ChIP” assay by combination of ISH and PLA methods. Moreover, using this new methodology, we demonstrate that H3K4dime of the *MYH11* gene locus is a highly specific marker of SMC lineage *in vivo* that persists even in phenotypically

modulated SMC within atherosclerotic lesions that lack detectable expression of endogenous SMC marker genes.

Materials and Methods

Human tissues

Coronary and carotid arteries specimens from patients (n =10) were collected during Coronary artery bypass graft (CABG) and carotid endarterectomy surgery as well as during autopsy. These specimens were processed, fixed in paraformaldehyde and paraffin-embedded blocks were cut into 5 µm sections. Human temporal lobe sections were from autopsy cases from the University of Virginia, Department of Pathology. Brain tissue was immersion-fixed in 10% zinc-buffered formalin, and embedded in paraffin using standard procedures. The institutional review board at University of Virginia approved the use of all autopsy specimens.

Mice

Animal protocols were reviewed and approved by the University of Virginia Animal Care and Use Committee. *Myh11-CreER^{T2}* mice were generously provided by Stefan Offermanns (Max Planck Institute, Germany)²¹; ROSA26 STOP flox eYFP and ApoE^{-/-} were obtained from Jackson Laboratories. All mouse strains have been backcrossed to a C57BL/6J for greater than six generations. *Myh11-CreER^{T2}* mice were genotyped by PCR as previously described²¹. ROSA26 STOP flox eYFP mice were genotyped using the following primers: oIMR0316 5'-GGAGCGGGAGAAATGGATATG-3', oIMR0872 5'-AAGTTCATCTGCACCACCG-3', oIMR1416 5'-TCCTTGAAGAAGATGGTGCG-

3', oIMR3621 5'-CGTGATCTGCAACTCCAGTC-3'. Cre Recombinase was activated with a series of ten 1 mg tamoxifen intraperitoneal injections (Sigma Aldrich) from six to eight weeks of age for a total of 10 mg of tamoxifen/25 g mouse. Mice were fed a high-fat (Western type) diet containing 21% milk fat and 0.15% cholesterol (Harlan Teklad) for 18 weeks starting at eight weeks of age. Mice were euthanized by CO₂ asphyxiation then perfused via the left ventricle with 5 mL PBS followed by 10 mL 4% paraformaldehyde and an additional 5 mL PBS. Brachiocephalic arteries and various organs were carefully dissected and fixed for 30 min in 4% paraformaldehyde prior to embedding in paraffin.

Cell culture and harvesting

Mouse SMCs were cultured in growth medium (DMEM/F12, Gibco) supplemented with Fetal Bovine Serum (10%), L-glutamine (1.6mM, Gibco) and Penicillin-Streptomycin (100U/mL, Gibco). Cells were starved for three days in serum-free medium and treated with 10µg/mL POV-PC (1-(palmitoyl)-2-(5-oxovaleroyl)-*sn*-glycero-3-phosphatidylcholine, Cayman Chemical). Human coronary SMCs, human coronary ECs, U937 (human monocyte) and RAW264.7 (human macrophage) cell lines were purchased from Lonza and ATCC. Cells were grown in corresponding medium in the presence of serum to confluence. For ISH/PLA, SMCs and ECs were harvested and fixed in 10% phosphate buffered formalin (PBF, Fisher). After formalin fixation, cells were pelleted and

suspended in 1% agarose (Sigma). Cell pellets were processed and paraffin-embedded blocks were cut into 5 μ m sections.

Immunofluorescent staining

Sections were de-paraffinized and rehydrated in xylene and ethanol series. After antigen retrieval (antigen retrieval solution, Vector), section were blocked with Fish Skin Gelatin/PBS (6 g/L) containing 10% of goat or horse serum for one hour at room temperature. Endogenous mouse IgG in mouse tissue sections was blocked by incubation with unconjugated Fab Fragment Goat anti-mouse IgG (H+L) (Jackson ImmunoResearch Labs) for 1h at room temperature. Slides were incubated with the following antibodies: mouse monoclonal SM α -actin-FITC (ACTA2) (4.4 μ g/mL, clone 1A4, Sigma Aldrich), rat monoclonal SM Myosin Heavy Chain (MYH11) (1 μ g/mL, clone KM3669, Kamiya Biomedical Company), goat polyclonal anti-PECAM-1 (CD31) (2 μ g/mL, # sc-1506, Santa Cruz), mouse monoclonal dimeH3K4 (4 μ g/mL, clone CMA303, Millipore) and goat polyclonal anti-GFP (4 μ g/mL, # ab6673, Abcam) for detection of eYFP. The secondary antibodies were donkey anti-rat conjugated to Alexa 555 (5 μ g/mL, Abcam), donkey anti-goat conjugated to Alexa-647 (4 μ g/mL, Invitrogen), donkey anti-mouse conjugated to Alexa-555 (4 μ g/mL, Invitrogen).

Probe preparation & hybridization

Human *MYH11*, mouse *Myh11*, human *CDH5*, mouse *Cdh5* and mouse *Tagln* biotin-labeled probes were generated. The proximal 2kb of these promoters were amplified by PCR (see primers in Supplemental Table 1). PCR products were cloned into pCR2.1 vector for amplification (TOPO cloning kit, Invitrogen). Probes were generated by Nick Translation (Roche) using biotin-14-dATP (Invitrogen). Nick translation efficiency was assessed by migration on 1% agarose gel. Labeled-DNA probes (40 ng/slide) undergo denaturation in Hybridization Buffer (2× SSC, 50% high grade formamide, 10% dextran sulfate, 1µg of human or mouse Cot-1 DNA) for 5 min at 80°C. Directly after immunostaining, slides were dehydrated in ethanol series and incubated in 1mM EDTA (pH 8.0) for 20 min. Then, samples were incubated with pepsin (0.5%) in buffer (0.05M Tris, 2mM CaCl₂, 0.01M EDTA, 0.01M NaCl) at 37°C for 20 min, as previously described²⁴. Hybridization mixture containing biotinylated probes or 5-TAMRA-dUTP labeled Y chromosome probe (Clone RP11–88F4, Empire Genomics) was applied on sections. Sections were incubated at 80°C for 5 min, followed by 16–24h incubation at 37°C. Hybridization was followed by multiple washes in 2× SSC, 0.1% NP-40 buffer.

Proximity Ligation assay (PLA)

PLA was performed directly after ISH following manufacturer's instructions (Olink). After blocking, sections were incubated with mouse H3K4dime (5 µg/mL, clone CMA303 Millipore), mouse H3K27trime (5 µg/mL, # ab6002, Abcam),

mouse H4ac (5 µg/mL, clone 3HH4–4C10, Millipore) and rabbit Biotin (5 µg/mL, # ab53494, Abcam) antibodies overnight at 4°C, followed by incubation with secondary antibodies conjugated with PLA probe at 37°C for 1h as recommended by manufacturers. Then, ligation and amplification were performed (Duolink detection kit Orange, 555nm). Finally, mounting medium with DAPI was used.

Image acquisition and analysis

Images were acquired with Olympus BX41 fitted with a Q imaging Retiga 2000R camera. Image acquisition was performed with the Q Capture Pro software (Media Cybernetics & QImaging Inc). Settings were fixed at the beginning of both acquisition and analysis steps and were unchanged. Brightness and contrast were lightly adjusted after merging. Image analysis was performed with Image J. Confocal images were acquired using a Zeiss LSM700 scanning confocal microscope with 405nm, 488nm, 555nm, and 637nm solid state lasers. Analysis of confocal images was completed using Zeiss Zen 2009 software.

Chromatin Immunoprecipitation

ChIP was performed on cultured cells as previously described¹⁰⁸. Cells were fixed with 1% paraformaldehyde for 10 min at room temperature. Cross-link was stopped by addition of 125 mM glycine for 10 min. The cross-linked

chromatin was sonicated to shear chromatin into fragments of 200–600 base pairs. The sheared chromatin was immunoprecipitated with 2 μg of diethylamine-modified H3K4 antibody (clone CMA303, Millipore), while negative control was incubated with mouse IgG and input DNA without antibody, and immune complexes were recovered with magnetic beads (Millipore).

Quantitative PCR

Total RNA was prepared from cultured cells using Trizol (Invitrogen) according to the manufacturer's protocol. One microgram of RNA was used for reverse transcription with iScript cDNA synthesis kit (BioRad). Real-time PCR was performed (iQ SYBR Green Supermix, Biorad) on cDNA or DNA extracted after CHIP using primers listed in Supplemental Table 1.

Statistics

Values are expressed as means \pm s.d. For CHIP, three independent experiments were performed. Each experiment was repeated in triplicate. Comparison between groups was tested using ANOVA test. A value of $P < 0.05$ was considered significant.

Results

Our overall strategy made use of the Proximity Ligation Assay (PLA)¹²³⁻¹²⁵, to detect proximity between a biotin-labeled probe targeting the *MYH11* promoter and H3K4dime at this locus (Fig. 3a). PLA is widely performed for detection of protein/protein interaction or protein post-translation modifications in both cultured cells and tissue sections^{124, 126} but to our knowledge has not been used for assessing histone modifications at specific gene loci. We sought to combine PLA with ISH methods using two primary antibodies targeting: 1) histone modifications; and 2) biotin residues included in a probe annealing to the genomic locus of interest. The feasibility of the approach was first assessed by estimating intermolecular distances between DNA and histone tails to ascertain the compatibility with the PLA range of detection of approximately 40 nm (Supplemental Fig. 1). The major methodological steps included the following (Fig. 3b): 1) immunostaining of human or mouse formalin-fixed paraffin embedded tissue sections with antibodies to SMC or non-SMC markers; 2) ISH with a biotinylated DNA probe targeting the *MYH11* locus; 3) PLA including incubation with anti-biotin (rabbit) and H3K4dime (mouse) primary antibodies. We validated that nuclear detection of H3K4dime was preserved following the ISH procedure (Supplemental Fig. 2) and mapped H3K4dime enrichment of the *MYH11* promoter to identify boundaries for our ISH probe (Supplemental Fig. 3). Moreover, for validation of our ISH procedure, we used a 5-TAMRA dUTP labeled Y chromosome probe in human samples from male patients, and we

observed similar hybridization efficiencies of the Y chromosome in SMCs and non-SMCs cell types (Supplemental Fig. 4).

ISH-PLA: a new method of detection of histone modifications at a single genomic locus in tissue sections

We performed ISH-PLA detection of H3K4dime at the *MYH11* locus in human coronary arteries since these are highly relevant to atherosclerotic disease, and these vessels contain three distinct cell layers: 1) the intima consisting of endothelial cells (ECs); 2) the media composed primarily of Smooth muscle α -actin⁺ (ACTA2⁺) SMCs; and 3) the adventitia mainly composed of fibroblasts negative for SMC markers but with abundant small blood vessels (Fig. 3c). We initially focused on small arteries within the adventitia of coronary arteries which have a well-defined SMC layer. *MYH11* H3K4dime PLA⁺ signal (i.e. visualized by red spots within the nucleus) was observed exclusively within ACTA2⁺ medial SMCs (Fig. 3d) whereas adventitial cells and ECs (CD31⁺) were negative. An empty biotinylated vector was used as a negative control and showed no PLA amplification in SMCs and non-SMCs demonstrating that the *MYH11* probe was required for PLA amplification (Fig. 3e). To further validate our ISH-PLA method, we compared results of ISH-PLA and ChIP assays in cultured cells (Fig. 3f,g and Supplemental Fig. 5). These results showed complete concordance in that H3K4dime enrichment of the *MYH11* locus was observed exclusively in SMCs by both ChIP and ISH-PLA analyses.

To provide a model system for testing the stability of the *MYH11* H3K4dime mark in phenotypically modulated SMCs *in vivo*, we developed a SMC lineage tracing system by crossing *Myh11-CreER^{T2}* mice²¹ with ROSA26 STOP-floxeYFP^{+/+} mice (SMC-eYFP^{+/+} mice) (Fig. 4a). Tamoxifen treatment of mice from age six to eight weeks induced high efficiency eYFP expression exclusively in SMCs in all tissues examined (Fig. 4b,c and Supplemental Fig. 6). In contrast, no detectable expression of eYFP was observed without tamoxifen treatment (Fig. 4b) or in SMC-eYFP^{-/-} mice treated with tamoxifen (Fig. 4d), whereas >95% of medial cells within SMC-eYFP^{+/+} mice were YFP⁺ (Fig. 4e) indicating high efficacy of SMC specific recombination. Moreover, a substantial fraction of eYFP⁺ SMCs within large arteries (i.e. aorta) of these SMC-eYFP^{+/+} mice were *Myh11* H3K4dime PLA⁺ (Fig. 4e). In contrast, non-SMCs including ECs were *Myh11* H3K4dime PLA⁻. No PLA signal was seen in negative controls using an empty cloning vector as probe in place of the MYH11 *in situ* probe (Fig. 4f). We estimated that ISH-PLA has an equivalent efficiency (66%) compared with regular FISH procedures (64%) (Supplemental Figs.4 and 7). Moreover, we found comparable efficiency using human and mouse tissue sections.

Validation of ISH-PLA using SMC lineage tracing mouse model

To test whether ISH-PLA can be readily adapted to examination of additional gene loci or histone modifications, we performed ISH-PLA experiments using a probe targeting the Vascular Endothelial-Cadherin (VEC) promoter

(*CDH5*). *CDH5* is a specific marker of the EC lineage¹²⁷, and enrichment of H3K4dime is found on this promoter specifically in cultured ECs based on conventional ChIP assays¹⁰⁸. Results of analyses of mouse and human tissue sections of healthy vessels showed specific *CDH5* H3K4dime PLA+ staining of ECs. In contrast, SMCs (medial ACTA2+ human, eYFP+ in SMC-eYFP^{+/+} mouse) were strictly PLA- (Supplemental Fig. 8). We also performed PLA analysis of H4 acetylation of SM22 α (*Tagln*), a gene selectively expressed in SMC within healthy adult blood vessels^{11, 13}. Consistent with expectations, *Tagln* H4 acetylation PLA+ staining was restricted to SMC (Supplemental Fig. 9).

Multiple non-SMC including ECs, fibroblasts and ESCs in culture show marked enrichment of H3K27trime of the *MYH11* gene locus based on ChIP assays, consistent with its transcriptional silencing in these cells¹⁰⁸. Thus, to further validate our PLA method *in vivo*, we evaluated not only H3K4dime but also H3K27trime of the *MYH11* locus in human carotid arteries (Fig. 5a). Consistent with PLA results in small arteries within the adventitia (Fig. 3d), and ChIP results in cultured cells (Supplemental Fig. 5), *MYH11* H3K4dime PLA+ cells were restricted to ACTA2+ SMCs within the media (Fig. 5b) whereas adventitial fibroblasts and endothelial cells were negative (Fig. 5b and Supplemental Fig. 12). We did not observe any PLA amplification when we used a non-relevant probe (Fig. 5c). Medial SMC were negative for H3K27trime of the *MYH11* locus, whereas ECs (CD31+ cells) (Fig. 5d) and adventitial fibroblasts (ACTA2- cells) (data not shown) were positive for this silencing mark based on

PLA analyses. Consistent with these results in human coronary arteries, PLA analyses of human brain sections (Fig. 5e and Supplemental Fig. 11) showed exclusive *MYH11* H3K4dime PLA labeling of SMC whereas neuronal cells were *MYH11* H3K4dime PLA⁻ but *MYH11* H3K27trimePLA⁺. These results provide compelling evidence of the reliability of our ISH-PLA method to specifically detect histone modifications at specific gene loci in single cells in human and mouse tissue sections and are consistent with results of our previous studies using conventional CHIP assays on cultured cells¹⁰⁸. However, the preceding studies are the first to identify a cell-type and locus-specific histone modification in cells *in vivo* within intact tissue sections within a complex multicellular tissue specimen. Furthermore, we provide evidence that H3K4dime of the *MYH11* gene locus represents a unique and specific epigenetic signature of cells of the SMC lineage *in vivo*. Finally, we show that our PLA methodology is readily adaptable to multiple gene loci and histone modifications.

Mature SMCs retain remarkable plasticity and can undergo phenotypic switching characterized by markedly decreased SMC marker gene expression and increased proliferation and migration in pathological environments such as atherosclerosis^{5, 128, 129}. However, because phenotypically modulated SMCs down-regulate expression of SMC markers (including ACTA2 and MYH11) there are major ambiguities as to which cells within lesions are derived from SMCs³⁰. Previous studies demonstrated that PDGF-BB-induced phenotypic switching of cultured SMCs was associated with marked reductions in SMC marker

expression and reduced H4 acetylation but no changes in H3K4dime enrichment of the *ACTA2* or *MYH11* promoters¹⁰⁸. We extended these studies herein by showing that induction of SMC phenotypic switching with the pro-atherogenic oxidized phospholipid, 1-(palmitoyl)-2-(5-oxovaleroyl)-*sn*-glycero-3-phosphatidylcholine (POVPC), had similar effects, including reduced MYH11 expression but no change in *MYH11* H3K4dime enrichment (Fig. 6a–b). To determine if *Myh11* H3K4dime persists during SMC phenotypic switching *in vivo*, we generated advanced atherosclerotic lesions by crossing our SMC-eYFP^{+/+} mice with ApoE^{-/-} mice and fed them a Western diet for 18 weeks. Remarkably, we identified large numbers of phenotypically modulated SMCs within lesions which show no detectible expression of MYH11 (Fig. 6c) or ACTA2 (Fig. 6d) and are identifiable as being of SMC origin only through detection of the SMC-specific eYFP lineage tracing gene product. Importantly, our SMC lineage tracing model is conditionally activated through an ER^{T2}-Cre system allowing us to permanently lineage tag mature SMCs that were expressing MYH11 during the tamoxifen treatment period (i.e. 6–8 weeks of age). These cells and their progeny constitutively express eYFP, allowing us to lineage trace these cells independent of the expression of traditional SMC markers which can be down-regulated. In contrast, any SMC derived from a non-SMC source at a later time point, will not express eYFP. Remarkably, results of our studies with this highly rigorous SMC lineage tracing system showed that >95% of SMC-derived cells within atherosclerotic lesions within brachiocephalic arteries of SMC-eYFP^{+/+} ApoE^{-/-}

ice were not detectable as being of SMC origin based on ACTA2 (Fig. 6f) or MYH11 immunostaining (Fig. 6c). Moreover, of major significance, we showed that the majority of these cells were *Myh11* H3K4dime PLA⁺ (Fig. 6f). Taken together, the preceding results not only establish the SMC specificity of H3K4dime of the *MYH11* gene locus, but also show that this epigenetic mark is stable *in vivo* even in SMC that are not identifiable as being of SMC origin based on detection of endogenous marker genes. Moreover, results indicate that one may use detection of *MYH11* H3K4dime by ISH-PLA as an epigenetic lineage tracing system for assessing the role of SMC in the pathogenesis of a number of major human diseases in which SMC phenotypic switching is postulated to play an important role including atherosclerosis, cancer, asthma, and hypertension. Indeed, consistent with this possibility, we found that a large fraction of cells within advanced atherosclerotic lesions within human coronary arteries do not express SMC marker genes such as ACTA2 and MYH11 (Fig. 7a and Supplemental Fig. 12) but are *MYH11* H3K4dime PLA⁺ (Fig. 7b). In addition, we detected *MYH11* H3K27trime PLA⁺ cells only in ACTA2⁻ cells within the lesions but not in medial ACTA2⁺ SMCs (Fig. 7c). In contrast, *MYH11* H4ac was restricted to medial ACTA2⁺ SMCs and was absent within lesion cells (Supplemental Fig. 13). Fig 5d presents a summary model of histone modifications in differentiated mature SMC *versus* phenotypically modulated SMC based on observations *in vivo* in the present studies and our previous studies in cultured SMCs¹⁰⁸.

Discussion

Herein we develop and validate a new method for visualizing histone modifications at a single genomic locus within single cells in histological sections, and using it provide novel evidence that H3K4dime of the *MYH11* gene locus is: 1) a highly specific marker of SMC lineage *in vivo*; and 2) this epigenetic mark persists even in SMC that have undergone phenotypic transitions to a less differentiated state wherein the cell is unidentifiable as being of SMC origin except using genetic lineage tracing methodologies. We believe these observations are highly important for the following reasons:

First, although several groups^{130, 131} have employed PLA to detect protein-nucleic acid interactions *in vitro*, our studies are the first to our knowledge to describe a method that permits detection of specific histone modifications at a given gene locus in single cells in fixed histological specimens which we believe will have tremendous utility for investigating the role of epigenetic changes in development and disease. Indeed, there is a large body of research that have investigated the role of epigenetic regulation and chromatin signature during stem cell differentiation or development of specific types of cancer¹³². Nevertheless, the technical limitations of ChIP assays described previously do not allow the *in vivo* characterization of such epigenetic signatures except in the study of hematopoietic stem cells¹³³ or leukemia¹³⁴ in which cell sorting can be performed without extensive tissue dissociation prior to ChIP analyses. Thus, we believe that ISH-PLA will be a powerful tool for the investigation of epigenetic

regulation in solid tumors in which it is virtually impossible to ascertain if a given epigenetic change is present within tumor or stromal cells. Similarly, our ISH-PLA method will have tremendous utility in investigating the role of specific histone modifications at selective gene loci during development of complex multicellular tissues during development. Moreover, the fact that the method can be applied to paraformaldehyde fixed paraffin embedded tissue specimens, the standard protocol for archiving human biopsy specimens, will allow unprecedented studies of the role of epigenetic changes in the pathogenesis of human diseases using existing tissue banks. Finally, we believe that our ISH-PLA method may be adapted for the detection and visualization of DNA methylation or transcription factor binding on specific promoters with single-cell resolution which will further expand our ability to investigate transcriptional regulation of a given gene locus within its native context within complex multicellular tissues *in vivo*.

Second, our results are the first to show persistence of a cell specific epigenetic signature when cells undergo phenotypic transitions to a less differentiated or altered phenotypic state *in vivo*, wherein the cell origin cannot be identified by detection of endogenous cell selective marker genes. Evidence of appearance and maintenance of cell-specific epigenetic signature (other than the SMC lineage) have been previously described but with the limitation that results were based on studies in cultured cells under conditions that fail to recapitulate complex cell-cell, cell-matrix, and other critical environmental cues that exist *in vivo*^{135, 136}. In addition, to having important implications for lineage tracing of cells

in complex tissues including human biopsy specimens, these observations may also have critical implications for the propagation of epigenetic mechanisms that control cell lineage memory and cell specific bookmarking during cell mitosis, normal development, and disease progression^{135, 137}. However, it remains to be determined whether persistence of H3K4diMe of SMC gene loci is important in the ability of SMC to undergo reversible phenotypic switching during repair of vascular injury. As such, our studies have provided no evidence as to whether this histone modification plays a causal role in controlling SMC lineage and phenotype and further mechanistic studies are needed in this important area but at present are not possible due to the lack of an approach to selectively remove this mark exclusively at SMC gene loci.

Third, of major significance, our results indicate that numerous studies of atherosclerosis that relied on identification of intimal SMC based on detection of ACTA2 have grossly under-estimated the frequency of SMCs within lesions, and likely failed to detect possible transition of these cells to alternative phenotypes that may be critical in the pathogenesis of the disease. Until now, lineage tracing of lesion cells *in vivo* in human studies has been restricted to studying the possible role of hematopoietic cells within lesions based on analyses of cross-gender bone marrow transplant specimens combined with Y chromosome detection by *in situ* hybridization²⁴. However, these approaches are highly limited due to such samples being extremely rare, the approach does not allow rigorous lineage tracing of non-hematopoietic cells, and results are confounded by

development of transplant atherosclerosis which has a different etiology than normal atherosclerosis. Of major interest, we believe that ISH-PLA will greatly advance studies of human atherosclerosis by facilitating novel studies of the mechanisms and factors that regulate phenotypic transitions in SMC within atherosclerotic lesions and their possible functional roles in plaque development, progression and end-stage events leading to clinical complications such as myocardial infarction or stroke.

Figure 3: ISH-PLA: a new method of detection of histone modifications at a single genomic locus in tissue sections.

(a) Schematic of the combined *in situ* hybridization (ISH) and Proximity Ligation Assay (PLA) method for detecting H3K4dime of the *MYH11* promoter. (b) Immunostaining of 5 μm -thick sections of human carotid artery for ACTA2 and DAPI (diamidinophenyindole). Two distinct layers are identified: the media (M) and the adventitia (A). Small vessels consisting of ACTA2+ SMCs are visualized within the adventitia (arrows). Scale bar = 100 μm . (c) ISH-PLA in adventitial small arteries ($n = 5$). PLA amplification (PLA+) is visualized as a red spot localized within nuclei. *MYH11* H3K4dime PLA+ signal is restricted to ACTA2+ medial SMCs (arrows) and is absent from CD31+ ECs (stars) as well as adventitial fibroblasts (arrow heads). (i–iii): High magnification with i) ACTA2, ii) PLA and iii) merge. Scale bar = 50 μm . (d) ISH-PLA negative control using an empty vector probe in adventitial vessel of human carotid artery sections. A total absence of PLA amplification demonstrates that hybridization of the biotin-labeled *MYH11* probe is required for ISH-PLA amplification. Scale bar = 50 μm . (e) Conventional ChIP assays showing enrichment of H3K4dime of *MYH11* in SMCs but not in ECs. Mean \pm s.d.; $n = 3$; $*P < 0.05$. (f,g) ISH-PLA in SMCs ($n = 3$) and ECs ($n = 3$) *in vitro*. *MYH11* H3K4dime PLA amplification is restricted to SMCs. Scale bars = 10 μm .

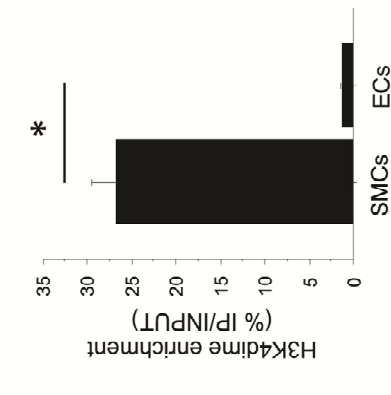
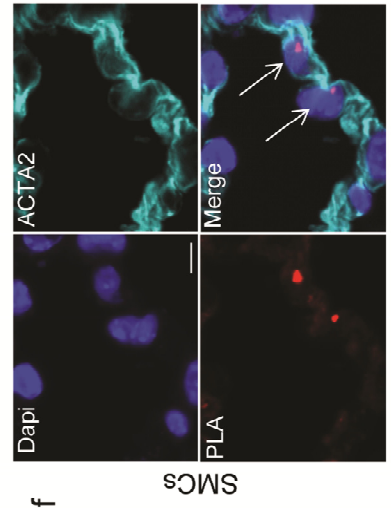
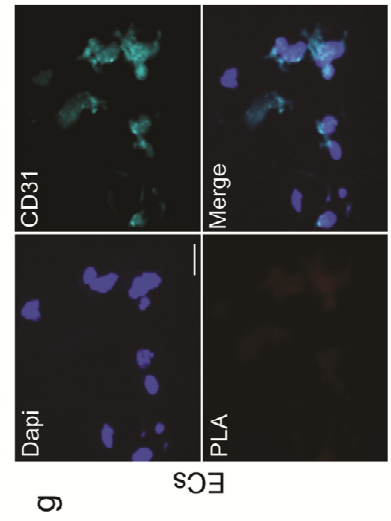
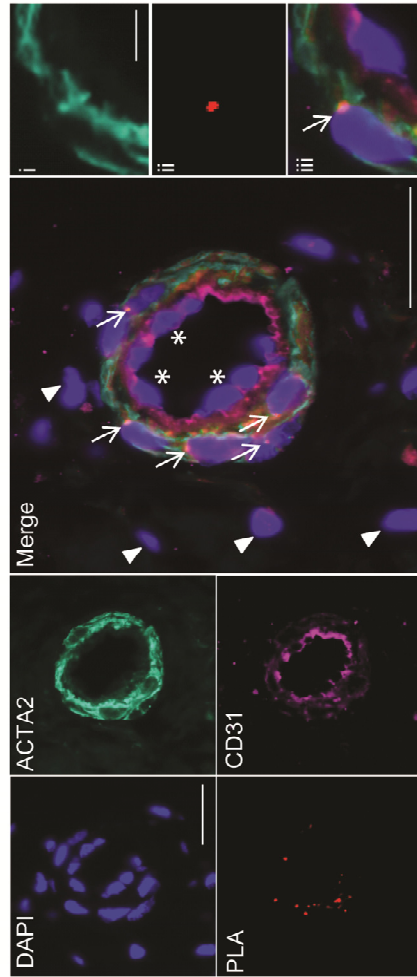
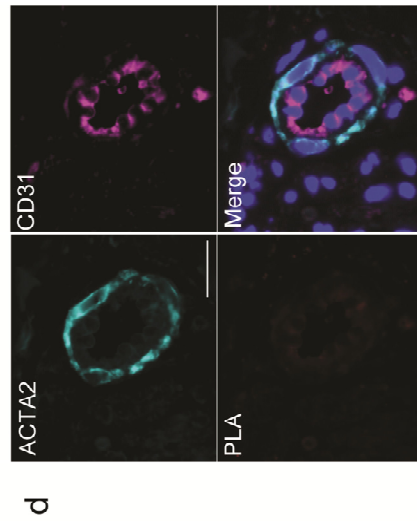
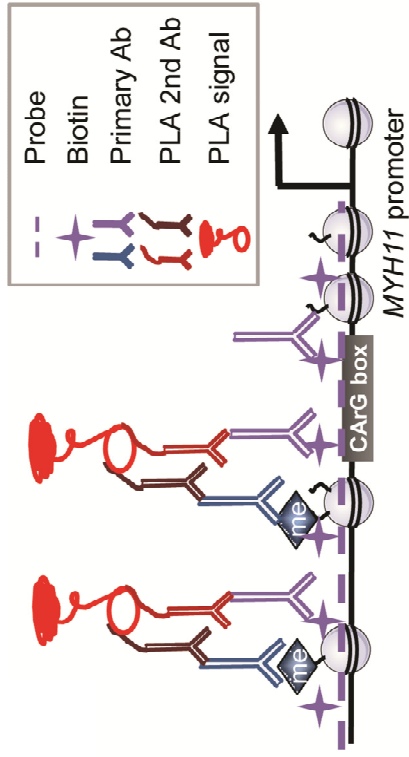
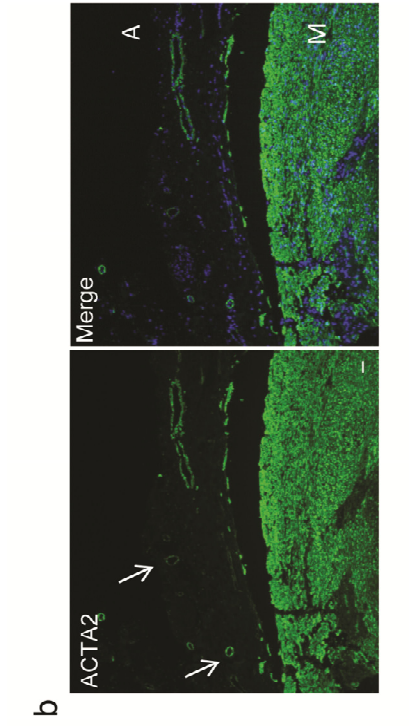


Figure 4: Validation of ISH-PLA using SMC lineage tracing mouse model.

(a) SMC lineage tracing was done by crossing Myh11-CreERT2 transgenic mice with ROSA26 STOPfloxeYFP^{+/+} mice and treating mice with tamoxifen between six and eight weeks of age thereby providing SMC-specific and permanent lineage tagging of SMCs with eYFP (n = 5). (b) Immunostaining of the aorta of SMC-eYFP^{+/+} mice for eYFP and ACTA2 with (bottom image) and without (top image) tamoxifen injections. eYFP expression was observed only after tamoxifen treatment and was exclusively observed in SMCs within the media (M), compared with the intima (I) and the adventitia (A) negative for eYFP staining. L: lumen. Scale bar = 10 μ m. (c) Assessment of eYFP expression in heart tissue sections of SMC-eYFP^{+/+} mice by immunostaining for eYFP (cyan), ACTA2 (red) and Dapi (blue). eYFP expression is strictly restricted to ACTA2⁺ cells. (d) SMC-eYFP^{-/-} mice present a complete lack of eYFP expression in ACTA2⁺ cells in heart tissue sections. Scale bar (c–d) = 100 μ m. (e) Results of ISH-PLA in aortas from SMC-eYFP^{+/+} mice showing that Myh11 H3K4dime PLA positivity was restricted to eYFP⁺ medial SMCs (arrows) (media: M). No Myh11 H3K4dime PLA signal was detected in ECs (stars) (intima: I). L: lumen. i–iii show eYFP⁺ PLA⁺ SMCs at higher magnification with i) eYFP, ii) PLA and iii) merge. Scale bar = 10 μ m. (f) Negative control wherein ISH was done using an empty biotinylated vector in SMC-eYFP^{+/+} mice. No Myh11 H3K4dime PLA⁺ cells were identified. Scale bar = 10 μ m.

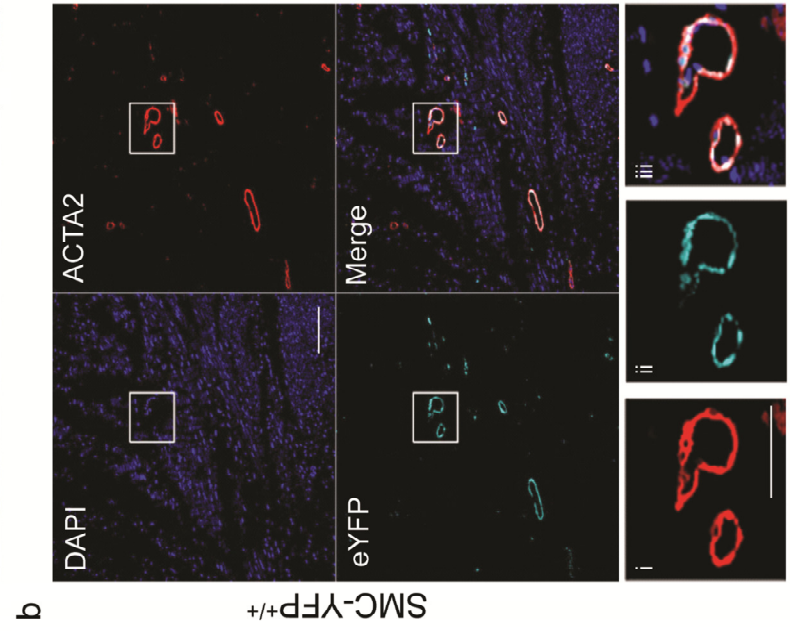
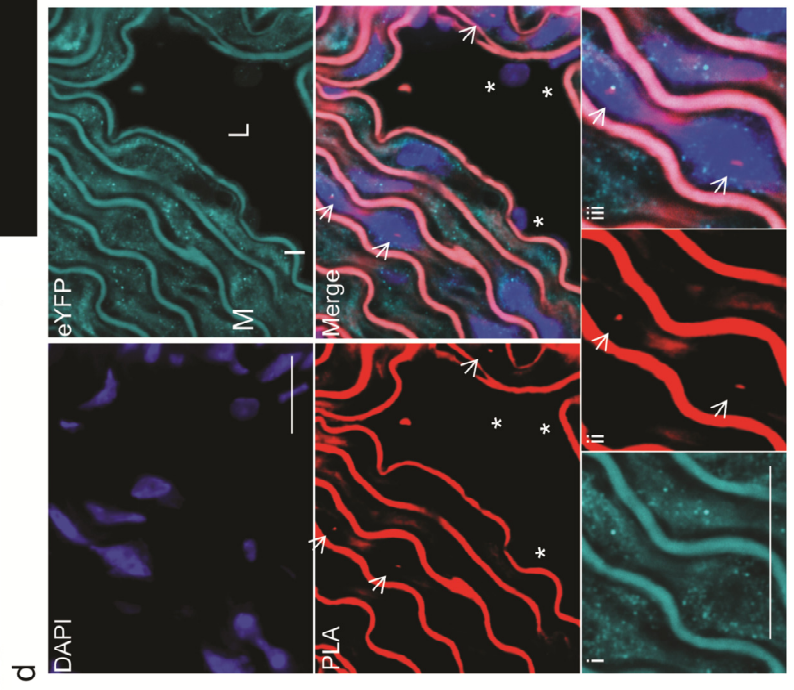
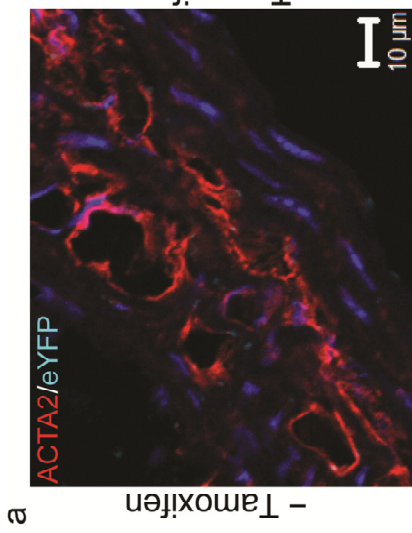
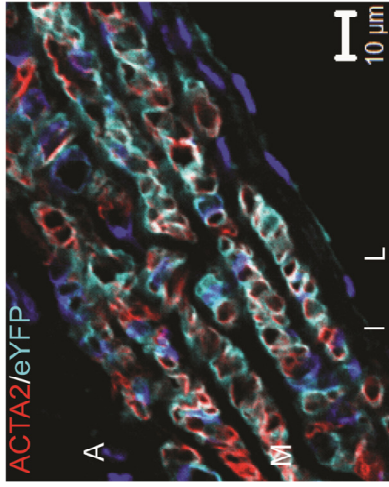
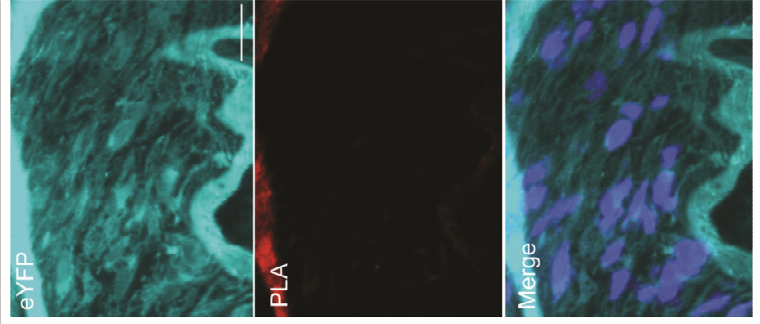
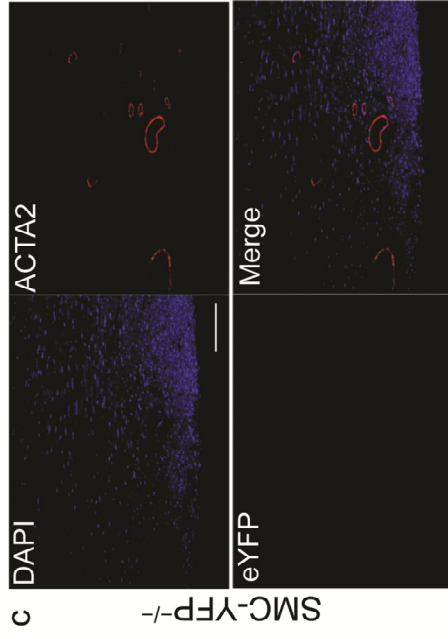


Figure 5: Visualization of H3K4dime on the MYH11 promoter in SMCs in situ in histological sections of human carotid arteries.

(a) Immunostaining of human carotid artery sections illustrating the media (M) consisting primarily of ACTA2+SMCs, as well as the adventitia (A), intima (I) and the vessel lumen (*) ($n=5$). Scale bar = 100 μm . (b) Results of *MYH11* H3K4dime PLA in human carotid artery sections with DAPI (blue) and ACTA2 (cyan). PLA signal (red) was exclusively observed in ACTA2+ medial SMCs (arrows). None of the ACTA2- cells within the adventitia were *MYH11* H3K4dime PLA+. Scale bar = 50 μm . Higher magnification from **b** with i) DAPI (blue), ii) ACTA2 (cyan), iii) PLA (red), and iv) merged image. (c) Negative control where ISH was done with an empty biotinylated vector followed by PLA with biotin and H3K4dime antibodies. Scale bar = 50 μm . (d) Detection of H3K27trime on the *MYH11* promoter in human carotid artery sections. Results showed a positive *MYH11* H3K27trime PLA signal in CD31+ ECs (arrows). In contrast, ACTA2+ cells were *MYH11* H3K27trime PLA-. Scale bar = 50 μm . i-iv) Higher magnification images with: i) ACTA2 (cyan), ii) CD31 (purple), iii) PLA (red), and iv) merged, DAPI (blue). (e) *MYH11* H3K4dime PLA analysis of human brain tissues stained with ACTA2 (cyan). SMCs in brain vessels are *MYH11* H3K4dime PLA+ (arrow). Scale bar = 10 μm . i-iv) Small capillary within brain tissue with DAPI (i), ACTA2 (ii), PLA (iii) and merged image (iv).

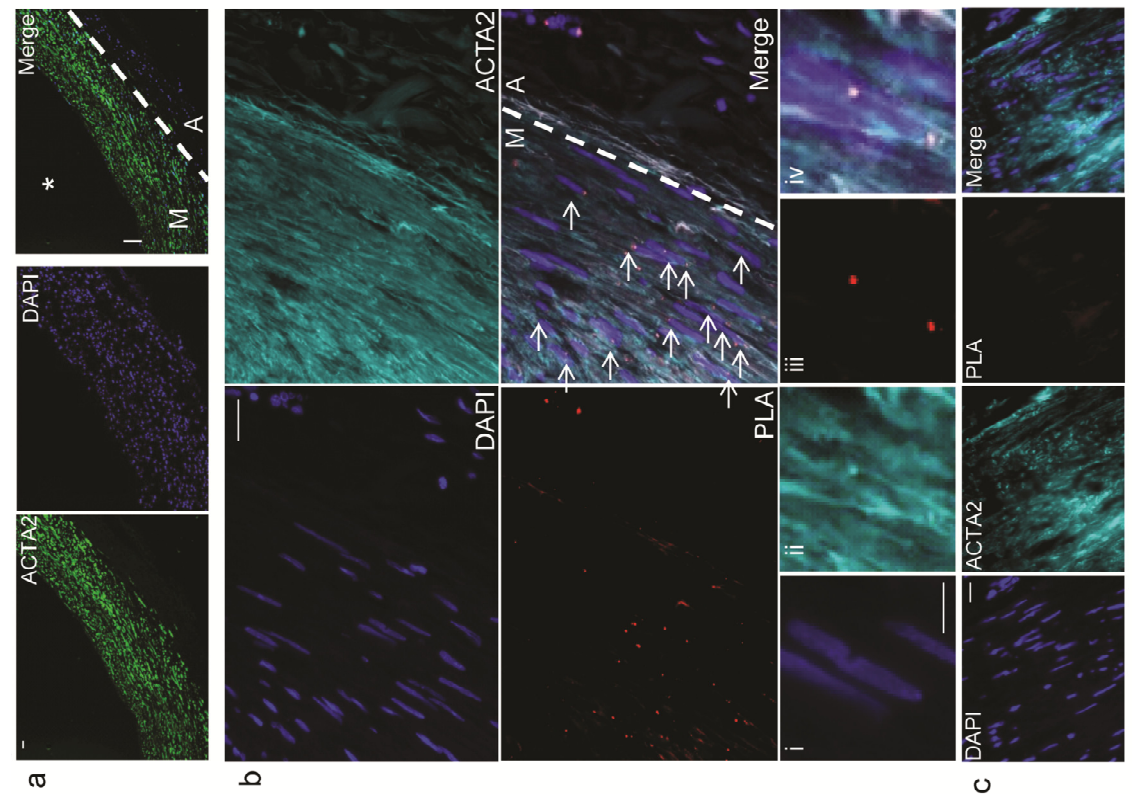
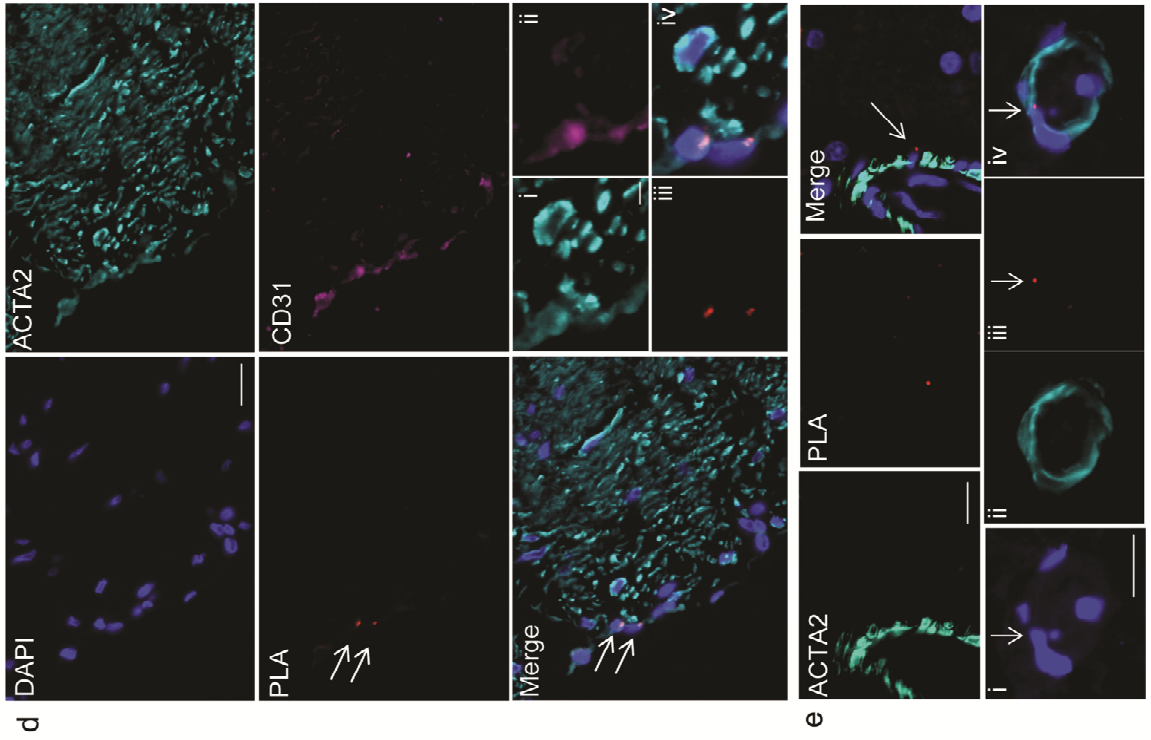
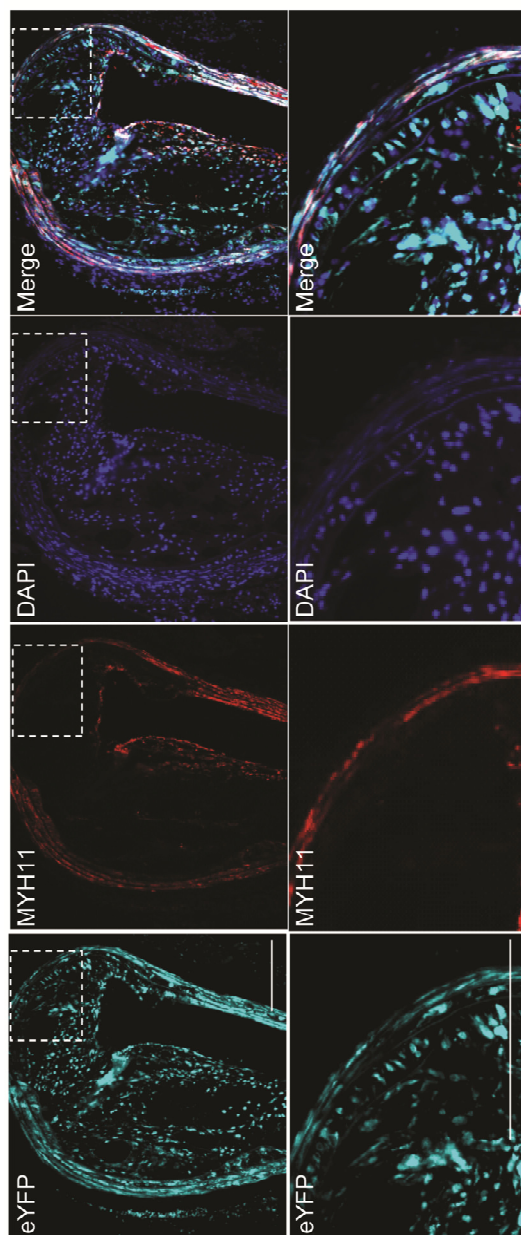
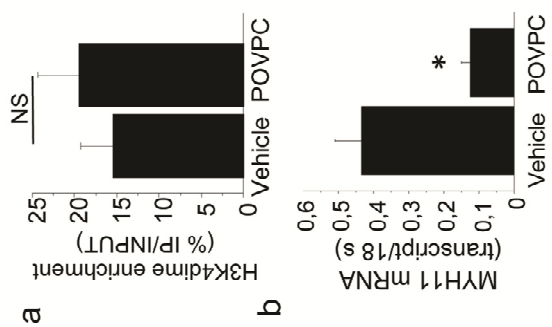


Figure 6: H3K4dime on the MYH11 promoter persists during phenotypic switching in vivo in SMC lineage tracing mice developing atherosclerosis.

(a) ChIP assay performed in cultured SMCs treated with vehicle (DMSO) or POVPC (10 µg/mL, 24h) showing similar H3K4dime enrichment on the *MYH11*. Mean s.d.; $n = 3$. (b) mRNA quantification of *MYH11* showing POVPC-induced decrease in *MYH11* mRNA level compared with vehicle. Mean \pm s.d; $n = 3$; * $P < 0.01$. (c) Identification of modulated SMCs in SMC-eYFP^{+/+} ApoE^{-/-} mice fed with Western diet for 18 weeks. Brachiocephalic arteries (BCA) sections of these mice were stained with eYFP (cyan) and MYH11 (red). eYFP⁺ SMCs were identified within the media where they co-express MYH11 and within the atherosclerotic lesion where they lose expression of MYH11. Scale bar = 100 µm. (d) BCA sections of SMC-eYFP^{+/+} ApoE^{-/-} mice were stained with eYFP (cyan) and ACTA2 (yellow) and were analyzed for MYH11 H3K4dime PLA. Scale bar = 100 µm. (e). Image corresponding to region 1 boxed in (d) Medial SMCs are ACTA2⁺ eYFP⁺ and *Myh11* H3K4dime PLA⁺ (arrows). Higher magnification with eYFP (i), PLA (ii) and merged image with Dapi (iii). (f) Image corresponding to region 2 boxed in (d). Within the atherosclerotic lesion, a substantial fraction of eYFP⁺ACTA2⁻ cells is *Myh11* H3K4dime PLA⁺ indicating cells of SMC origin not identifiable based on detection of endogenous SMC markers (arrows). Scale bar (e–f) = 10 µm. Higher magnification with eYFP (i), PLA (ii) and merged image with Dapi (iii).

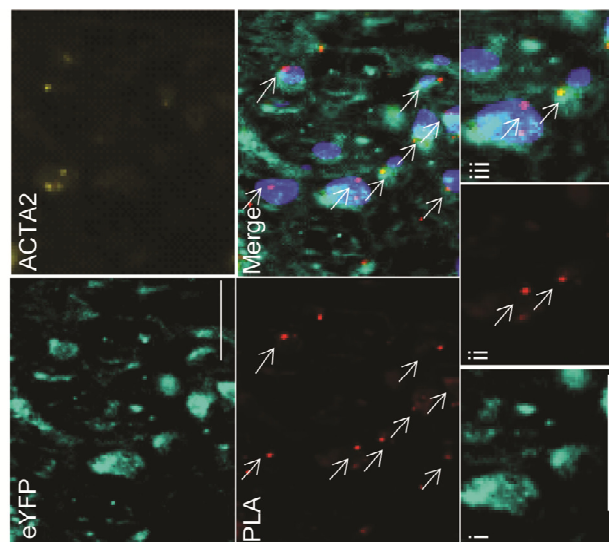


c

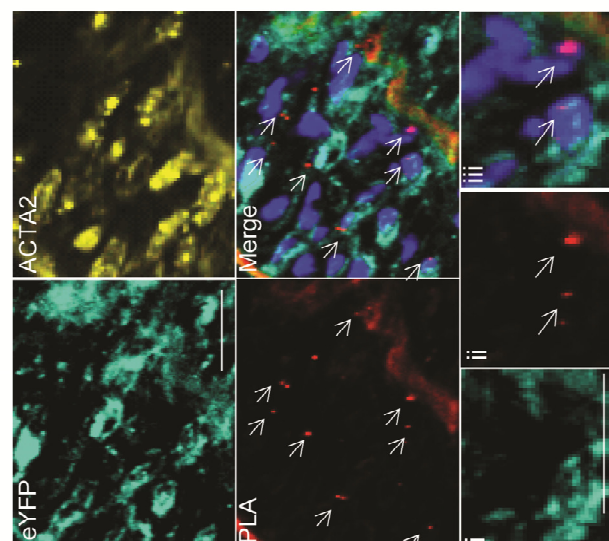


a

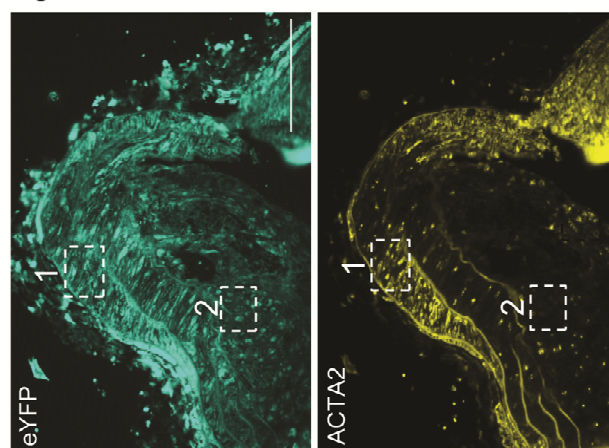
b



f



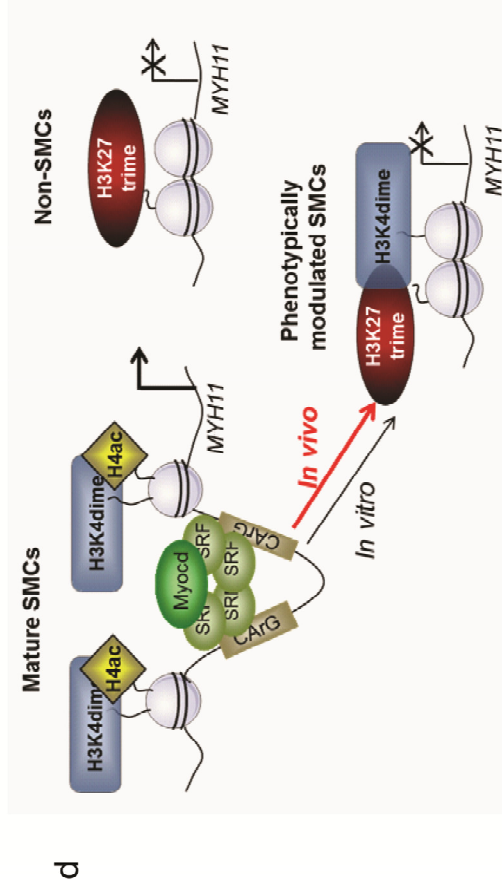
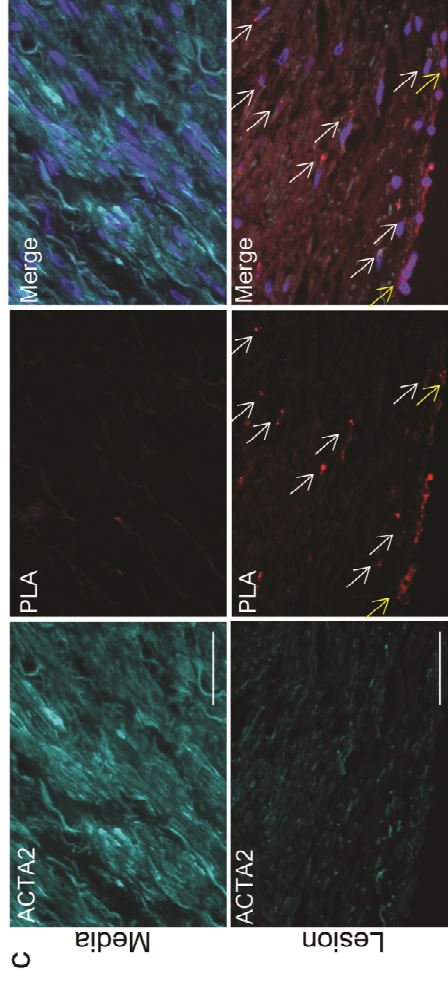
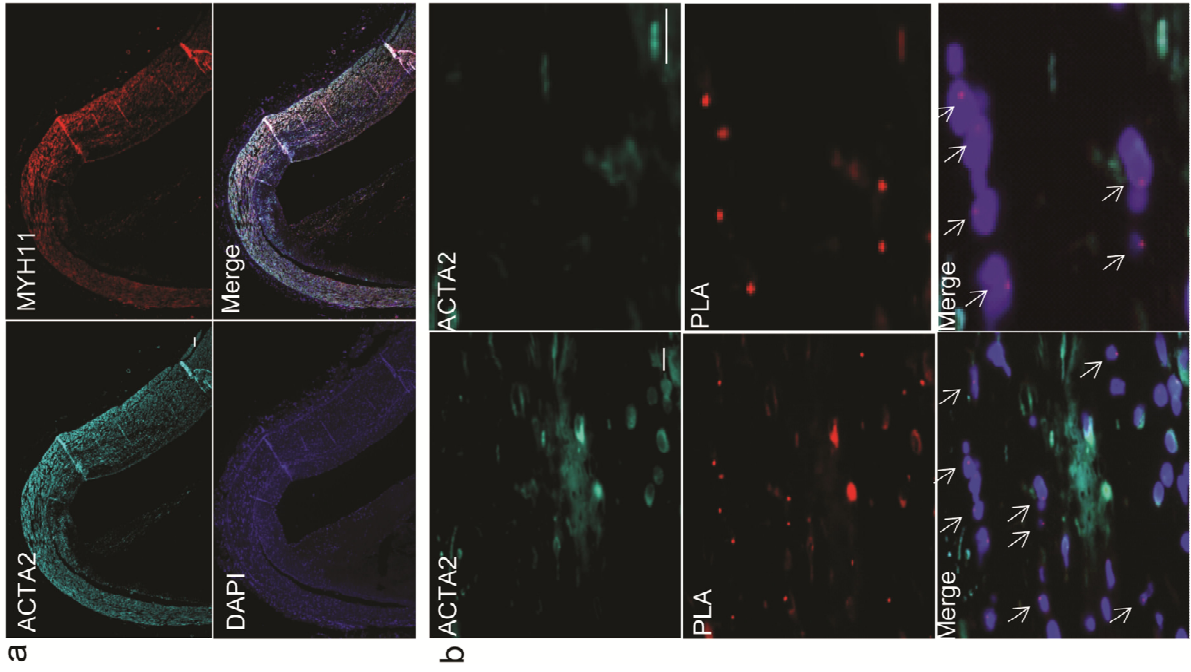
e



d

Figure 7: Identification of epigenetic regulation of phenotypically modulated SMCs within human coronary atherosclerotic lesions by ISH/PLA.

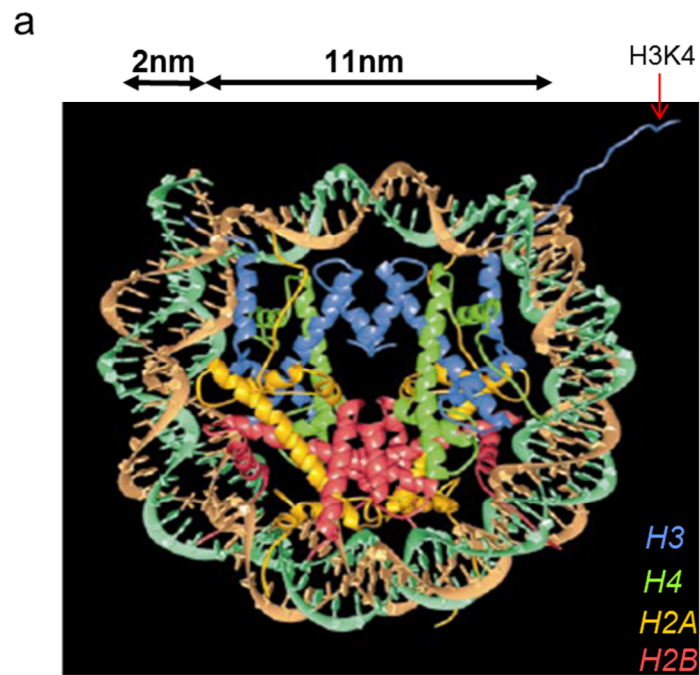
(a) Immunostaining of 5 μm -thick sections of human coronary arteries illustrates loss of SM marker genes expression within the atherosclerotic lesion: ACTA2 (cyan), MYH11 (red) and Dapi (blue). Scale bar = 100 μm . (b) Immunostaining was combined with *MYH11* H3K4dime ISH/PLA with ACTA2 (cyan), PLA (red) and Dapi (blue). A large fraction of ACTA2⁻ lesion cells are positive for *MYH11* H3K4dime PLA (arrows), suggesting that these cells are of SMC origin. Higher magnification on the right panels. Scale bar = 10 μm . (c) *MYH11* H3K27trime ISH-PLA in human coronary atherosclerotic lesions. Medial SMCs are strictly *MYH11* H3K27trime PLA⁻ whereas lesion SMCs (white arrows) and ECs (yellow arrows) are *MYH11* H3K27trime PLA⁺. The lower panels are the higher magnification of the middle panels. Scale bar = 50 μm . (d) Cartoon summarizing the epigenetic regulation on the *MYH11* promoter in mature SMCs, phenotypically modulated SMCs and non-SMCs *in vivo*.



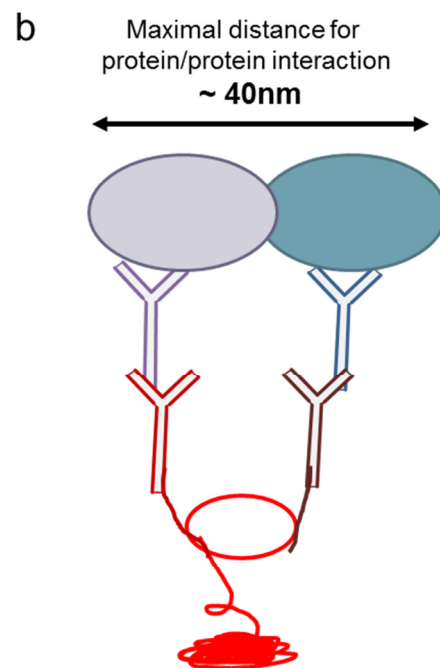
Supplemental Figure 1: Compatibility between PLA and chromatin structure.

(a) Reprinted partially from Luger *et al. Nature* 1997 389:251-260 (reproduced with permission: 3020231289008). The diameter of the nucleosome and the DNA double strand helix is approximately 11 nm and 2 nm, respectively. The distance between two biotinylated ATPs within the DNA strand is estimated to be 2 nm.

(b) Together, these estimates establish the feasibility of PLA for the detection of H3K4dime on the *MYH11* promoter based on the maximal distance of 40 nm between two entities that can be detected by PLA.

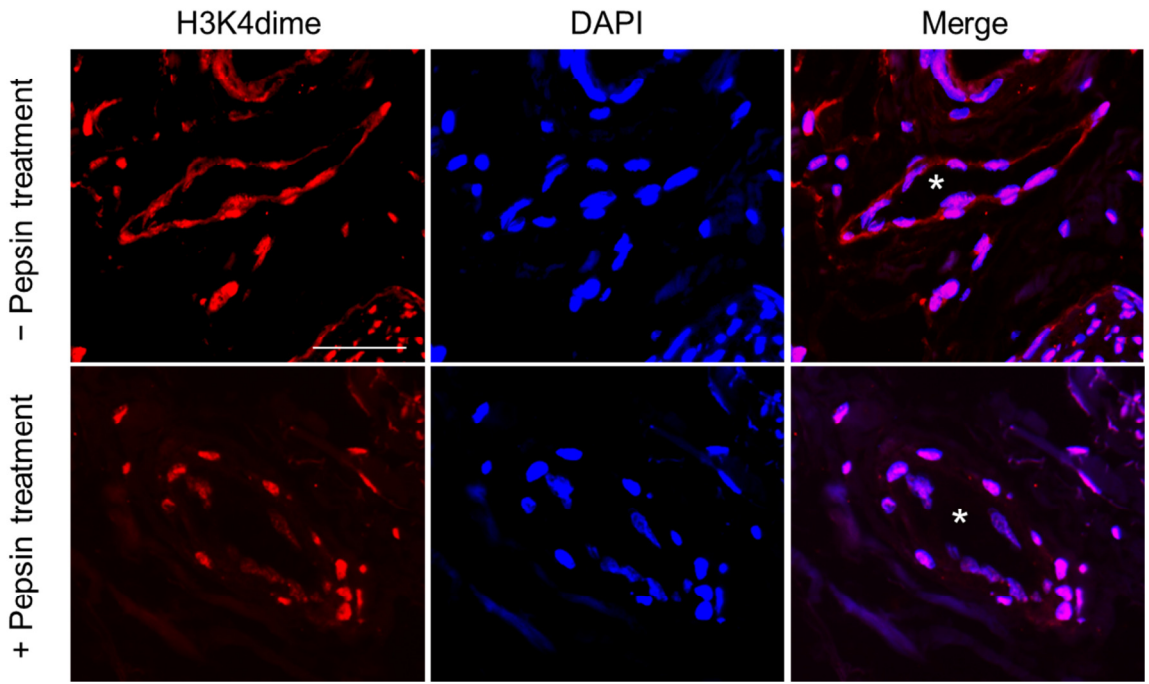


Estimated distance between two biotinylated ATPs within the DNA strand ~2 nm



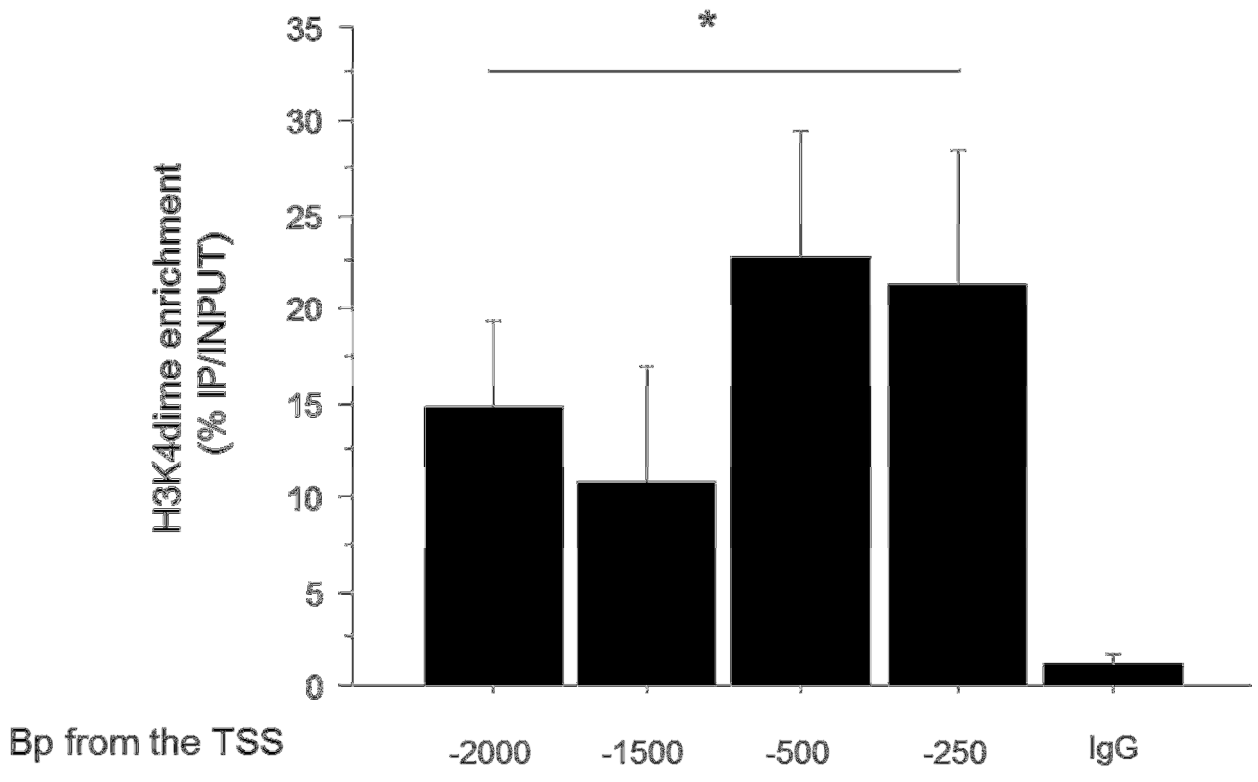
Supplemental Figure 2: Pepsin treatment does not affect H3K4dime staining in tissue sections.

Immunostaining of H3K4dime (red) in the adventitia of formalin-fixed paraffin-embedded (FFPE) human coronary arteries with and without pepsin treatment. The adventitial layer consists of fibroblasts and small vessels containing SMCs and ECs. These vessels were identified with a star corresponding with the lumen of the vessel (*). Nuclear H3K4dime staining is similar in all cell types within the adventitia and remains unchanged after pepsin treatment and ISH procedure. Scale Bar = 50 μ m.



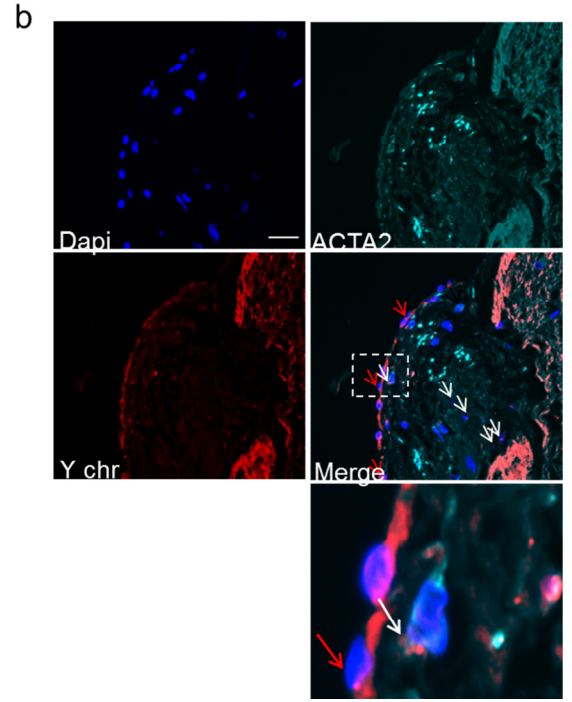
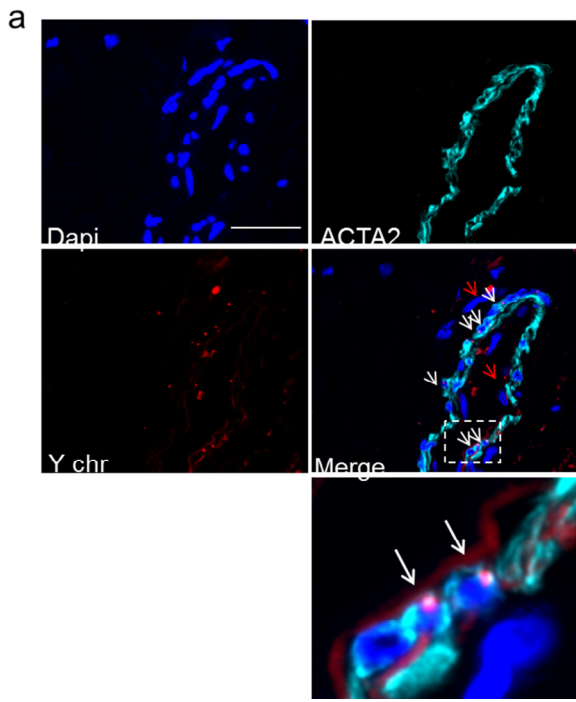
Supplemental Figure 3: Mapping of H3K4dime enrichment on the MYH11 promoter.

Conventional ChIP assay of H3K4dime on the *MYH11* promoter in cultured SMCs. H3K4dime enrichment was assessed along the *MYH11* promoter between the transcription start site (TSS) and –2000 base pairs. A significant enrichment of H3K4dime is quantified on the *MYH11* promoter region chosen for *MYH11* probe design compared with control IgG. Error bars = s.d.; $n = 3$ independent experiments; * $P < 0.005$.



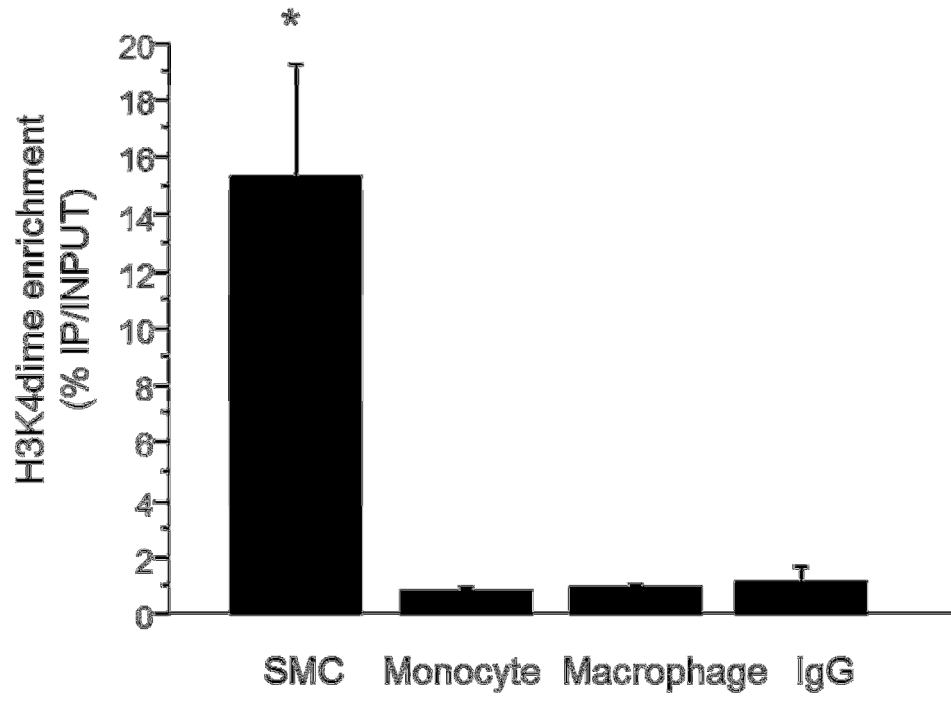
Supplemental Figure 4: Y chromosome FISH in male patient tissue sections.

Fluorescent *In Situ* Hybridization (FISH) in FFPE carotid samples from male patients using a Red-dUTP labeled probe designed for hybridization with human Y chromosome (clone RP11-88F4). Y chromosome probe hybridization was analyzed in small vessels within the adventitia (**a**) and in large carotid arteries (**b**). Red spots corresponding with Y chromosome probe hybridization is visualized in small and large vessels with similar hybridization efficiencies within SMCs (white arrows) and ECs (red arrows) providing validation of the ISH protocol. The efficiency of detection of the Y-chromosome was estimated to be 64%, which is similar to the overall efficiency of our ISH-PLA assays. Scale bar = 50 μm .



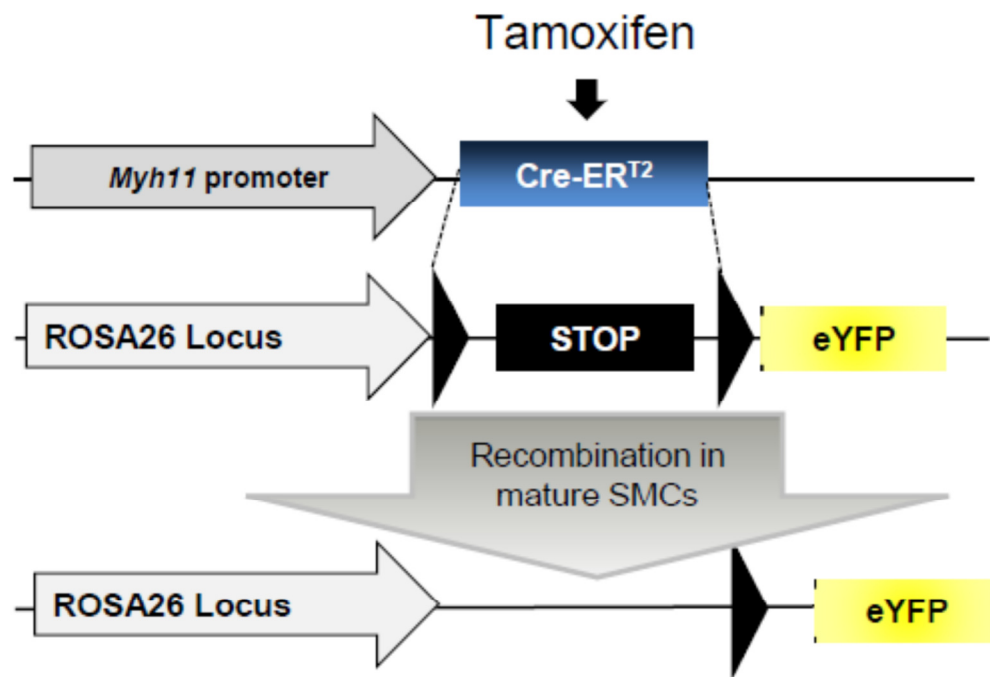
Supplemental Figure 5: Assessment of H3K4dime enrichment at MYH11 promoter in various cultured cell lines.

Conventional ChIP assays were performed in SMC, macrophage and monocyte cell lines. The absence of H3K4dime on *MYH11* in monocyte and macrophage cell lines further extends results showing that *MYH11* H3K4dime is a specific mark of SMC lineage. Data represent means \pm s.d.; $n = 3$ independent experiments; * $P < 0.001$ vs IgG control.



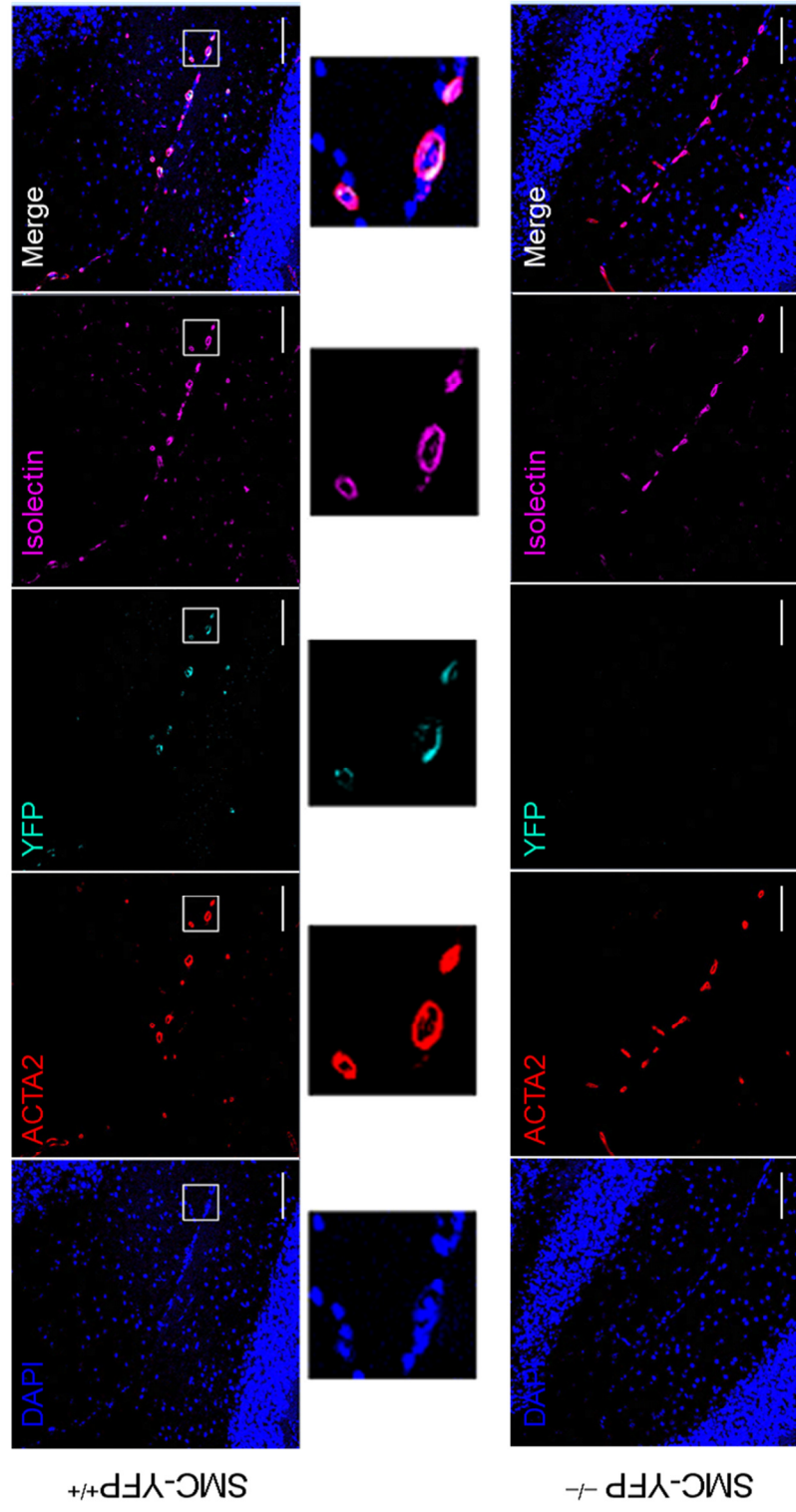
Supplemental Figure 6: Assessment of eYFP expression in Myh11-CreERT2 ROSA26 STOP flox eYFP+/+ and eYFP-/- mice.

(a) SMC lineage tracing was done by crossing *Myh11-CreERT2* transgenic mice with ROSA26 STOP flox eYFP+/+ mice and treating mice with tamoxifen between six and eight weeks of age thereby providing SMC-specific and permanent lineage tagging of SMCs with eYFP.



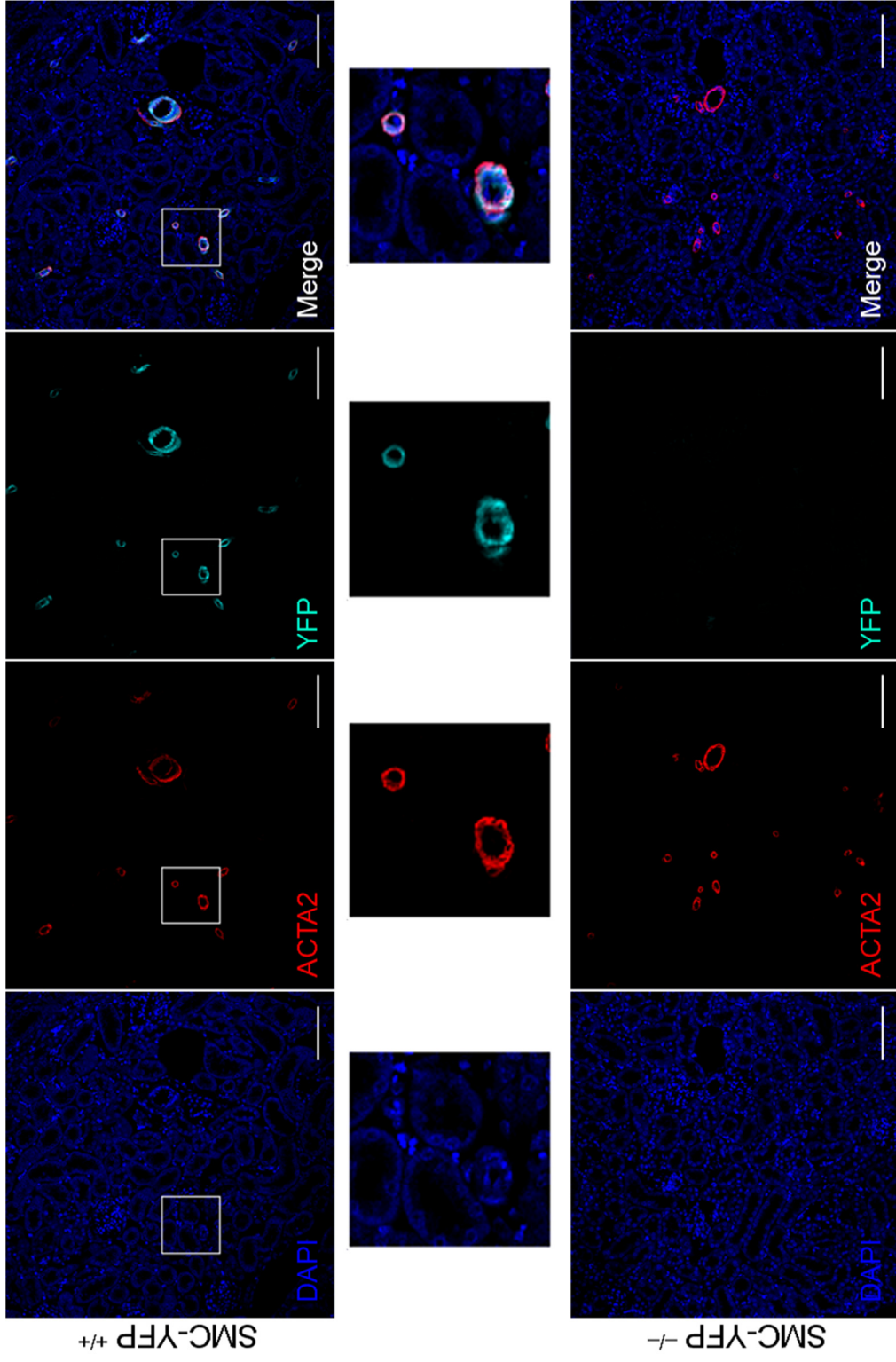
Supplemental Figure 6

Assessment of eYFP expression in *Myh11*-CreERT2 ROSA26 STOP flox eYFP^{+/+} and eYFP^{-/-} mice. (b) Assessment of eYFP expression in cerebellum tissue sections of *Myh11* CreERT2 ROSA26 STOP flox eYFP^{+/+} and eYFP^{-/-} mice by immunostaining for eYFP (cyan), ACTA2 (red), isolectin (purple) and Dapi (blue). eYFP staining was observed in eYFP^{+/+} mice whereas no eYFP staining was detected in eYFP^{-/-} mice. Scale bar = 100 μ m.



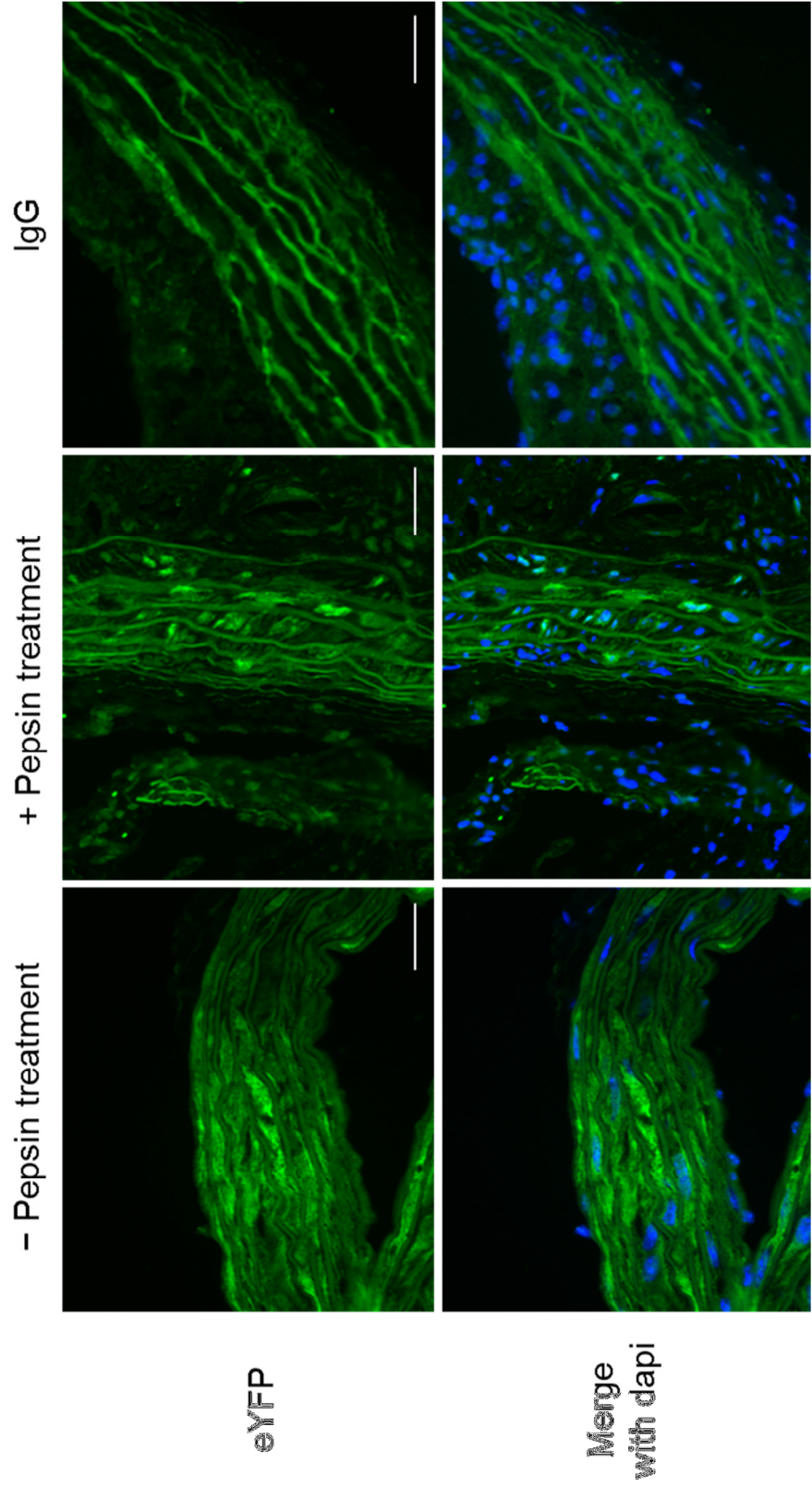
Supplemental Figure 6

Assessment of eYFP expression in *Myh11*-CreERT2 ROSA26 STOP flox eYFP^{+/+} and eYFP^{-/-} mice. (c) Assessment of eYFP expression in kidney tissue sections of *Myh11* CreERT2 ROSA26 STOP flox eYFP^{+/+} and eYFP^{-/-} mice by immunostaining for eYFP (cyan), ACTA2 (red), isolectin (purple) and Dapi (blue). eYFP staining was observed in eYFP^{+/+} mice whereas no eYFP staining was detected in eYFP^{-/-} mice. Scale bar = 100 μ m.



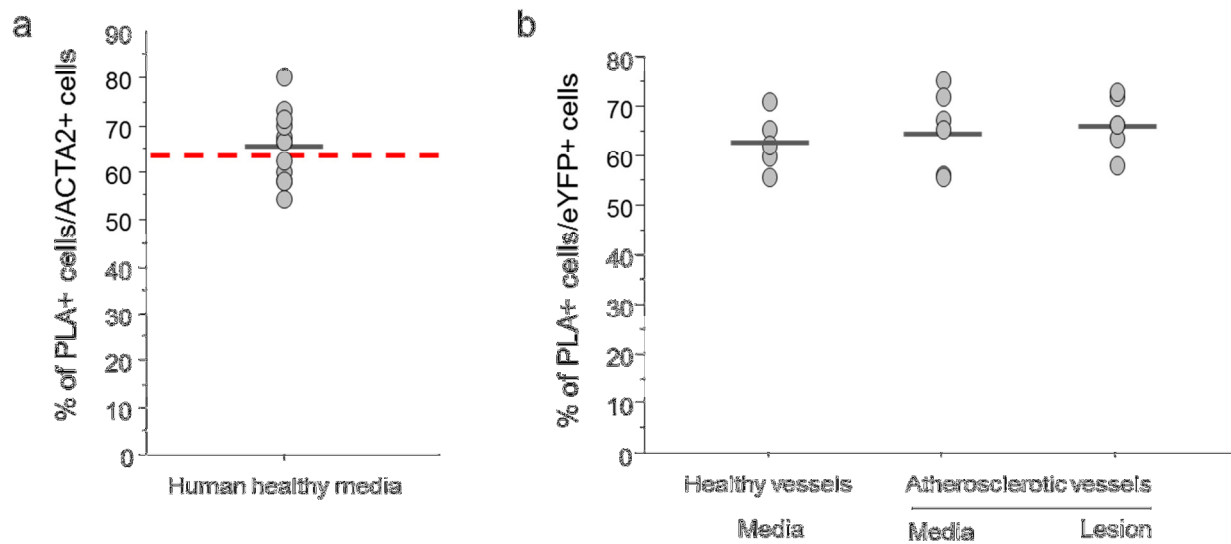
Supplemental Figure 6

Assessment of eYFP expression in *Myh11*-CreERT2 ROSA26 STOP flox eYFP^{+/+} and eYFP^{-/-} mice. (d) The reliability of the eYFP staining (green) with and without pepsin treatment was assessed in aorta tissue sections. eYFP detection was preserved after pepsin treatment. Scale bar = 10 μ m.



Supplemental Figure 7: Quantification of ISH-PLA efficiency.

(a) Percentage of *MYH11* H3K4dime PLA⁺ cells/ACTA2⁺ medial cells detected by ISH-PLA in healthy human vessels. Results indicate that approximately 66% (grey line) of ACTA2⁺ medial cells are detected (PLA⁺) by ISH-PLA. The efficiency of ISH-PLA is compared with the estimated efficiency of the FISH procedure (64%, red line) based on our Y-chromosome FISH analyses on parallel histological sections (data presented in Supplemental Fig. 4). (b) Percentage of *Myh11* H3K4dime PLA⁺ cell/eYFP⁺ cells detected by ISH-PLA in brachiocephalic arteries of SMC-eYFP^{+/+} mice. The ISH-PLA efficiency was 63% in healthy BCA of SMC-eYFP^{+/+} mice, 65% in the media of atherosclerotic BCA, and 67% in the lesion of atherosclerotic BCA of SMC-eYFP^{+/+}-ApoE^{-/-} mice. Mean, s.d and *n* for these quantifications are indicated in Supplemental Fig. 6c).



Supplemental Figure 7

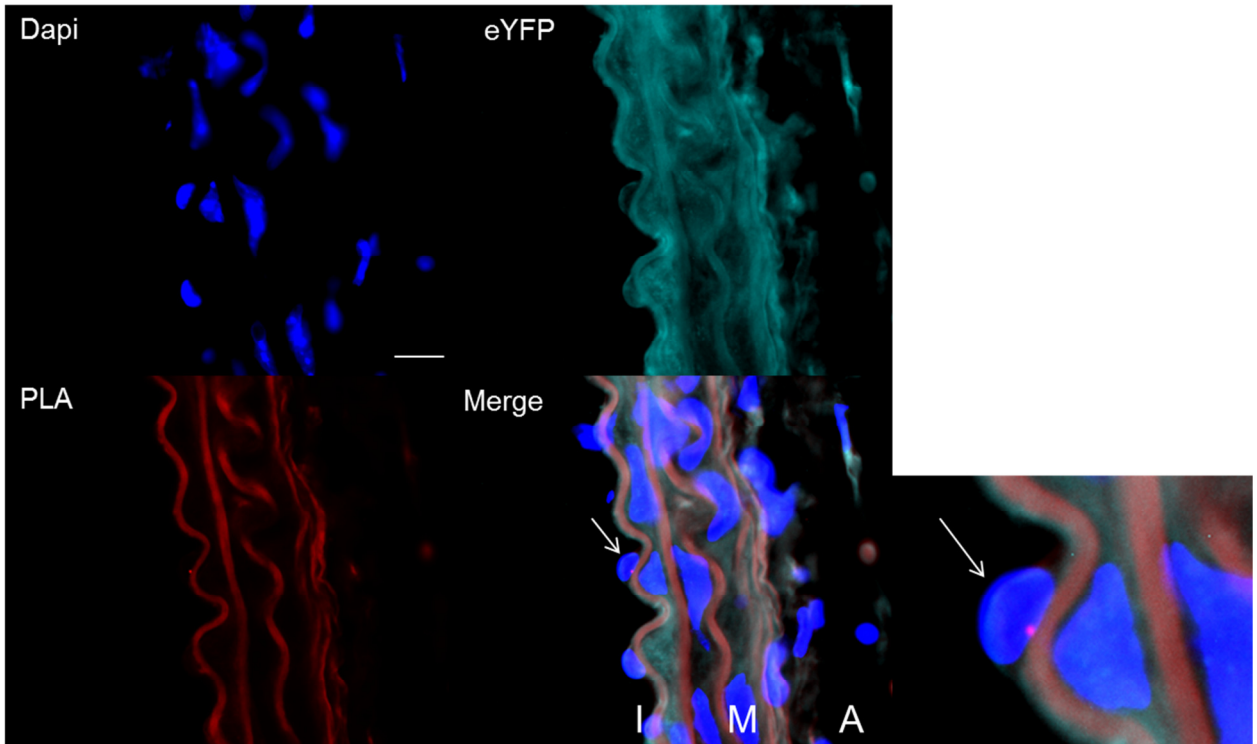
Quantification of ISH-PLA efficiency. (c) Table summarizing quantitative analyses including the number of sections, the means of the percentage of PLA+ cells/ACTA2+ cells for human specimens, or the percentage of PLA+ cells/eYFP+ cells for SMC-eYFP+/+ mouse specimens.

C

Species	Samples	Method	Target gene	Nb of sections	Mean (%)	St Dev
Human	Healthy vessels	ISH/PLA	<i>MYH11</i> (H3K4dime)	15	66	0.7
Human	Healthy vessels	FISH	Y chromosome	5	64	0.8
Mouse	Healthy vessels	ISH/PLA	<i>Myh11</i> (H3K4dime)	7	63	0.6
Mouse	Atherosclerotic vessel: media	ISH/PLA	<i>Myh11</i> (H3K4dime)	6	65	0.8
Mouse	Atherosclerotic vessel: lesion	ISH/PLA	<i>Myh11</i> (H3K4dime)	6	67	0.6

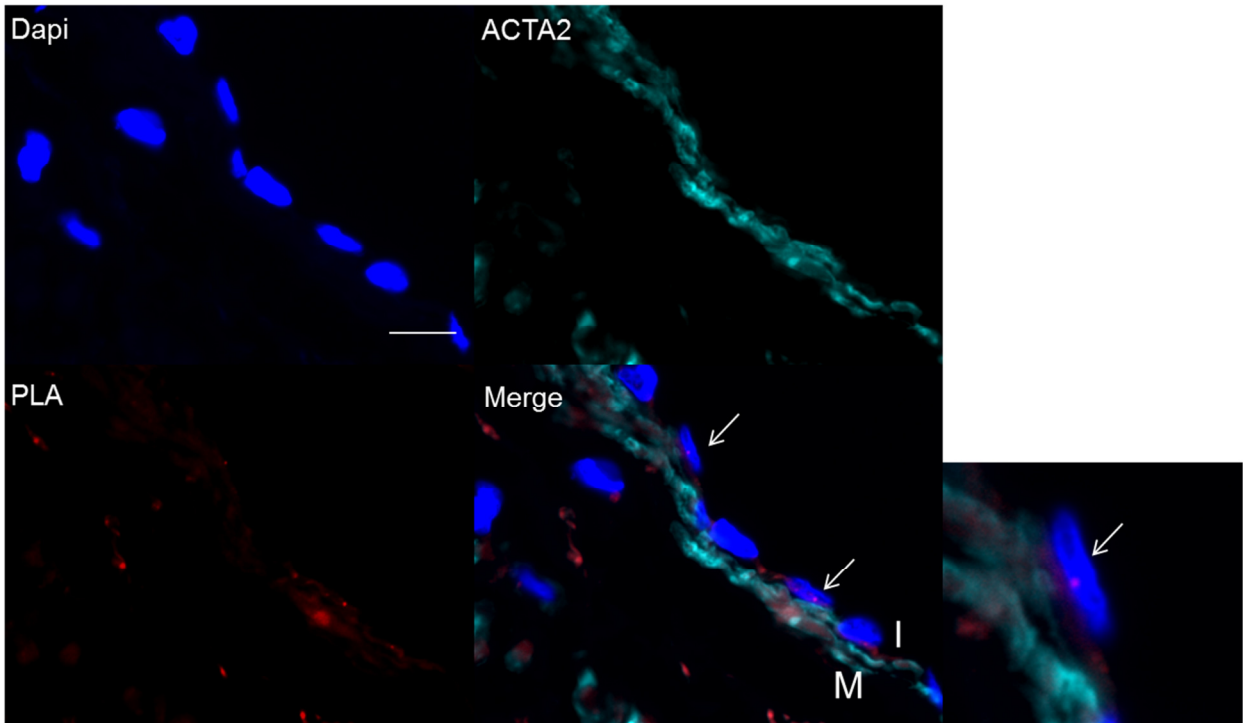
Supplemental Figure 8: CDH5 H3K4dime PLA in human and mouse tissue sections.

(a) Results of *Cdh5* H3H4dime ISH-PLA assays in paraformaldehyde-fixed paraffin embedded histological sections of the brachiocephalic arteries (BCA) from SMC-eYFP^{+/+} mice. PLA⁺ signals (red dots) were exclusively observed in Endothelial Cells (ECs) lining the lumen of the blood vessel intima (I) (arrow). In contrast, no PLA signal was detected in eYFP⁺ SMCs in the media (M) or in fibroblasts of the adventitia (A). Scale bar = 10 μ m.



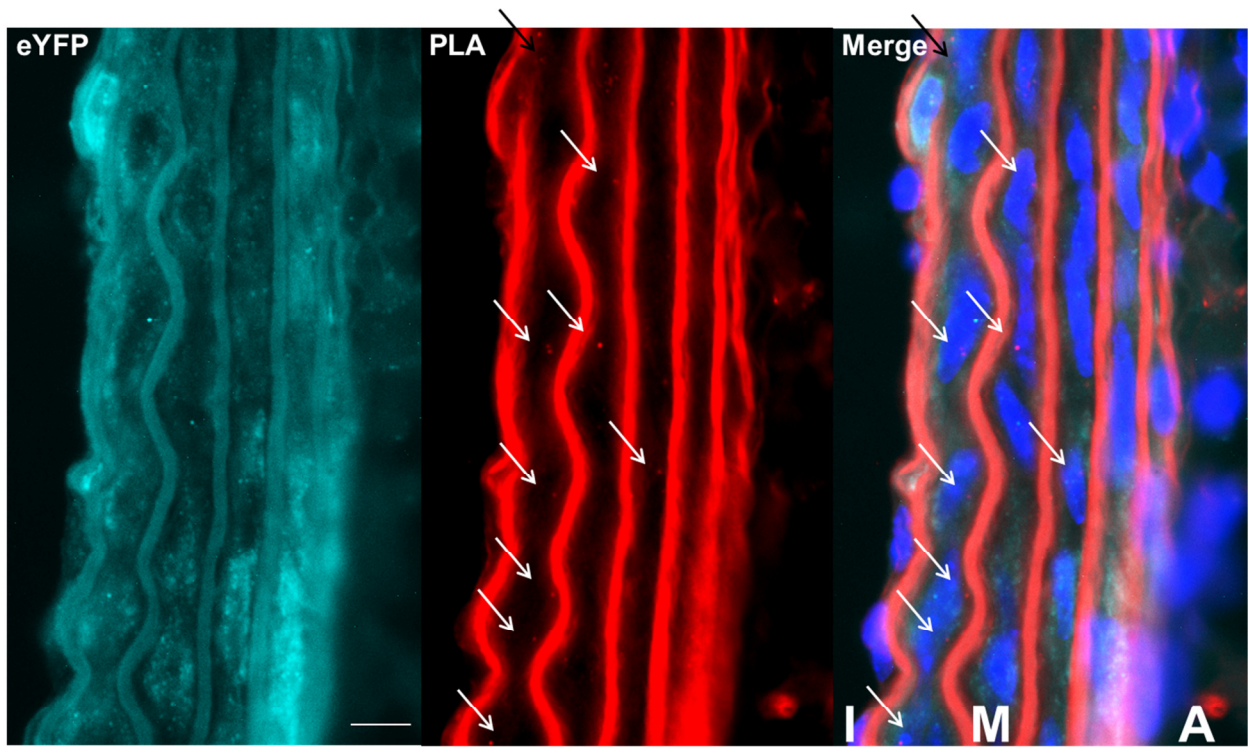
Supplemental Figure 8

***CDH5* H3K4dime PLA in human and mouse tissue sections.** (b) Similar *CDH5* H3K4dime PLA assays were performed in FFPE human carotid arteries. *CDH5* H3K4dime PLA⁺ cells were strictly found within the intimal layer (I) and correspond to ECs (arrows). No medial SMCs (M) were PLA⁺. Scale bar = 10 μm .



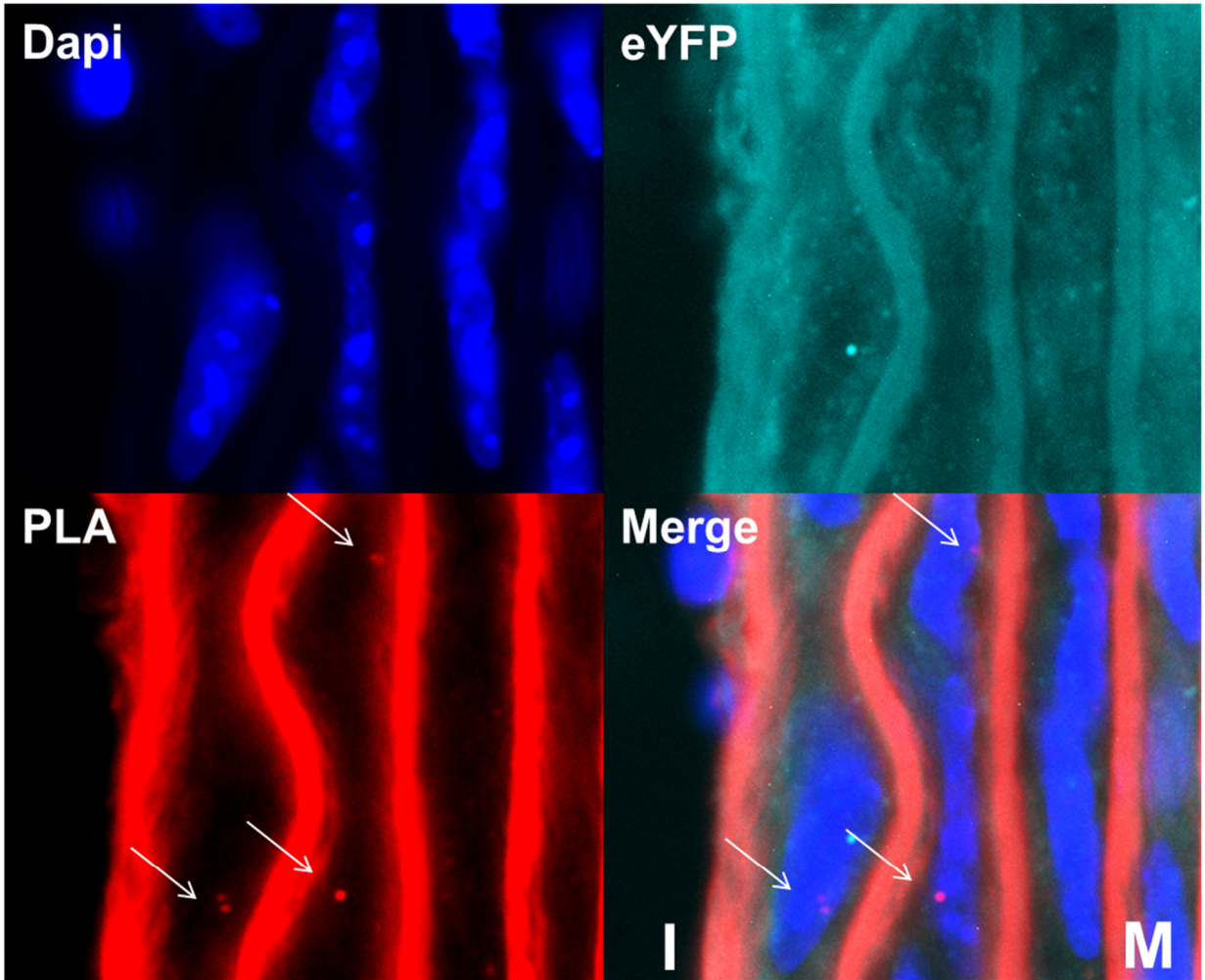
Supplemental Figure 9: Tagln H4ac PLA in mouse tissue sections.

(a) Results of *Tagln* H4ac ISH-PLA assays in BCA sections from SMC-eYFP^{+/+} mice. Results showed that a large fraction of eYFP⁺ medial SMC were *Tagln* H4ac PLA⁺ (media, M) whereas ECs (intima, I) and advential cells (Adventitia, A) were negative. Scale bar = 10 μ m.



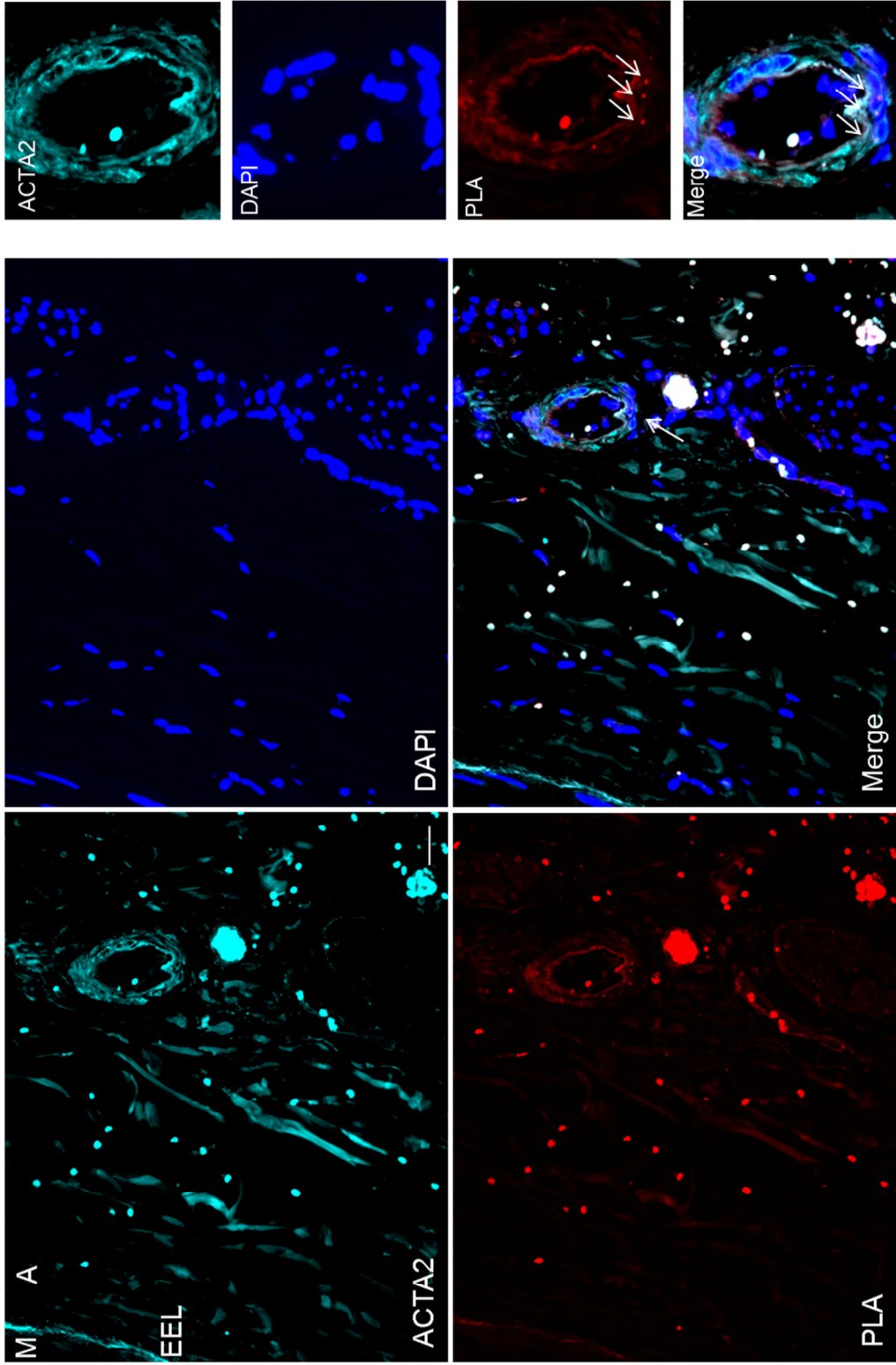
Supplemental Figure 9

***Tagln* H4ac PLA in mouse tissue sections.** (b) Zoom in corresponding to the previous images (**Supplemental Fig. 9a**) focused on *Tagln* H4ac PLA⁺/eYFP⁺ SMCs (Arrows).



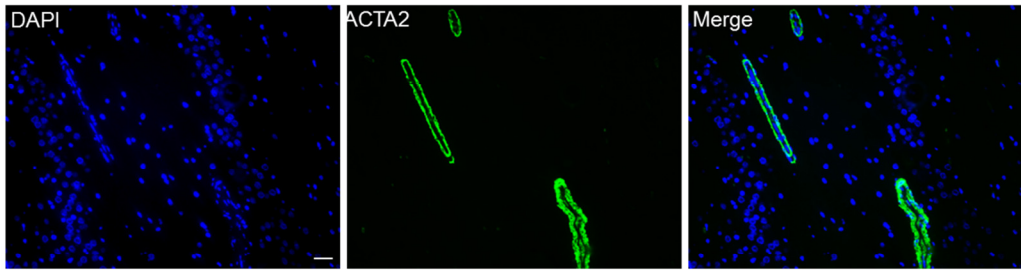
Supplemental Figure 10: MYH11 H3K4dime ISH-PLA assay in FFPE human carotid arteries.

General view of the adventitia showing PLA+ signal only in SMCs associated with small vessels (arrows). Staining for ACTA2 (cyan), PLA (red), Dapi (blue) and merge of images. Scale bar = 50 μ m. Higher magnification of the main image is shown in the right panels centered on an adventitial vessel.

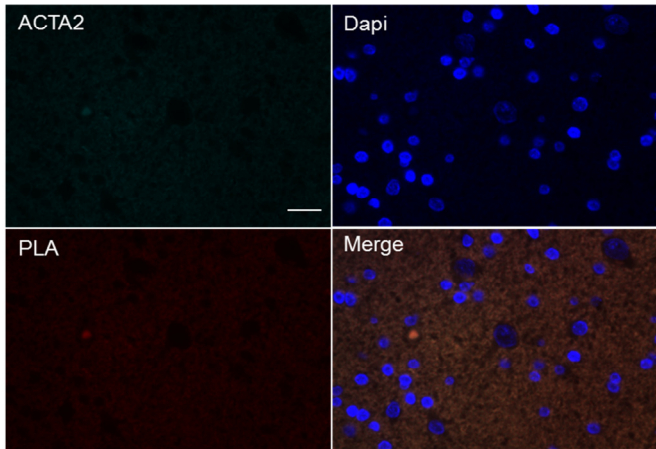


Supplemental Figure 11: MYH11 H3K4dime ISH-PLA assay in FFPE human brain sections.

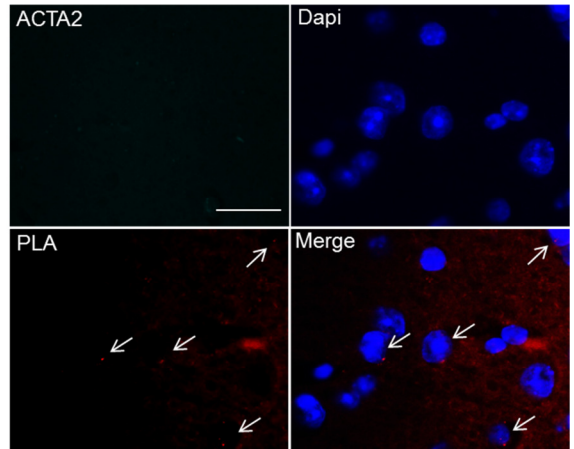
(a) A general view of brain sections showing the presence of vessels including ACTA2+ SMCs. Scale bar = 100 μ m. (b) Non-SMC cells within the brain (ACTA2-) are strictly MYH11 H3K4dime PLA-. (c) In contrast, non-SMCs within the brain are MYH11 H3K27trime PLA+ (arrows), similar to observations in ECs (Fig. 5d). Scale bars for (b) and (c) = 10 μ m.



b

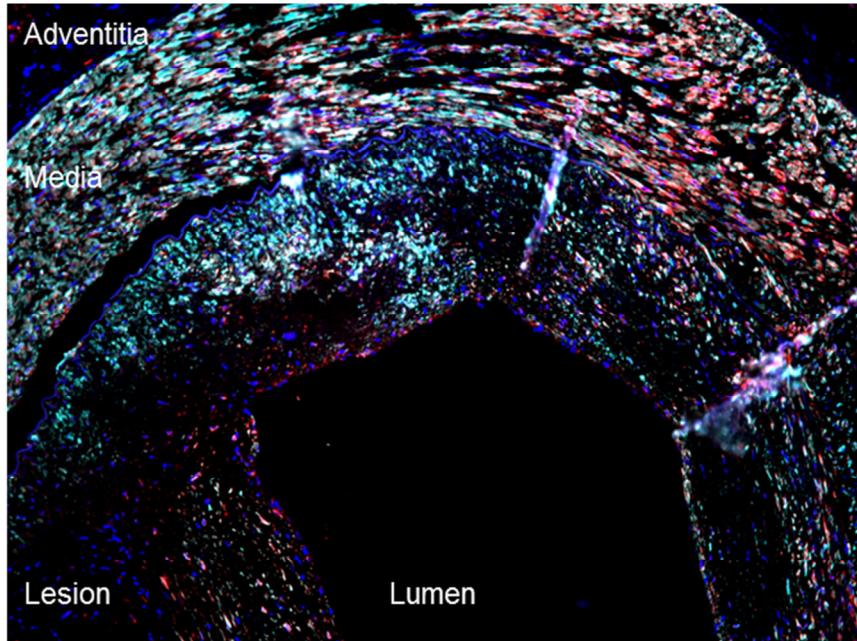
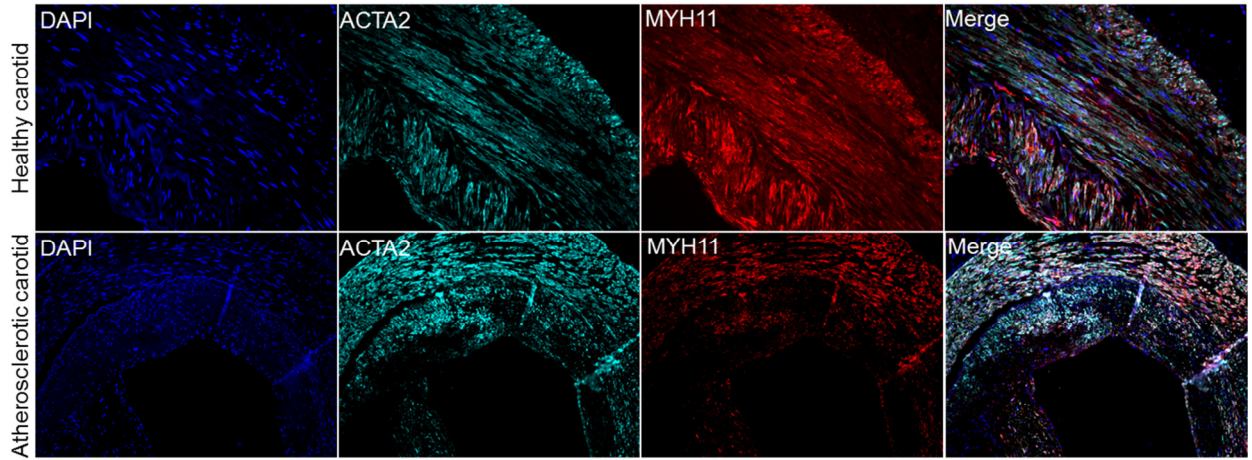


c



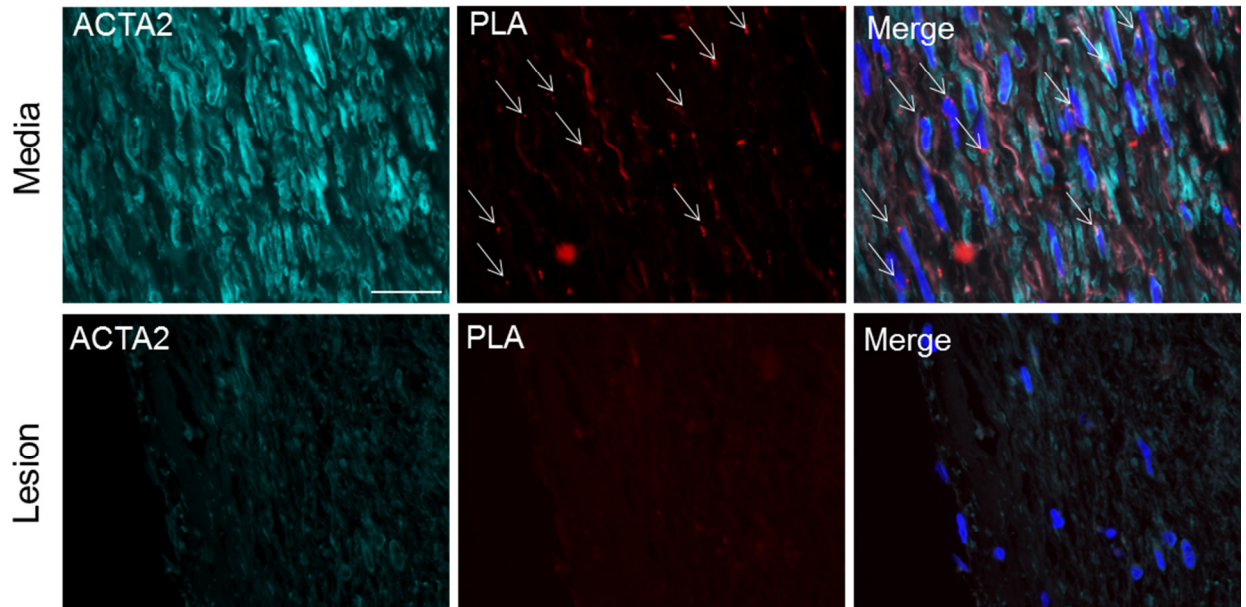
Supplemental Figure 12: Immunofluorescent staining of SMC marker proteins in healthy and atherosclerotic human carotids.

ACTA2 (cyan) and MYH11 (red) are highly expressed in the medial layer. Within atherosclerotic lesions, a significant decrease in ACTA2 and MYH11 expression is observed. Scale bar = 100 μ m.



Supplemental Figure 13: MYH11 H4ac PLA in human atherosclerotic vessel tissue sections.

MYH11 H4ac PLA (red) combined with ACTA2 (cyan) staining within the atherosclerotic coronary artery shows that medial SMCs (ACTA2+) are *MYH11* H4ac PLA+ (arrows) whereas no *MYH11* H4ac PLA+ cells are found within the lesion. Scale bar = 50 μ m.



Supplemental Table 1: Primer table

Human <i>MYH11</i> promoter	For	F1-GAGATGGCAAGTTGGGAAAA
	Rev	R1-GCTGTGGTGGATCTGACTT
	For	F2-CTCGACCCCCTTTCTCTAG
	Rev	R2-GCTGTGGTGGATCTGACTT
	For	F3-AGAGCCTGGGGAAGAGAGA
	Rev	R3- CTCGCCTAAAATTGCATTCC
Mouse <i>Myh11</i> promoter	For	F1 AGTTTGAGGCCAACGAGCTA
	Rev	R1-GCTGTGGTGGATCTGACTT
	For	F2- CCCTCCCTTTGCTAAACACA
	Rev	R2- CCAGATCCTGGGTCCTTACA
	For	F3- TAGGGTCTTAGCACGCATCC
	Rev	R3-GTCACCGCATATCCTCCAGT
	For	F4-TTCCCTCTTCCATTCTCCT
	Rev	R4-CACTGGGCAGCAATACACAG
Mouse <i>Myh11</i> cDNA	For	TGGACACCATGTCAGGGAAA
	Rev	ATGGACACAAGTGCTAAGCAGTCT
Mouse <i>Cdh5</i> promoter	For	TCCTTCTCCAGCTTGCATCT
	Rev	GAGCACAGTTGATTGCCTCA
Human <i>CDH5</i> promoter	For	TCTGAGACCCAGCAGGAAG
	Rev	GGGATGTTTCTGTTCCGTTG
Mouse <i>Tagln</i> promoter	For	AGCACCTGACTACCCACCAC
	Rev	TTTGGGCCTAACACATAGCC

Chapter 3: Transition of smooth muscle cells to a macrophage-like state within advanced atherosclerotic lesions plays a key role in regulating indices of plaque stability and is regulated by Krüppel-like factor 4

Authors: Laura S. Shankman, Delphine Gomez, Morgan Salmon, Olga A. Cherepanova, Elizabeth Greene, and Gary Owens

Adapted from manuscript submission to *Nature Medicine*

Abstract

Cardiovascular disease is the leading cause of death in developed countries and there is compelling evidence that the majority of these fatalities are secondary to rupture of unstable atherosclerotic plaques. However, the mechanisms that control plaque stability are poorly understood, although it is widely believed that plaques having a decreased ratio of cells positive for smooth muscle cell (SMCs) markers such as ACTA2 relative to macrophage markers are more likely to rupture with consequent clinical sequelae. Herein we show that traditional methods for staining and detecting SMCs are unable to detect $\geq 80\%$ of SMC-derived cells within advanced atherosclerotic lesions of *ApoE*^{-/-} mice following 18 weeks of Western diet feeding and that nearly a quarter of macrophages identified by markers such as LGALS3 are of SMC origin. Moreover, using a novel single cell epigenetic assay developed by our lab, we provide evidence that significant numbers of SMC-derived cells within advanced human coronary artery atherosclerotic lesions also express the macrophage marker CD68. We further demonstrate that SMC specific conditional knockout (KO) of pluripotency factor, Krüppel-like factor 4 (KLF4), greatly reduced the number of SMCs expressing macrophage markers and improved multiple indices of plaque stability as well as reducing plaque size. Finally, we show that global heterozygous conditional KO of KLF4 in mice resulted in changes very similar to those seen with SMC specific KLF4 KO, indicating that KLF4-dependent

phenotypic switching of SMC can play a dominant role in determining overall plaque size and composition.

Introduction

Atherosclerosis is a disease of chronic inflammation and is the leading cause of morbidity and mortality worldwide. Research in the last two decades has revealed a causal link between thrombotic events caused by unstable plaques and the majority of coronary syndromes^{69, 138, 139}. Plaque instability has been associated with disruption of the fibrous cap, an atheroprotective layer of smooth muscle α -actin (ACTA2) positive cells that cover the atherosclerotic plaque^{55, 69, 70, 140, 141}, and the presence of a large foam cell laden necrotic core within the plaque^{69, 70, 139, 142}. The distribution, content, and ratio of these two major cell types, the smooth muscle cells (SMCs) and the macrophages, has long been considered one of the strongest components for determining plaque stability and the probability of plaque rupture leading to coronary events.

Despite the overwhelming research demonstrating that ACTA2 (traditional marker for SMCs) positive cells are beneficial for plaque stability and LGALS3 (Mac2) or CD68 (commonly used markers for macrophages) positive cells are detrimental, there are major ambiguities regarding the accurate contribution of each cell type to lesion progression^{1, 55} including: 1) SMCs and macrophages are capable of down-regulating lineage specific marker genes typically used to identify each respective cell type^{8-10, 100-107}; 2) results of studies in cultured cells have shown that both cell types are capable of expressing “definitive” markers of the other cell type under conditions likely to exist within atherosclerotic lesions [reviewed in Gomez and Owens³⁰]; and 3) there is a lack of rigorous cell lineage

tracing studies to unambiguously identify cells of SMC origin within the lesion. For example, studies by Andreeva et al.⁵² showed the presence of cells within advanced human coronary atherosclerotic lesions that co-stained with SMC marker ACTA2 and macrophage marker CD68, raising uncertainties if these cells are derived from SMC, monocyte-macrophages, both, or neither. Similarly, Caplice et al.²⁴ provided evidence based on Y-chromosome FISH analysis of atherosclerotic lesions from patients who had undergone a cross gender bone marrow transplantation (BMT) suggesting that approximately 10% of ACTA2+ cells in human coronary artery lesions were of myeloid and not SMC origin. Results of bone marrow lineage tracing studies in mouse models of experimental atherosclerosis are also controversial with Bentzon et al.²² claiming that myeloid cells do not give rise to SMC-like cells within lesions, whereas Nagai et al.^{16, 23} concluded that bone-marrow derived cells can express several markers of SMCs including ACTA2 and TAGLN, but not MYH11. Similar bone marrow lineage tracing studies were conducted by Nemenoff et al.²⁰ also noted that hematopoietic derived cells could express ACTA2 in a femoral wire-injury mouse model, but did not see bone marrow derived cells express MYH11. Further confounding the issue are results of *in vitro* studies showing that treatment of cultured macrophages with TGF β or thrombin results in activation of various SMC markers including ACTA2^{25, 143}, whereas cholesterol loading of cultured SMC is associated with marked suppression of SMC marker genes and activation of multiple macrophage markers⁴¹.

Our lab previously demonstrated that mutation of a G/C rich region within the *Tagln* promoter, which is targeted during SMC marker gene down-regulation, resulted in persistent expression of a *Tagln* promoter-driven lacZ transgene (*Tagln* G/C-mut lacZ) within cells negative for ACTA2 and TAGLN within advanced atherosclerotic lesions of Western diet fed *Apoe*^{-/-} mice¹⁴. In contrast, *Apoe*^{-/-} mice containing the wild-type *Tagln* promoter lacZ transgene showed virtually no lacZ⁺ cells within advanced lesions or the media underlying these lesions. These findings suggest that there is a population of phenotypically modulated SMCs within atherosclerotic plaques that were previously unidentifiable based on immunostaining for SMC markers used in virtually all previous studies in the field. However, there are several limitations of these studies that prevent rigorous SMC lineage tracing. First, TAGLN is not SMC specific and recent evidence has shown that it can be activated by hematopoietic cells¹⁶. Second, the *Tagln* G/C-mut lacZ mouse is not conditionally regulated therefore we cannot rule out that SMC might down-regulate the *Tagln* G/C-mut lacZ transgene in response to environmental cues that exist within some lesions such that we would underestimate the contribution of SMC to lesion cells. This may also lead to non-SMCs activating the gene and being falsely identified as a SMC. Third, the X-GAL staining system used in these studies could not be used for confocal z-stack microscopy to rigorously assess if markers were present within a single cell or to determine if the de-differentiated SMC-derived population might be activating markers of other cell types.

To overcome these limitations we utilized a highly stringent tamoxifen-inducible SMC conditional lineage tracing *Myh11-CreER^{T2}* ROSA floxed STOP eYFP *Apoe^{-/-}* mice recently developed by our lab¹⁴⁴ to identify SMC-derived cells within advanced atherosclerotic lesions of *Apoe^{-/-}* mice fed a high fat Western diet, and to define phenotypic transitions of these cells. Using these mice, we generated data that challenge many of our fundamental assumptions regarding the origins of cells within atherosclerotic lesions, and show that the embryonic stem cell (ESC) and induced pluripotency stem (iPS) cell factor Krüppel-like factor 4 (KLF4) regulates phenotypic transitions of SMC within atherosclerotic lesions and knockout of this gene within SMC is associated with marked reductions in lesion size and multiple changes consistent with plaque stabilization.

Materials and Methods

Mice

Myh11-CreER^{T2} mice were generously provided by S. Offermanns (Max Planck Institute)²¹; *ROSA26 STOP-flox eYFP^{+/+}* and *Apoe^{-/-}* mice were obtained from Jackson Laboratories. *Klf4^{fl/fl}*¹⁴⁵ were provided by Dr. Kaestner, and transgenic tamoxifen-inducible Cre recombinase mice (ERT-Cre¹⁴⁶) were provided by Dr. Anton Berns from The Netherlands Cancer Institute, Amsterdam, Netherlands. *Myh11-CreER^{T2}*, *ROSA26 STOP-flox eYFP*, *Klf4 fl/fl*, and ERT-Cre mice were genotyped by PCR as previously described^{21, 144-146}. Cre recombinase was activated in male mice with a series of ten 1-mg tamoxifen intraperitoneal injections (Sigma T-5648) from 6 to 8 weeks of age for a total of 10 mg of tamoxifen per 25 g mouse for both the *Myh11-CreER^{T2}* and ERT-Cre mouse models. Next, mice were fed a high-fat diet containing 21% milk fat and 0.15% cholesterol (Harlan Teklad) for 18 weeks starting at the end of tamoxifen treatment. Mice were euthanized by CO₂ asphyxiation and then perfused via the left ventricle as follows: 5 mL PBS, 10 mL 4% paraformaldehyde, 5mL PBS. Brachiocephalic arteries were carefully dissected and fixed for an additional hour in 4% paraformaldehyde before they were embedded in paraffin. Assays for determining total plasma cholesterol and triglyceride levels (Abbott Laboratories) were performed by the University of Virginia Clinical Pathology Laboratory.

Analysis of Atherosclerotic Plaques

Paraffin-embedded brachiocephalic arteries (BCAs) were serially sectioned at 10 μm thickness from the aortic arch to the right subclavian artery. For immunofluorescent analysis of LGALS3+ SMCs within the, BCA three sections were taken 300 μm apart, spanning the length of the BCA. Slides were stained with antibodies to GFP (Abcam ab6673), ACTA2 (Sigma F3777), LGALS3 (Cedarlane CL8942AP), MKI67 (Abcam ab15580), CASP3 (Cell Signaling 9661S), KLF4 (R&D Systems AF3158), and MYH11 (Kamiya Biomedical Company MC-352). Using a Zeiss LSM700 confocal microscope a series of 8 z-stack images of 1 μm thickness were acquired for further analysis. Five 14283 μm^2 locations within each z-stack of every BCA were analyzed using Zen 2009 Light Edition Software for the presence of immunofluorescent staining coinciding with a single DAPI+ nucleus to determine the average cell populations within each lesion. Every plane of the z-stack was used to assess the co-localization of cellular markers within a single cell. The region of the lesion within 30 μm of the luminal boundary, as determined using Zen 2009 Light Edition Software, was analyzed to determine the cellular composition of the lesion cap, the area within this region was compared to the entire area of the atherosclerotic lesion to determine cap area/lesion area. Cap coverage analyses and morphometric analyses of lesion size were completed using ImagePro Plus as described in Alexander et al¹⁴⁷.

Flow Cytometry

SMC YFP^{+/+} *ApoE*^{-/-} mice were euthanized by CO₂ asphyxiation after 18 weeks of Western diet treatment. Mice were then perfused with 10mL of PBS and the aorta from the iliac bifurcation to the aortic root was gently cleaned of fat and fascia before removal from the animal. Once cleaned, the tissue was placed into an enzyme cocktail containing 4U/mL Liberase TM (Roche 05401119001), 0.1mg/mL DNaseI, and 60U/mL Hyaluronidase in RPMI-1640. Once immersed in the digestion cocktail, the tissue was cut longitudinally, minced, and placed in a 37°C incubator for 1.5 hours. After a two minute red blood cell lysis (BD PharmLyse 555899), macrophage marker expressing SMCs were identified using antibodies to F4/80 (eBioscience 17-4801), PTPRC (eBioscience 47-0451), ITGAM (eBioscience 45-0112), DAPI (Invitrogen), LGALS3 (BioLegend 125405), and ITGAX (eBioscience 25-0114). All samples were run on a Beckman Coulter CyAn ADP LX flow cytometer equipped with 405nm, 488nm, and 633nm lasers.

Human Samples

De-identified human coronary arteries specimens from patients (n = 5) collected during Coronary artery bypass graft (CABG) surgery as well as during autopsy were kindly provided by Nicole McGinn from the Department of Pathology, University of Virginia Hospital. These specimens were processed, fixed in paraformaldehyde and paraffin-embedded blocks were cut into 5µm sections. The coronary artery specimens from male patients who received heart transplant from a female donor was kindly provided by Dr. Joseph Maleszewski

(Mayo Clinic, Rochester, Department of laboratory medicine and pathology). The institutional review board at University of Virginia approved the use of all autopsy specimens.

ISH-PLA

Human *MYH11*, mouse *Myh11*, and mouse *Tagln* probes were generated by Nick Translation (Roche) using biotin-14-dATP (Invitrogen). Labeled-DNA probes (40 ng/slide) underwent denaturation in Hybridization Buffer (2x SSC, 50% high grade formamide, 10% dextran sulfate, 1 µg of human or mouse Cot-1 DNA) for 5 min at 80 °C. After immunostaining, slides were dehydrated in ethanol series and incubated in 1mM EDTA (pH 8.0) for 20 min. Then, samples were incubated with pepsin (0.5%) in buffer (0.05M Tris, 2mM CaCl₂, 0.01M EDTA, 0.01M NaCl) at 37 °C for 20 min, as previously described²⁴. Hybridization mixture containing biotinylated probes or 5-TAMRA-dUTP labeled Y chromosome probe (Clone RP11-88F4, Empire Genomics) was applied on sections. Sections were incubated at 80 °C for 5 min, followed by 16-24h incubation at 37 °C. Hybridization was followed by multiple washes in 2x SSC, 0.1% NP-40 buffer.

PLA was performed directly after ISH following manufacturer's instructions (Olink). After blocking, sections were incubated with mouse H3K4dime (5 µg/mL, clone CMA303 Millipore) and rabbit Biotin (5 µg/mL, # ab53494, Abcam) antibodies overnight at 4 °C, followed by incubation with secondary antibodies conjugated with PLA probe at 37 °C for 1hr as recommended by manufacturers.

Then, ligation and amplification were performed (Duolink detection kit Orange, 555nm). Finally, mounting medium with DAPI was used to coverslip the slides. Images were acquired with an Olympus BX41 fitted with a Q imaging Retiga 2000R camera. Image acquisition was performed using Q Capture Pro software (Media Cybernetics & QImaging Inc). Settings were fixed at the beginning of both acquisition and analysis steps and were unchanged. Brightness and contrast were equally adjusted after merging. Image analysis was performed with ImageJ.

ChIP Assays

ChIP was performed on cultured cells as previously described¹⁴⁸. Cells were fixed with 1% paraformaldehyde for 10 min at room temperature. The cross-linked chromatin was sonicated to shear chromatin into fragments of 200–600 base pairs. The sheared chromatin was immunoprecipitated with 2 µg of dimeH3K4 antibody (clone CMA303, Millipore), while negative control was incubated with mouse IgG and input DNA without antibody, and immune complexes were recovered with magnetic beads (Millipore). *In vivo* KLF4 ChIP assays were performed using flash frozen BCAs from mice that had been fed either 18 weeks of high-fat or standard chow (Harlan 7012) beginning at 8 weeks of age as previously described^{86, 87}.

Cell Culture Studies

Primary mouse aortic SMCs were isolated from 8 week old SMC-lineage tracing mice after a series of 10 tamoxifen injections using a previously described protocol¹⁴⁹. Cells isolated from SMC YFP^{+/+} *Klf4*^{wt/wt} and SMC YFP^{+/+} *Klf4*^{Δ/Δ} mice were passaged three times before undergoing a cell selective sort for eYFP+. Cholesterol assays were performed using water-soluble cholesterol from Sigma (C4951-30MG) as previously published⁴¹ with minor modification: Cholesterol was reconstituted in DMEM-F12 media from Gibco containing; 0.2% FBS (Gibco); 100 U/mL penicillin/streptomycin (Gibco); 1.6 mmol/l L-glutamine, (Gibco). Cells were allowed to grow to ~70% confluency before being switched to 0, 20, 40, or 80 μg/mL cholesterol containing media. After 72hrs cells were harvested for mRNA, protein, or ChIP analysis.

Statistics

Fisher's exact test was used for categorical data. Two-way ANOVA with Tukey post-hoc tests were used for multiple group comparisons determined to have normal distribution by the Kolmogorov-Smirnov test. Two analyses showed statistical difference across multiple locations, ACTA2/DAPI, and eYFP/DAPI, using 2-way ANOVA. All other analyses across multiple locations were therefore not reported in the manuscript. Non-parametric data were analyzed using the Wilcoxon rank sum test. There were no significant interactions between genotype and location for any of the end points analyzed by the 2-way ANOVA. $p < 0.05$

was considered significant. SAS v9.3 with Enterprise Guide v5.1 software (SAS Institute Inc.) was used for all statistical analyses.

Study approval

Animal protocols used in this study were approved by the Animal Care and Use Committee at the University of Virginia.

Results

The majority of smooth muscle cells within atherosclerotic plaques were not identifiable by ACTA2 staining

SMCs are distinguished from other cell types by expression of a unique repertoire of genes including ACTA2, TAGLN, and MYH11, which are coordinately down-regulated, at least *in vitro*, during SMC phenotypic switching such that they may be undetectable using traditional immunohistochemical staining methods^{30, 120}. In order to further define the contribution of phenotypically modulated SMC within advanced atherosclerotic lesions, we utilized a SMC specific lineage tracing mouse model, *Myh11-CreER^{T2} ROSA floxed STOP eYFP Apoe^{-/-}* (SMC YFP^{+/+} *Apoe^{-/-}*), recently developed by our lab^{21, 144} which label >95% of medial SMCs following a series of tamoxifen injections between 6-8 weeks of age (Supplemental Fig. 27, Fig. 2a of Gomez et al.¹⁴⁴) and prior to initiation of Western diet feeding. To further ensure the fidelity and SMC specificity of this lineage tracing model we completed a number of further validation studies beyond those shown in previous reports^{20, 21, 144}. Results showed the following: 1) no detectable expression of the YFP indicator gene in the absence of tamoxifen injection or in SMC YFP^{+/+} *Apoe^{-/-}* mice (Supplemental Fig. 27a, Supplemental Fig. 15a); 2) SMC specific YFP labeling within brachiocephalic arteries (BCAs) and vasculature/airways of the lungs (Supplemental Fig. 27b); 3) no detectable YFP⁺ cells within blood or bone marrow preparations based on flow cytometry (Supplemental Fig. 15a); 4) no

evidence of YFP⁺ cells within lesions of SMC YFP^{+/+} *ApoE*^{-/-} mice that were not given tamoxifen following 18 weeks of Western diet feeding (Supplemental Fig. 16a); 5) no detectable YFP⁺ cells in the blood of SMC YFP^{+/+} *ApoE*^{-/-} mice given a high fat diet for 18 weeks (Supplemental Fig. 16b); and 6) YFP⁺ labeling of approximately 60% of freshly enzymatically dissociated cells from the ascending, descending thoracic aorta plus the abdominal aorta to the iliac bifurcation based on flow cytometry (Supplemental Fig. 15b). The latter analyses include contributions of numerous non-SMC including ECs, adventitial cells, and blood cells resident within the tissue and are an important control for interpreting results of flow cytometric analyses. Since cre excision is permanent, this SMC lineage tracing model system provides **permanently lineage tagging of mature (MYH11+) SMC that exist at the time of tamoxifen injection and subsequent determination of what they or their progeny become irrespective of continued expression of ACTA2, MYH11, or other SMC-marker genes.**

After 18 weeks of Western diet treatment, BCAs were harvested from SMC YFP^{+/+} *ApoE*^{-/-} mice and immunostained for eYFP, ACTA2, and LGALS3. Confocal microscopy z-stacks of the collected tissues were acquired and analyzed to accurately profile each cell (Fig. 8a). Remarkably, 86% of SMCs within atherosclerotic lesions (eYFP⁺DAPI⁺ cells) were ACTA2 negative, indicating that the majority of SMCs within the lesion cannot be identified using traditional SMC markers. In addition, results showed that phenotypically modulated SMCs (eYFP⁺ACTA2⁻/DAPI⁺) comprised approximately 25% of the

total cellular composition of the lesions (Table 1, Supplemental Table 2, and Supplemental Fig. 17). These data are the first to our knowledge to clearly define the overall composition of SMC within atherosclerotic lesions in either animal models or man.

Smooth muscle cells expressed multiple markers of macrophages

When characterizing these phenotypically modulated SMCs we discovered that a large portion of the cells took on characteristics of hematopoietic derived cells. Using a common marker for macrophages, LGALS3 (i.e. MAC-2), we found that 23% of LGALS3+ cells within advanced atherosclerotic lesions were eYFP+, indicating that nearly a quarter of cells that would normally be classified as macrophages in previous studies originated from SMCs, not myeloid cells (Fig. 8a, Table 1).

To independently validate the presence of phenotypically modulated SMCs that express LGALS3 we utilized a novel *in situ* hybridization proximity ligation assay (ISH-PLA) recently developed by our lab¹⁴⁴ that permits identification of phenotypically modulated SMCs based on detection of H3K4dime of the *Myh11* promoter (PLA+), a stable epigenetic signature of SMCs^{108, 144}. With this method we identified SMCs that were PLA+ eYFP+ LGALS3+ positive cells, confirming that phenotypically modulated SMCs can express macrophage markers within atherosclerotic lesions of 18 week Western diet fed mice (Fig. 8b). To test whether or not macrophages were capable of

acquiring H3K4dime on the *Myh11* promoter we treated cultured RAW 264-7 mouse macrophage cells with the pro-atherogenic, oxidized-phospholipid POVPC (1-palmitoyl-2-(5-oxovaleroyl)-sn-glycero-3-phosphorylcholine), an oxidative product of LDL which is known to be a potent repressor of SMC marker gene expression in vascular SMCs^{40, 88}, and activator of an inflammatory phenotype in macrophages^{150, 151}. Chromatin Immunoprecipitation (ChIP) assays showed that macrophages did not acquire the H3K4 dimethyl mark at the *Myh11* promoter under these conditions (Supplemental Fig. 18).

In order to maintain the ultrastructure of the plaque for detailed lesion analysis, most of our studies were performed in paraffin embedded samples which limited the antigenicity of the specimen, including many markers of macrophage phenotype. Therefore, to determine if eYFP+ (SMC-derived) lesion cells can activate multiple macrophage/hematopoietic markers, we performed flow cytometric analyses of freshly dissociated cells from the aortic region from the aortic root through the iliac bifurcation of 18 week Western diet fed SMC YFP^{+/+} *ApoE*^{-/-} mice to assess expression of LGALS3, ITGAM (CD11b), ITGAX (CD11c), and F4/80 (Fig. 8c). Results demonstrated that significant numbers of SMC-derived cells express each of these markers including cells that co-express ITGAM and F4/80. Importantly, by no means do our results prove that SMCs are actually transitioning to macrophages with their many associated functions since this cannot be assessed simply on the basis of marker gene expression. However, we ascertain through three independent methods that SMCs undergo

phenotypic transition to a macrophage-like state *in vivo*. These cells represent a population of would be synthetic state SMCs that have been diverted to a macrophage-like state, changing the ratio of LGALS3+/ACTA2+ cells believed to be critical in plaque stabilization, and could have overall profound effects on overall lesion size, composition, and indices of stability.

Smooth muscle cells within human coronary artery atherosclerotic lesions expressed the macrophage marker CD68

To determine if the preceding studies in *ApoE*^{-/-} mice are relevant to human pathology, we stained human coronary artery atherosclerotic lesions for CD68, ACTA2, and *MYH11* H3K4dime PLA. Within human atherosclerotic lesions, we detected a large number of CD68+ cells that were also positive for the *MYH11* H3K4dime SMC-specific epigenetic signature based on PLA assays (Fig. 9a, b) , indicating that they were of SMC origin. Although highly unlikely based on the SMC specificity of MYH11 expression and results of our previous studies showing that H3K4dime of the *MYH11* promoter occurs exclusively in SMC^{108, 144}, we assessed by ChIP assay whether macrophages might undergo enrichment of H3K4dime on the *MYH11* promoter when exposed to POVPC. There was no enrichment of H3K4dime on the *MYH11* promoter in human macrophages treated with POVPC (Fig. 9c); in contrast, a stable H3K4dime enrichment was observed in SMCs, consistent with our previous observations¹⁰⁸. In addition, to determine if *MYH11* H3K4dime PLA+ CD68+ cells might be

derived from circulating progenitor cells, we acquired coronary artery samples from men that had received a cross gender heart transplant (female heart) in order to lineage trace hematopoietic derived cells using Y-chromosome fluorescent *in situ* hybridization (FISH). Results showed detection of *MYH11* H3K4dime PLA⁺ CD68⁺ cells that were Y-chromosome negative (Supplemental Fig. 19), consistent with these macrophage-like cells being of SMC and not hematopoietic origin. Importantly, as further validation of the fidelity of our *MYH11* H3K4dime PLA⁺ epigenetic method for identifying phenotypically modulated SMC, we never saw cells that were *MYH11* H3K4dime PLA⁺ and Y-chromosome⁺ (Supplemental Fig. 19 and unpublished data). In summary, we have identified a population of SMCs that cannot be identified using traditional SMC lineage markers that constitute a portion of the macrophage marker expressing population within advanced mouse and human atherosclerotic lesions.

Transition of SMC to a macrophage-like state was dependent on the pluripotency factor KLF4

Krüppel-like factor 4 (KLF4) is an ESC and iPS cell pluripotency factor that we have previously shown to be required for SMC phenotypic switching in several *in vitro* models, including stimulation with PDGF or POVPC^{40, 88}. Our lab has also shown that global conditional genetic knockout of *Klf4* transiently decreases the ability of SMCs to down-regulate their SM-marker genes following

vascular injury⁸⁹. Moreover, we previously presented evidence indicating that the functional effects that mutating the G/C repressor element has in abrogating down-regulation of the *Taglin* gene promoter following vascular injury, are likely mediated by binding of KLF4 to the G/C repressor element⁸⁷. Since all CArG-dependent SMC marker genes characterized to date have conserved putative KLF4 binding sites within their promoters¹²⁰, we believe KLF4 plays a key role in mediating coordinate suppression of SMC marker genes during phenotypic switching, at least in *in vitro* culture model systems. However, as yet, there is no direct evidence that KLF4 regulates SMC phenotype in atherosclerotic lesions. Equally intriguing, results of an elegant series of studies by the Jain lab^{152, 153} have provided evidence that KLF4 directly binds to promoters of macrophage specific genes promoting monocyte differentiation and macrophage polarization, making KLF4 a likely candidate that may be involved in modulating phenotypic transitions of SMC to macrophage-like state¹⁵²⁻¹⁵⁴.

To ascertain if KLF4 is required for phenotypic switching of SMC to a macrophage-like state during atherosclerotic plaque development *in vivo* and if loss of KLF4 in SMC impacts overall lesion size, composition, and/or indices of plaque stability we crossed the SMC YFP^{+/+} *Apoe*^{-/-} mouse with a *Klf4*^{flox/flox} mouse line¹⁴⁵ thereby permitting simultaneous SMC lineage tracing and SMC specific conditional knockout of KLF4. We observed highly efficacious recombination of the floxed KLF4 alleles selectively in the SMC-rich media of the BCA after tamoxifen treatment (Supplemental Fig. 20a) including what we

estimate to be nearly 100% recombination in the aorta based on 55% recombination in DNA extracted from aortic tissue specimens (Supplemental Fig. 20b) which contain about 60% SMCs as assessed by flow cytometry (Supplemental Fig. 15b). Although there was no significant difference in the number of phenotypically modulated SMCs (eYFP+ACTA2-/DAPI+) within BCA atherosclerotic lesions of SMC YFP^{+/+} *Klf4*^{Δ/Δ} *ApoE*^{-/-} mice compared to SMC YFP^{+/+} *Klf4*^{wt/wt} *ApoE*^{-/-} mice (Supplemental Fig. 21a), there was a greater than 50% decrease in the SMC-derived macrophage-like cells (YFP+ LGALS3+/DAPI+) (Fig. 10a). Also, of major significance SMC YFP^{+/+} *Klf4*^{Δ/Δ} *ApoE*^{-/-} mice exhibited a 40% decrease in overall lesion area (Fig. 15b), and a 100% increase in the fibrous cap area relative to lesion size (Fig. 10c) as compared to control SMC YFP^{+/+} *Klf4*^{wt/wt} *ApoE*^{-/-} mice. These changes were not associated with an overall decrease in the medial area, lumen area (Supplemental Fig. 22a), or changes in cholesterol or triglyceride levels (Supplemental Fig. 22b). We also noted several other indicators of increased plaque stability, including: decreased LGALS3+ cells within the lesion (Fig. 10a), increased ACTA2 cap coverage (Fig. 10d, Supplemental Fig. 21c, d), and decreased LGALS3 cap coverage (Supplemental Fig. 21e). SMC-specific *Klf4* knockout also resulted in a reduced proliferation of SMC-derived cells (Supplemental Fig. 21f) as well as reduced apoptosis within both SMC- and non-SMC derived cells (Supplemental Fig. 21g) which likely contributed to reduced overall lesion size and inflammation. Taken together, results show that selective

loss of KLF4 in SMC resulted in marked reductions in SMC-derived macrophage-like cells and major overall beneficial effects on lesion size, and indices of plaque stability.

Global heterozygous conditional KO of *Klf4* decreased plaque size and increased indices of plaque stability

Recent studies using *VE-cadherin-Cre Klf4 Apoe^{-/-}* and *LysM^{cre/cre} Klf4 Apoe^{-/-}* mouse models provided evidence that KLF4 plays an atheroprotective role in endothelial cells and myeloid cells respectively with knockout resulting in increased lesion size^{155, 156}. Paradoxically, results of our studies showed the opposite effects of loss of KLF4 in SMCs. As such, there is major ambiguity regarding the overall role of KLF4 in lesion development and whether it would be beneficial or detrimental to inhibit its action *in vivo*. In order to ascertain the dominant effect of loss of KLF4, we generated tamoxifen-inducible heterozygous KLF4 floxed mice, ERT-Cre+ *Klf4^{flox/wt} Apoe^{-/-}*, as a model of partial inhibition of KLF4 across all cell types. Note that a parallel study of tamoxifen dependent homozygous KLF4 KO mice was terminated at ten weeks of Western diet due to excessive weight loss, and severe skin lesions in the mice. ERT-Cre+ *Klf4^{flox/wt} Apoe^{-/-}* mice treated with tamoxifen (ERT-Cre+ *Klf4^{Δ/wt} Apoe^{-/-}*) demonstrated 50% recombination, the maximum possible recombination for heterozygous KO, in the aorta, liver, and colon (Supplemental Fig. 23a, b), but exhibited no changes in body weight, heart weight, or cholesterol and triglyceride levels when

compared to ERT-Cre- *Klf4*^{flox/wt} *ApoE*^{-/-} littermate control mice (Supplemental Fig. 24).

Results showed that ERT-Cre+ *Klf4*^{Δ/wt} *ApoE*^{-/-} mice had virtually identical changes in atherosclerotic lesions as observed in our SMC specific conditional KLF4 KO mice. For example, these mice showed a dramatic decrease in lesion size (Fig. 11a), and exhibited several indices of increased plaque stability, including increased ACTA2 cap coverage (Fig. 11c), decreased macrophage content (Fig. 11d), and decreased evidence of hemorrhagic events, as measured by TER119 staining (Fig. 11b). ERT-Cre+ *Klf4*^{Δ/wt} *ApoE*^{-/-} BCA atherosclerotic lesions also exhibited decreased apoptosis and proliferation, as indicated by cleaved CASP3 and MKI67 staining respectively (Supplemental Fig. 25). Taken together, these results indicate that loss of one KLF4 allele has beneficial overall effects on plaque development, including the ideal therapeutic goal of smaller more stable lesions. Moreover, results suggest that the dominant effect of loss of one KLF4 allele is mediated through SMCs, given the similarities between these results and those of our SMC specific KLF4 KO studies.

Mechanisms by which KLF4 induces transition of SMCs to a macrophage-like state

We have previously presented evidence showing that long term Western diet feeding caused an up-regulation of *Klf4* expression with an associated down-regulation of SMC marker genes⁸⁸. We have also shown that *Klf4* is induced in

cultured SMC by treatment with oxidized phospholipids such as POVPC⁸⁸ and suppresses expression of SMC marker genes through several mechanisms including binding to the G/C repressor element found in most SMC marker gene promoters including *Acta2*, *Tagln*, and *Myh11*, and inhibiting binding of SRF to CARG elements^{11, 14, 87}. To determine if similar mechanisms contribute to suppression of SMC marker genes within atherosclerotic lesions *in vivo*, we performed ChIP assays on chromatin extracted from BCA regions of *ApoE*^{-/-} transgenic mice containing either a wild type *Tagln* promoter driving lacZ or a *Tagln* promoter with a mutation of the GC repressor element (*Tagln* GC repressor mutant lacZ mouse). We previously showed that these mice retain normal developmental expression of *Tagln*, but the GC repressor mutant mouse retained expression of lacZ after wire injury¹¹ and atherosclerosis¹⁴. Results showed marked enrichment of KLF4 binding to *Acta2*, *Tagln*, *Myh11*, and *Cnn1* endogenous promoters in Western diet fed animals (Fig. 12a) consistent with prior *in vitro* results^{40, 88}. Moreover, we showed that enhanced Klf4 binding to the *Tagln* promoter was dependent on the G/C repressor element in that enrichment was not observed to the GC repressor mutant transgene (Supplemental Fig. 26a). Finally, we provide direct evidence for KLF4 binding to the G/C repressor element within intact lesions based on ISH-PLA assay with a biotinylated probe to the GC repressor region of the *Tagln* promoter and looking for the proximity of KLF4 to the biotin residues (Supplemental Fig. 26b).

We next asked whether KLF4 is required for transition of cultured SMC to a macrophage-like state *in vitro* following cholesterol loading since Rong et al.⁴¹ previously showed that this induces not only suppression of SMC marker genes, but also activation of multiple markers of macrophages. Due to recent controversies about the origins and purity of SMCs cultured from mouse vessels^{18, 19}, we utilized our SMC-lineage tracing mice to harvest SMC populations from 8 week old tamoxifen injected SMC YFP^{+/+} *ApoE*^{-/-} mice. Flow cytometry results indicated that >98% of the cells were YFP+ (Supplemental Fig. 27), indicating they are derived from mature differentiated SMC *in vivo* and not a stem cell source as has been speculated^{18, 19}. We confirmed that treatment with cholesterol up-regulated expression of Lgals3 in pure primary cultures of mouse aortic SMCs and also noted that *Klf4* expression was also induced in these samples (data not shown). Of major interest, we showed that cholesterol loading induced increased expression of Lgals3 in cultured mouse aortic SMCs derived from SMC YFP^{+/+} *Klf4*^{wt/wt} but not in SMC derived from SMC YFP^{+/+} *Klf4*^{Δ/Δ} mice (Fig. 12b), which lack *Klf4* expression (Supplemental Fig. 28). We also observed KLF4 expression in phenotypically modulated SMCs *in vivo*, with a large population of the SMC-derived macrophage-like cells expressing KLF4 (Fig. 12c, yellow arrows). Taken together, the preceding results provide evidence that KLF4 plays a direct role in inducing both suppression of SMC marker genes and induction of macrophage marker genes in the setting of advanced atherosclerotic lesions.

Discussion

Despite numerous papers in the field showing that cultured SMCs down-regulate expression of ACTA2 and other SMC differentiation marker genes following exposure to environmental cues likely to be present in lesions including: cholesterol⁴¹, POVPC⁴⁰, PDGF-BB¹⁵⁷, and IL-1 β ⁴², the field has relied almost entirely on detection of these markers to ascertain if a given cell within a lesion is a SMC or from another lineage. Indeed, this practice has contributed to the well-established dogma in the field that the role of SMCs within plaques is rather limited, albeit presumed to be beneficial by virtue of phenotypically modulated SMC secreting extracellular matrix and contributing to fibrous cap formation. Herein we report for the first time definitive evidence for the presence of a large population (86%) of phenotypically modulated SMCs that have previously gone undetected, which constitute ~25% of the total cellular composition of the lesion. Moreover, we show that an essential fraction of these phenotypically modulated SMC transition to a macrophage-like state within both advanced human (Fig. 9) and mouse atherosclerotic lesions (Fig. 1), and that selective loss of KLF4 within SMCs (Fig. 10, Supplemental Fig. 21), or global loss of one *Klf4* allele in all cell types (Fig. 11, Supplemental Fig. 25), results in large reductions in lesion size as well as multiple changes consistent with plaque stabilization. Taken together results provide compelling evidence that irrespective of the exact functions of SMC-derived macrophage-like cells within lesions, results indicate that transitions in SMC phenotype can play a dominant role in overall lesion

development, plaque composition, and stability. Previous studies have provided evidence that diphtheria toxin-induced SMC-selective apoptosis can exacerbate lesion development^{33, 158, 159}, and that there are ACTA2+ lesion cells which exhibit a macrophage-like phenotype including presumptive antigen presentation¹⁶⁰, and phagocytosis^{24, 41, 52}. However, the present studies are the first to provide definitive evidence that SMCs transition to a macrophage-like state within advanced human and mouse atherosclerotic lesions, and that these transitions are critical in disease pathogenesis.

A key question is how did loss of KLF4 within SMCs or global loss of one allele of *Klf4* in all cell types result in marked reductions in overall lesion size as well as multiple changes consistent with increased plaque stability. Although there was a 40% reduction in the number of SMCs that became macrophage-like (Fig. 10a), this only correlated with ~10% reduction in the overall number of macrophages present within the lesion, and would not seem sufficient to explain the large overall effects on plaque size and stability. Since we show that there was no significant reduction in the fraction of SMC-derived cells within lesions (Supplemental Fig. 8a) this would suggest that phenotypically modulated SMCs are being diverted from entering a macrophage-like state to a phenotypic state that is beneficial for reductions in plaque size and increased plaque stability. In other words, simultaneously reducing the number of macrophages and increasing the number of plaque stabilizing cells. Indeed, we present evidence in support of this idea in that SMC specific KLF4 KO mice had decreased CASP3

and MKI67 staining in the eYFP+ plaque population (Supplemental Fig. 8f, g), symptomatic of SMCs being in a more synthetic state. Given evidence in this (Fig. 12a, b, and Supplemental Fig. 26a) and previous papers showing that KLF4 can not only result in silencing of SMC marker genes^{40, 87, 88, 90, 161} but also active multiple pro-inflammatory genes^{152, 153}, we postulate that loss of KLF4 can exert a dominant overall effect on plaque size, composition, and indices of stability by reducing overall plaque inflammation and increasing SMC transitions to a matrix producing “synthetic” or myofibroblast-like state. Although this has long been postulated to be the primary role of SMC within lesions (see reviews^{1, 5, 30, 45, 57, 120}), the present studies are the first to precisely identify phenotypically modulated SMC within advanced lesions, to show that these cells transition to a macrophage-like state, and to identify a key pathway that regulates SMC phenotypic transitions *in vivo*.

A very surprising observation was that global KO of one allele of *Klf4* within *Apoe*^{-/-} Western diet fed mice resulted in changes virtually identical to those observed with complete KO of this gene in SMCs (Fig. 11 and Supplemental Fig. 25) and were opposite to effects reported in recent publications involving depletion of KLF4 from other major players in plaque development, including macrophages (*LysM*^{cre/cre} *Klf4* *Apoe*^{-/-})¹⁵⁵ and endothelial cells (ECs) (*VE-cadherin-Cre* *Klf4* *Apoe*^{-/-})¹⁵⁶. Specifically, studies showed that *LysM*^{cre/cre} *Klf4*^{Δ/Δ} *Apoe*^{-/-} mice exhibited increased Sudan IV and macrophage infiltration into lesions of mice fed a Western diet for 20 weeks as compared to

wild type control *ApoE*^{-/-} mice. However, the loss of KLF4 in macrophages also resulted in increased triglycerides, cholesterol, and LDL levels¹⁵⁵, which may have led to many of the proatherogenic findings in *LysM*^{cre/cre} *Klf4*^{Δ/Δ} *ApoE*^{-/-} mice secondary to the macrophage-specific loss of KLF4. The studies investigating the role of KLF4 in endothelial cells elegantly described how loss of KLF4 can cause endothelial cell dysfunction and lead to larger *en face* lesions with a higher percentage of hematopoietic derived (PTPRC/CD45+) cells. However, neither of these studies included an in-depth analysis of plaque composition or stability following long term Western diet feeding. Taken together, it is possible that at least some of the differences observed between SMC-, EC- and macrophage-selective *Klf4* KO in *ApoE*^{-/-} mice may be a function of differences in experimental design. However, our observations that global heterozygous KO of *Klf4* in all cell types pheno-copied the effects of SMC specific *Klf4* knockout provide strong evidence suggesting that: 1) KLF4 exhibits strong gene dosage effects within SMC that appear to be dominant over any beneficial effects of loss of KLF4 in non-SMC including ECs and macrophages; and 2) KLF4 as a possible novel therapeutic target for achieving both reductions in the size and stabilization of atherosclerotic plaques. However, given the difficulty in achieving long term efficacious inhibition of transcription factors *in vivo*, this would likely be through targeting an as yet unidentified upstream signaling pathway required for activating KLF4 expression or down-stream effector pathways selectively linked to beneficial phenotypes in lesion cells. Indeed, such studies will be difficult as

they would require rigorous lineage tracing for each of the major cell types present within the atherosclerotic lesion for in vivo validation of effects of candidate inhibitors on phenotypic transitions of each cell type.

Figure 8: Multiple SMC lineage tracing methods provide evidence for large populations of phenotypically modulated SMCs within brachiocephalic arteries (BCA) of 18 Week WD fed SMC eYFP^{+/+} Apoe^{-/-} mice some of which have activated multiple markers of macrophages.

(a) BCAs were paraffin embedded, and sectioned for immunostaining from SMC eYFP^{+/+} Apoe^{-/-} mice that were injected with tamoxifen and placed on Western diet for 18 weeks as described in Methods. Results show that differentiated SMCs present at the time of tamoxifen injection (eYFP⁺) subsequently give rise to multiple phenotypes including: (i) phenotypically modulated SMCs (eYFP⁺ ACTA2⁻ cells highlighted in white rectangle), and (ii) phenotypically modulated macrophage-like SMCs (eYFP⁺ ACTA2⁻ LGALS3⁺) (marked by yellow arrows). Scale bar represents 50µm for the larger panel and 10µm for the smaller panels.

(b) Independent validation of the SMC origin of phenotypically modulated SMC within lesions using a single cell epigenetic assay designated *Myh11* H3K4dime ISH-PLA showed the presence of macrophage-like SMCs eYFP⁺ LGALS3⁺ cells that are also positive for the SMC specific histone modification (yellow arrows). White arrows indicate eYFP⁺ H3K4dime *Myh11* PLA⁺ cells. (c) Flow cytometry of single cell suspension from 18 Week WD fed SMC eYFP^{+/+} Apoe^{-/-} mouse aortas, from the iliac bifurcation to the aortic root as described in Methods. The gating strategy included: (i) forward versus side scatter gate; (ii) a singlets gate; (iii) and eYFP⁺ cell gate. A sub-population of eYFP⁺ cells were found to be double positive for ITGAM (CD11b) and F4/80 (iv). We also saw populations of

eYFP⁺ cells expressing hematopoietic markers, ITGAX (CD11c) (v), and LGALS3 (mac-2) (vi). $n=6$.

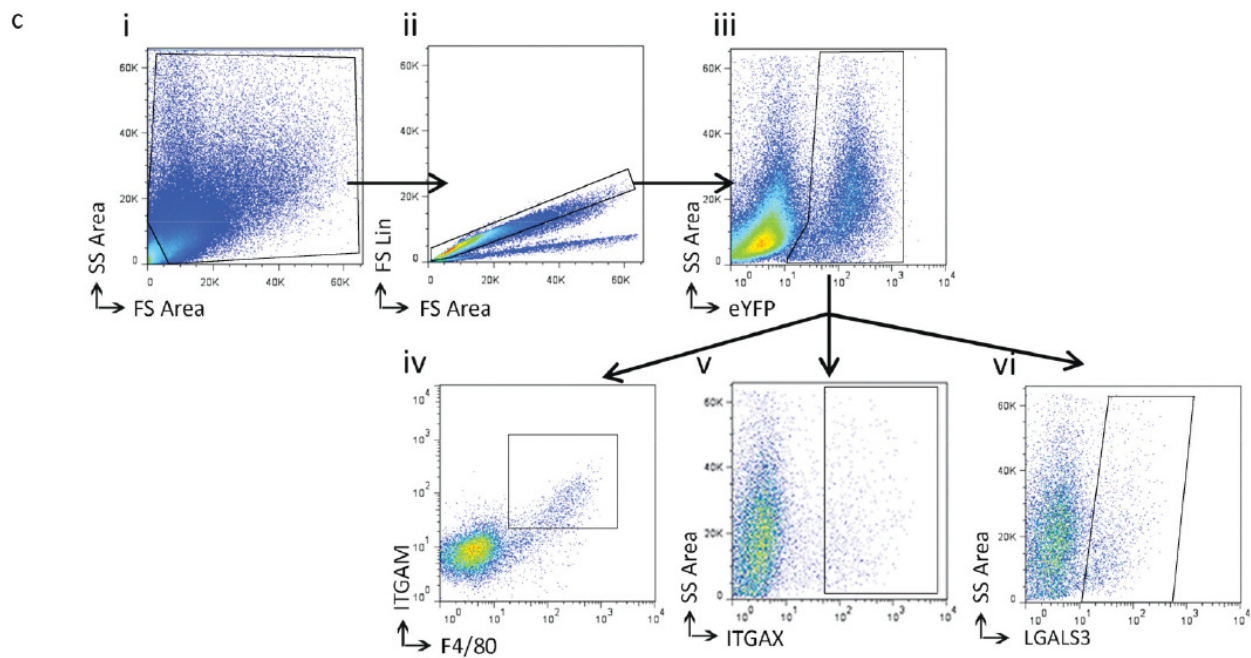
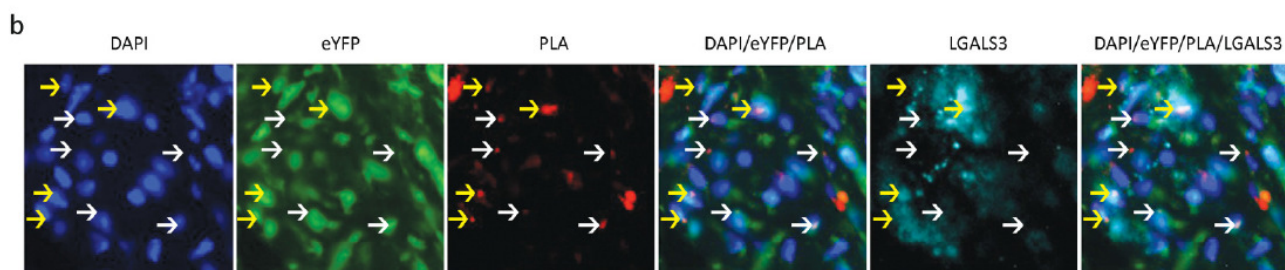
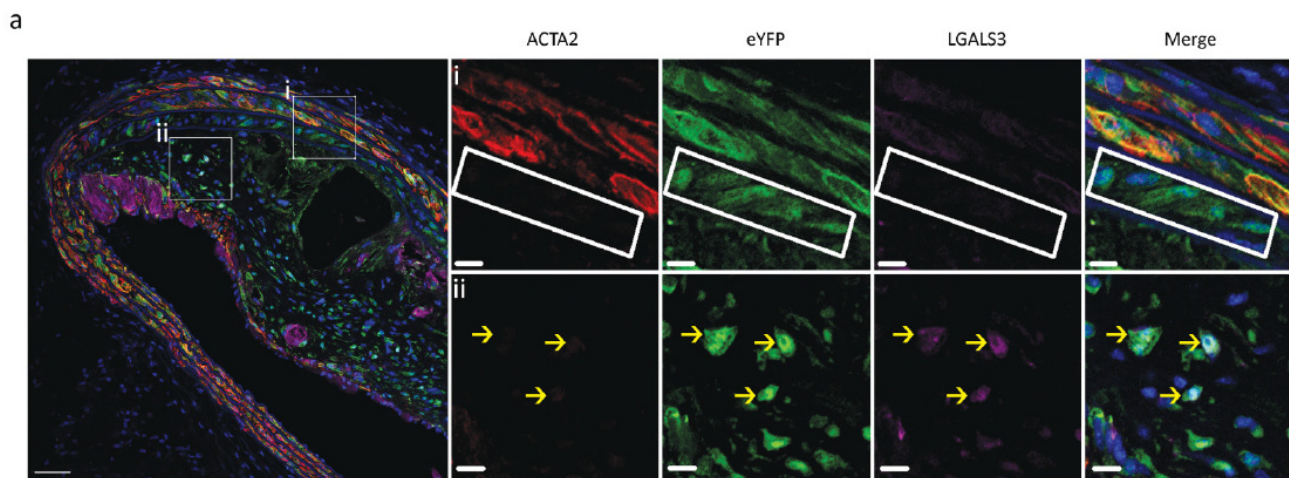


Figure 9: Evidence that SMCs within advanced human coronary artery lesions express the macrophage marker CD68.

(a) SMCs within advanced atherosclerotic lesion specimens were identified based on PLA detection of the SMC specific stable epigenetic signature H3K4dime on the *MYH11* promoter. *MYH11* H3K4dime PLA+ cells exhibit a punctate red dot within the nucleus while the non-nuclear amorphous red staining is autofluorescence or non-specific background. Samples were also immunostained for CD68 (green) and for DNA (blue). Results showed three distinct cell populations shown in enlarged panels to the right and highlighted with white arrows: (i) *MYH11* H3K4dime PLA+ SMCs that are CD68-, (ii) *MYH11* H3K4dime PLA- CD68+ presumably hematopoietic derived macrophages, and (iii) H3K4dime *MYH11* H3K4dime PLA+CD68+ SMC derived macrophage-like cells. (b) Shoulder regions within plaques exhibited a high incidence of phenotypically modulated (ACTA2-) smooth muscle cell derived (*MYH11* H3K4dime PLA+) macrophage marker (CD68+) expressing cells (yellow arrows) and a few phenotypically modulated SMC negative for CD68 (white arrows) *MYH11* H3K4dime PLA+ ACTA2- CD68- cells. (c) Cultured human coronary SMCs fail to show loss of the *MYH11* H3K4dime mark after 24 hours treatment with POVPC, whereas human monocytes lack this mark with or without POVPC treatment. Statistics were then performed using two-way ANOVA with a Tukey post-test. * $P < 0.05$. Error bars are based on S.E.M.

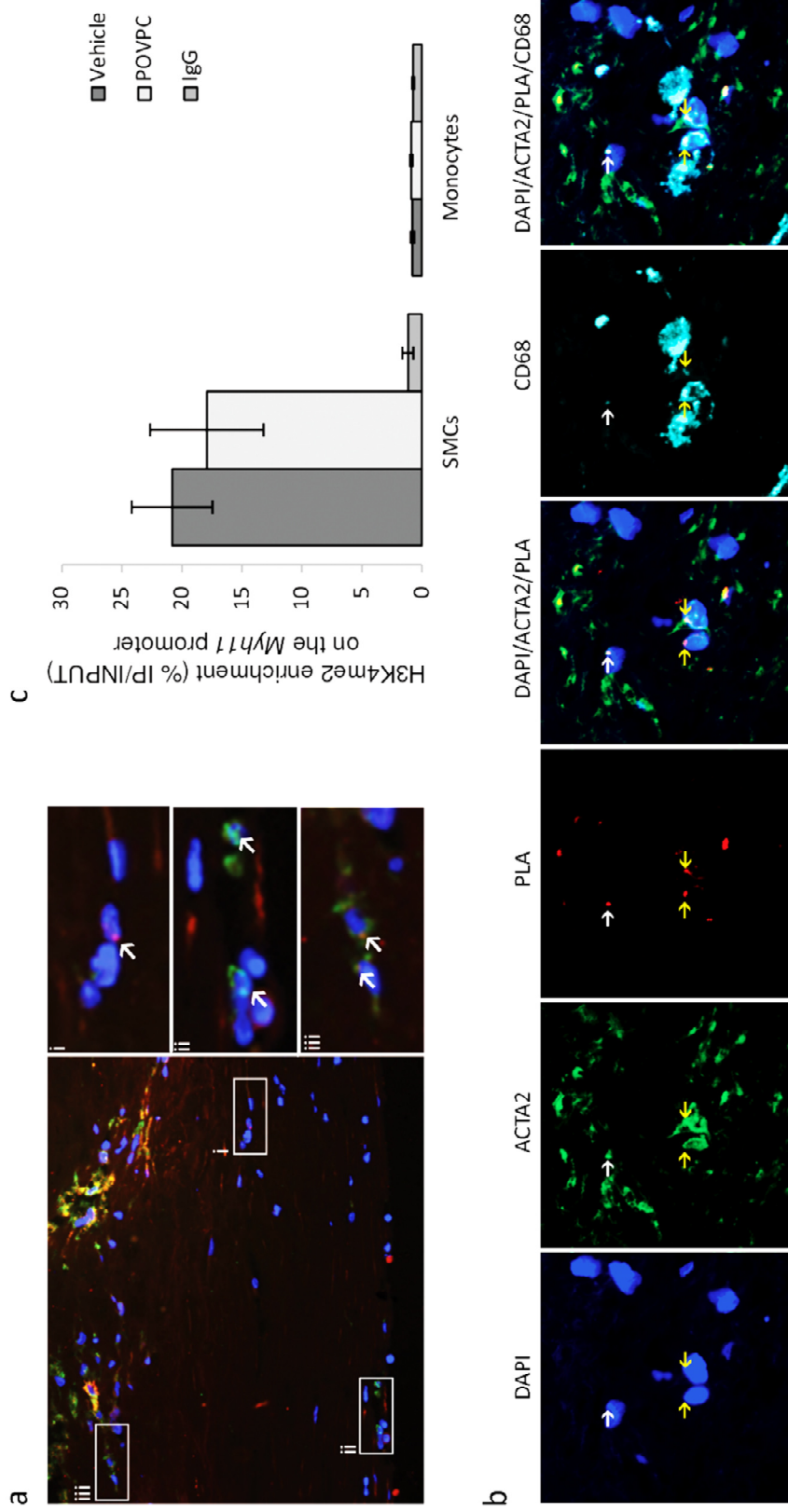


Figure 10: SMC specific *Klf4* conditional knockout in *Apoe*^{-/-} mice fed a high fat diet for 18 weeks resulted in decreased lesion size and increased indices of plaque stability.

SMC eYFP^{+/+} *Apoe*^{-/-} mice crossed to *Klf4* floxed mice were tamoxifen treated and given Western diet for 18 weeks prior to analysis. Results showed the following: (a) Loss of KLF4 in SMCs resulted in an overall decrease in the fraction of LGALS3⁺ cells, and a large decrease in the fraction of SMC-derived LGALS3⁺ cells (YFP+LGALS3⁺); (b) decreased total lesion area (μm^2); (c) increased fibrous cap area (defined as the region of the lesion within 30 μm of the luminal surface) relative to the size of the lesion; (d) and increased ACTA2⁺ cells within the lesion. Analysis completed by 2-way ANOVA comparing genotyping and distance from start of the BCA, p-values indicated on graphs, data represent mean \pm SEM. (e) Representative image demonstrating the changes in lesion morphology and cell composition. Quantification is based on analysis of five 71415 μm^2 regions in each of three sections per mouse spanning a 600 μm length of the BCA. Scale bar = 50 μm . SMC YFP^{+/+} *Klf4*^{wt/wt} *Apoe*^{-/-} *n*=11, SMC YFP^{+/+} *Klf4* ^{Δ/Δ} *Apoe*^{-/-} *n*=8.

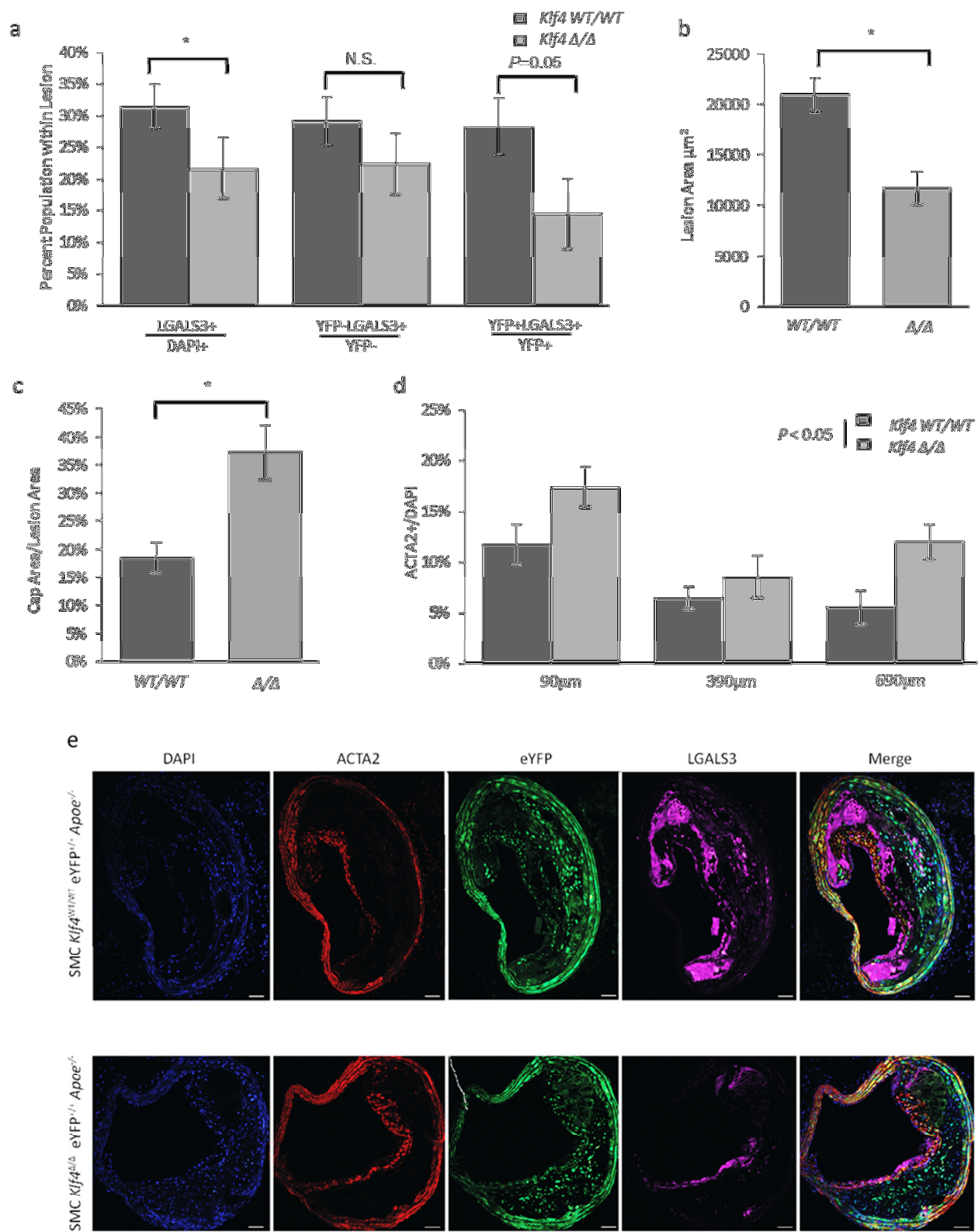


Figure 11: Global conditional knockout of one *Klf4* allele increased indices of plaque stability.

ERT Cre⁻ ($n=12$) and ERT Cre⁺ ($n=10$) animals were crossed with floxed *Klf4* *ApoE*^{-/-} mice and treated with tamoxifen between 6-8 weeks to generate mice that were *Klf4*^{flx/wt} *ApoE*^{-/-} and *Klf4* ^{Δ /wt} *ApoE*^{-/-} respectively. Mice were then fed a Western diet for 25 weeks before BCA lesions analysis. Mice with loss of one *Klf4* allele exhibited BCA lesions that were smaller (a) and exhibited multiple indices consistent with increased plaque stability including (b) reduced intraplaque hemorrhage (TER119 staining measured by presence or absence of TER119 in the plaque), (c) increased fibrous cap ACTA2 lumen coverage, and (d) decreased LGALS3 staining. Scale bar = 50 μ m. *Fisher's exact test (b), one-way ANOVA (a, c, d) $P<0.05$. Data represent mean \pm SEM.

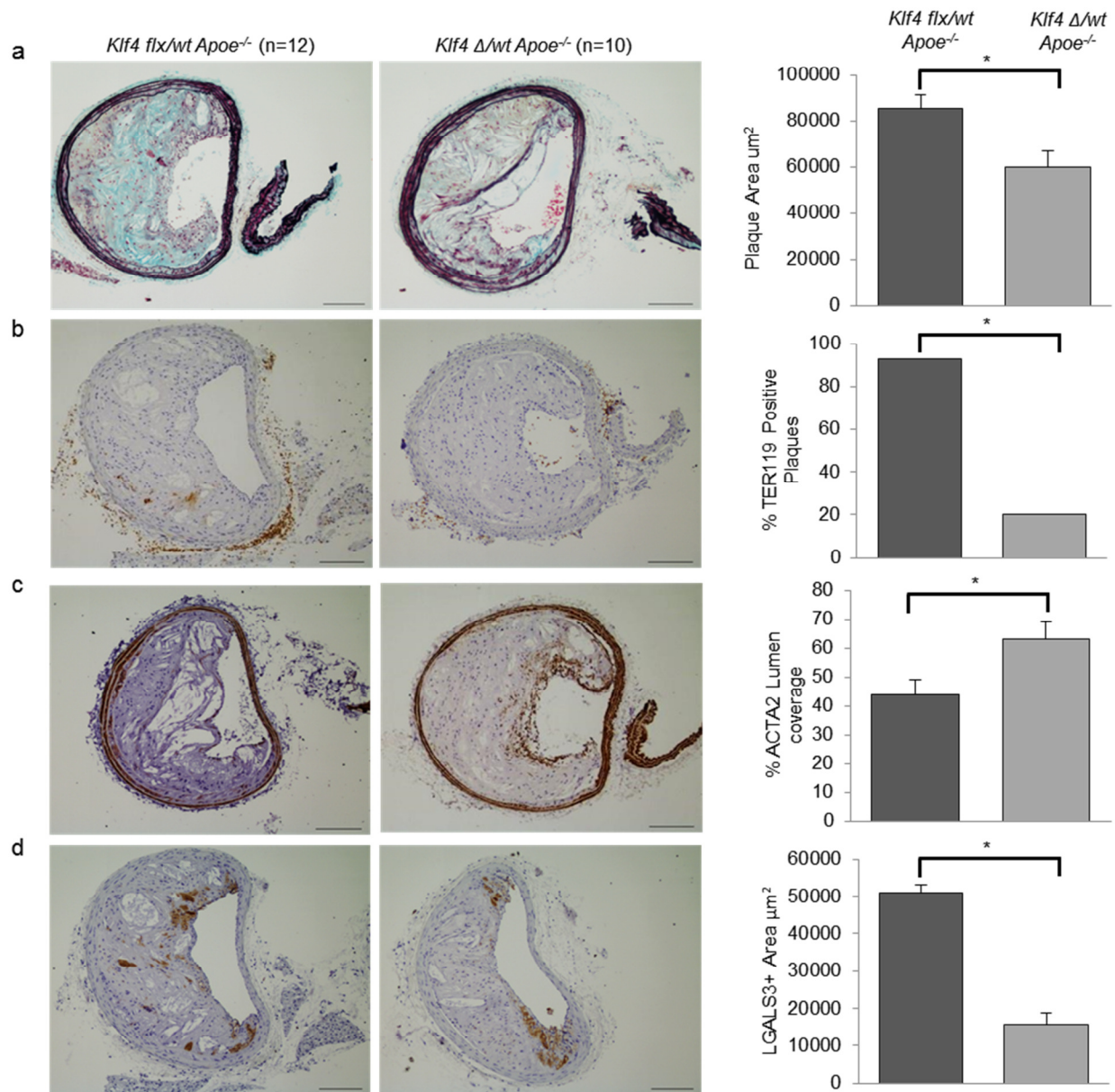
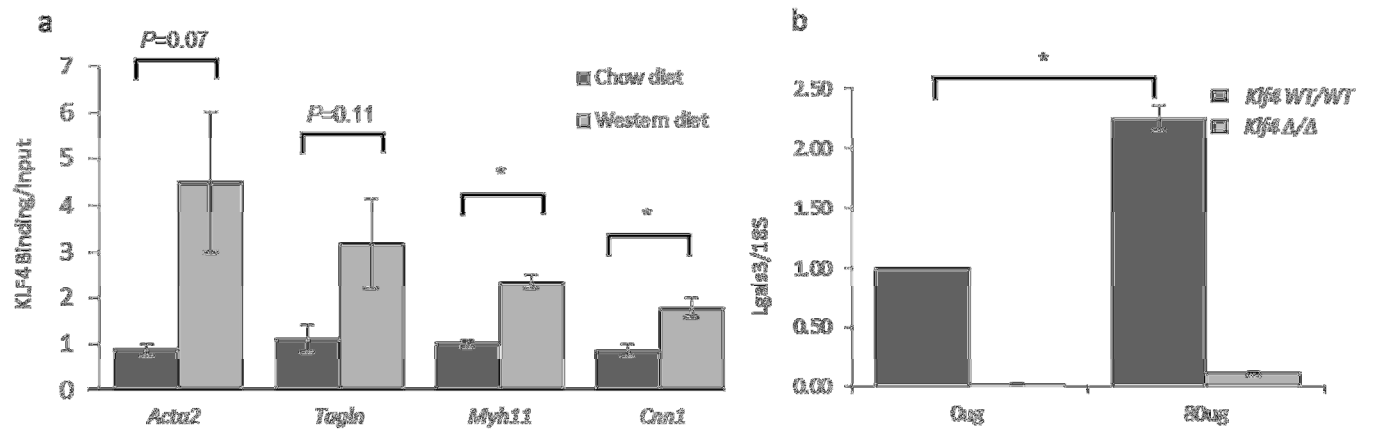


Figure 12: KLF4 is upregulated in SMCs during atherosclerosis, binds to the promoters of SM marker genes, and loss of KLF4 diminishes LGALS3 expression.

(a) *in vivo* ChIP assays on BCAs obtained from 18 week Western diet fed *ApoE*^{-/-} mice show increased binding of KLF4 to SM marker gene promoters compared to *ApoE*^{-/-} mice fed a chow diet. (b) Aortic SMCs were isolated from SMC YFP^{+/+} *Klf4*^{wt/wt} and SMC YFP^{+/+} *Klf4*^{Δ/Δ} and sorted for YFP. LGALS3 mRNA expression in these cells was assessed after treatment with either 0 or 80 μg/mL cholesterol for 72 hours to induce a macrophage-like state. (c) Staining of the BCA from 18 week Western diet fed SMC-lineage tracing mouse for DAPI (blue), eYFP (green), LGALS3 (magenta), and KLF4 (red) shows that KLF4 was upregulated in phenotypically modulated SMCs (white arrows) and also in phenotypically modulated SMCs that express LGALS3 (yellow arrows). (i) scale bar = 20 μm (ii) zoom in from boxed region, scale bar = 10 μm. Data normalcy was determined using Kolmogorov-Smirnov test. Statistics were then performed using two-way ANOVA with a Tukey post-test. **P*<0.05. Data represent mean±SEM.



c

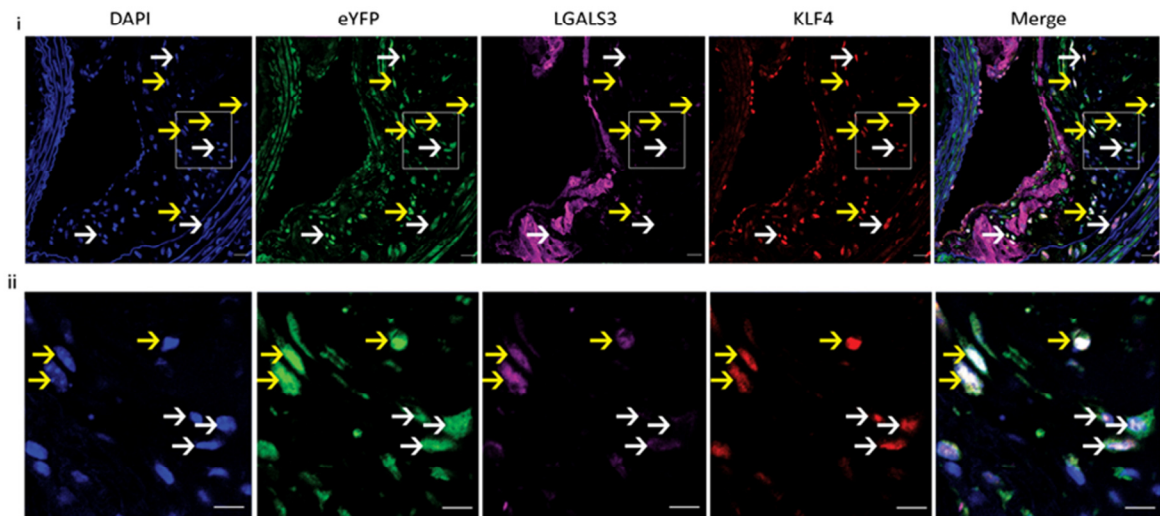


Table 1: Cellular composition of 18 week Western diet SMC eYFP^{+/+} *ApoE*^{-/-} mice.

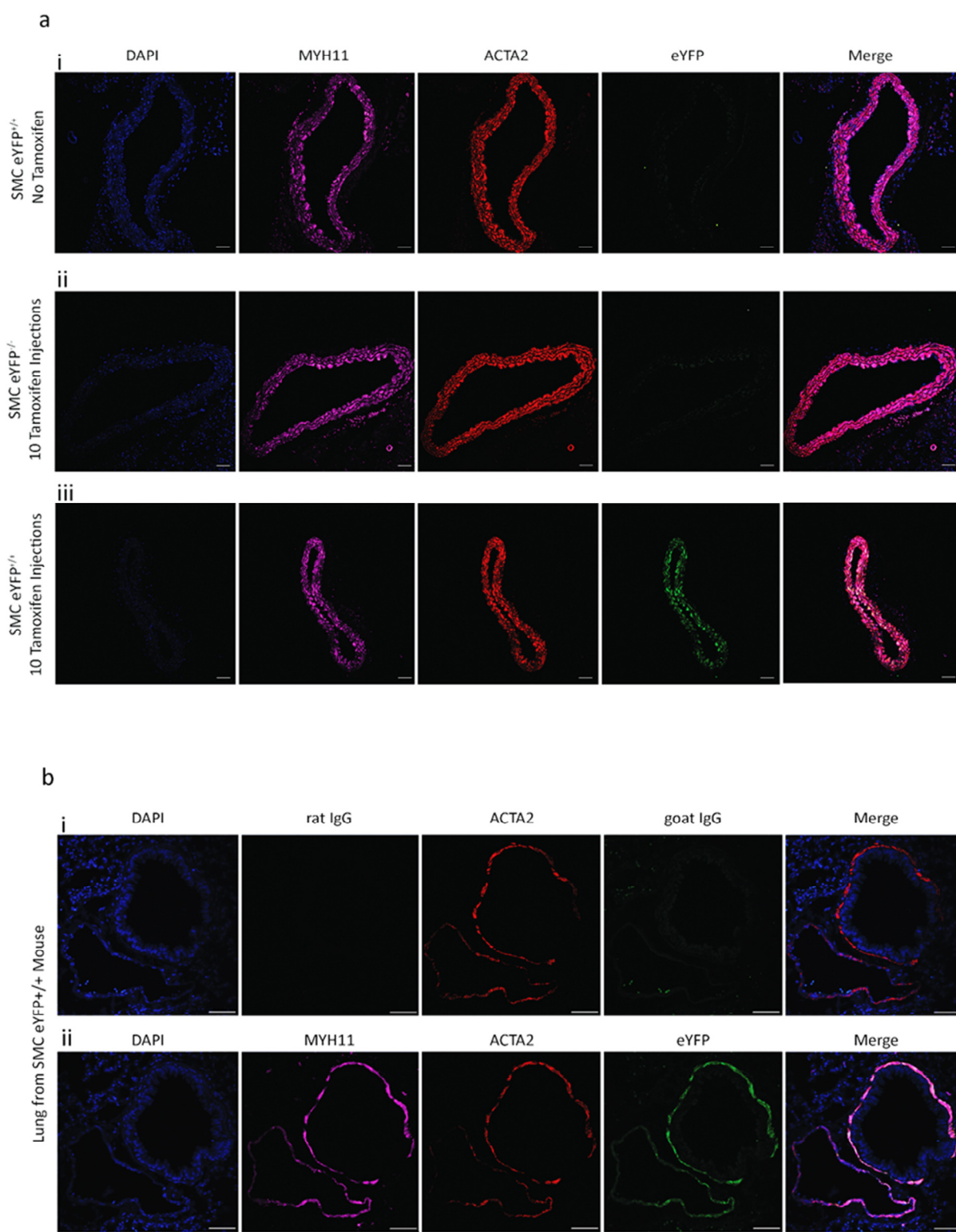
Quantification of immunofluorescent stained slides from 18 week WD fed SMC eYFP^{+/+} *ApoE*^{-/-} mouse lesions reveal shocking new SMC populations. Cells stained with markers for nuclei (DAPI), traditional SMC marker (ACTA2), lineage tracing mark (eYFP), and macrophage marker (LGALS3), were counted in five 71415 μm^2 regions in each of three sections per mouse spanning a 600 μm length of the braciocephalic artery. $n=10$.

18 Week WD Fed SMC eYFP^{+/+} <i>ApoE</i>^{-/-} Mice		
Cell Population	Percent	Std Err
eYFP+ACTA2-/eYFP+	86.87%	±2.53%
eYFP+ACTA2-/DAPI+	27.11%	±3.09%
eYFP+LGALS3+/LGALS3+	22.82%	±3.83%
eYFP+LGALS3+/eYFP+	22.72%	±3.43%
eYFP+LGALS3+/DAPI+	6.65%	±1.01%

Supplemental Figure 14: SMC lineage tracing mice exhibit recombination exclusively in the SMCs of tamoxifen treated SMC eYFP^{+/+} mice.

(a) eYFP expression within aortas of SMC eYFP^{+/+} mice treated either with or without tamoxifen co-localized with staining for the SMC markers MYH11 and ACTA2. SMC eYFP^{+/+} mice given no tamoxifen had no recombination of the ROSA STOP eYFP allele (i). SMC eYFP^{-/-} mice given 10 intraperitoneal (IP) injections of tamoxifen have no recombination of the ROSA STOP eYFP allele (ii). Only with SMC eYFP^{+/+} mice given 10 IP tamoxifen injections is there recombination of the ROSA STOP eYFP allele (iii). Scale bar represents 20 μ m.

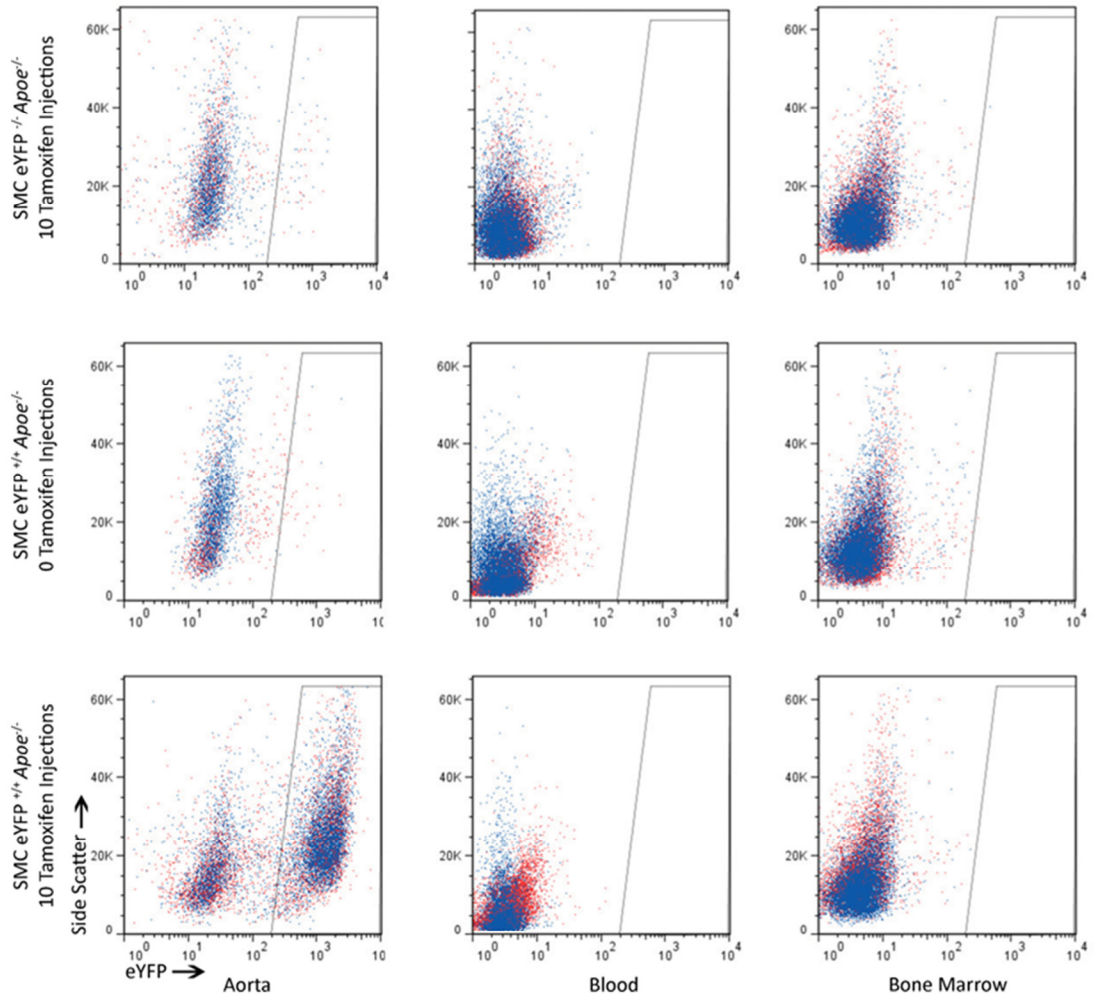
(b) eYFP expression within the lungs of SMC eYFP^{+/+} mice with 10 IP tamoxifen injections (panel ii). Results show the eYFP staining is co-localized exclusively with MYH11⁺ and ACTA2⁺ SMCs within the lung tissue. A goat IgG control antibody shows that the antibody used to detect eYFP has no non-specific binding (i). Scale bar represents 50 μ m.



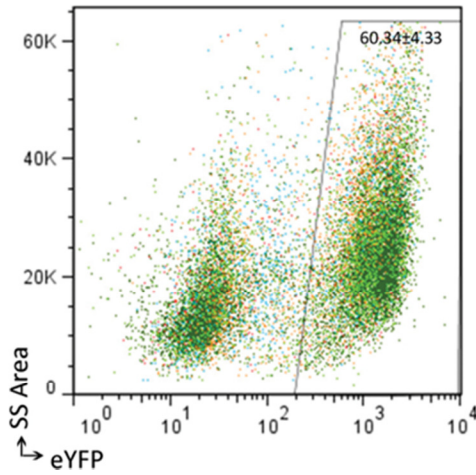
Supplemental Figure 15: Recombination of the ROSA STOP eYFP locus is not present in cells within the blood or bone marrow of tamoxifen treated SMC eYFP mice, but is abundant in freshly dissociated cell preparations from the aorta.

(a) SMC eYFP^{+/+} mice with (bottom panel) and without (middle panel) 10 IP injections of tamoxifen between 6-8 weeks of age. Aortas, blood, and bone marrow samples were processed for flow cytometry. Samples from tamoxifen injected SMC eYFP^{-/-} mice are also shown as a control for background staining (top panel). SMC eYFP^{+/+} mice treated with tamoxifen showed no eYFP⁺ signal in the blood or bone marrow but a large fraction of positive aortic cells (lower left panel). ($n=2$). (b) Dissection and dissociation of aortas from six independent SMC eYFP^{+/+} mice for flow cytometry revealed ~60% of the preparation were eYFP⁺.

a



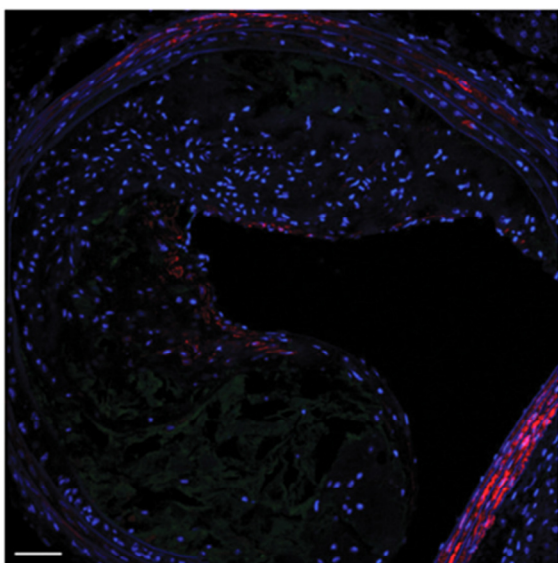
b



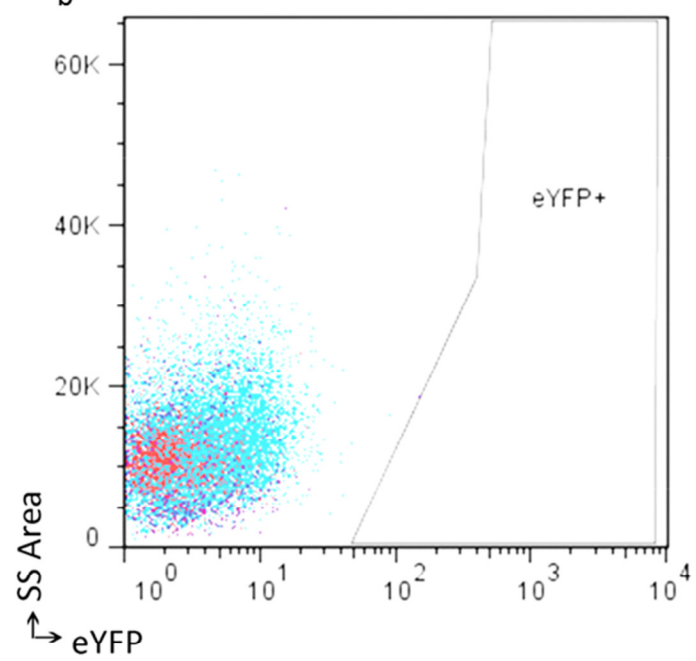
Supplemental Figure 16: Absence of spontaneous recombination of the ROSA STOP eYFP locus or appearance of circulating eYFP+ cells following long term Western diet feeding.

(a) SMC eYFP^{+/+} *ApoE*^{-/-} mice not given tamoxifen do not show spontaneous recombination of the ROSA STOP eYFP^{+/+} locus even following Western diet feeding for 18 weeks based on the absence of eYFP signal in BCA sections. 10µm thick section immunostained for DAPI (blue), ACTA2 (red), and eYFP (green) (*n*=3). Scale bar = 50µm. (b) Flow cytometry of blood samples from 18 week WD fed SMC eYFP^{+/+} *ApoE*^{-/-} mice treated with tamoxifen have no detectable eYFP⁺ cells (*n*=3).

a

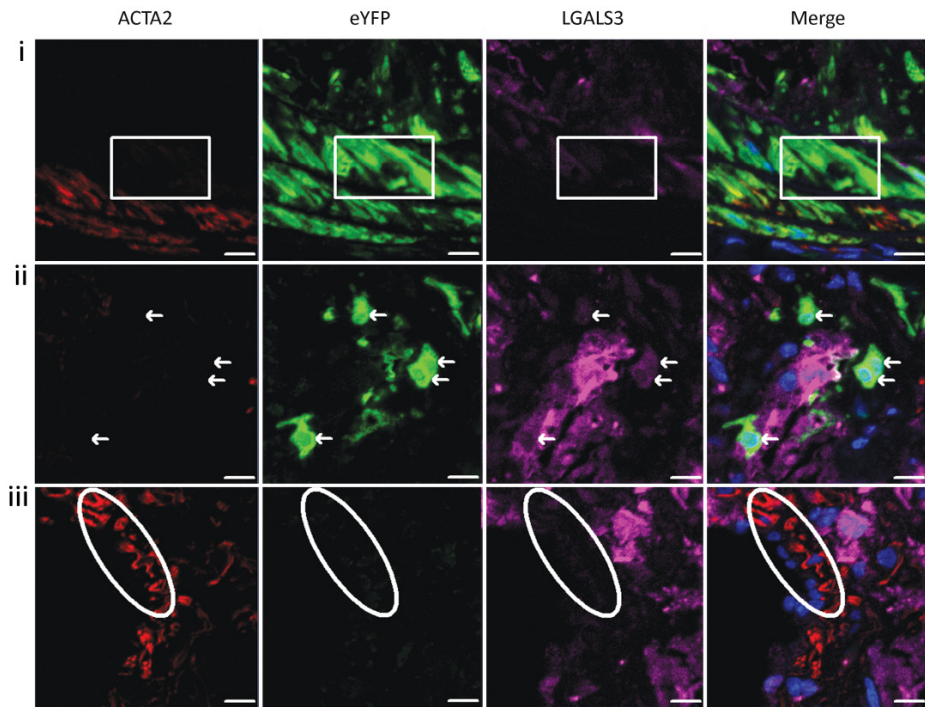
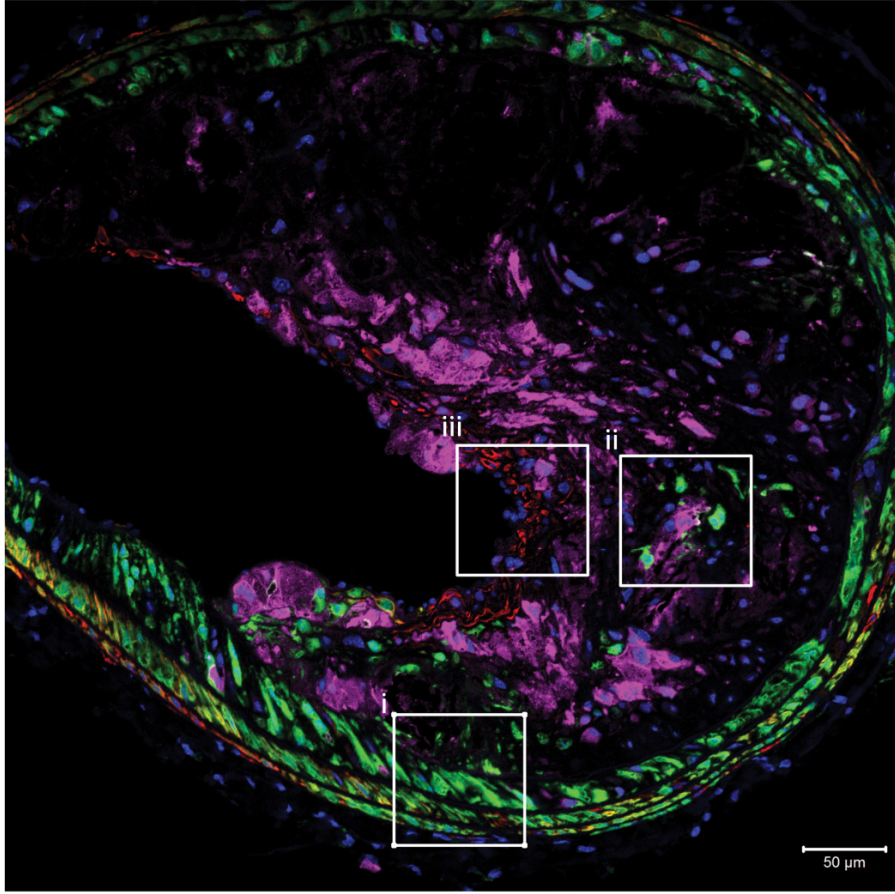


b



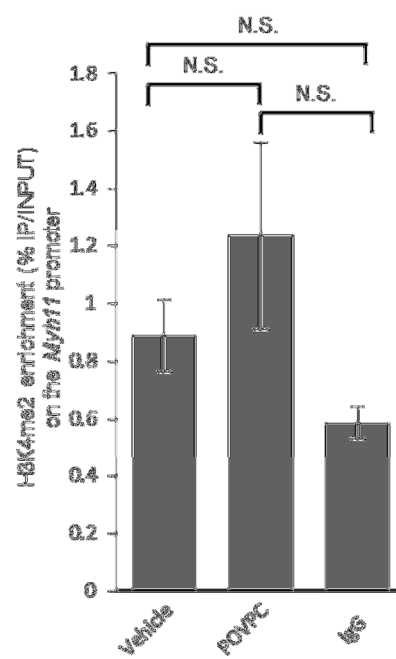
Supplemental Figure 17: SMC lineage tracing studies provide evidence for large populations of phenotypically modulated SMCs within brachiocephalic arteries (BCA) of 18 Week Western diet fed SMC eYFP^{+/+} Apoe^{-/-} mice that cannot be identified using conventional SMC marker genes including some of which have activated multiple markers of macrophages.

10µm paraffin sections from the BCAs from SMC eYFP^{+/+} Apoe^{-/-} mice that had been injected with tamoxifen and placed on Western diet for 18 weeks as described in Methods. Results show that differentiated SMC present at the time of tamoxifen injection (eYFP⁺) subsequently give rise to multiple phenotypes including: (i) phenotypically modulated SMCs (eYFP⁺ ACTA2⁻ cells highlighted in white rectangle), and (ii) phenotypically modulated macrophage-like SMCs (eYFP⁺ ACTA2⁻ LGALS3⁺) (marked by white arrows). Also revealed was a population of ACTA2⁺eYFP⁻ cells near the fibrous cap (as seen in ellipse) believed to be an alternative source of fibrous cap SMCs (iii). Scale bar represents 50µm for the larger panel and 10µm for the smaller panels.



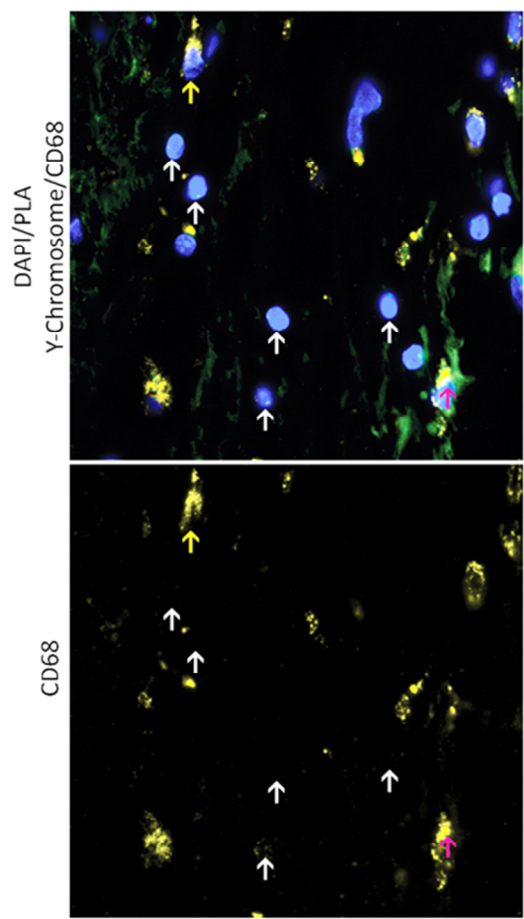
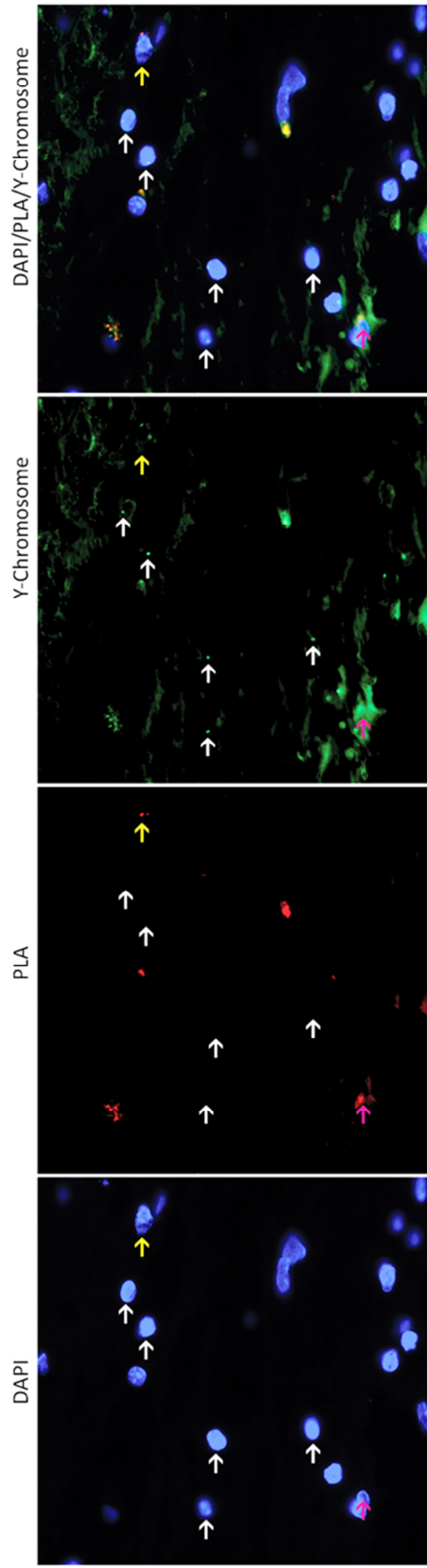
Supplemental Figure 18: Mouse macrophages do not acquire the H3K4dime mark on the Myh11 promoter when treated with the oxidized phospholipid POVPC.

RAW264.7 mouse macrophage cells were treated with 10 µg/mL of POVPC or vehicle for 24 hours. Chromatin was harvested from these cells for CHIP analysis of the *Myh11* H3K4dime mark showed that mouse macrophages lack this mark with or without POVPC treatment. Statistics were then performed using two-way ANOVA with a Tukey post-test. * $P < 0.05$. Data represent mean ± SEM.



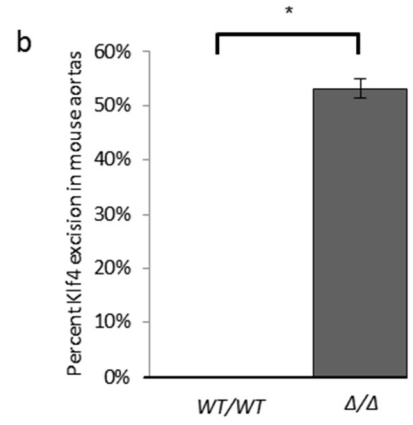
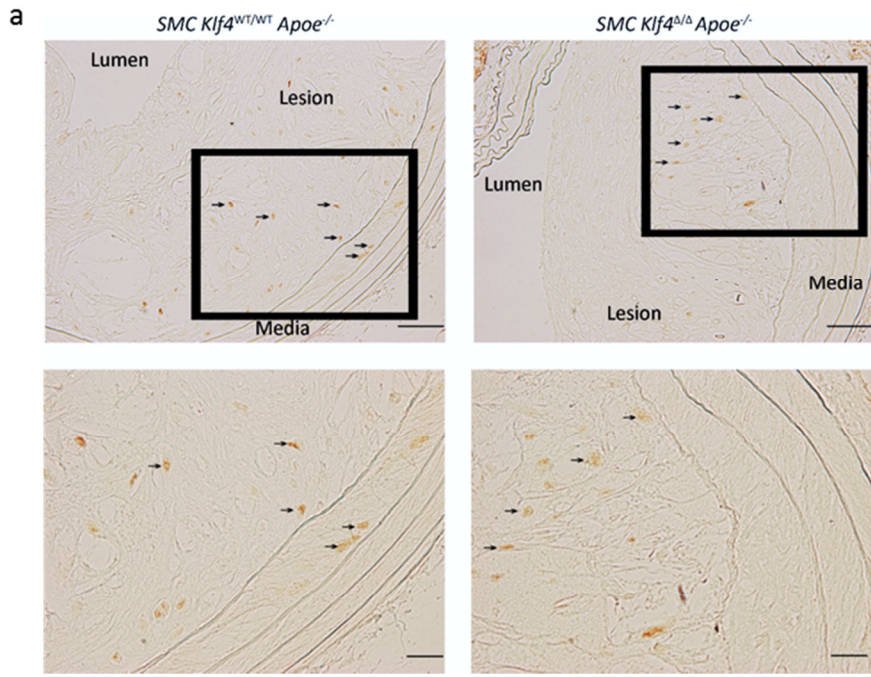
Supplemental Figure 19: Combinatorial epigenetic SMC and Y chromosome lineage tracing analyses of cross gender heart transplant samples provides further evidence for SMC-derived macrophage-like samples in advanced atherosclerotic lesions of human coronary artery samples.

Coronary artery specimens from a male patient who received a female heart were processed for simultaneous *MYH11* H3K4dime PLA epigenetic analyses to identify phenotypically modulated SMC, Y-chromosome FISH to detect cells of hematopoietic origin (i.e. derived from the male heart transplant recipient), and CD68 staining (yellow). Results showed numerous cells within coronary artery lesions which were *MYH11* H3K4dime PLA+ Y-chromosome – and CD68+ (yellow arrows) reflecting a SMC-derived macrophage-like cell that is not of hematopoietic origin. In contrast, macrophages of hematopoietic origin are *MYH11* H3K4dime PLA- Y-chromosome+ CD68+ (red arrows). In no case did we see *MYH11* PLA+ cells that were also Y-chromosome+ thus further validating the SMC specificity of the *MYH11* H3K4dime epigenetic mark and that it is not activated in hematopoietic cells within the context of advanced human atherosclerotic lesions.



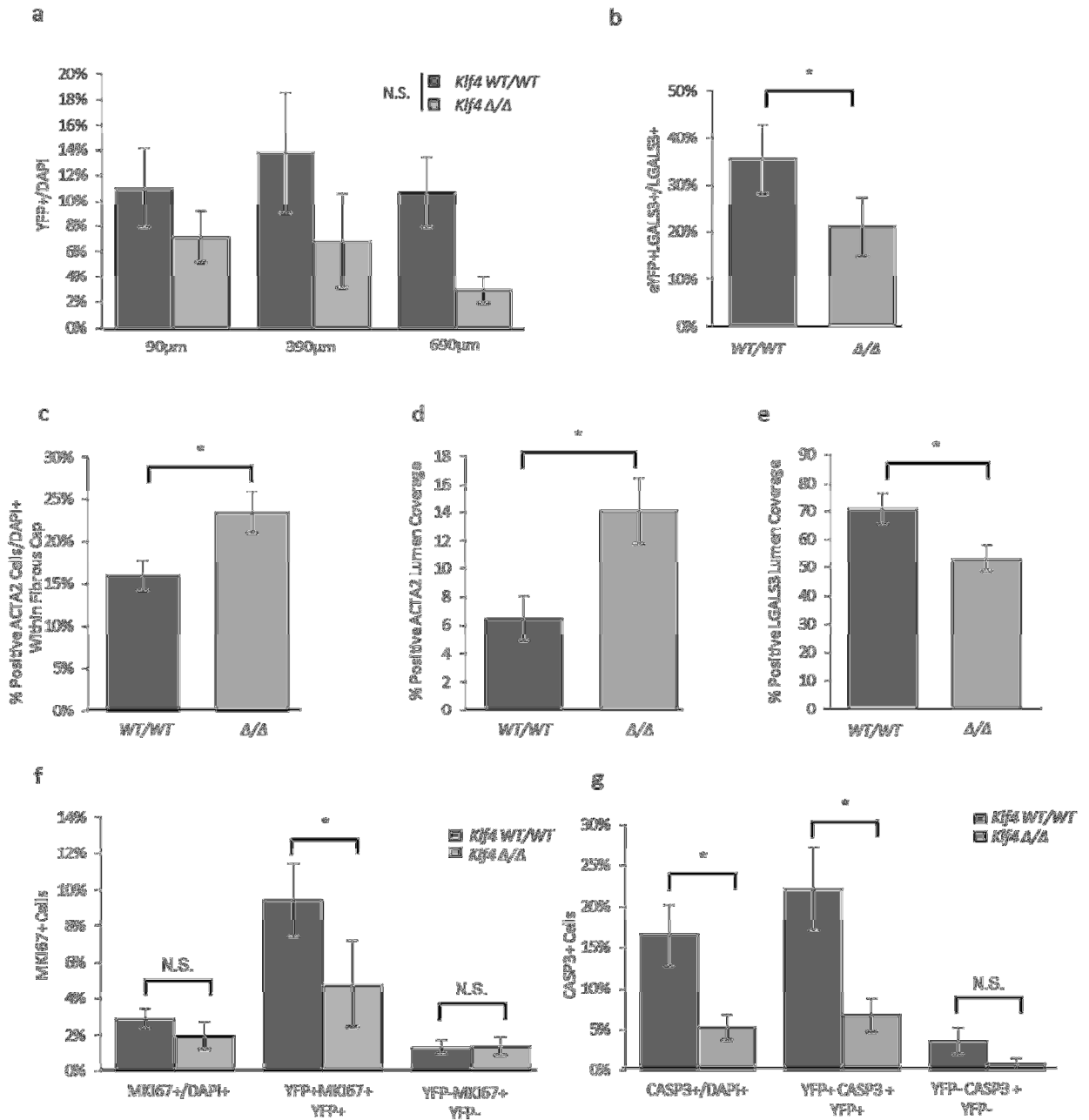
Supplemental Figure 20: Tamoxifen treatment between 6-8 weeks of age induced high efficiency SMC-specific recombination of the floxed *Klf4* gene locus.

(a) Immunohistochemical stain for KLF4 demonstrates efficient recombination of KLF4 selectively in the SMC-containing medial layer. (b) Genotyping PCR of thoracic aortas shows complete lack of the KLF4 excision product in the SMC *Klf4^{wt/wt} Apoe^{-/-}* control mice ($n=10$) and greater than 50% recombination in the tamoxifen treated SMC *Klf4^{Δ/Δ} Apoe^{-/-}* mice ($n=11$). Based on flow cytometric results showing that these aortic preparations used in genotyping contain approximately 50-60% SMC versus non-SMC (Supplemental Fig. 15b), results indicate virtually 100% recombination in SMC. *P*-values based on two-way student's t-test. * $P<0.05$. Data represent mean \pm SEM.



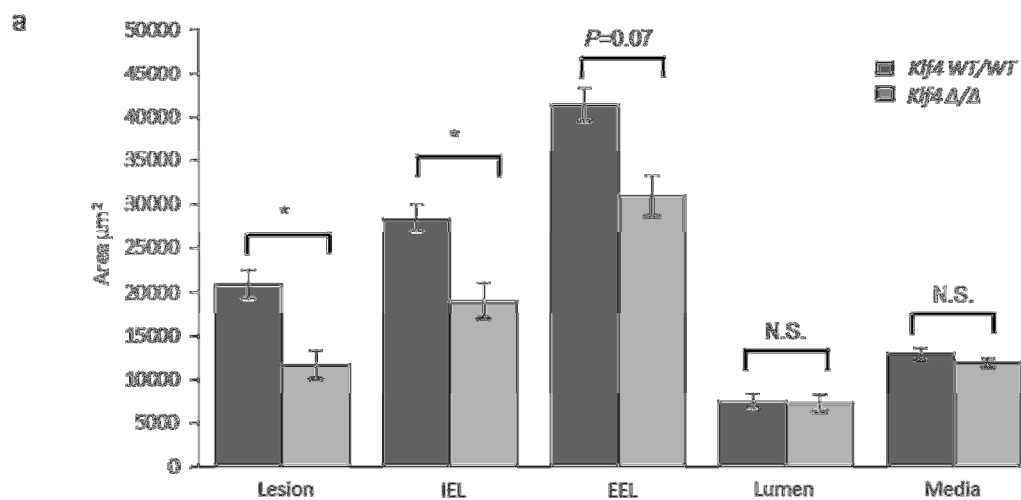
Supplemental Figure 21: Smooth muscle cell specific KLF4 knockout SMC eYFP^{+/+} Apoe^{-/-} mice exhibited marked changes in the cellular composition of plaques.

Analysis of the cellular composition of atherosclerotic lesions from BCAs of 18 week Western diet fed SMC *Klf4*^{wt/wt} eYFP^{+/+} *Apoe*^{-/-} and SMC *Klf4*^{Δ/Δ} eYFP^{+/+} *Apoe*^{-/-} mice showed the following: (a) No difference in total SMC content (YFP+ cells) within the atherosclerotic plaque, (b) a decrease in the percentage of macrophages derived from SMCs (eYFP+ LGALS3+/LGALS3+), (c) an increase in the number of ACTA2+ cells in the fibrous cap region, as defined by the region within 30 μm of the lumen, is increased, (d) and an increase in ACTA2+ cells lining the lumen (as defined by cells in the lesion that are in direct contact with the lumen). (e) There is also a decrease in LGALS3+ cells lining the lumen (as defined by cells in the lesion that are in direct contact with the lumen). The lesions also show decreases in (f) proliferating SMCs (eYFP+ MKI67+), and (g) apoptosing SMCs (eYFP+ CASP3+) within atherosclerotic lesions of SMC specific KLF4 knockout animals. Quantification is based on five 71415 μm² regions in each of three sections per mouse spanning a 600 μm length of the brachiocephalic artery. SMC *Klf4*^{wt/wt} eYFP^{+/+} *Apoe*^{-/-} *n*= 11, SMC *Klf4*^{Δ/Δ} eYFP^{+/+} *Apoe*^{-/-} *n*=8. *P*-values based on two-way ANOVA statistical test with Tukey post-test. * *P* <0.05. Data represent mean±SEM.



Supplemental Figure 22: SMC specific KLF4 knockout decreases lesion size without affecting overall body weight or cholesterol levels.

Modified Russell-Movat pentachrome (Movat) staining was performed for morphometric analysis of paraffin embedded BCAs from SMC $Klf4^{WT/WT}$ eYFP^{+/+} $ApoE^{-/-}$ and SMC $Klf4^{\Delta/\Delta}$ eYFP^{+/+} $ApoE^{-/-}$ mice using ImagePro Plus v7.0. (a) SMC $Klf4^{\Delta/\Delta}$ eYFP^{+/+} $ApoE^{-/-}$ mice had decreased lesion area, and interelastic lamina area (IEL), but no changes in external elastic lamina area (EEL), lumen area or medial area as compared to SMC $Klf4^{wt/wt}$ eYFP^{+/+} $ApoE^{-/-}$ control animals. (b) Blood work revealed no changes in triglycerides or total cholesterol levels, and there were no statistical differences between total body weight, spleen (% of body weight), or heart weight (% of body weight). *P*-values based on two-way ANOVA statistical test. * *P*<0.05. Data represent mean±SEM.

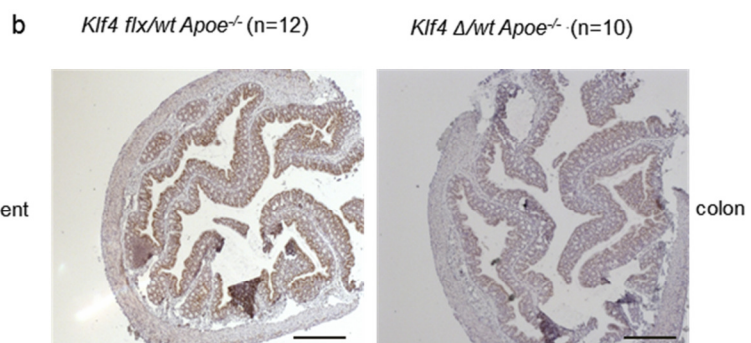
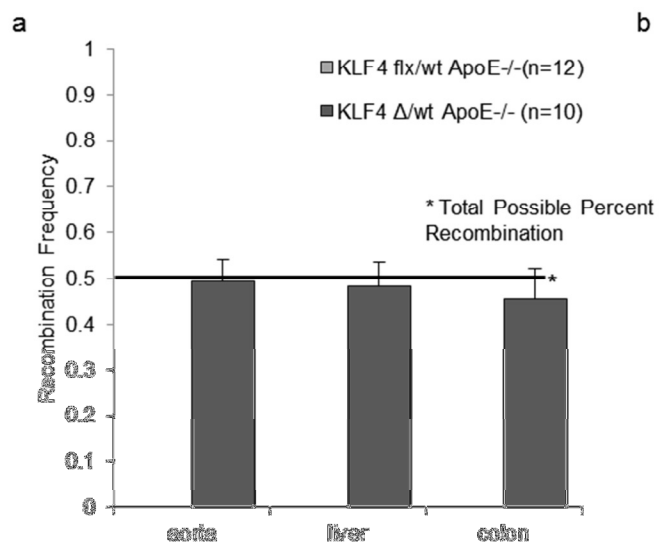


b

	N.S.		N.S.	
	<i>Klf4</i> ^{WT/WT} <i>ApoE</i> ^{-/-} (n=8)	<i>Klf4</i> ^{Δ/Δ} <i>ApoE</i> ^{-/-} (n=6)	<i>Klf4</i> ^{WT/WT} <i>YFP</i> ^{-/-} <i>ApoE</i> ^{-/-} (n=26)	<i>Klf4</i> ^{Δ/Δ} <i>YFP</i> ^{-/-} <i>ApoE</i> ^{-/-} (n=20)
Total Cholesterol, mg/dL	1094 \pm 257	613 \pm 256	N.D.	N.D.
Triglycerides, mg/dL	183 \pm 28	178 \pm 54	N.D.	N.D.
Body weight, g	32.9 \pm 2.3	35.3 \pm 2.2	39.5 \pm 1.6	42.6 \pm 1.5
Heart weight, % body weight	0.49 \pm 0.03	0.60 \pm 0.06	0.51 \pm 0.02	0.49 \pm 0.03
Spleen weight, % body weight	2.52 \pm 0.72	4.36 \pm 1.25	1.60 \pm 0.19	2.03 \pm 0.26

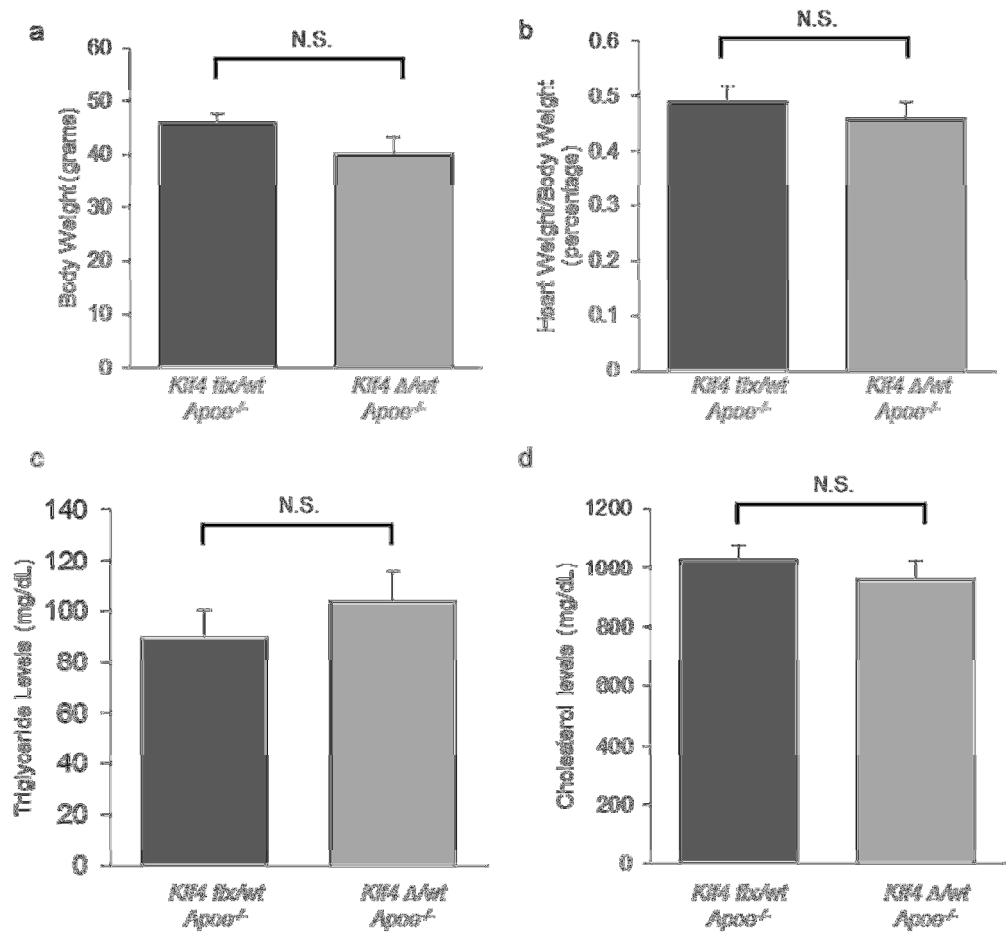
Supplemental Figure 23: Confirmation of global conditional knockout of one *Klf4* allele as assessed by PCR and immunohistochemical analysis.

ERT Cre⁻ and ERT Cre⁺ *Klf4*^{flx/wt} *Apoe*^{-/-} mice were treated with tamoxifen for ten days to recombine the *Klf4* floxed allele in mice containing ERT Cre. (a) PCR genotyping for the KLF4 excised band reveals 50% KLF4 recombination in aorta, liver, and colons, indicating a near 100% recombination of the single floxed allele. Data represent mean±SEM. (b) Sections from paraffin embedded colons showed decreased KLF4, as detected by immunohistochemistry, in ERT Cre⁺ tamoxifen treated *Klf4*^{flx/wt} *Apoe*^{-/-} mice compared to their ERT Cre⁻ littermates.



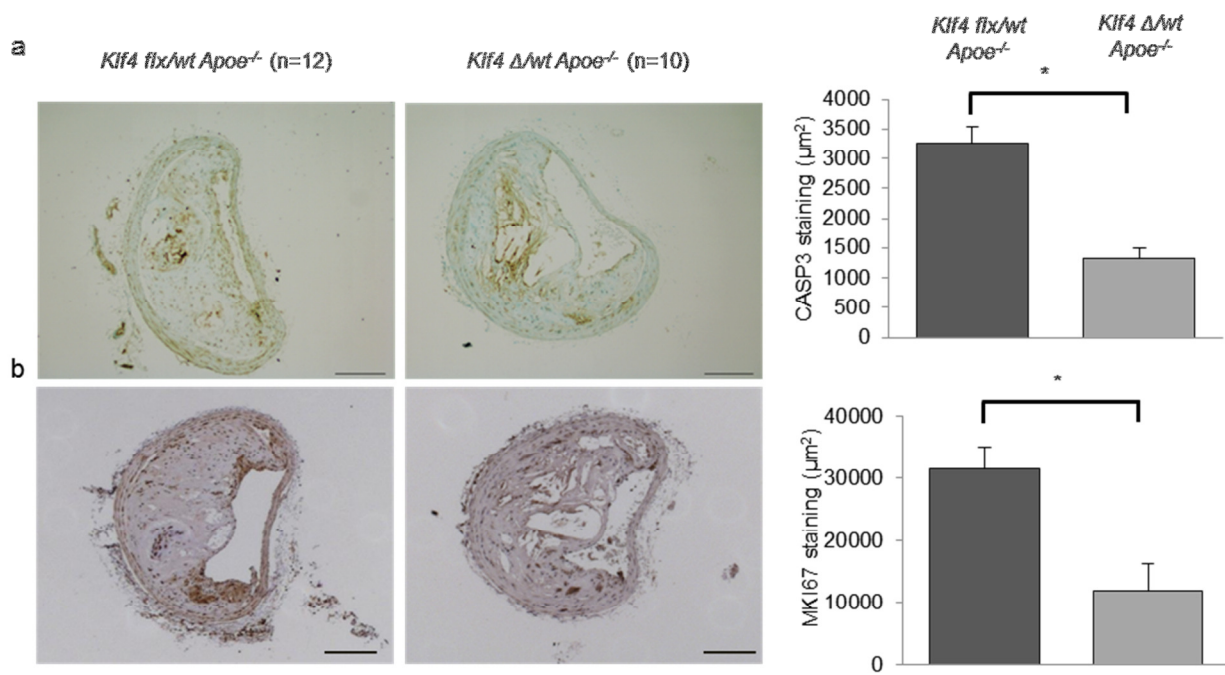
Supplemental Figure 24: Global conditional knockout of one *Klf4* allele does not affect overall body weight or cholesterol levels.

ERT Cre+ *Klf4*^{flx/wt} *ApoE*^{-/-} tamoxifen treated mice and their ERT Cre- littermate controls were placed on Western diet for 25 weeks immediately following tamoxifen treatment. At time of euthanasia, there were no statistical differences in (a) total body weight, (b) heart weight (%body weight), (c) triglycerides, or (d) cholesterol levels between the ERT Cre+ *Klf4*^{Δ/wt} *ApoE*^{-/-} (n=10) and ERT Cre- *Klf4*^{flx/wt} *ApoE*^{-/-} (n=12) mice. *P*-values based on two-way student's t-test. Data represent mean±SEM.



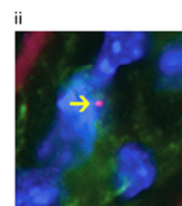
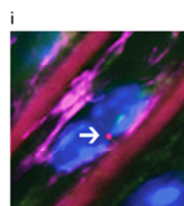
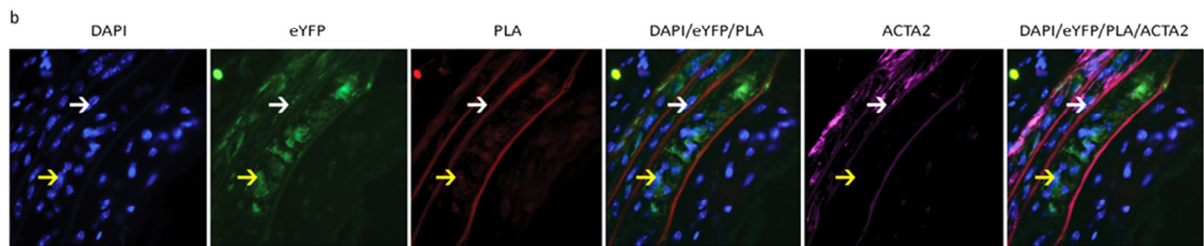
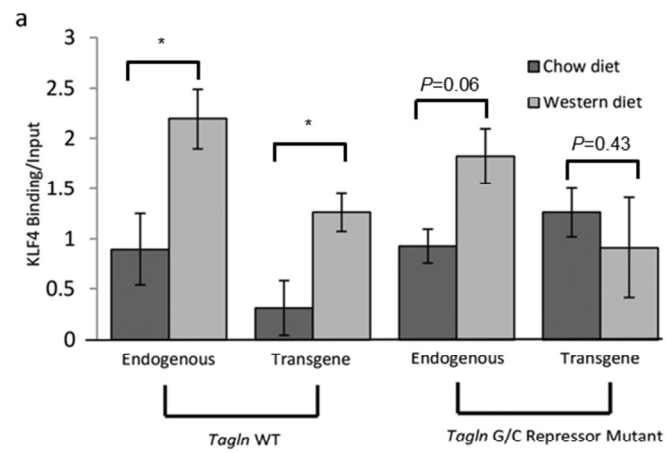
Supplemental Figure 25: Global conditional knockout of one Klf4 allele decreased cellular proliferation and apoptosis.

ERT Cre⁺ *Klf4*^{flx/wt} *ApoE*^{-/-} tamoxifen treated mice and their ERT Cre⁻ littermate controls were placed on Western diet for 25 weeks immediately following tamoxifen treatment. 5µm paraffin sections from the BCAs were then analyzed for indices of plaque stability by immunohistochemistry. ERT Cre⁺ *Klf4*^{Δ/wt} *ApoE*^{-/-} mice demonstrated indices of more stable atherosclerotic plaques including: (a) decreased apoptosis (CASP3 staining) and (b) decreased proliferation (MKI67 staining) compared to their ERT Cre⁻ *Klf4*^{flx/wt} *ApoE*^{-/-} littermate controls. ERT Cre⁺ *Klf4*^{Δ/wt} *ApoE*^{-/-} (n=10) and ERT Cre⁻ *Klf4*^{flx/wt} *ApoE*^{-/-} (n=12). * *P* <0.05. *P*-values are based on Fisher's Exact test. Data represent mean±SEM.



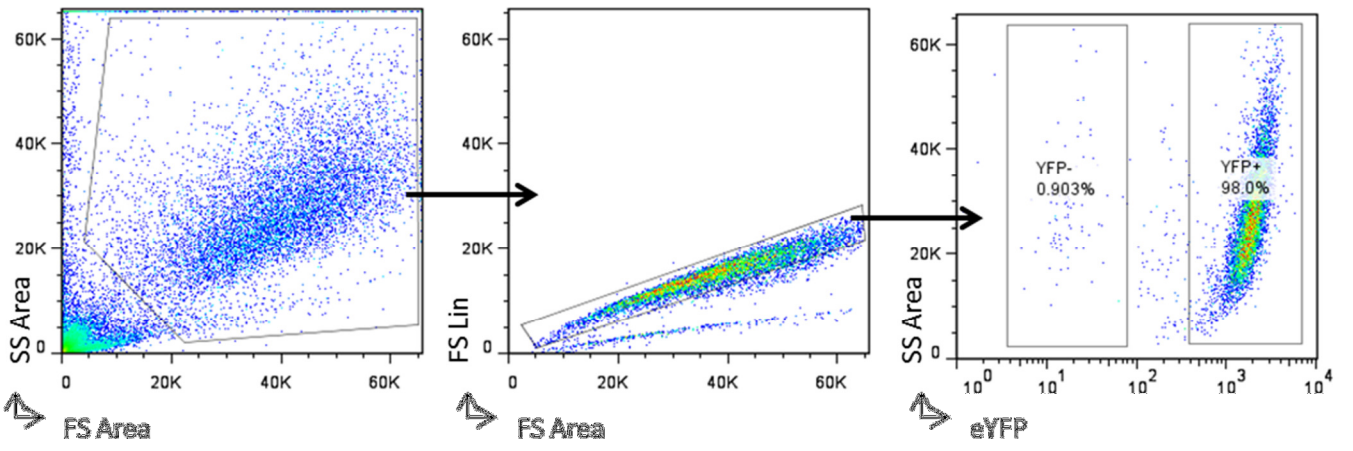
Supplemental Figure 26: KLF4 binds to the *Tagln* promoter in response to Western diet treatment is dependent on the GC repressor element.

(a) *Apoe*^{-/-} mice crossed to either a *Tagln* wild type (WT) transgene or *Tagln* G/C repressor mutant transgene to assess the importance of the G/C repressor element on KLF4 binding to SMC marker genes. At the end of 18 weeks of a high-fat or chow diet, BCAs were snap frozen in liquid nitrogen for *in vivo* ChIP analysis. Western diet treatment caused KLF4 enrichment on both the endogenous and transgene WT promoters, as well as the endogenous *Tagln* promoter in the *Tagln* G/C repressor mutant mice. There was no KLF4 enrichment in response to Western diet on the *Tagln* G/C repressor mutant transgene compared to chow diet fed animals as assessed by *in vivo* ChIP assay of the BCA region. *P*-values based on two-way ANOVA with Tukey post-test. **P*<0.05. Data represent mean±SEM. (b) KLF4 binding to the G/C repressor element of the *Tagln* promoter *in vivo* was established using *Tagln* ISH-PLA. The white arrow indicates a cell where KLF4 is actively binding to the *Tagln* promoter of a differentiated SMC (i), while the yellow arrow identifies a phenotypically modulated SMC (ii).



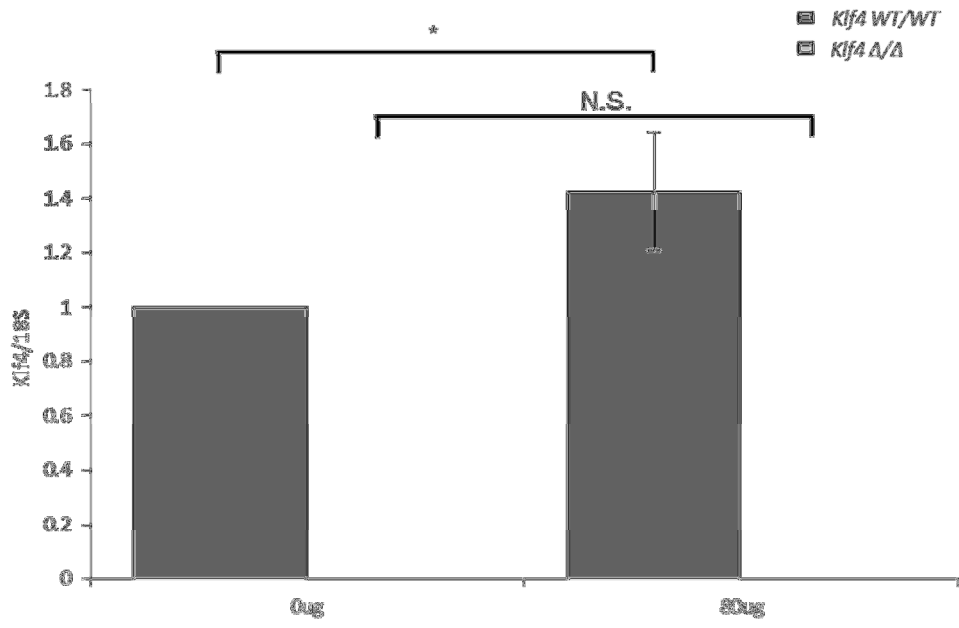
Supplemental Figure 27: Cultured aortic SMCs from SMC YFP^{+/+} ApoE^{-/-} mice are 98% pure by flow cytometry.

Primary aortic SMCs isolated from SMC-lineage tracing mice were run on a CyAn ADP flow cytometer to check for eYFP expression. After a forward/side scatter gate, and gating for singlets, the cultured cells are analyzed for eYFP.



Supplemental Figure 28: Pure aortic SMCs from SMC YFP^{+/+} Klf4^{Δ/Δ} mice do not express KLF4 when exposed to water soluble cholesterol.

Primary aortic SMCs were isolated from SMC YFP^{+/+} Klf4^{fl/fl} or SMC YFP^{+/+} Klf4^{WT/WT} mice that had been treated with tamoxifen (Klf4^{Δ/Δ} and Klf4^{WT/WT} respectively). Cells were sorted using a FACSVantage SE DIVA to ensure a pure SMC (eYFP+) cell population. Klf4^{Δ/Δ} and Klf4^{WT/WT} cells were then treated with either 0 or 80 μg/mL water soluble cholesterol to check for Klf4 expression. n=3. *P*-values based on two-way ANOVA with Tukey post-test. **P*<0.05. Data represent mean±SEM.



Supplemental Table 2: Quantification of immunofluorescent stained slides from 18 week WD fed SMC eYFP^{+/+} *ApoE*^{-/-} mouse lesions reveal new SMC populations.

Cells stained with markers for nuclei (DAPI), traditional SMC marker (ACTA2), lineage tracing mark (eYFP), and macrophage marker (LGALS3), were counted in five 71415 μm^2 regions in each of three sections per mouse spanning a 600 μm length of the brachiocephalic artery. (a) Cell counts normalized to area counted. (b) Cell counts expressed as subpopulations of other cell types. $n=10$.

a

Average Cell Counts Within Atherosclerotic Lesions (71415 μm^2)	Absolute Cell Count	Std Err
DAPI+	208.24	± 12.36
eYFP+	68.95	± 10.13
LGALS3+	62.43	± 4.60
eYFP+ LGALS3+	14.86	± 2.82
ACTA2+	12.05	± 2.14
eYFP+ACTA2+	8.71	± 1.85
LGALS3+ACTA2+	1.10	± 0.45
eYFP+LGALS3+ACTA2+	0.76	± 0.42

b

Populations of Interest Within Atherosclerotic Lesions	Percent of Population	Std Err
eYFP+/DAPI+	31.37%	$\pm 3.32\%$
LGALS3+/DAPI+	31.90%	$\pm 2.91\%$
ACTA2+/DAPI+	5.78%	$\pm 0.91\%$
eYFP+LGALS3+/LGALS3+	22.82%	$\pm 3.83\%$
eYFP+LGALS3+/eYFP+	22.72%	$\pm 3.43\%$
eYFP+LGALS3+/DAPI+	6.65%	$\pm 1.01\%$
eYFP-ACTA2+/DAPI+	1.83%	$\pm 0.42\%$
eYFP+ACTA2-LGALS3-/eYFP+	64.95%	$\pm 3.14\%$
eYFP+ACTA2-/eYFP+	86.87%	$\pm 2.53\%$
eYFP+ACTA2-/DAPI+	27.11%	$\pm 3.09\%$

Chapter 4: The pluripotency factor Oct4 modulates blood vessel remodeling in atherosclerotic lesions

Authors: Olga A. Cherepanova, Laura S. Shankman, Delphine Gomez, Olga F. Sarmiento, Melissa H. Bevard, Elizabeth S. Greene, Meera Murgai, Alexey Tomilin, and Gary K. Owens.

Adapted from manuscript submission to *Nature*

Abstract

Octamer-binding transcriptional factor 4A (Oct4) is a protein that regulates embryonic stem cell (ESC) totipotency^{162, 163} and is the only gene thought to be indispensable for production of induced pluripotent stem (iPS) cells^{96, 97}. Although there is evidence that Oct4 may be expressed in non-ESC, this evidence is controversial and as yet there is no direct evidence that Oct4 plays a functional role within somatic cells (reviewed in *Lengner, C.J. et al.*⁹⁹).

Here we provide evidence that Oct4 is markedly induced in cells within atherosclerotic lesions from *ApoE*^{-/-} mice fed a high-fat diet as well as within human coronary artery atherosclerotic lesions. We show that smooth muscle cell (SMC)-specific conditional knockout (KO) of *Oct4* within Western diet-fed *ApoE*^{-/-} mice resulted in marked alterations in the size of atherosclerotic lesions and in multiple properties consistent with decreased plaque stability including increased necrotic core area and intraplaque hemorrhage as well as decreased *Acta2* (SM α -actin) and increased *Lgals3* (Mac2) fibrous cap coverage. In addition, using a novel SMC lineage tracing mouse developed in our lab¹⁴⁴, we also show that lesions from SMC-specific conditional *Oct4* KO mice contained far fewer de-differentiated (*Acta2*-) SMC likely as the result of impaired SMC migration from the media into the intima and not to altered proliferation or apoptosis. Further mechanistic studies showed that migration of cultured SMC was Oct4-dependent. We also show that activation of *Oct4* in cultured cells was dependent on *Klf4* and *Hif1 α* , and we demonstrate that these factors bind to the *Oct4*

promoter based on CHIP assays on lesion specimens. These results are the first to show that Oct4 plays a direct functional role in regulating phenotypic transitions in somatic cells, and provide a foundation for future studies investigating the role of Oct4 in the pathogenesis of multiple vascular diseases.

Introduction

The pluripotency gene *Oct4* (*octamer-binding transcriptional factor 4*, also known as *Pou5f1* and *Oct3/4*) was believed to be permanently epigenetically silenced in adult somatic cells¹⁶⁴. However, recent evidence suggests that *Oct4* may be activated in cultured pulmonary artery SMCs exposed to chronic hypoxia¹⁶⁵, some somatic cells⁹⁹ and tumor cells^{166, 167}. As reviewed by *Lengner, C.J. et al.*¹⁶⁴ the evidence that *Oct4* is expressed in somatic cells is highly controversial, due to possible antibody cross-reactivity with other non-pluripotent *Oct4* isoforms (*Oct3/4b* and *Oct3/4c* in mouse and *OCTB* and *OCTB1* in human)^{168, 169}, possible detection of *Oct4* pseudogenes, extraordinarily low expression levels¹⁷⁰, and/or lack of appropriate controls (e.g., *Oct4* genetic knockout (KO) cells). Moreover, there is no evidence that *Oct4* has any functional effects within these cells. Indeed, *Lengner, C.J. et al.*⁹⁹ showed that conditional *Oct4* KO mice had no observed functional defects or alterations in tissue regeneration following skin injury, partial hepatectomy, irradiation exposure, or bone marrow transplantation. As such, the most conservative and authoritative data at this time indicate that *Oct4* is stably silenced in adult somatic cells and is dispensable for proliferation and phenotypic transitions of somatic cells, as well as adult tissue regeneration and self-renewal of somatic stem cells. Consistent with the idea that *Oct4* may be exclusively expressed and function within ESC, Yamanaka and co-authors⁹⁷ have shown that *Oct4* is essential for reprogramming of somatic cells into induced pluripotential stem (iPS) cells. That

is, whereas other iPS cell pluripotency genes such as Sox2, c-myc, and Klf4 can be substituted with other ESC pluripotency genes, Oct4 is indispensable.

Of interest, we and others have previously shown that following vascular injury, or during development of atherosclerosis, vascular SMC undergo a de-differentiation or phenotypic switching process that is characterized by loss of expression of SMC specific marker genes such as *Acta2* and SM myosin heavy chain (*Myh11*) coincident with increased cell proliferation, migration, and production of extracellular matrix⁵. Indeed, this process, is believed to have evolved to enable blood vessels in mature animals to repair and remodel, and has been implicated in playing a critical role in a number of major human diseases including atherosclerosis, hypertension, asthma, tumor angiogenesis, and aneurysms that in aggregate account for greater than 40% of all deaths in developed societies¹⁴². For example, during development of atherosclerosis SMC within the media are believed to undergo phenotypic switching, and migration into the intima where they undergo proliferation and production of extracellular matrix components thought to be critical in determining plaque size and the probability of plaque rupture^{142, 171}. As such, there has been tremendous interest in identifying mechanisms and factors that regulate SMC phenotypic transitions. Of major interest, we^{28, 40, 89} and others¹⁶¹ have provided evidence that the iPS cell pluripotency gene Klf4 plays a key role in regulating SMC phenotypic switching both *in vitro* and *in vivo*. However, as yet no studies have tested if other iPS/ESC pluripotency factors are required.

Materials and Methods

Mice

Animal protocols were approved by the University of Virginia Animal Care and Use Committee. *Oct4^{Flox/Flox}* (*Pou5f1^{tm1Scho}*) mice were generously provided by H. Schöler (Max Planck Institute, Germany) and *Myh11-CreER^{T2}* (*Tg(Myh11-cre/ER^{T2})1Soff*) mice by S. Offermanns (Max Planck Institute, Germany).

Oct4^{Flox/Flox} mice were bred with *Myh11-CreER^{T2}* mice to generate *Oct4^{Flox/WT}Myh11-CreER^{T2}* mice. The *Myh11-CreER^{T2}* transgene is located on the Y-chromosome thus preventing use of Cre-negative mice as controls since these all are females. Therefore, we bred *Oct4^{Flox/WT}; Myh11-CreER^{T2}* males with *Oct4^{Flox/WT}* females to generate a cohort of experimental *Oct4^{Flox/Flox};Myh11-CreER^{T2}* and control *Oct4^{WT/WT};Myh11-CreER^{T2}* male littermate mice. Conditional *Oct4* mice and *Myh11-CreER^{T2}* mice were genotyped as described previously^{21, 162}. *Oct4^{Flox/Flox};Myh11-CreER^{T2}* mice were then crossed with *ApoE^{-/-}* mice (B6.129P2-*ApoE^{tm1Unc}/J*, #002052; Jackson Laboratory) to generate *Oct4^{Flox/WT};Myh11-CreER^{T2};ApoE^{-/-}* males and *Oct4^{Flox/WT};ApoE^{-/-}* females that we used as breeders to generate experimental littermate mice.

ROSA26-STOP^{Flox}eYFP^{+/+} mice (B6.129X1-*GT(ROSA)26Sor^{tm1(EYFP)Cos}/J*, #006148; Jackson Laboratory) were crossed with *ApoE^{-/-}* mice and *Myh11-CreER^{T2}* mice to generate *ROSA26-STOP^{Flox}eYFP^{+/+};Myh11-CreER^{T2};ApoE^{-/-}* mice using the same strategy as was described for *Oct4* mice above. *Oct4^{Flox/Flox}; Myh11-CreER^{T2}; ApoE^{-/-}* mice were then crossed with *ROSA26-*

STOP^{Flox}eYFP^{+/+};Myh11-CreER^{T2};ApoE^{-/-} mice to generate *Oct4^{Flox/WT};ROSA26-STOP^{Flox}eYFP^{+/+};Myh11-CreER^{T2};ApoE^{-/-}* males and *Oct4^{Flox/WT};ROSA26-STOP^{Flox}eYFP^{+/+};ApoE^{-/-}* females that we used as breeders to get experimental littermate mice. *ROSA26-Stop^{Flox}eYFP* mice were genotyped as previously described¹⁴⁴.

Activation of Cre-recombinase was achieved through eight intraperitoneal injections of tamoxifen (Sigma-Aldrich) (1 mg in 100 μ L peanut oil [Sigma-Aldrich]) starting 5-6 weeks of age.

Animal diet feeding

Oct4 ^{Δ/Δ} ;Myh11-CreER^{T2};ApoE^{-/-} or *Oct4 ^{Δ/Δ} ;ROSA26-STOP^{Flox}eYFP^{+/+};Myh11-CreER^{T2};ApoE^{-/-}* and control *Oct4^{WT/WT};Myh11-CreER^{T2};ApoE^{-/-}* or *Oct4^{WT/WT};ROSA26-STOP^{Flox}eYFP^{+/+};Myh11-CreER^{T2};ApoE^{-/-}* male mice were fed a high-fat (Western type) diet containing 21% milk fat and 0.15% cholesterol (TD.88137, Harlan Teklad) for 18 weeks starting 7-8 weeks of age. All mice were euthanized after a 4-hour fast, and blood plasma was collected. Brachiocephalic artery region (region from the aortic arch to the middle of the left carotid artery) were harvested, fixed in 4% paraformaldehyde and paraffin-embedded. Brachiocephalic arteries were sectioned at 10 μ m (mice with *ROSA26-STOP^{Flox}eYFP*) or 5 μ m thickness from the aortic arch to the right subclavian artery. Morphometric and immunohistochemical analyses were performed using 2-4 sections per artery. Assays for determining total plasma

cholesterol and triglyceride levels (Abbott Laboratories) were performed by the University of Virginia Clinical Pathology Laboratory.

Carotid ligation injury

Carotid artery ligation injury was performed in *Oct4^{Δ/Δ};Myh11-CreER^{T2}* and control *Oct4^{WT/WT};Myh11-CreER^{T2}* as described previously^{89, 172}. The right carotid artery was completely ligated proximal to the carotid bifurcation. The left carotid artery served as an uninjured control. The right and left carotid arteries were harvested 21 days after injury and fixed in 4% paraformaldehyde. Paraffin-embedded carotids were sectioned at 5 μm thickness from the ligature to the aortic arch. Morphometric and immunohistochemical analyses were performed using 3-4 sections per artery.

Aortic explants

Aortic explants were isolated from *Oct4^{WT/WT}SMC-eYFP^{+/+}* or *Oct4^{Δ/Δ}SMC-eYFP^{+/+}* mice following tamoxifen injections. Briefly, aortas were harvested, perivascular fat removed, and aortas digested in 1 mg mL⁻¹ collagenase II, 0.744 U mL⁻¹ elastase and 1 mg mL⁻¹ Soybean Trypsin inhibitor (all reagents from Worthington Biochemical Corp.) in Hank's balanced salt solution for 10 minutes. Following digestion the adventitia was carefully removed and the intimal surface was gently washed with PBS. Aortas were cut into ~3 mm pieces and placed on plastic chamber slides. Aortic explants were then grown and maintained in 20%

serum-containing media (DMEM/F12 [Gibco], fetal bovine serum [Hyclone], 100 U mL⁻¹ penicillin/streptomycin [Gibco], 1.6 mM L⁻¹ L-glutamine [Gibco]). After 2 weeks aortic explants were stained with antibodies for eYFP/eGFP (Abcam, ab6673).

Immunohistochemical and morphometric analyses

Modified Russell-Movat (Movat) staining was performed for morphometric analysis of carotid and brachiocephalic arteries. The areas within the external and internal elastic lamina, lesion, lumen and media areas were measured directly from the digitized images. Necrotic area analysis was performed independently by O.A.C, M.M. and L.S.G. PicroSirius red staining was performed for analysis of collagen content by measuring birefringence to plane-polarized light. Immunohistochemistry (IH) was performed with antibodies for Oct4-biotin (clone C10, Santa-Cruz Biotechnology Inc.), Acta2-biotin (clone1A4, Santa Cruz Biotechnology Inc.), Lgals3 (clone M3/38, Accurate Chemical), Ter119 (rat anti-mouse, Santa-Cruz Biotechnology Inc.). Staining for IH was visualized by DAB (Acros Organics). Images were acquired with Zeiss Axioskope2 fitted with an AxioCamMR3 camera. Image acquisition was performed with AxioVision40 V4.6.3.0 software (Carl Zeiss Imaging Solution). Settings were fixed at the beginning of both acquisition and analysis steps and were unchanged. Vessel morphometry and areas of positive immunohistochemical or PicroSirius red

staining were quantified using ImagePro Plus 7.0 software (Media Cybernetics, Inc) as previously described¹⁴⁷.

Immunofluorescence was performed with antibodies for eYFP/eGFP (Abcam, ab6673), Acta2-Cy3 (clone1A4, Sigma-Aldrich), Ki67 (Abcam, ab15580), cleaved caspase-3 (Cell Signaling, 9661S) and sections were counterstained with DAPI. The secondary antibodies were donkey anti-rabbit 647 (Invitrogen, A31573) and donkey anti-goat 488 (Invitrogen, A11055). Incubation with irrelevant species- and isotope-matched IgG was used as a negative control for all immunostaining. Confocal images were acquired using Zeiss LSM700 scanning confocal microscope. Brightness and contrast in Fig. 11f, 12a, Supplemental Fig. 35 and 36 were lightly adjusted uniformly across all images. Numbers of cells were counted in 5 fields (14283 μm^2) per cross-section/per location based on eYFP (eYFP+), cleaved caspase-3 (caspase-3+) or Ki67 (Ki67+) staining normalized to either total number of cells based on DAPI staining or number of eYFP+/eYFP- cells. Analysis of confocal images was completed using Zeiss Zen Lite 2009 software.

Smooth muscle cell culture

Mouse aortic SMCs were isolated from thoracic aortas of 6 week old male C57BL/6 mice or *Oct4*^{WT/WT} and *Oct4* ^{Δ/Δ} mice following tamoxifen injections. Briefly, aortas were harvested, perivascular fat removed, and aortas were digested in 1 mg mL⁻¹ collagenase II, 0.744 U mL⁻¹ elastase and 1 mg mL⁻¹

Soybean Trypsin inhibitor (all reagents from Worthington Biochemical Corp.) in Hank's balanced salt solution for 10 minutes. Following digestion the adventitia was carefully removed and the intimal surface was gently washed with PBS. Aortas were cut into ~0.5 mm pieces and placed in the enzyme solution for ~1 hour. Disaggregated SMCs were then grown and maintained in 20% serum-containing media (DMEM/F12 [Gibco], fetal bovine serum [Hyclone], 100 U mL⁻¹ penicillin/streptomycin [Gibco], 1.6 mM L⁻¹ L-glutamine [Gibco]). After 2 passages SMCs were switched to 10% serum. For experiments with POVPC, cells were grown to 100% confluence and then switched to serum-free media (SFM) (DMEM/F12 [Gibco], 100 U mL⁻¹ penicillin/streptomycin [Gibco], 1.6 mM L⁻¹ L-glutamine [Gibco]). After culturing in SFM for 2 days, passages 5–12 of post-confluent mouse aortic SMCs were treated with DMSO-vehicle or POVPC (Cayman Chemical). siRNA oligonucleotide smart pools specific for Oct4 (ON-TARGETplusSMARTpool, mouse *Pou5f1*, NM_013633) and control non-targeting pool were purchased from Dharmacon (ThermoScientific). The transient transfection of siRNA oligonucleotides was carried out using Oligofectamine (Invitrogen) according to the manufacturer protocol.

RNA isolation, cDNA preparation and quantitative real-time RT-PCR

Total RNA was isolated from cultured cells using Trizol reagent (Invitrogen) according to the manufacturer protocol. Isolated RNA was treated with DNaseI (Invitrogen), and one microgram of RNA was reverse-transcribed

with iScript cDNA synthesis kit (BioRad). Real-time RT-PCR was performed by C1000TM Thermal Cycler CFX96TM (BioRad) using SensiFASTTM SYBR NO-ROX Mix (Bioline) and primers specific for mouse *Pou5f1*, *Mmp3*, *Mmp13*, *Opt*, *Col5a2*, *Col6a2*, *Col15a1* and *18s RNA* (Supplemental Table 3). Expression of the genes was normalized to *18s RNA*.

SMC migration assay

Cell migration assays were performed on HTS Transwell plates containing 8 μm pores (Corning). Briefly, a cell suspension (1×10^5 cells mL^{-1} , 70 μL) of mouse aortic SMC after 1 day of SFM-starvation was added to the upper well in serum-free media containing 0.1% bovine serum albumin (BSA) (Sigma-Aldrich). Concentrations of POVPC from 0 to 10 $\mu\text{g mL}^{-1}$ were added to the bottom chamber in SFM with 0.1% BSA and 5 $\mu\text{g mL}^{-1}$ fibronectin (Sigma-Aldrich). Cells were incubated at 37 °C in CO₂ incubator for 18 hours, fixed in 4% formalin and stained with 0.2% Crystal Violet in 7% ethanol. Upon removing cells from the upper surface of each Transwell, the remaining cells were counted in 8-10 randomly chosen high-power fields (magnification x20).

Chromatin Immunoprecipitation (ChIP) assay

For *in vitro* ChIP mouse aortic SMC treated with 10 $\mu\text{g mL}^{-1}$ POVPC or DMSO-vehicle for 3, 6 or 12 hours were fixed with 1% paraformaldehyde for 10 min at room temperature. For *in vivo* ChIP, mouse aortas (arch, thoracic and

abdominal regions) were quickly dissected from surrounding tissue, washed in ice-cold PBS to remove blood and debris, snapped frozen in liquid nitrogen, and stored at -80°C . Tissues were later ground with a mortar and pestle with liquid nitrogen cooling, transferred directly to 37°C 1% formaldehyde for 10 min. Cross-link was stopped by adding of 125 mM glycine for 10 min. The cross-linked chromatin was sonicated to shear chromatin into fragments of 200-600 base pairs. The sheared chromatin was immunoprecipitated with 2 μg of Klf4 antibodies (Santa-Cruz, sc-20691) or Hif1 α antibodies (Abcam, ab1), while negative control was incubated with control IgG, and immune complex were recovered with magnetic beads (Millipore). Real time RT-PCR was performed using SensiFASTTM SYBR NO-ROX Mix (Bioline) and primers specific for *Oct4* promoter (Supplemental Fig. 42).

Site-Directed Mutagenesis, Luciferase assay

Mouse 1.5 kb *Oct4* promoter was cloned into the pGL3 luciferase plasmid. Site direct mutagenesis of the wild-type *Oct4* promoter was performed using QuikChange II XL Site-Directed Mutagenesis Kit (Agilent) and primers presented in Supplemental Table 3. Mutations of the Klf4 and Hif1 α were confirmed by sequencing.

Cultured rat aortic SMCs were transiently transfected with reporter plasmids (1 μg) using FuGENE reagent (Roche Diagnostics Corp.) at approximately 75% confluency according to the manufacturer's protocol and

treated with vehicle, POVPC ($10 \mu\text{g mL}^{-1}$), oxLDL ($100 \mu\text{g mL}^{-1}$) or LDL ($100 \mu\text{g mL}^{-1}$) for 24 hours. Luciferase activity was measured using the Luciferase Assay System Kit (Promega) and normalized to total protein content (Coomassie Plus protein Assay reagent, Pierce).

Results

To test the hypothesis that the pluripotency factor Oct4 plays a functional role in modulating SMC phenotypic transition *in vivo*, we generated conditional SMC-specific tamoxifen-inducible *Oct4* KO mice by breeding *Oct4*^{Flox/Flox} mice^{99, 162} with mice carrying a tamoxifen-inducible Cre recombinase/estrogen receptor fusion protein under transcriptional control of the *Myh11* promoter (*Myh11-CreER*^{T2})²¹ (Supplemental Fig. 29a). Tamoxifen-treated *Oct4*^{Flox/Flox};*Myh11-CreER*^{T2} mice demonstrated selective recombination of *Oct4* (*Oct4*^{Δ/Δ} mice) in SMC-rich tissues such as aorta and femoral artery (Supplemental Fig. 29b) as well as lung and carotid artery (data not shown), but no significant recombination in non-SMC-rich tissues such as liver (Supplemental Fig. 29b) or skin (data not shown). In addition, cultured SMC isolated from the aortas of *Oct4*^{Δ/Δ} mice following tamoxifen treatment exhibited >90% recombination (Supplemental Fig. 29c).

To study the role of the SMC-derived Oct4 during the development of atherosclerosis we crossed *Oct4*^{Flox/Flox};*Myh11-CreER*^{T2} mice with atheroprone *ApoE*^{-/-} mice¹⁷³ (*Oct4*^{Δ/Δ}*ApoE*^{-/-} mice). *Oct4*^{Δ/Δ}*ApoE*^{-/-} mice exhibited no significant differences in cholesterol or triglyceride levels after 18 weeks of high-fat Western diet feeding, as well as no significant differences neither in body weight or heart, lung and spleen weights relative to body weight (Supplemental Fig. 30) as compared to control *Oct4*^{WT/WT}*ApoE*^{-/-} mice.

Immunostaining using an antibody specific to the pluripotency isoform of Oct4 showed that Oct4 expression was markedly induced within atherosclerotic lesions as well as in medial and adventitial cells within the brachiocephalic arteries of *Oct4^{WT/WT}ApoE^{-/-}* mice after 18 weeks of high-fat Western diet feeding (Fig. 11a). *Oct4^{Δ/Δ}ApoE^{-/-}* mice demonstrated reduced Oct4 staining within the brachiocephalic artery, particularly within the medial layer, consistent with SMC-specific KO of *Oct4*.

Of major significance, *Oct4^{Δ/Δ}ApoE^{-/-}* mice had a 40-50% increase in lesion size, area within the internal elastic lamina (IEL), and total vessel area, but reduced lumen size as compared to *Oct4^{WT/WT}ApoE^{-/-}* mice (Fig. 11b-d and Supplemental Fig. 31a,b). In contrast, there were no significant differences in vessel tunica media area (Supplemental Fig. 31c).

To determine whether *Oct4* deficiency altered atherosclerotic plaque composition, we analyzed brachiocephalic artery lesions for *Acta2* and *Lgals3*, markers that have been used routinely for assessing SMC and macrophage content respectively. Lesions from *Oct4^{Δ/Δ}ApoE^{-/-}* mice did not show a significant difference in overall *Acta2* or *Lgals3* staining relative to control mice (Supplemental Fig. 32), but exhibited marked differences in the distribution of both *Acta2* and *Lgals3* staining, particularly in the fibrous cap region (Fig. 11b). That is, *Acta2* staining in KO mice was far more diffuse whereas *Lgals3* staining was highly concentrated in the shoulder regions of the plaque. These differences were quantified as *Acta2* and *Lgals3* coverage indices by determining the fraction

of the fibrous cap stained with each marker (Fig. 11e). Results showed a significant increase in *Lgals3* fibrous cap coverage and decrease in *Acta2* coverage in *Oct4^{Δ/Δ}ApoE^{-/-}* lesions, suggesting that *Oct4^{Δ/Δ}ApoE^{-/-}* mice have less stable lesions^{171, 174}.

To extrapolate our studies in the atherosclerotic mouse model to human we tested if Oct4 is expressed within human atherosclerotic lesions by performing Oct4 immunostaining in human carotid artery. Of particular importance, results showed marked increases in Oct4 staining in the tunica media and within atherosclerotic lesions of human coronary arteries (Supplemental Fig. 33), indicating that re-activation of Oct4 also occurs within somatic cells in humans.

Since phenotypically modulated SMC show decreased expression of differentiation marker genes, many SMC-derived intimal cells cannot be detected based on traditional immunostaining with antibodies to *Acta2* or *Myh11*³⁰. Therefore, to provide unambiguous identification of SMC-derived cells within atherosclerotic lesions, we recently generated a novel SMC lineage-tracing mouse by breeding tamoxifen-inducible *Myh11-CreER^{T2}* mice with *ROSA26-Stop^{Flox}eYFP^{+/+}* mice (*SMC-eYFP^{+/+}*). These mice show high efficiency eYFP labeling of SMC in all tissues examined following tamoxifen treatment, with no detectable eYFP expression in non-SMC or in the absence of tamoxifen¹⁴⁴. Importantly, this conditional SMC-specific lineage-tracing model permits high efficiency labeling of mature, fully differentiated SMC at the time of tamoxifen

injections, and subsequent determination of the fate of these cells and their progeny independent of continued expression of detectable levels of endogenous SMC marker genes. Next, we crossed our *Oct4^{Flox/Flox} ApoE^{-/-}* and *Oct4^{WT/WT} ApoE^{-/-}* mice with the *SMC-eYFP^{+/+}* mice to test if genetic KO of *Oct4* in SMC was associated with changes in distribution and/or frequency of phenotypically modulated SMC within atherosclerotic lesions. Remarkably, the number of SMC-derived cells (eYFP+) within lesions was dramatically reduced in *Oct4^{Δ/Δ} ApoE^{-/-} SMC-eYFP^{+/+}* versus control *Oct4^{WT/WT} ApoE^{-/-} SMC-eYFP^{+/+}* mice (Fig. 11f,g), indicating that Oct4 is a critical factor required for the presence of phenotypically modulated SMCs within lesions.

SMC phenotypic switching is also well documented in several models of acute vascular injury⁵. Therefore, to study whether Oct4 plays a role in non-atherogenic vascular pathogenesis, *Oct4^{Δ/Δ}* and *Oct4^{WT/WT}* mice were subjected to carotid ligation injury¹⁷². Results of Oct4 immunostaining studies showed marked induction of Oct4 expression 3 days following carotid ligation in *Oct4^{WT/WT}* injured carotid arteries, but not in uninjured arteries (Supplemental Fig. 34a). This induction was greatly attenuated within medial cells of *Oct4^{Δ/Δ}* injured carotid arteries, consistent with SMC-specific gene targeting in a manner similar to our results in atherosclerotic lesions. *Oct4^{Δ/Δ}* mice showed an increase in intimal, medial and total vessel area of the injured carotid artery (Supplemental Fig. 34b-e).

To distinguish whether the dramatic decrease in eYFP+ cells within atherosclerotic lesions of SMC-specific conditional *Oct4* KO mice was a result of impaired migration, proliferation, and/or increased apoptosis, we analyzed apoptosis (cleaved caspase-3 staining) and proliferation (Ki67 staining) in eYFP+ cells within lesions. Results showed no difference in caspase-3+ (Fig.2a,b and Supplemental Fig. 35) or Ki67+ (Supplemental Fig. 36) cell number within eYFP+ lesion cells. Unexpectedly, however, we observed a >3-fold increase in the number of caspase-3+ cells within eYFP- (non-SMC derived) lesion cells (Fig. 14 b), indicating that: 1) SMC within lesions normally play a key role in survival of non-SMCs; and/or 2) phenotypically modulated SMC play an important role in phagocytic clearance of lesion cells, consistent with reports by *Bennett, M.* and co-workers suggesting that SMC-derived cells play an important role in apoptotic cell clearance during atherosclerogenesis¹⁷⁵. Whichever the case, these processes appear to be dependent on Oct4 expression within SMC.

Proliferation marker Ki67 is present in cells during active phases of cell cycle, such as G1, G2, S and mitosis, whereas SMC migration occurs in the G1 phase of cell cycle¹⁷⁶. Therefore, it is not possible to distinguish proliferative versus migrating cells based only on proliferation marker staining. To further elucidate the role of Oct4 in SMC, we tested the effect of genetic KO or siRNA-induced suppression of *Oct4* on proliferation and migration of cultured SMC induced by the pro-atherogenic oxidized phospholipids^{40, 88}. Aortic SMC isolated from *Oct4*^{WT/WT} SMC demonstrated >3-fold increase in Oct4 mRNA expression in

response to POVPC (1-palmitoyl-2-(5-oxovaleroyl)-sn-glycero-3-phosphorylcholine) and oxLDL, but no response to a non-oxidized form of LDL. These effects were completely abrogated in *Oct4*^{Δ/Δ} SMC (Supplemental Fig. 37a). Results also showed that genetic inactivation of Oct4 completely blocked POVPC-induced migration of SMC (Fig. 14c), but did not affect cell adhesion to fibronectin and type I collagen (data not shown). Effects on SMC proliferation were small and varied depending on the experimental conditions in that genetic inactivation of *Oct4* resulted in modest increases in cell number in SMC grown in 2% serum, but had no effect on POVPC-induced proliferation of cells (Supplemental Fig. 37b). In addition, results showed that siRNA-induced knockdown of *Oct4* blocked POVPC-induced migration of cultured mouse aortic SMC (Fig. 14d), but did not change POVPC-induced proliferation (Supplemental Fig. 37a). Conversely, lentivirus-mediated over-expression of Oct4 increased SMC migration and decreased proliferation of SMC grown in 2% serum (Supplemental Fig. 38).

To determine whether knockout of Oct4 inhibits SMC migration in blood vessels we studied SMC outgrowth from aortic explants isolated from *Oct4*^{WT/WT}*SMC-eYFP*^{+/+} and *Oct4*^{Δ/Δ}*SMC-eYFP*^{+/+} lineage tracing mice. Results showed that migration of the eYFP⁺ cells was completely inhibited in *Oct4*^{Δ/Δ} aortic explants (Fig. 14e). Next, we tested expression levels of several extracellular matrix (ECM)-related genes in *Oct4*^{WT/WT} and *Oct4*^{Δ/Δ} SMC and found that multiple genes required for SMC migration including matrix

metalloproteinases *Mmp3*, *Mmp13*, collagens *Col15a1*, *Col5a2*, *Col6a2*, as well as *Opn* (osteopontin) and *Timp1* (tissue inhibitor of matrix metalloproteinase 1) were up-regulated in *Oct4*^{WT/WT} SMC in response to POVPC, but not in *Oct4*^{Δ/Δ} SMC (Fig. 2*f-i*, Supplemental Fig. 39). These findings suggest that the decrease in the migration rate in *Oct4*^{Δ/Δ} SMC was due at least in part to modified *de novo* synthesis of MMPs and ECM proteins in KO cells.

Taken together, these results indicate that the primary mechanism responsible for the decrease in SMC-derived (eYFP+) cells within lesions of *Oct4*^{Δ/Δ}*ApoE*^{-/-} SMC-eYFP^{+/+} mice is impaired migration of SMC from the media into the intima. However, we cannot rule out the possibility that alterations in SMC proliferation or apoptosis at earlier time points may have also contributed to this phenotype.

Clinical data indicate that atherosclerotic plaque destabilization rather than lesion size is the most critical determinant of clinical events from lesion thrombosis including myocardial infarction and stroke¹⁴¹. To further validate if *Oct4* deficiency in SMCs alters atherosclerotic plaque stability, we analyzed cellular versus non-cellular composition of lesions, lipid accumulation, collagen content by PicroSirius Red staining and intraplaque hemorrhage based on staining for the red blood cell (RBC) marker Ter119. Necrotic non-cellular areas were markedly increased in *Oct4*^{Δ/Δ}*ApoE*^{-/-} as compared to *Oct4*^{WT/WT}*ApoE*^{-/-} lesions (Fig. 15*a*), whereas cell density in the non-necrotic areas was decreased (Fig. 15*b*). No difference was detected in lipid accumulation based on Oil Red O

staining (Supplemental Fig. 40). Although there was no significant difference in total collagen content (Supplemental Fig. 41), *Oct4^{Δ/Δ}ApoE^{-/-}* mice showed significantly more intermediate collagen fibers versus thick collagen fibers (Fig. 15c,d), indicating a decrease in the amount of mature collagen fibrils in *Oct4^{Δ/Δ}ApoE^{-/-}* as compared to *Oct4^{WT/WT}ApoE^{-/-}* lesions. Moreover, lesions within brachiocephalic arteries of *Oct4^{Δ/Δ}ApoE^{-/-}* mice exhibited significantly increased intraplaque hemorrhage based on Ter119 staining (Fig. 15e,f). Taken together, our results indicate that loss of Oct4 within SMC leads to marked reduction in number of SMC within lesions (Fig. 13f,g), but paradoxically results in an increase rather than a decrease in overall lesion size (Fig. 13b,c). We postulate that this is due to lesions being less stable with recurrent episodes of plaque rupture and healing in addition to trapping of RBC and other blood products, as well as to increased apoptosis of non-SMC. As such, our results indicate that Oct4-dependent phenotypic transition is a critical determinant of plaque size, composition, and stability.

Given the dogma that Oct4 is epigenetically silenced in somatic cells¹⁷⁷, a critical question is what molecular mechanisms contribute to the re-activation of *Oct4* expression within SMC in response to injury or in the setting of atherosclerosis. The *Oct4* promoter contains potential binding sites for the transcriptional factors Klf4 (Krüppel-like factor 4) and Hif1 α (Hypoxia-inducible factor 1 α) (Supplemental Fig.42), which both have been previously shown to be activated in the phenotypically modulated SMC^{40, 89, 178}. Adenovirus-mediated

over-expression of Klf4 increased expression of the pluripotency factor *Oct4* in cultured SMC (Fig. 16a). Klf4 was also enriched at the *Oct4* gene promoter based on Chromatin Immunoprecipitation (ChIP) analyses of cultured SMC treated with POVPC (Fig. 16b). Next, we tested the involvement of potential Klf4 and Hif1 α binding sites for activation of *Oct4* gene transcription in cultured aortic SMC. POVPC and oxLDL induced transcriptional activity of the 1.5 kb *Oct4* promoter–luciferase construct by 5- and 3-fold correspondingly, but the induction was reduced by mutation of either one of these *cis* elements (Fig. 15c,d). Simultaneous mutations of all Klf4 or Hif1 α binding sites completely abolished the response. In addition, we found that Klf4 and Hif1 α were enriched at the *Oct4* gene promoter in ChIP analyses of chromatin isolated from blood vessels of *ApoE*^{-/-} mice after 18 weeks of high-fat Western diet feeding as compared with control *ApoE*^{+/+} mice fed a chow diet (Fig. 15e,f). Taken together, results indicate that induction of *Oct4* in SMC within atherosclerotic lesions is mediated by combined action of Klf4 and Hif1 α . These observations are of interest in that it has previously been shown that oxLDL can activate Hif1 α even under normoxic conditions¹⁷⁹, and since hypoxia is well known to play a key role in maintaining *Oct4* expression within stem cell niches¹⁸⁰.

Discussion

In conclusion, our results provide novel evidence showing induction of the pluripotency factor Oct4 in SMC during experimental atherosclerosis and following vascular injury. Oct4-dependent loss of SMC-derived cells in atherosclerotic lesions results in larger, less stable lesions as indicated by: reduced Acta2, increased Lgals3 fibrous cap coverage, increased numbers of apoptotic cells, increased necrotic core area, and increased intraplaque hemorrhage. These findings provide the first evidence, to our knowledge, of a critical functional role for the pluripotency factor Oct4 in somatic cells. Further studies are needed to determine: 1) the role of Oct4 in SMC in the context of different cardiovascular diseases including hypertension, myocardial infarction, and arterial aneurysms, as well as in vascular remodeling in the setting of tissue repair and tumor growth; 2) whether therapeutic augmentation of Oct4 functions within SMC might promote plaque stability and/or improved vascular remodeling.

Figure 13: SMC-specific conditional KO of the pluripotency gene *Oct4* was associated with an increased size of lesions, as well as a marked reduction in phenotypically modified SMC within the atherosclerotic lesions of 18 weeks Western diet fed *ApoE* KO mice.

(a) Oct4 protein levels were markedly induced within cells of the tunica media and atherosclerotic lesions of the *Oct4*^{WT/WT}*ApoE*^{-/-} mice (middle panel) following 18 weeks of high-fat Western diet feeding as compared to the control age-matched *Oct4*^{WT/WT}*ApoE*^{+/+} mice fed a chow diet (top panel). In contrast, the frequency of Oct4 positive cells was markedly attenuated in conditional SMC-specific *Oct4*^{Δ/Δ}*ApoE*^{-/-} mice on Western diet for 18 weeks (bottom panel), including a virtual absence of Oct4 positive cells within the tunica media, consistent with high efficacy SMC-specific Oct4 KO. Micrographs show cross-sections of brachiocephalic artery: *adv* – adventitia, *lum* – lumen, *med* – tunica media, *les* – lesion. Scale bar = 50 μm. (b) Movat, SM α-actin (*Acta2*) and Mac-2 (*Lgals3*) staining of representative brachiocephalic arteries of *Oct4*^{WT/WT}*ApoE*^{-/-} and *Oct4*^{Δ/Δ}*ApoE*^{-/-} mice. Scale bar = 100 μm. (c) Atherosclerotic lesion area and (d) lumen area. Values represent mean ± s.e.m. (e) Quantification of lesion SMC coverage index based on *Acta2* staining and macrophage coverage index based on *Lgals3* staining. Values represent mean ± s.e.m. (f) Immunostaining of representative brachiocephalic arteries of *Oct4*^{WT/WT}*ApoE*^{-/-}*SMC-eYFP*^{+/+} and *Oct4*^{Δ/Δ}*ApoE*^{-/-}*SMC-eYFP*^{+/+} SMC lineage-tracing mice fed a Western diet for 18 weeks showing a remarkable decrease in the number of AMC-derived cells

within lesions of Oct4 KO mice (**f**, third panel (eYFP), compare the upper versus the lower panel). Scale bar = 50 μ m. (**g**) Quantification of eYFP+ cells within atherosclerotic lesions. Values represent the percent of eYFP+ cells within the total cell population based on DAPI staining, mean \pm s.e.m. P values for *Oct4*^{WT/WT}*ApoE*^{-/-} (n=12) vs. *Oct4* ^{Δ/Δ} *ApoE*^{-/-} (n=14) mice (**c,d,e**) or *Oct4*^{WT/WT}*ApoE*^{-/-}*SMC-eYFP*^{+/+} (n=10) vs. *Oct4* ^{Δ/Δ} *ApoE*^{-/-}*SMC-eYFP*^{+/+} (n=14) mice (**g**) across multiple locations along the brachiocephalic arteries were generated by 2-way ANOVA (**c,d,g**) or one-way ANOVA (**e**).

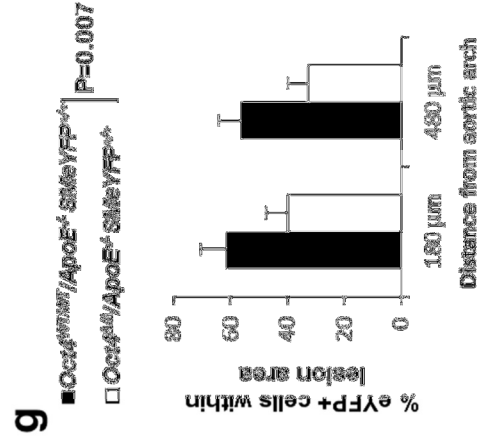
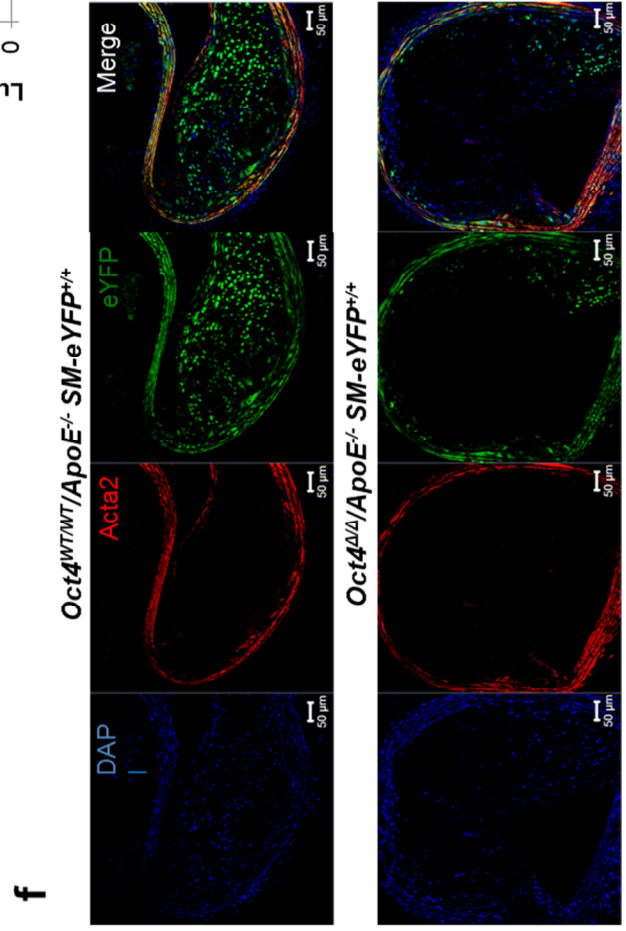
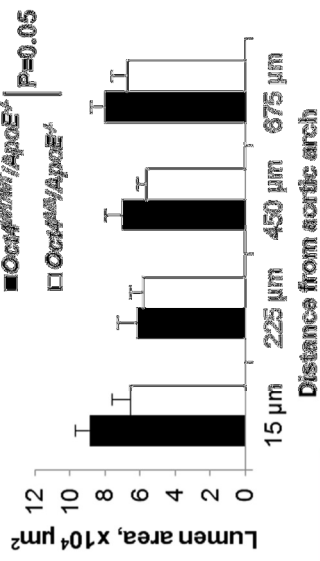
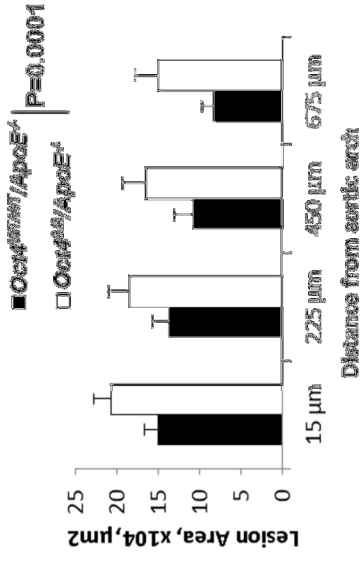
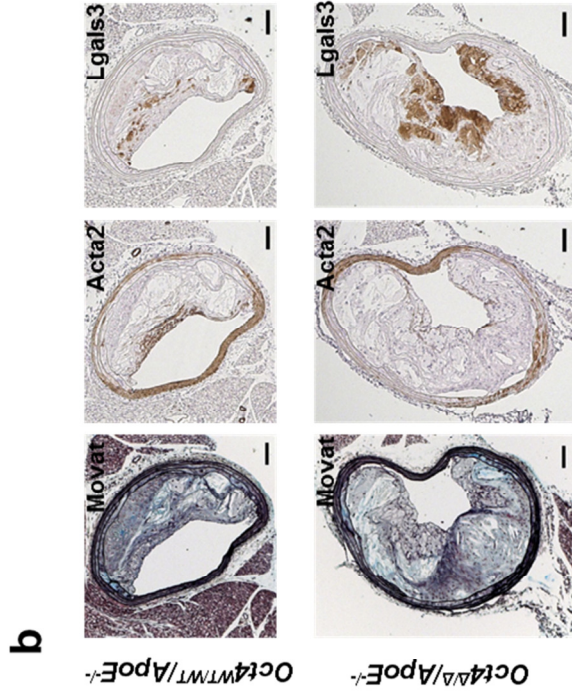
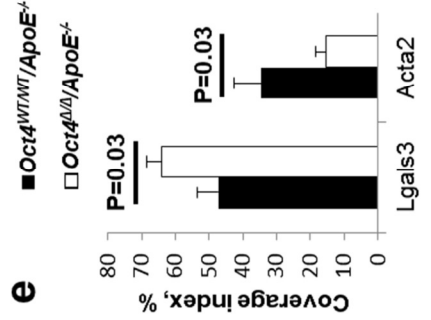
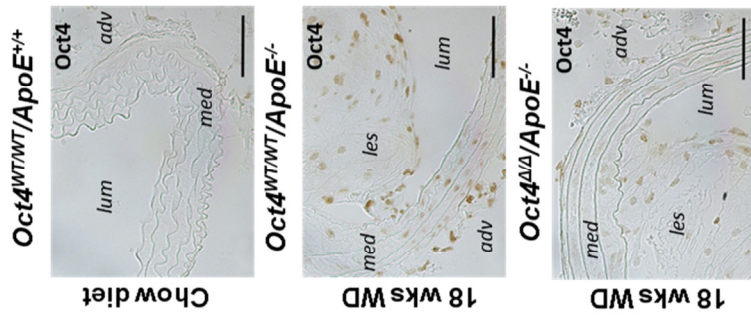


Figure 14: Role of the pluripotency factor Oct4 in regulating SMC proliferation, migration and apoptosis.

(a) Co-immunostaining of representative brachiocephalic arteries of $Oct4^{WT/WT}ApoE^{-/-}SMC-eYFP^{+/+}$ and $Oct4^{\Delta/\Delta}ApoE^{-/-}SMC-eYFP^{+/+}$ mice fed a Western diet for 18 weeks for DAPI, Acta2, eYFP and cleaved caspase-3 (a). Arrows indicate examples of double-positive eYFP+/caspase-3+ cells ($Oct4^{WT/WT}ApoE^{-/-}SMC-eYFP^{+/+}$ panel) or eYFP-/caspase3+ cells ($Oct4^{\Delta/\Delta}ApoE^{-/-}SMC-eYFP^{+/+}$ SMC panel). Scale bar = 20 μ m. (b) Quantification of total caspase-3+ cells, eYFP+/caspase3+ over eYFP+ cells and eYFP-/caspase-3+ over eYFP- cells within atherosclerotic lesions. Values represent mean \pm s.e.m. P values for $Oct4^{WT/WT}ApoE^{-/-}SMC-eYFP^{+/+}$ (n=9) vs. $Oct4^{\Delta/\Delta}ApoE^{-/-}SMC-eYFP^{+/+}$ (n=14) mice were generated by non-parametric (P*) or one-way parametric (P) ANOVA. (c,d) Boyden chamber transmigration assays were performed using the pro-atherogenic phospholipid POVPC as a chemo-attractant in the bottom chamber. (c) Mouse aortic SMC isolated from $Oct4^{WT/WT}$ and $Oct4^{\Delta/\Delta}$ mice following tamoxifen injections. (d) Mouse aortic SMCs transfected with siRNA specific to Oct4 (siOct4) or control non-targeting siRNA (siNT). Values represent cell counts (means \pm s.e.m) from 8–10 randomly chosen high-power fields, n = 3 independent experiments. P values for siOct4 vs. siNT or Oct4 WT vs. KO SMC were generated by 2-way ANOVA. (e) Aortic explants were isolated from $Oct4^{WT/WT}SMC-eYFP^{+/+}$ or $Oct4^{\Delta/\Delta}SMC-eYFP^{+/+}$ mice and grown on plastic for 2 weeks. Immunostaining for eYFP. Scale bar = 50 μ m. (f,g) Mouse aortic

Oct4^{WT/WT} and *Oct4*^{Δ/Δ} SMC were treated with vehicle, POVPC 5 or 10 μg mL⁻¹ for 24 hours and expression of *Mmp3* (**f**), *Mmp13* (**g**) was measured by quantitative real-time RT-PCR. Data represent mean ± s.d. (**h,i**) *Oct4*^{WT/WT} and *Oct4*^{Δ/Δ} SMC were treated with vehicle (V) or POVPC 10 μg mL⁻¹ (P) for 48 hrs. Conditioned media were analyzed by gelatin (**h**, top panel) or casein (**h**, bottom panel) zymography or Western blot (**i**).

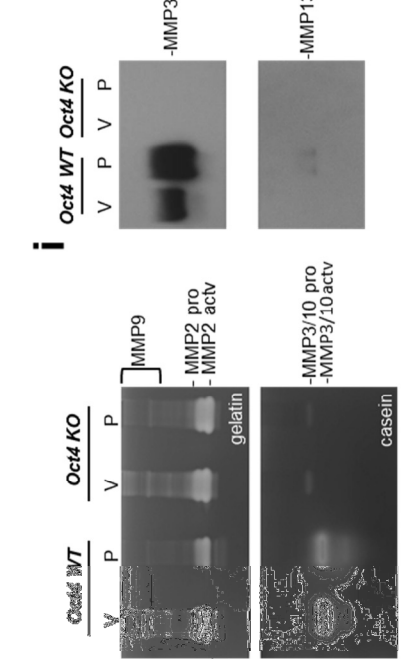
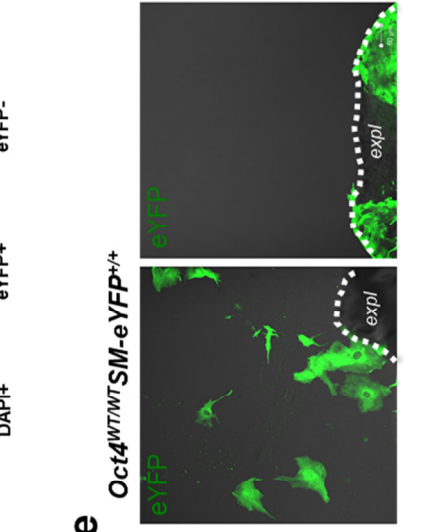
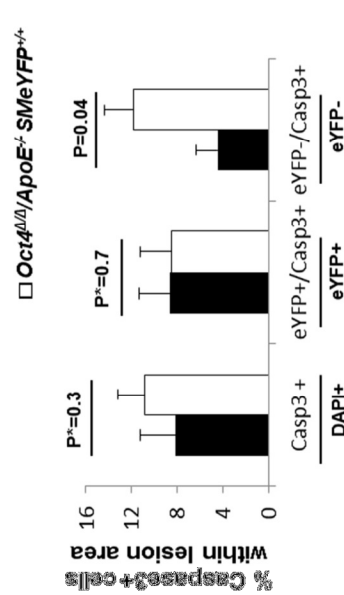
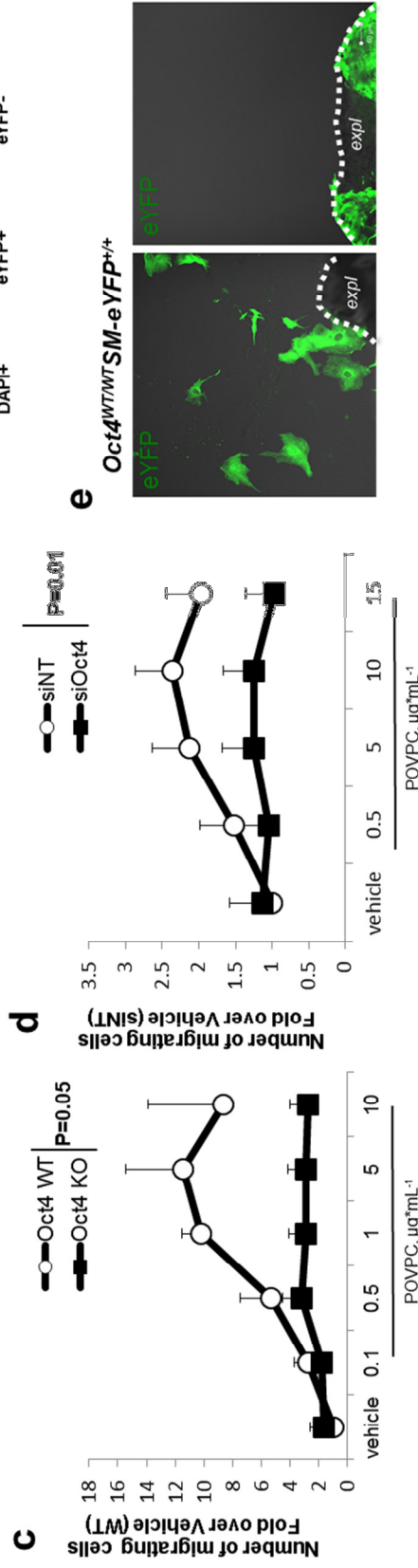
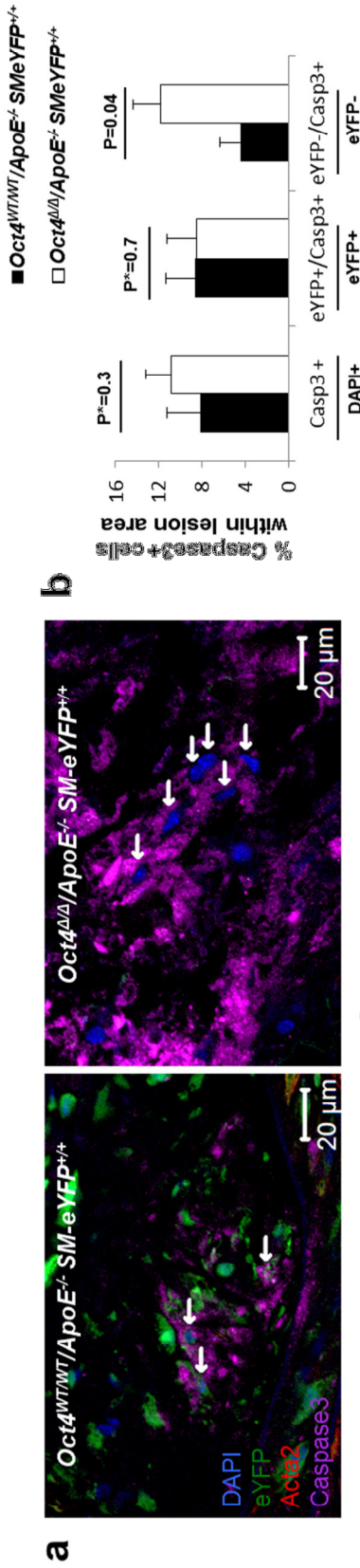


Figure 15: SMC-specific conditional KO of the pluripotency gene *Oct4* increased multiple indices of atherosclerotic plaque instability.

(a) Necrotic core area based on Movat staining. Values represent mean \pm s.e.m. P values for *Oct4*^{WT/WT}*ApoE*^{-/-} (n=12) vs. *Oct4* ^{Δ/Δ} *ApoE*^{-/-} (n=14) mice across multiple locations along the brachiocephalic arteries were generated by 2-way ANOVA. (b) Cell density analysis. Values represent the relative number of cells based on DAPI staining, mean \pm s.e.m. P value for *Oct4*^{WT/WT}*ApoE*^{-/-}*SMC-eYFP*^{+/+} (n=9) vs. *Oct4* ^{Δ/Δ} *ApoE*^{-/-}*SMC-eYFP*^{+/+} (n=14) mice was generated by one-way ANOVA. (c) PicroSirius red staining and polarized light microscopy for collagen detection of representative brachiocephalic arteries of *Oct4*^{WT/WT}*ApoE*^{-/-} and *Oct4* ^{Δ/Δ} *ApoE*^{-/-} mice. Scale bar = 100 μ m. (d) Collagen fiber hue variations. Ratio between the amount of thin (green/immature), intermediate (yellow) and thick (orange/mature) collagen fibrils showed significant decrease of thick fibrils in *Oct4* ^{Δ/Δ} *ApoE*^{-/-} atherosclerotic lesions as compared with control *Oct4*^{WT/WT}*ApoE*^{-/-} mice. P value for *Oct4*^{WT/WT}*ApoE*^{-/-} (n=11) vs. *Oct4* ^{Δ/Δ} *ApoE*^{-/-} (n=8) mice was generated by one-way ANOVA. (e) Immunostaining for the red blood cell marker Ter-119. Scale bar = 50 μ m. (f) The percentage of brachiocephalic arteries exhibiting intraplaque hemorrhage based on Ter-119 staining. P value for *Oct4*^{WT/WT}*ApoE*^{-/-} (n=12) vs. *Oct4* ^{Δ/Δ} *ApoE*^{-/-} (n=14) mice was generated by Fisher's exact test. Bottom panels in **c** and **e** represent magnified boxed areas from top panels.

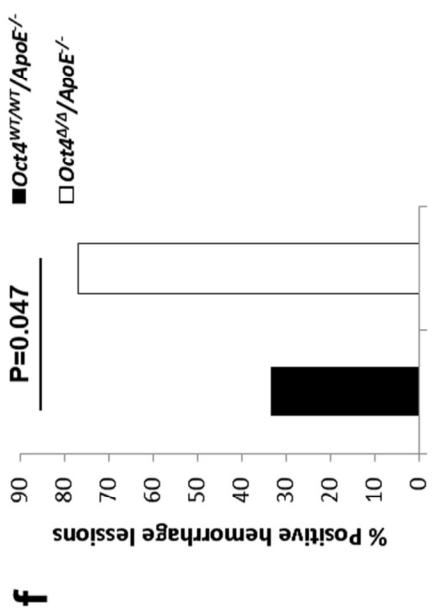
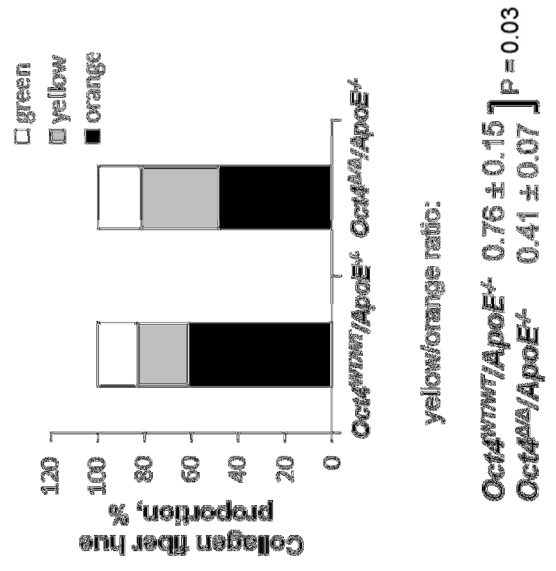
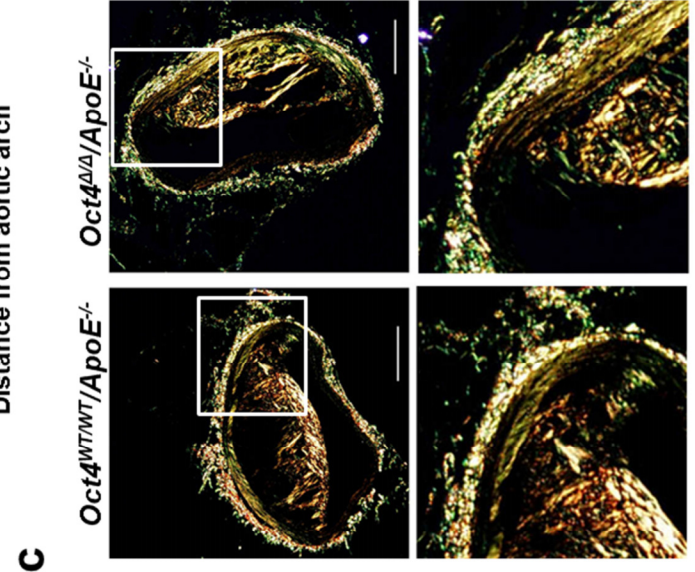
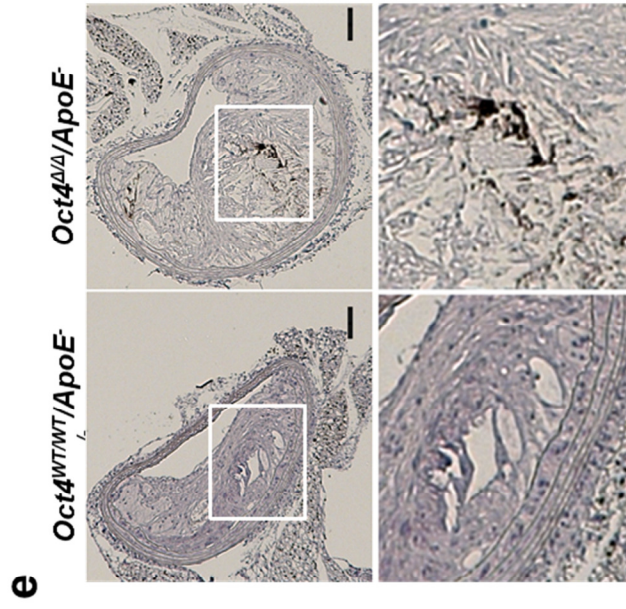
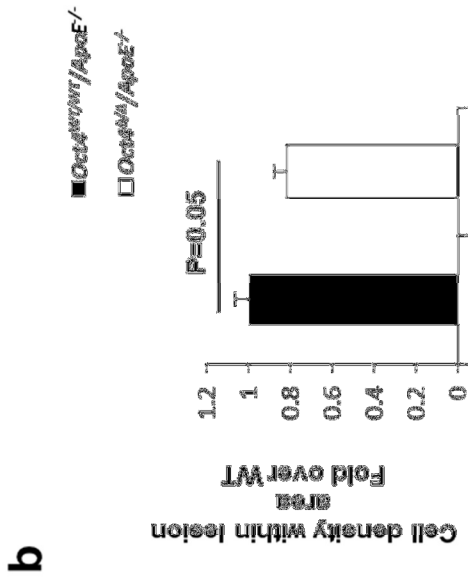
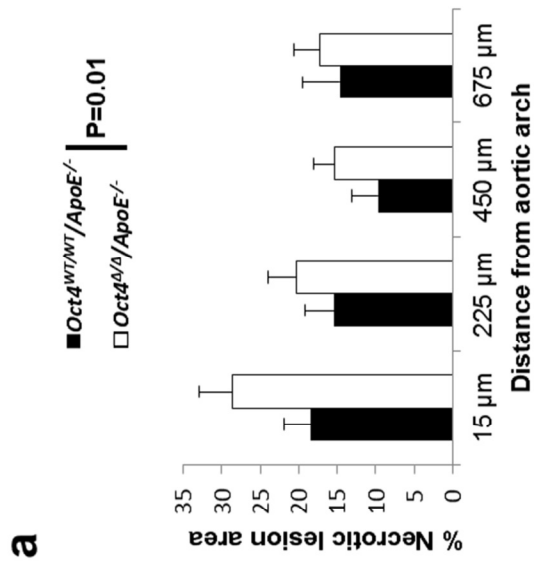
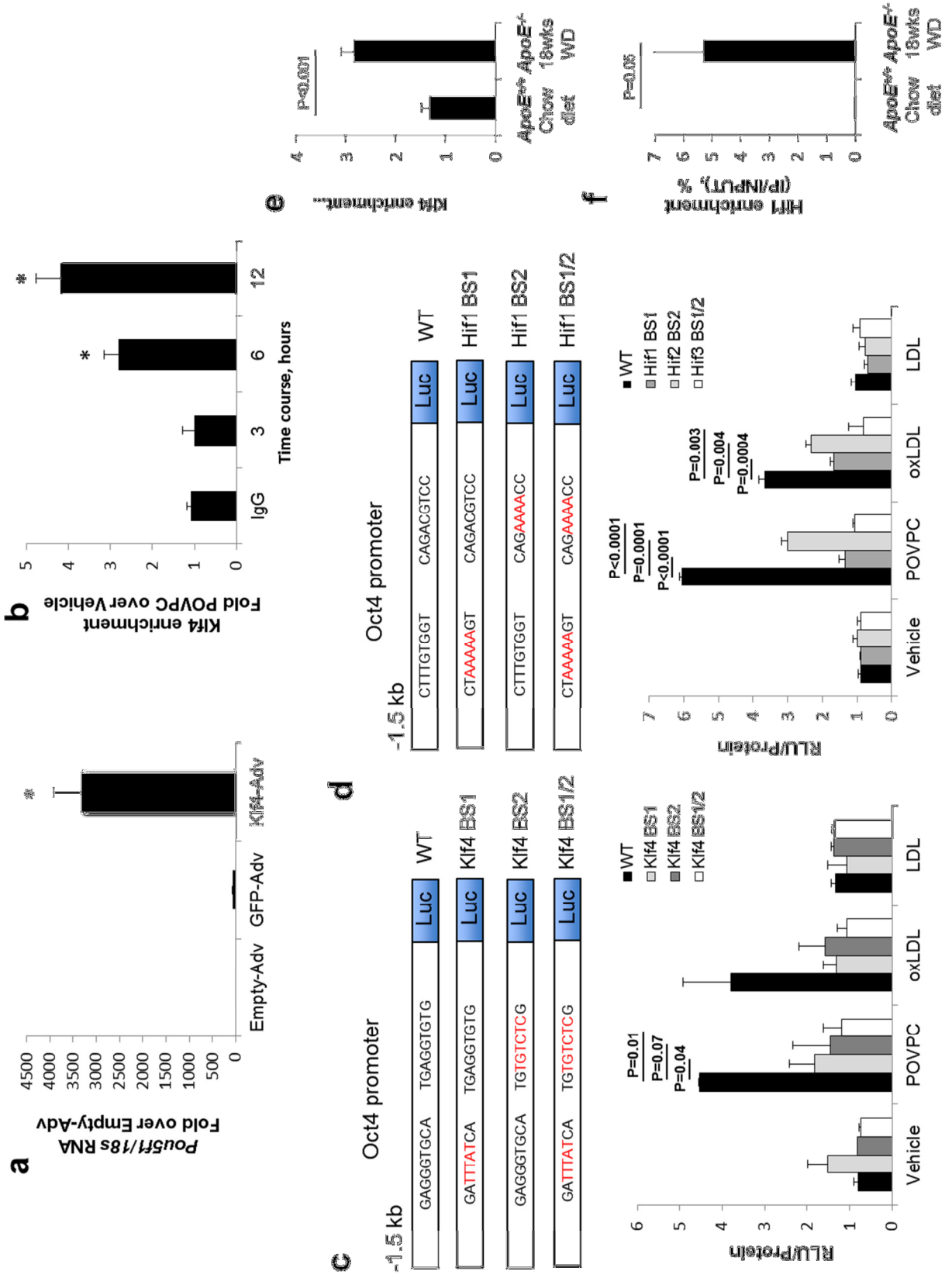


Figure 16: Activation of Oct4 in SMC was dependent on Klf4 and Hif1 α .

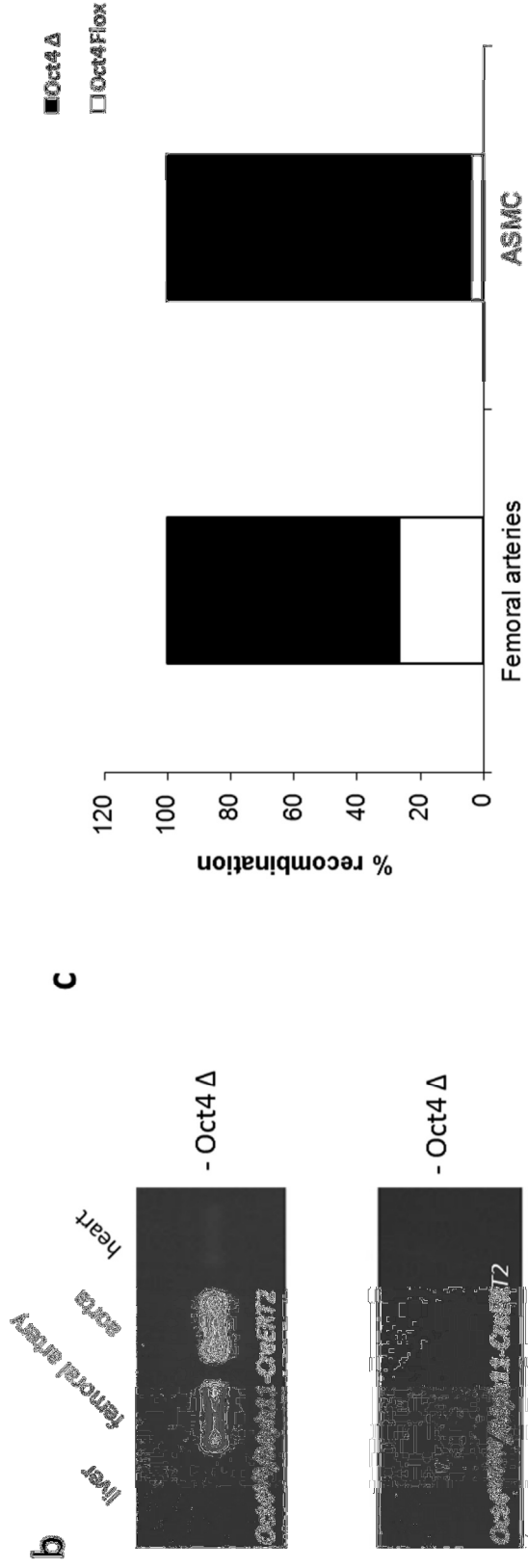
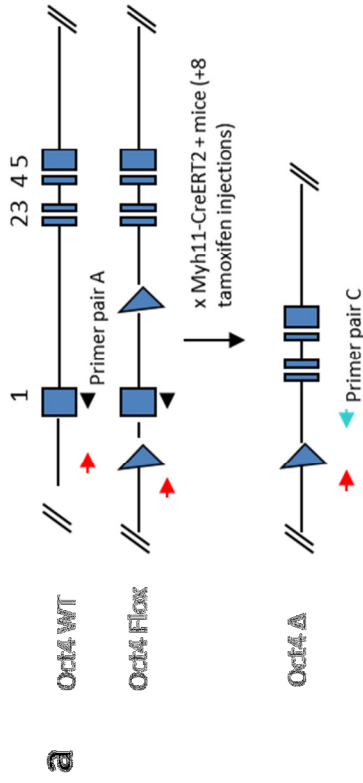
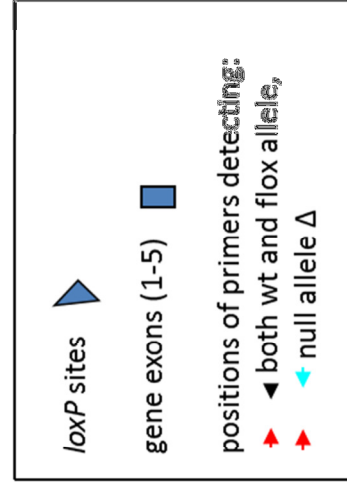
(a) Mouse aortic SMC were infected with adenoviruses expressing Klf4, GFP or were mock infected with Empty-adenovirus for 48 hours and expression of *Oct4* gene (*Pou5f1*) was measured by quantitative real-time RT-PCR. Data represent mean \pm s.e.m. * $P \leq 0.05$ vs. GFP by Student's *t*-test, $n = 3$ independent experiments. (b) Mouse aortic SMC were treated with either POVPC or DMSO-vehicle for 3, 6 or 12 hours. Association of Klf4 with the promoter region of *Oct4* gene was determined by CHIP assays. Chromatin either precipitated with antibody for Klf4 or with isotype control antibody (IgG) was subjected to the real-time RT-PCR. Results were normalized to the total Input and demonstrated as a fold-increased over vehicle. * $P \leq 0.05$ vs. IgG (12 hours) control by Student's *t*-test, $n = 3$ independent experiments. (c,d) Site-directed mutagenesis of the Klf4 or Hif1 α binding sites (BS) within 1.5 kb *Oct4* promoter region. Rat aortic SMC were transfected with the *Oct4* wild type (WT) promoter/enhancer-luciferase pGL3 construct or its mutants and treated with vehicle, POVPC, oxLDL or LDL for 24 hours before determining luciferase activity. Results were normalized to the total protein content and demonstrated as a fold-increased over empty pGL3, mean \pm s.e.m, $n = 3$ independent experiments. P values were generated by Student's *t*-test. (e) Klf4 and (f) Hif1 α were enriched at the *Oct4* gene promoter in *in vivo* CHIP analyses of chromatin isolated from blood vessels of *ApoE*^{-/-} mice fed a high-fat Western diet for 18 months as compared to the control age-matched *ApoE*^{+/+} mice fed a chow diet. Chromatin either precipitated with

antibodies for Klf4, Hif1 α or with isotope control antibody (IgG) was subjected to the real-time RT-PCR. Results were normalized to the total Input, mean \pm s.e.m. P values *ApoE*^{-/-} (n =5) vs. *ApoE*^{+/+} (n=5) were generated by one-way ANOVA.



Supplemental Figure 29: *Oct4* is recombined specifically in SMC rich tissues of *Oct4*^{Δ/Δ}*ApoE*^{-/-} versus *Oct4*^{WT/WT}*ApoE*^{-/-} mice.

(a) Schematic representation of the targeting DNA construct, wild-type (*Oct4* WT), Flox (*Oct4* Flox) and a null (*Oct4* Δ) alleles of the *Oct4* gene. (b) PCR genotyping of tissues from *Oct4*^{Δ/Δ}*Myh11-CreER*^{T2} and *Oct4*^{WT/WT}*Myh11-CreER*^{T2} mice after 8 tamoxifen injections using primers detecting *Oct4* Δ allele (primer pair C). (c) Recombination efficiency after 8 tamoxifen injections measured by real-time RT-PCR in femoral arteries of *Oct4*^{Δ/Δ}*Myh11-CreER*^{T2} mice or aortic SMC (ASMC) isolated from the same animals. Results of pilot experiments using fewer than 8 tamoxifen injections resulted in incomplete and variable efficacy of recombination of the floxed *Oct4* gene locus.



Supplemental Figure 30: Genetic knockout of Oct4 did not significantly change metabolic parameters in Oct4^{Δ/Δ}ApoE^{-/-} versus Oct4^{WT/WT}ApoE^{-/-} mice fed a Western diet.

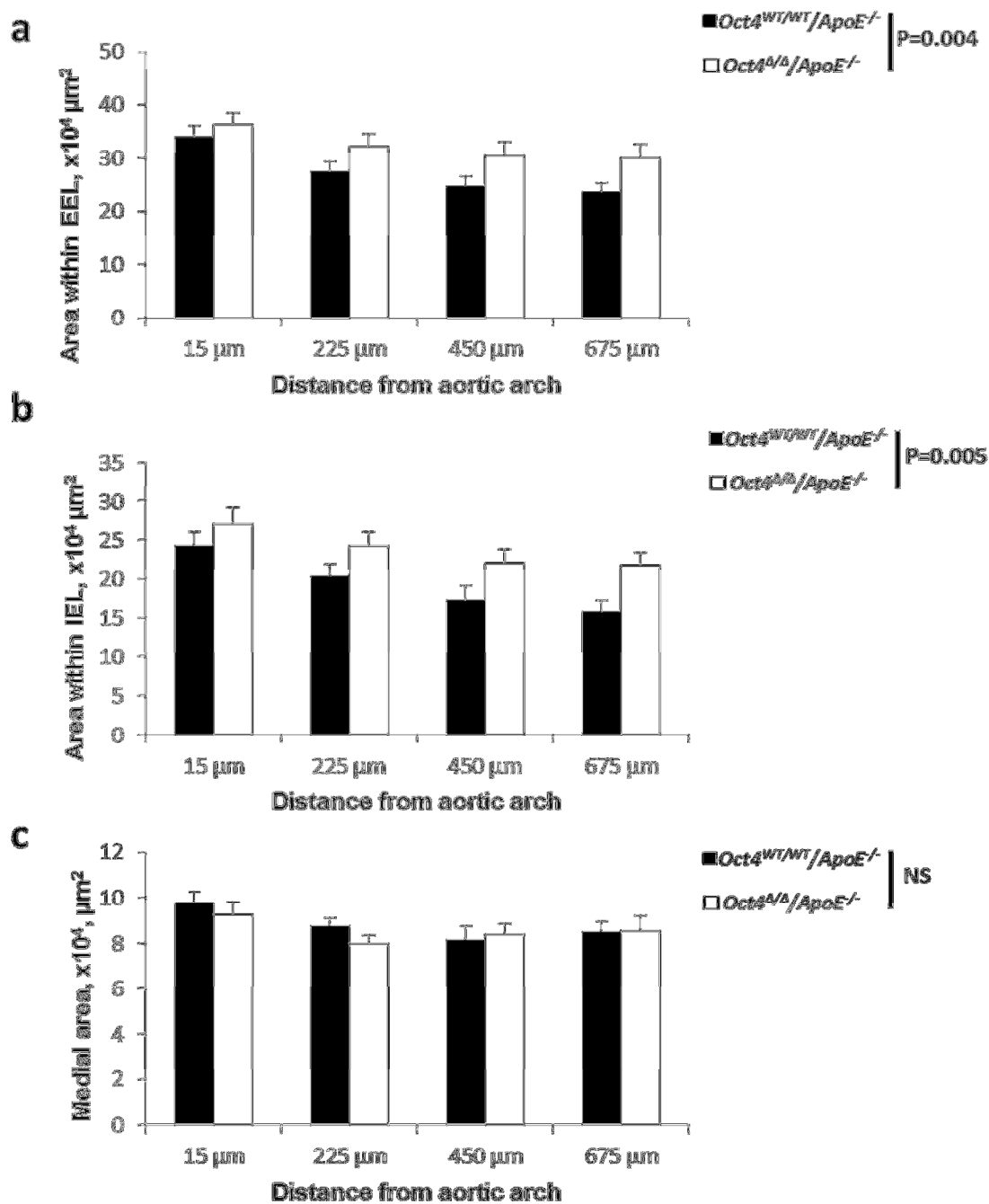
Plasma cholesterol and triglyceride levels, body weight, as well as heart weight, spleen weight and lung weight relative to body weight were quantified from Oct4^{WT/WT}ApoE^{-/-} versus Oct4^{Δ/Δ}ApoE^{-/-} or Oct4^{WT/WT}/ApoE^{-/-} SMC-eYFP^{+/+} versus Oct4^{Δ/Δ}/ApoE^{-/-} SMC-eYFP^{+/+} mice 18 weeks of Western diet feeding. Data represent mean ± s.e.m. $P > 0.05$ – not significant (NS) by one-way ANOVA.

	NS		NS	
	<i>Oct4^{WT/WT}/ApoE^{-/-}</i> (n=13)	<i>Oct4^{ΔΔ}/ApoE^{-/-}</i> (n=14)	<i>Oct4^{WT/WT}/ApoE^{-/-} SMC-eYFP^{+/+}</i> (n=6)	<i>Oct4^{ΔΔ}/ApoE^{-/-} SMC-eYFP^{+/+}</i> (n=6)
Total Cholesterol, mg/dL	934 ± 129	1217 ± 129	1418 ± 193	1176 ± 181
Triglycerides, mg/dL	183 ± 42	194 ± 38	142 ± 20	166 ± 24
Body weight, g	30.3 ± 1.6	27.9 ± 1.7	32.4 ± 1.6	29.2 ± 1.8
Heart, % body weight	0.7 ± 0.04	0.65 ± 0.03	0.61 ± 0.02	0.69 ± 0.03
Lungs, % body weight	0.8 ± 0.06	0.9 ± 0.06	ND	ND
Spleen, % body weight	1.7 ± 0.4	1.0 ± 0.2	0.9 ± 0.2	1.2 ± 0.2

NS - No statistically significant difference was determined for *Oct4^{WT/WT}/ApoE^{-/-}* versus *Oct4^{ΔΔ}/ApoE^{-/-}* or *Oct4^{WT/WT}/ApoE^{-/-} SMC-eYFP^{+/+}* versus *Oct4^{ΔΔ}/ApoE^{-/-} SMC-eYFP^{+/+}* mice.

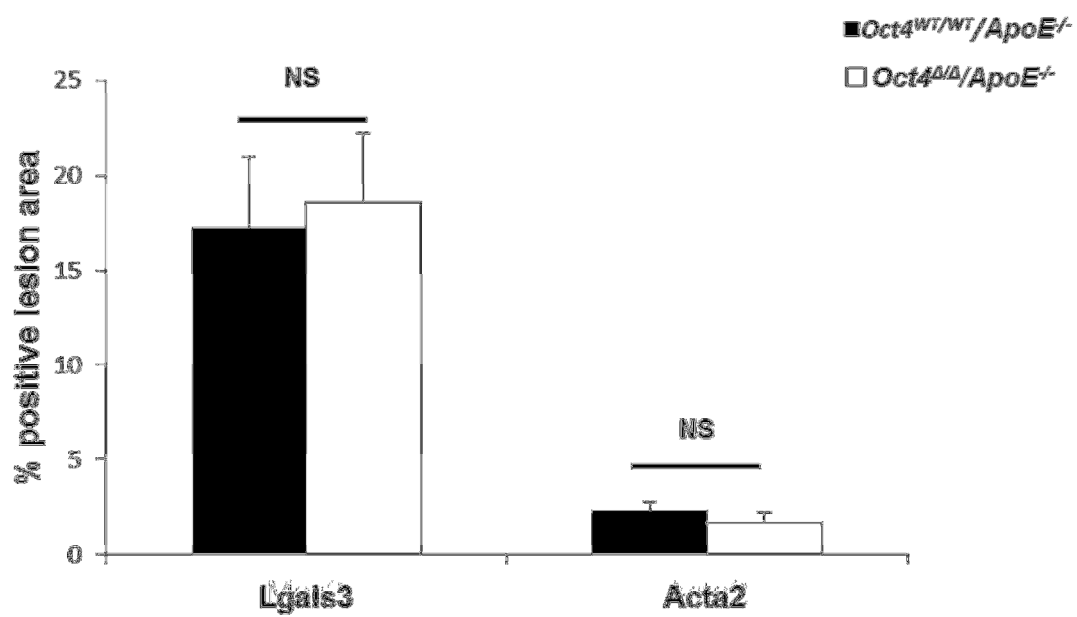
Supplemental Figure 31: SMC-specific conditional KO of the pluripotency gene *Oct4* increased atherosclerotic lesion size in brachiocephalic arteries.

Quantification of (a) area within external elastic lamina (EEL), (b) area within internal elastic lamina (IEL) and (c) medial area based on the Movat staining of the cross-sections of atherosclerotic lesions within brachiocephalic arteries from Fig. 13. Values represent mean \pm s.e.m. P values for *Oct4*^{WT/WT}*ApoE*^{-/-} (n=12) vs. *Oct4* ^{Δ/Δ} *ApoE*^{-/-} (n=14) mice across multiple locations along the brachiocephalic arteries were generated by 2-way ANOVA.



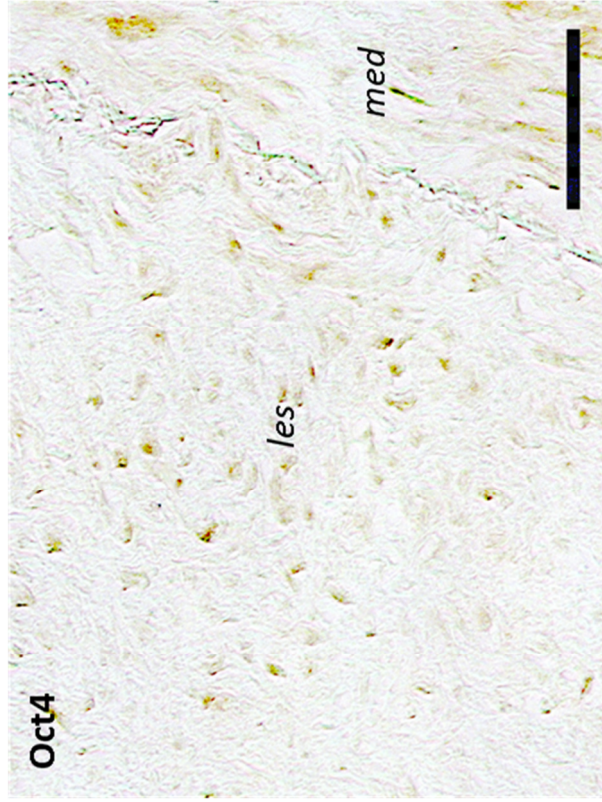
Supplemental Figure 32: SMC-specific conditional KO of the pluripotency gene *Oct4* did not change overall *Lgals3* (*Mac2*) staining or *Acta2* (SM α -actin) staining of brachiocephalic lesions.

Values represent mean \pm s.e.m. $P > 0.05$ – not significant (NS) *Oct4*^{WT/WT}*ApoE*^{-/-} ($n=12$) vs. *Oct4* ^{Δ/Δ} *ApoE*^{-/-} ($n=14$) mice.



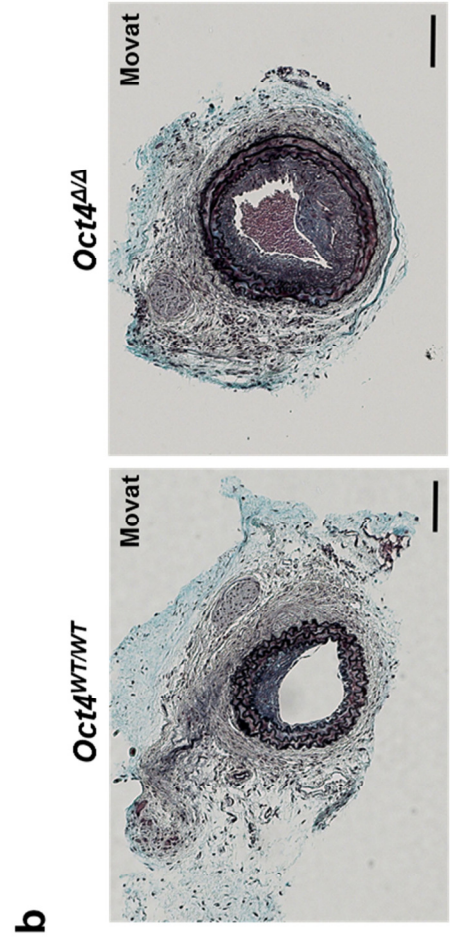
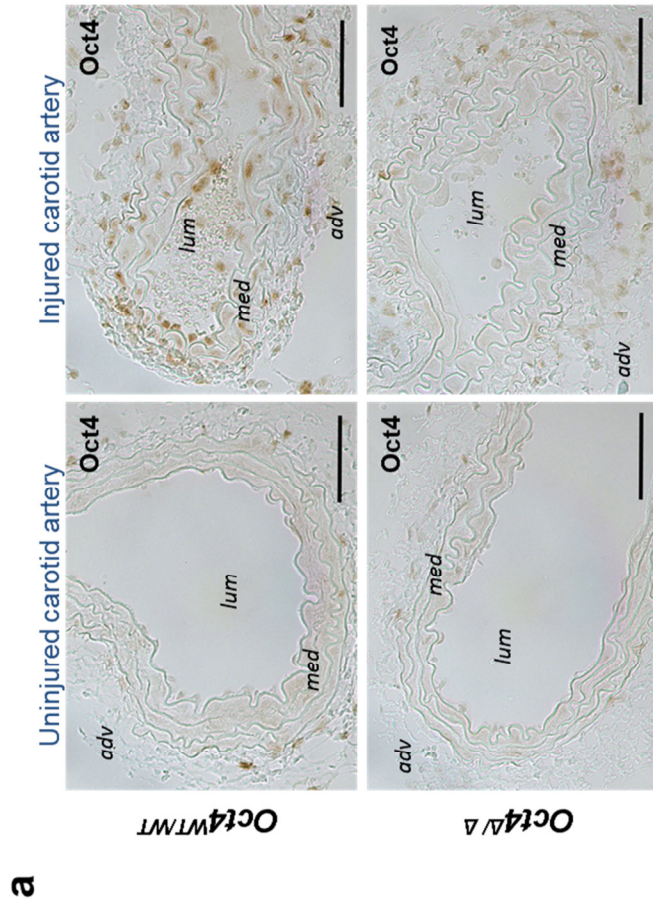
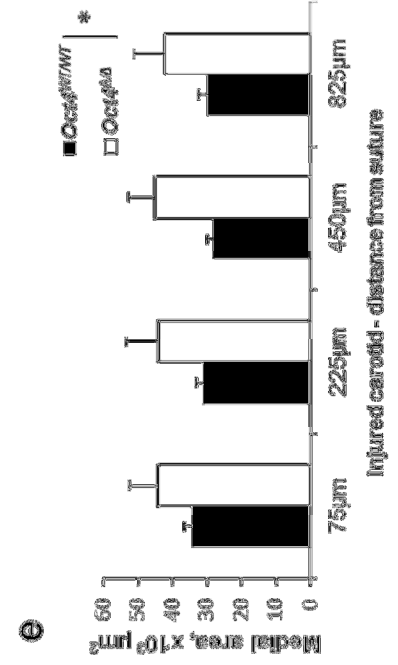
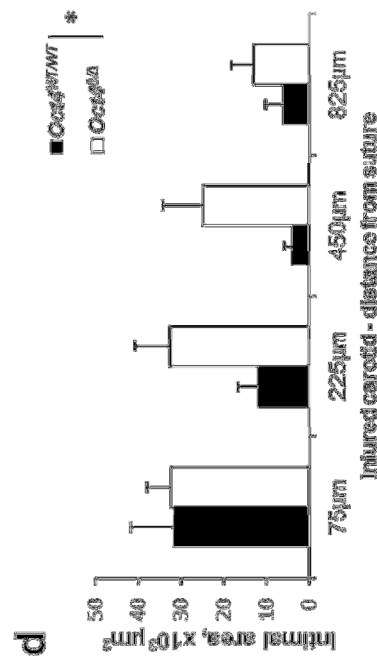
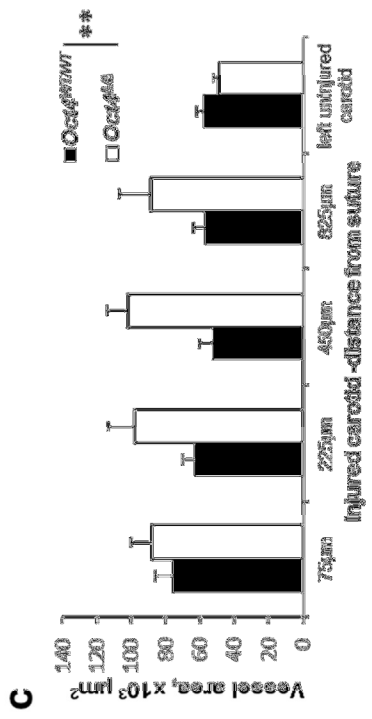
Supplemental Figure 33: Oct4 protein levels were markedly induced within cells of the tunica media and atherosclerotic lesions of the human atherosclerotic lesion.

Micrographs show cross-sections of left human coronary artery: *med* – tunica media, *les* – lesion. Scale bar = 100 μm .



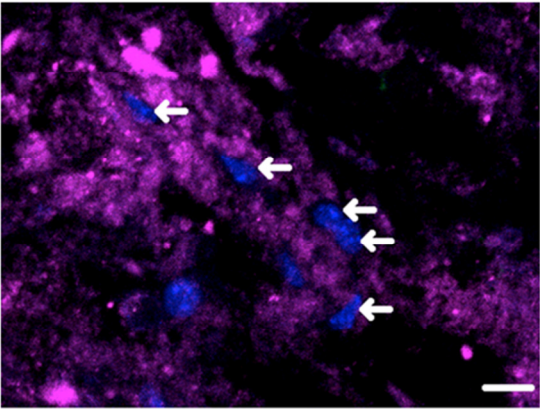
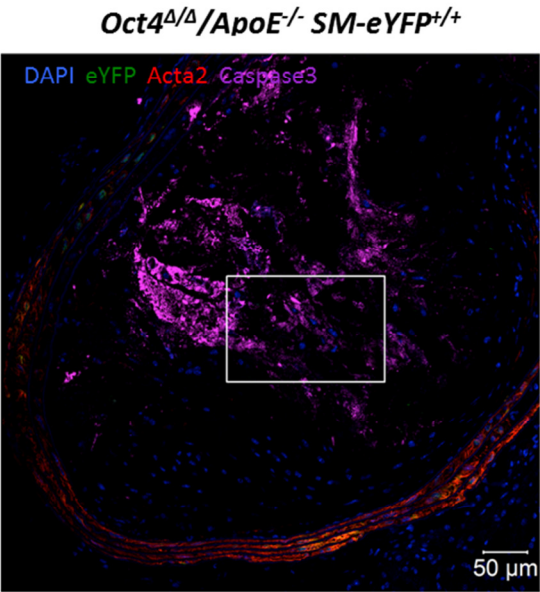
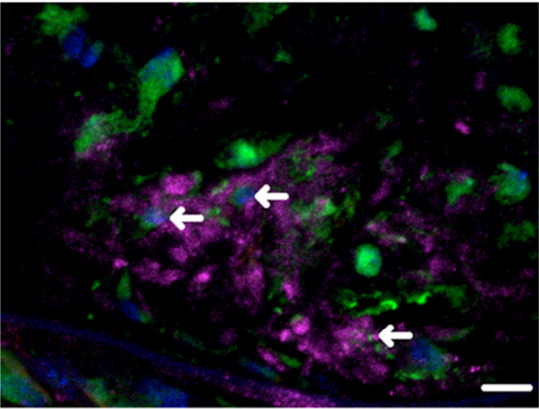
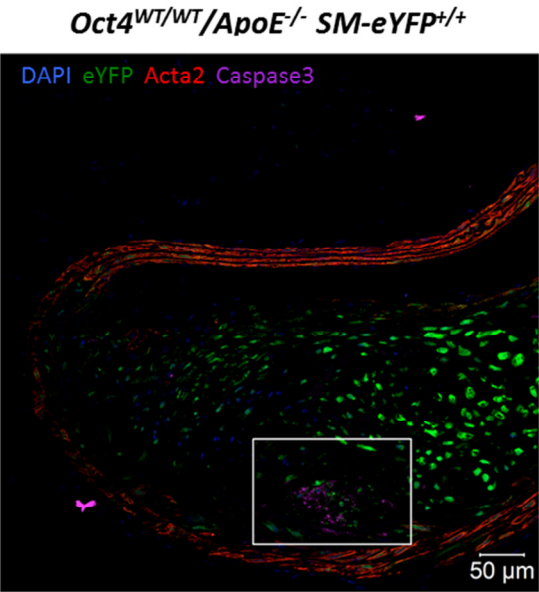
Supplemental Figure 34: SMC-specific conditional KO of the pluripotency gene *Oct4* accelerated neointima formation and tunica media following carotid artery ligation-induced vascular injury.

(a) *Oct4* protein levels were markedly induced in cells within the tunica media of the right injured carotid arteries of *Oct4*^{WT/WT}, but not SMC-specific conditional knockout *Oct4*^{Δ/Δ} mice at day 3 post-carotid ligation injury. Micrographs show cross-sections of injured and uninjured carotid arteries: adv – adventitia, lum – lumen, med – tunica media. Scale bar = 50 μm. (b) Movat staining of representative injured carotid arteries of *Oct4*^{WT/WT} and *Oct4*^{Δ/Δ} mice at day 21 post-carotid ligation injury. Scale bar = 50 μm. (c) Total vessel area within external elastic lamina, (d) intimal area and (e) medial area. Values represent mean ± s.e.m. **P*≤0.05, ***P*≤0.005 by 2-way ANOVA or #*P*≤0.05 *Oct4*^{WT/WT} (*n*=8) vs. *Oct4*^{Δ/Δ} (*n*=8) mice by non-parametric ANOVA across multiple locations from the ligation suture.



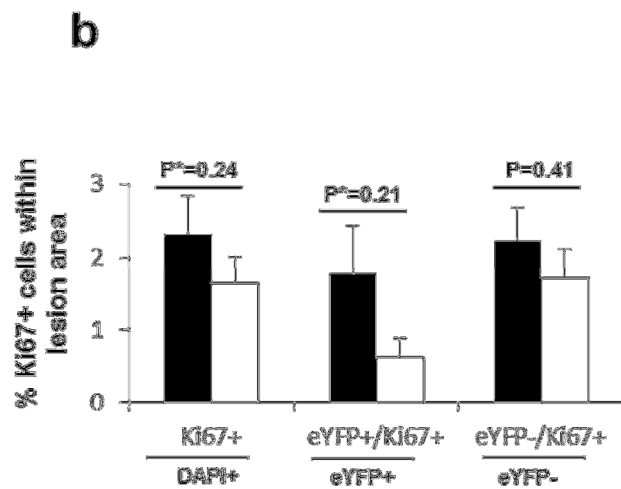
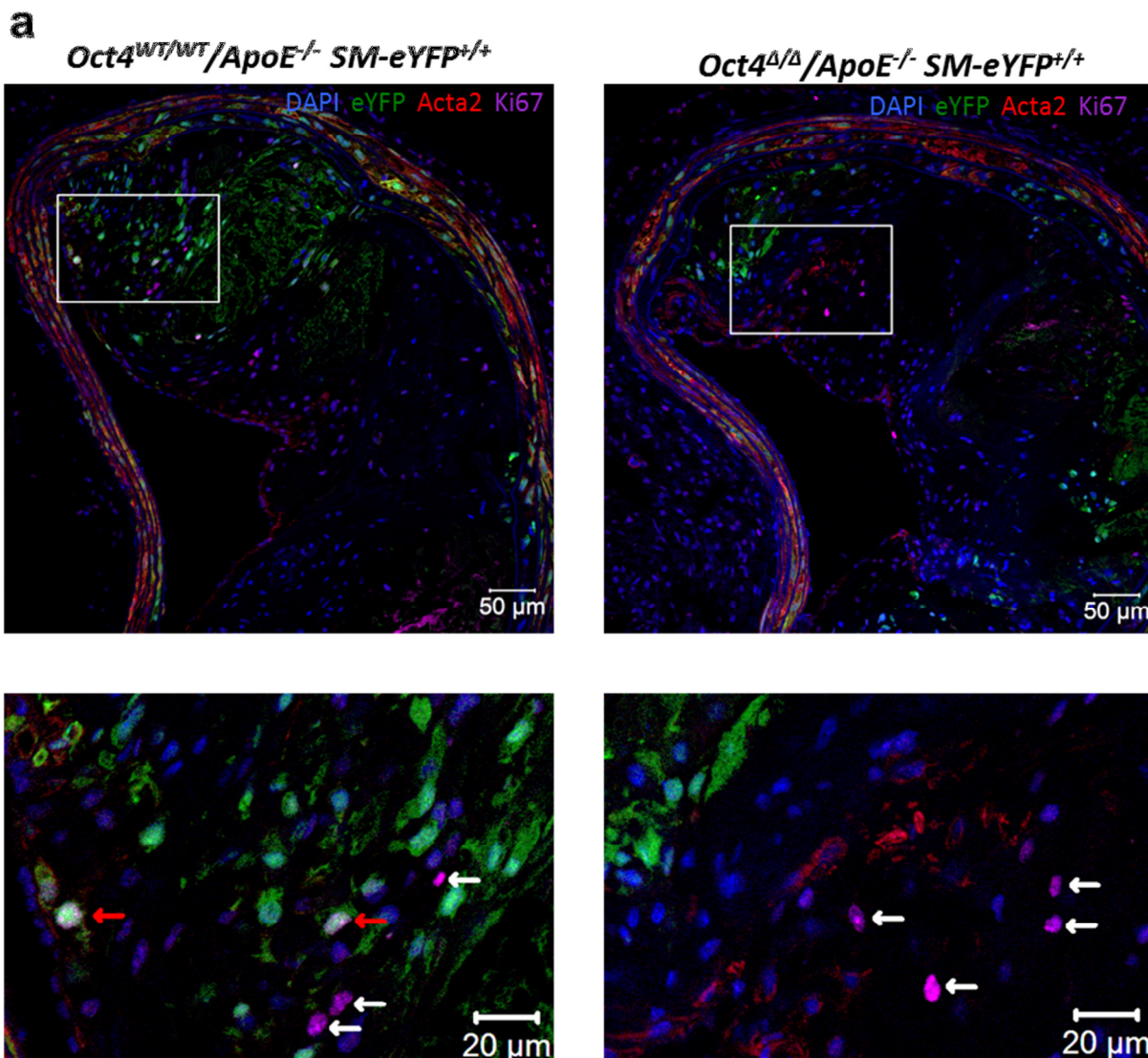
Supplemental Figure 35: Genetic loss of Oct4 in SMCs decreased non-SMC apoptosis.

Co-immunostaining of representative brachiocephalic arteries of $Oct4^{WT/WT}ApoE^{-/-}SMC-eYFP^{+/+}$ and $Oct4^{\Delta/\Delta}ApoE^{-/-}SMC-eYFP^{+/+}$ mice fed a Western diet for 18 weeks for DAPI, Acta2, eYFP and cleaved caspase-3. DAPI (blue), Acta2 (red), eYFP (green) and cleaved caspase-3 (magenta) staining of representative brachiocephalic arteries of $Oct4^{WT/WT}ApoE^{-/-}SMC-eYFP^{+/+}$ and $Oct4^{\Delta/\Delta}ApoE^{-/-}SMC-eYFP^{+/+}$ SMC lineage-tracing mice fed a Western diet for 18 weeks. Arrows indicate examples of double-positive eYFP+/caspase-3+ cells ($Oct4^{WT/WT}ApoE^{-/-}SMC-eYFP^{+/+}$ panel) or eYFP-/caspase3+ cells ($Oct4^{\Delta/\Delta}ApoE^{-/-}SMC-eYFP^{+/+}$ SMC panel).



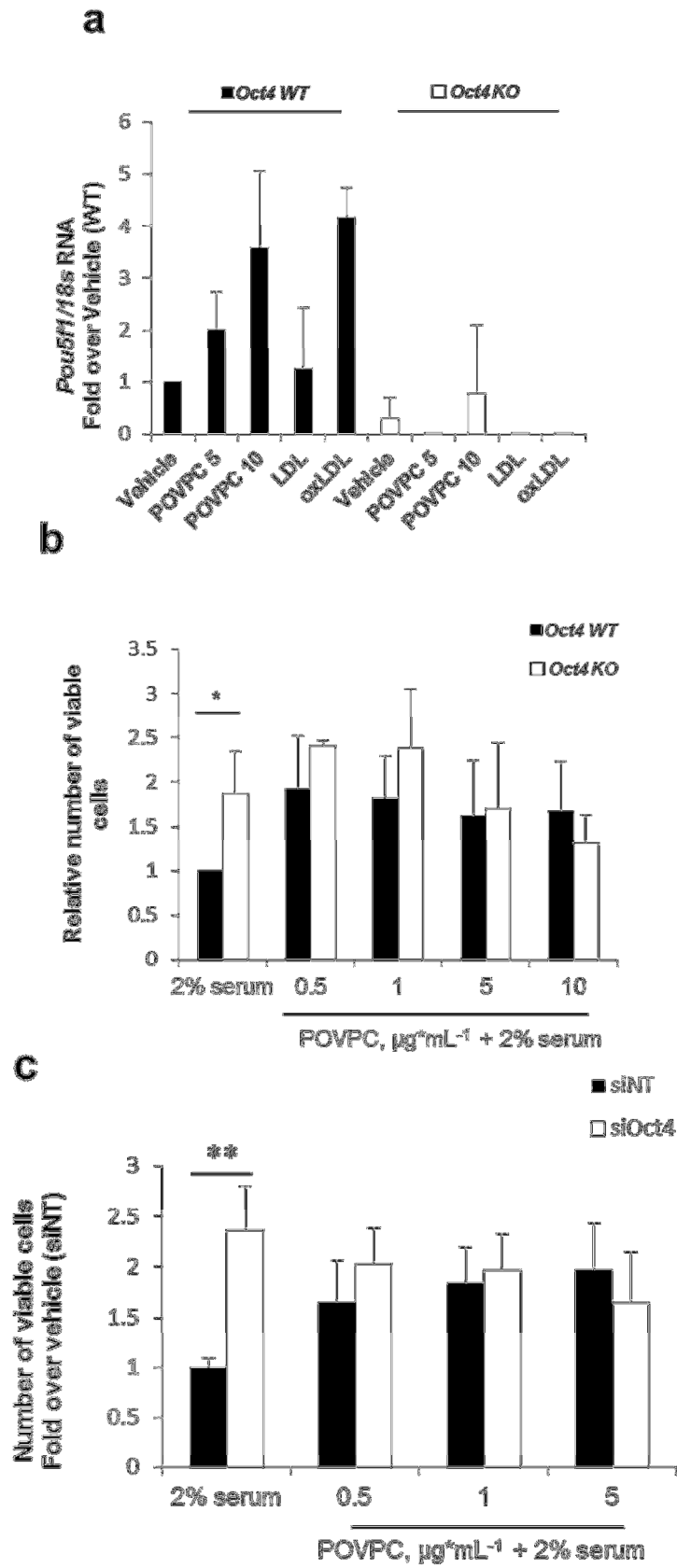
Supplemental Figure 36: SMC specific KO of Oct4 has no significant effect on cellular proliferation in atherosclerotic lesions.

(a) Co-immunostaining of representative brachiocephalic arteries of $Oct4^{WT/WT}ApoE^{-/-}SMC-eYFP^{+/+}$ and $Oct4^{\Delta/\Delta}ApoE^{-/-}SMC-eYFP^{+/+}$ mice fed a Western diet for 18 weeks for DAPI, Acta2, eYFP and Ki67 (magenta). Arrows indicate examples of eYFP+/Ki67 positive cells (red arrows) and eYFP-/Ki67+ cells (white arrows). **(b)** Quantification of total Ki67+ cells, eYFP+/Ki67+ over eYFP+ cells and eYFP-/Ki67+ over eYFP- cells within atherosclerotic lesions. Values represent the percent of Ki67+ and eYFP+ cells, mean \pm s.e.m. P values for $Oct4^{WT/WT}ApoE^{-/-}SMC-eYFP^{+/+}$ (n=9) vs. $Oct4^{\Delta/\Delta}ApoE^{-/-}SMC-eYFP^{+/+}$ (n=14) mice were generated by non-parametric (P*) or one-way parametric (P) ANOVA.



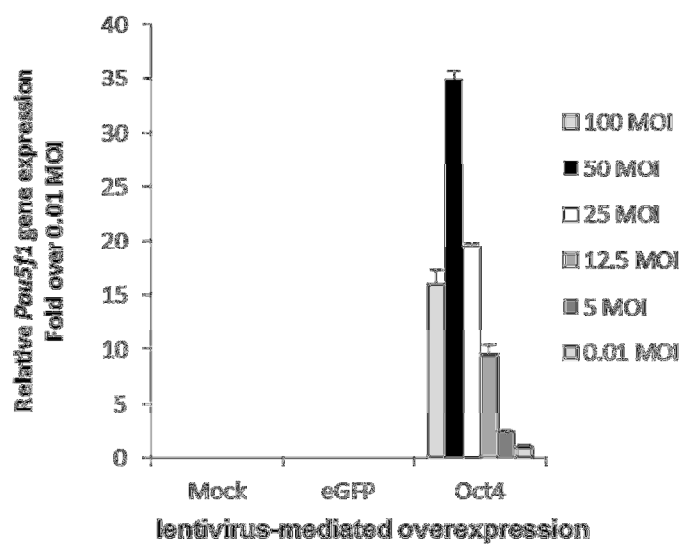
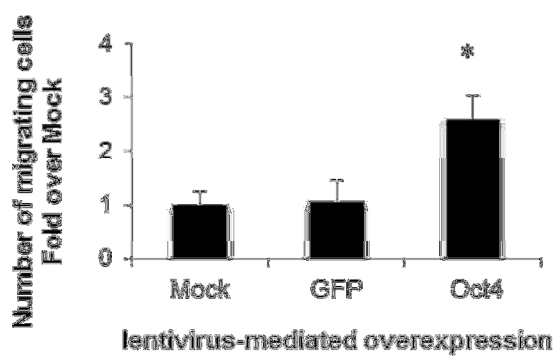
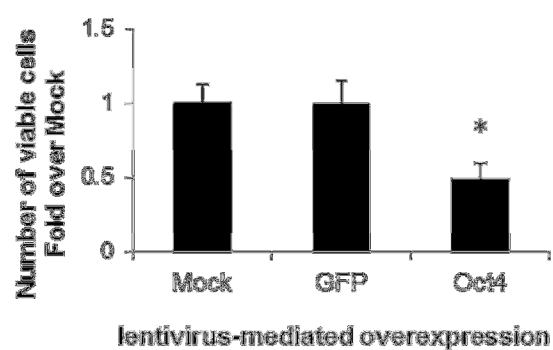
Supplemental Figure 37: Oct4 KO increases cellular proliferation in vitro in baseline conditions which is ameliorated during treatment with POVPC.

(a) Oxidized phospholipids induced expression of the endogenous Oct4 (*Pou5f1*) in SMC. Mouse aortic *Oct4*^{WT/WT} and *Oct4*^{Δ/Δ} SMC were treated with vehicle, POVPC 5 or 10 μg mL⁻¹, OxLDL 100 μg mL⁻¹ and LDL 100 μg mL⁻¹ for 24 hours and expression of *Oct4* gene was measured by quantitative real-time RT-PCR. Data represent mean ± s.e.m. **P*≤0.05 vs. vehicle by Student's *t*-test. (b) Mouse aortic *Oct4*^{WT/WT} and *Oct4*^{Δ/Δ} SMC or (c) SMC transfected with siOct4 or non-target siRNA (siNT) were grown in culture media containing 2% serum with 0–10 μg mL⁻¹ POVPC. Relative viable cell numbers were counted after 24 hours based on the absorbance at 485 nm using a CellTiter 96[®] AQ_{ueous} One Solution Cell Proliferation assay (MTS assay). Data represent mean ± s.e.m. **P*≤0.05, ***P*≤0.005 vs. vehicle by Student's *t*-test.



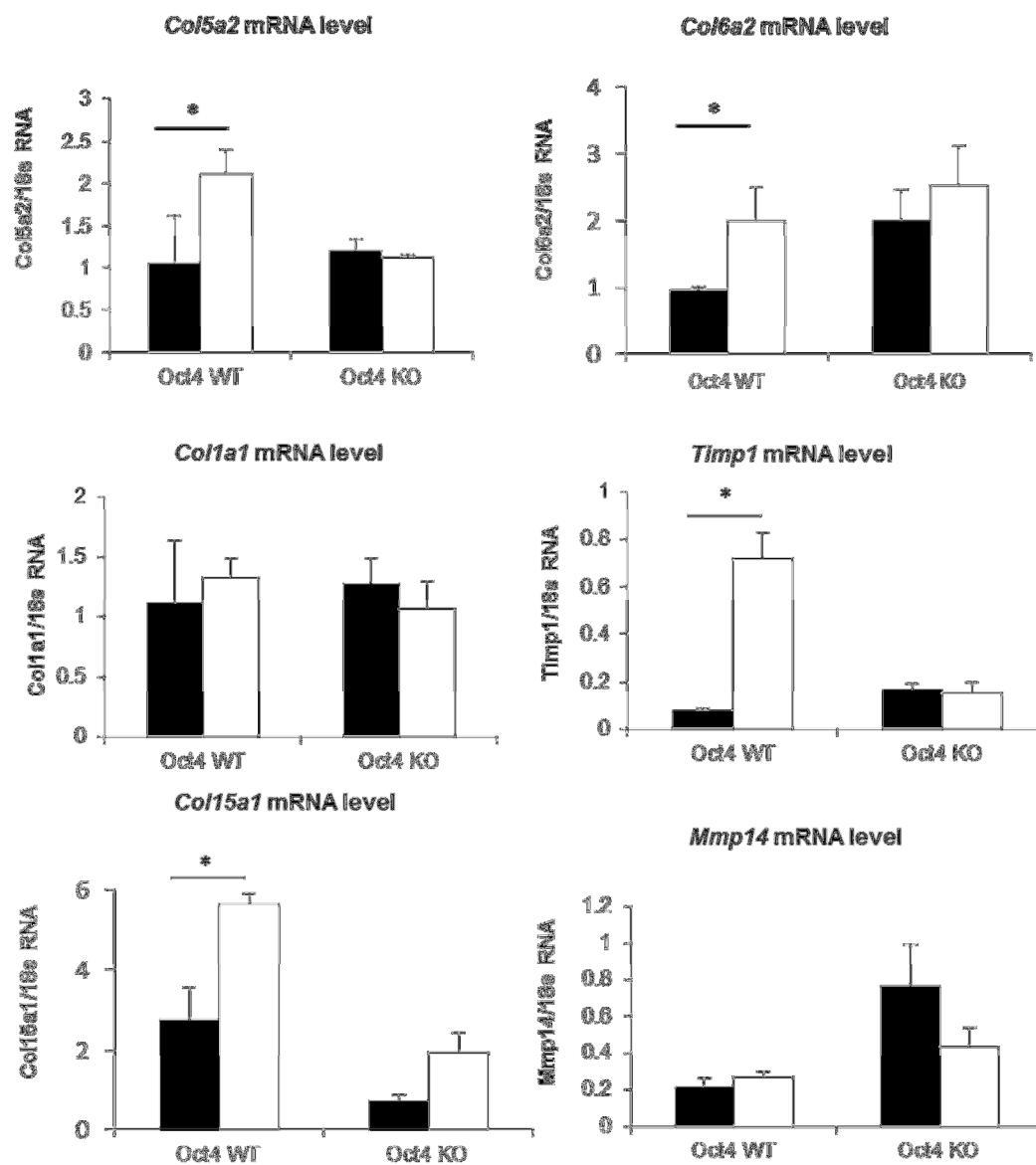
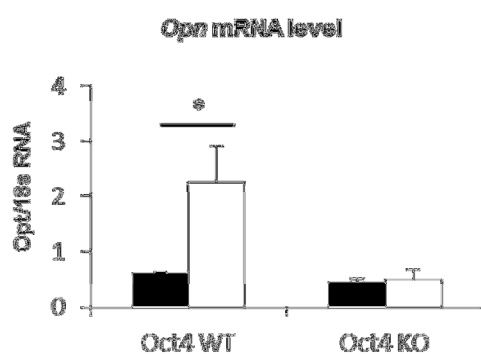
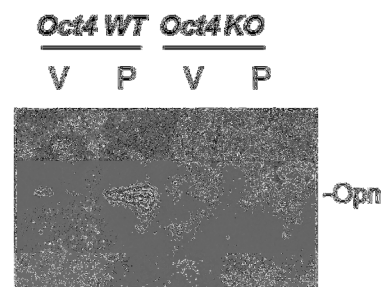
Supplemental Figure 38: Lentiviral-induced overexpression of the pluripotency factor Oct4 induced increased migration, but reduced proliferation of cultured SMC.

Mouse aortic SMCs were infected with lentiviruses expressing Oct4 or eGFP as a control lentivirus (GFP) or were mock infected (uninfected, Mock) for 48 hours. **(a)** Lentivirus infection of mouse aortic SMC was performed at 100, 50, 25, 12.5, 5 and 0.01 MOI. Expression of *Oct4* gene (*Pou5f1*) was measured by quantitative real-time RT-PCR. Data represent means \pm s.d. **(b)** Transmigration assays were performed using mouse aortic SMC infected with lentiviruses (50 MOI). Data represent cell counts in the Boyden chambers with mean \pm s.e.m. from 10 randomly chosen high-power fields, * $P < 0.05$ vs. Mock-infected cells by Student's *t*-test. **(b)** SMCs were infected with lentiviruses (50 MOI) and relative cell numbers determined using a CellTiter 96[®] AQ_{uneous} One Solution Cell Proliferation assay (MTS assay) (Cell Promega) involving measurement of absorbance at 485 nm. Data represent mean \pm s.e.m. * $P < 0.05$ vs. Mock-infected cells by Student's *t*-test.

a**b****c**

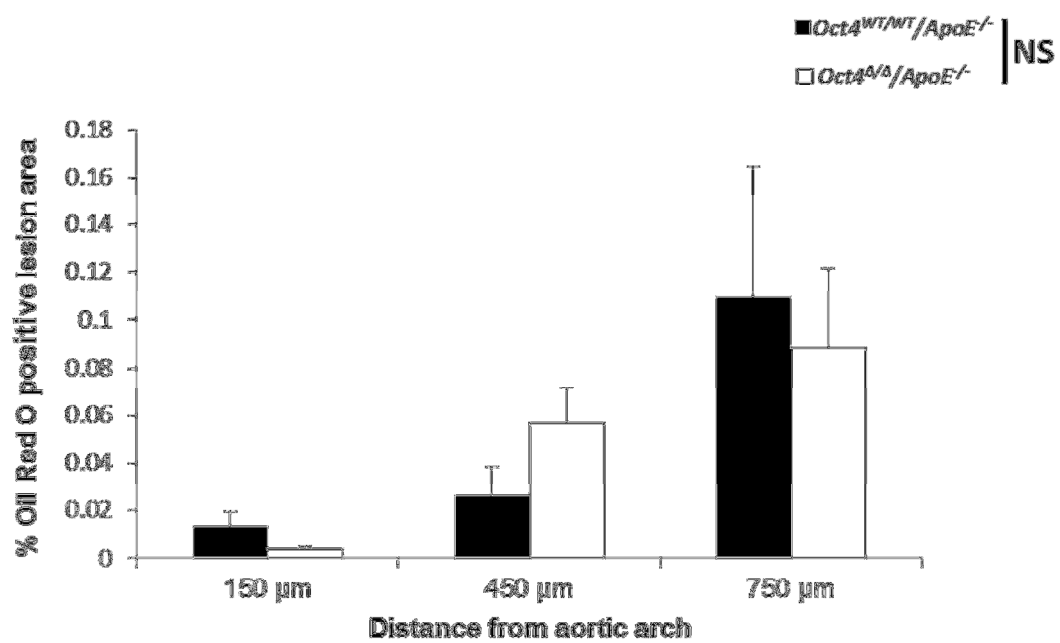
Supplemental Figure 39: Expression of the extracellular matrix-dependent genes was abolished in $Oct4^{\Delta/\Delta}$ SMC.

$Oct4^{WT/WT}$ and $Oct4^{\Delta/\Delta}$ SMC were treated with vehicle or POVPC $10 \mu\text{g mL}^{-1}$ for 24 hours and expression of (a) *Col5a1*, *Col6a2*, *Col1a1*, *Col15a1*, *Timp1*, *Mmp14*, (b) *Opn* was measured by quantitative real-time RT-PCR. Data represent mean \pm s.e.m. * $P \leq 0.05$ vs. vehicle by Student's *t*-test. (c) $Oct4^{WT/WT}$ and $Oct4^{\Delta/\Delta}$ SMC were treated with vehicle (V) or POVPC $10 \mu\text{g mL}^{-1}$ (P) for 48 hrs. Conditioned media were analyzed by Western blot using antibody for Osteopontin (Opn). POVPC-induced up-regulation of Opn protein was completely blocked in $Oct4^{\Delta/\Delta}$ SMC. Of note, it has been established that *Opn* gene is transcriptionally activated by Oct4 protein in pre-implantation mouse embryos and cultured pluripotent cells via the PORE enhancer in gene's first intron¹⁸¹.

a**b****c**

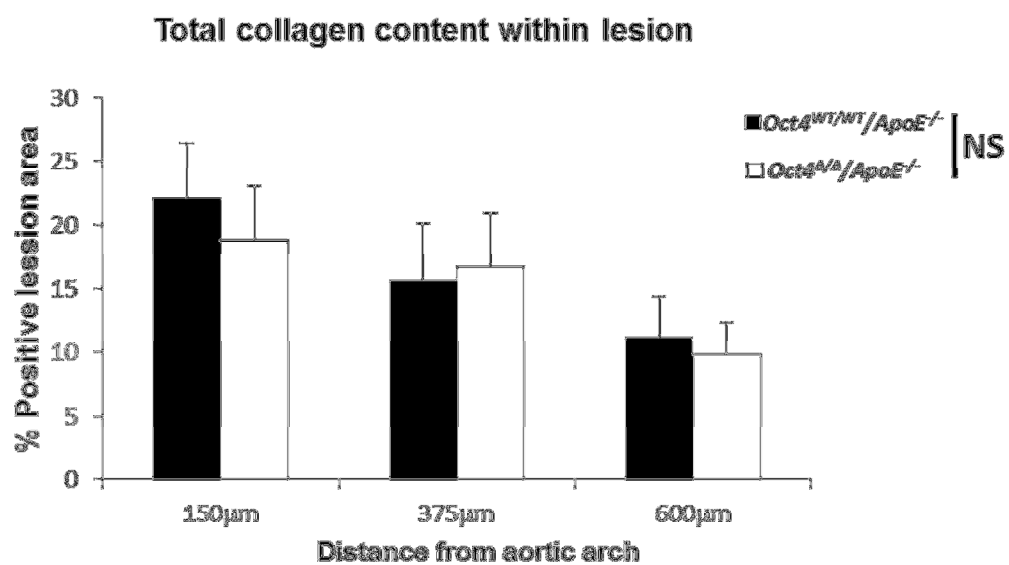
Supplemental Figure 40: SMC specific KO of Oct4 does not affect overall lipid accumulation as quantified by Oil Red O positive staining lesion area.

Values represent mean \pm s.e.m. $P > 0.05$ – not significant (NS) for $Oct4^{WT/WT} ApoE^{-/-} SMC-eYFP^{+/+}$ (n=8) vs. $Oct4^{\Delta/\Delta} ApoE^{-/-} SMC-eYFP^{+/+}$ (n=8) mice across multiple locations along the brachiocephalic arteries were generated by 2-way ANOVA.



Supplemental Figure 41: SMC-specific conditional KO of the pluripotency gene Oct4 did not alter total lesion collagen content.

Quantification of total collagen content based on PicroSirius Red staining. Values represent mean \pm s.e.m. $P > 0.05$ – not significant (NS) for *Oct4*^{WT/WT}*ApoE*^{-/-} ($n=11$) vs. *Oct4* ^{Δ/Δ} *ApoE*^{-/-} ($n=8$) mice by 2-way ANOVA across multiple locations along the brachiocephalic arteries.



Supplemental Figure 42: Schematic of the sequence of 1.5 kb mouse promoter region of the Pou5f1 gene.

Mus musculus strain 129X1/SvJ chromosome 17 genomic contig, NCBI Reference Sequence: NT_039662.3. Three primer sets were used for ChIP assays. Results for primer set #1 are demonstrated in Fig. 16 ***b,e,f***. Primer set #2 and 3 showed similar results (data not shown). Primer set #4 (For 1,823,064-1,823,083; Rev 1,823,200-1,823,219) showed no difference between vehicle- and POVPC-treated SMC (data not shown).

1,823,571 AGGCTCAGAACTCTGTCTGGCTATGTACACTGTGGGGTGTCTGGGCTTTTTGAGGCTGTGTGATTCACCCCTGGGGCCTTCG
 TTCAGAATGGTGTAGGAGCAGACAGACAAACACCATCCCTTGACAGACAGGCACCTTGAGGGCTATTCTCTTGCAAAGATAACT
 AAGCACCCAGGCCAGTAATGGGATCCTCAGACTGGGCCAGAAAACCACTCTAGGGAAGTTCAGGGTAGGCTCTCTGCACCCCC
 TCCTCCTAATCCCGTCTCCTTAGTGTCTTCCGCCAGCACAGGAATGGGGGAGGGTGGGTGACGAGGATGAACACCGGAGTC
 CCTGGAGGAAGGGAAGCAGGGTATCTCCATCTGAGGCTCTGTCTTTGAGGAGAGGTGGAGAGCTGGGGAAGTCTTGTGTGAGG
 GGATTGGGGCTCAGGAGGGGGTGGGGAGCAGGAAGTTGTCCCAGGGGAGCCATCCTGGCCCATCAAGGGTTGAGTACTTG
 TTTAGGGTTAGAGCTGCCCTCTGGGGACCAGGATTGTCCAGCCAAAGCCATTGTCTGCCCCCTCCCCCAGTCCCTCCCA
 GGCCCTTTGAACCTGAAGTCAGATATTTCTTCTCTACCCACCTCCCAACCCGTTGGGTTTCTCCACCCAGGAACTAGGCTG
 GAAGCCTGGGATGAGGAGGTGGGGGAGGGAGAAGTGAAGTCTTGAGGAAAGAGGCCCGGCCCTTAAGTGTGAGGGGATGGA
 GCCTGGGTGCAGGCTTATGGGGTGGGGGGTGGTTAGTGTCTAATCTACCAACCTGGACAACACAGATGGAATACTGTGC
 TCTGAAAACGCAGAGCCAGCACTTCTCTGGGGTCTCTGGGGACATATCTGGTTGGGGCTCGGGTCCCATGGTGTAGAGCCTC
 TAACTCTGGAGACTGGAGGTGCAATGGCTGTCTTGTCTGGCCCTTGACATGGGCTGAAATACTGGGTTCAACCATATCTA
 GGACTCTAGACGGGTGGGTAAGCAAGAACTGAGGAGTGGCCCCAGAAATAAATGGCACACGAACATCAATGGATGTTTTAGG
 CTCTCCAGAGGATGGCTGAGTGGGCTGTAAGGACAGGCCGAGAGGGTGCAGTGCCAACAGGCTTTGTGCGCGCATGGGGCATC
 CGAGCAACTGGTTTGTGAGGTGCGGGTACCCAAAGGCAGGGGTGAGAGGACCTTGAGGTTGAAAATGAAGGCCCTCCTGGGG
 TCCCGTCTTAGGGTTGTCTGTCCAGAGCCCAACCTCCGTCTGGAAGACACAGGCAGATAGCGCTCGCCTCAGTTTCTC
 CCACCCACAGCTCTGCTCCTCCACCCACCCAGGGGGCGGGCCAGAGGTCAAGGCTAGAGGGTGGGATTGGGGAGGGAAG
 GTGAAACCGTCCCTAGGTGAGCCGTCTTCCACCAGGCCCGGCTCGGGGTGCCACCTTCCCATGGCTGGACACCTGGCT 1,825,066
 TCAGACTTCGCCTTCTCACCCC

Klf4 Hif1 Pou5f1 start site

ChIP primer sets:

Forward KLF4 site 1&2 - Hif site 1&2: AGGCTCTCCAGAGGATGGCT #1
 Reverse KLF4 site 1&2 - Hif site 1&2: AGCGCTATCTGCCTGTGTCT

Forward KLF4 site 1: TAGACGGGTGGGTAAGCAAG #2
 Reverse KLF4 site 1: CACAAAGCCTGTTGGCACT

Forward Hif1 site 2: AAGGTTGTCTGTCC #3
 Reverse Hif1 site 2: ACCTAGGGACGGTTTCAC

Forward Neg : CTCTCGTCTAGCCCTTCCT #4
 Reverse Neg : CCTCCACTCTGTCATGCTCA

Supplemental Table 3: Primers used for quantitative real time RT-PCR and site-direct mutagenesis.

Real-time RT-PCR primers

<i>18s RNA</i>	For	CGGCTACCACATCCAAGGAA
	Rev	AGCTGGAATTACCGCGGC
<i>Pou5f1</i> exon1*	For	AAGTTGGCGTGGAGACTTT
	Rev	TTCCACCTTCTCCAACCTCAC
<i>Pou5f1</i> exon4*	For	TGCAAATCGGAGACCCTGGT
	Rev	CCAAGCTGATTGGCGATGTG
<i>Col5a2</i>	For	GTGTCTGTGACAATGGTGCC
	Rev	AGAGCCAGGCATGAGTCCTA
<i>Col6a2</i>	For	GAGCGAGTCAACTCCCTGTC
	Rev	CCATCCAGCAGGAAGACAAT
<i>Col15a1</i>	For	CTGTCCACTTTCCGAGCCTTT
	Rev	AAAGCACTTGGCCCTTGAGA
<i>Col1a1</i>	For	GGCTGCACGAGTCACAC
	Rev	TGGAGGGAGTTTACACGAAG
<i>Timp1</i>	For	ACTCGGACCTGGTCATAAGGGC
	Rev	TTCCGTGGCAGGCAAGCAAAGT

<i>Mmp14</i>	For	CAAGGCCAATGTTCTGGAGGAAG
	Rev	TCTCCATACTCGGAAGGCCTTC
<i>Mmp3</i>	For	ACCAACCTATTCCTGGTTGCTGCT
	Rev	ATGGAAACGGGACAAGTCTGTGGA
<i>Mmp13</i>	For	GCCACCTTCTTCTTGTTGAG
	Rev	AGTCGCAGGATGGTAGTATG
<i>Opn</i>	For	GATGATGATGACGATGGAGACC
	Rev	CGACTGTAGGGACGATTGGAG

* Both primer sets for *Pou5f1* gene showed similar results

Site-directed
mutagenesis

Hif1 BS1	CAGTGCCAACAGGCTAAAAAGTGCGATGGGGCATC
Hif1 BS2	GTTGTCCTGTCCAGAAAACCCCAACCTCCGTCT
Klf4 BS1	AAGGACAGGCCGAGATTTATCAGTGCCAACAGGCT
Klf4 BS2	AGCAACTGGTTTGTGTCTCGTCCGGTGACCCAAG

Chapter 5: Conclusions and Future Directions

Smooth muscle cell involvement in atherosclerotic development and stability has been regrettably underappreciated due to inadequate lineage tracing methodologies. While, the ability of SMCs to down-regulate their SMC marker genes in response to atherosclerotic stimuli has been well studied in the field, researchers, including members of our own lab, have relied heavily on the expression of a single SMC marker (ACTA2) to define a cell as a SMC. On the other hand, expression of ACTA2 and CD68 have been used as important biomarkers for plaque stability. However, controversy over the fidelity of these markers in identifying a cell as either a SMC or macrophage, leaves the exact contribution of each cell type to plaque stability largely unknown. In this dissertation I demonstrated that 86% of intimal SMCs have gone undetected by previous studies. I also showed that approximately one-quarter of cells deemed macrophages by traditional immunohistochemistry are in fact SMC in origin, and that manipulating phenotypic modulation through pluripotency factors OCT4 and KLF4 have profound and opposing effects on lesion size and stability. Taken together, these results indicate that SMCs play a much greater role in atherosclerotic development than previously reported and that the contribution of each cell type within the lesion needs to be closely re-evaluated using high-fidelity lineage tracing.

Development and uses of ISH-PLA in disease state models

Results of Chapter 2 outline the development of a novel method for detecting histone modifications at specific gene loci in single cells within histological sections, and how this method can be used to lineage trace SMCs in human atherosclerotic lesions *in vivo*. Through this method we were able to identify SMC derived macrophages in human atherosclerotic lesions (Figure 7) and discern KLF4 binding to the *Tagln* promoter in medial SMCs of 18 week Western diet fed SMC-lineage tracing mice in Chapter 3 (Supplemental Figure 26b). While traditional ChIP methods revealed that KLF4 binding was increased on SMC promoters after long-term Western diet feeding (Supplemental Figure 26a), ISH-PLA was able to determine the location of these cells within the lesion (Supplemental Figure 26b). By identifying the localization of transcription factor binding, researchers are able to further refine cell signaling models. For instance, KLF4 binding to the *Tagln* promoter was mainly observed in SMCs still contained within the medial layer, suggesting that KLF4 binding at this location initiates SMC phenotypic modulation, most likely through deacetylation of the promoter via recruitment of HDACs 2, 4, and 5 as reported previously in Salmon et al.⁸⁷ Furthermore we believe that ISH-PLA will allow researchers to more closely examine the role of different histone modifications and transcription factor binding in the microenvironments of the atherosclerotic lesion and have a high impact on other disease models including cancer.

Smooth muscle cell lineage tracing and atherosclerosis

Studies in Chapter 3 provide the first rigorous analysis of phenotypically modulated SMCs within advanced atherosclerotic plaques (Figure 8). The discovery that nearly all intimal SMCs are undetectable by traditional immunohistochemical techniques raises questions about the conclusions of hundreds of publications over the past thirty years. In particular, a recent article by Tang *et al.*¹⁸ concluded that the majority of SMCs are quiescent and that primary cultures of SMCs are actually derived from multipotent vascular stem cells (MVSCs) within the media, not SMCs. Our results show that these findings are incorrect. After 18 weeks of Western diet feeding YFP+ cells comprise ~30% of the total cellular composition within the atherosclerotic plaque (Supplemental Table 2). We also showed that a primary culture of SMCs from SMC YFP^{+/+} *ApoE*^{-/-} was 98% SMC pure based on flow cytometry for YFP+ of cultured cells (Supplemental Figure 27). Many studies still need to be done in order to fully assess the contribution of SMCs to the atherosclerotic lesion, but it is our sincere belief that these studies are the first of many that will lead to significant modifications in the dogma of how atherosclerosis develops.

Pluripotency factors KLF4 and OCT4 regulate SMC phenotypic modulation and differentially affect atherosclerotic plaque size and indices of plaque stability

KLF4 has been implicated as a necessary factor for SMC phenotypic switching *in vitro* for fifteen years, however, due to the lack of a high fidelity SMC conditional knock mouse model, no studies to date have been able to study the role of KLF4 in SMC phenotypic switching *in vivo*. Therefore, in Chapter 3 we utilized our new SMC lineage tracing mouse to investigate the role of SMC cell selective KLF4 KO in the development of atherosclerosis. When KLF4 was selectively knocked out in SMCs, atherosclerotic plaques were smaller and had increased indices of stability (Figure 10).

In contrast, when pluripotency factor OCT4 was selectively knocked out in SMCs, atherosclerotic lesions were bigger and had decreased indices of stability (Figure 13). Chapter 4 focused on the surprising finding that OCT4 is dramatically up-regulated in SMCs vascular injury and atherosclerosis despite previous reports that OCT4 is not expressed in somatic cells⁹⁹. One of the most shocking findings was that *Oct4* knock out in SMCs resulted in a 50% reduction in phenotypically modulated SMCs within the plaque (Figure 13) which appears to be due to a reduced ability to phenotypically modulate and migrate (Figure 14). A schematic diagramming the hypothesized mechanism of action of OCT4 and KLF4 on SMC differentiation can be found in Figure 17.

Both KLF4 and OCT4 are indicated as important transcription factors in the induction of a pluripotency state from terminally differentiated cell lineages⁹⁶,⁹⁷. Between the two, only OCT4 has been shown to be sufficient for cellular reprogramming⁹⁸, but before the aforementioned studies in Chapter 4, there was no convincing evidence of OCT4 expression in somatic cells⁹⁹. Indeed, SMCs are different from skeletal and cardiac muscle in that they are able to undergo profound phenotypic changes in response to environmental cues⁵. Given that we identified KLF4 and OCT4 expression in phenotypically modulated SMCs within the atherosclerotic lesion (Figures 12, Figure 18) and demonstrated dramatic changes in SMC phenotype (KLF4 KO) and their ability to phenotypically modulate/migrate (OCT4 KO), we believe that KLF4 and OCT4 are functioning to push SMCs into a more plastic state where they respond to environmental cues and take on characteristics of other cell types as a mechanism of injury repair. In corroboration with this theory is the finding that a subpopulation of SMCs (YFP+ cells) within the atherosclerotic lesions co-express several markers of mesenchymal stem cells (MSCs) as assessed by flow cytometry (Figure 19).

Smooth muscle cells as a therapeutic target

One of the major concerns that arose from Chapter 3 was whether or not the source of LGALS3+ cells in the lesion had any bearing on the use of the marker as an index of plaque instability. In SMC specific KLF4 KO mice, there was a decrease in the overall LGALS3+ population, which was mainly a result of

a decrease in LGALS3+YFP+ cells. However, there were no significant changes in the total eYFP+ population within the lesion, suggesting that specifically altering the phenotypic state of SMCs can affect the LGALS3+ population. Due to the fact that the lesions from these mice also demonstrated reduced indices of plaque stability we hypothesize that the cells that would have been LGALS3+YFP+ are now being pushed into a different phenotypic state that is beneficial for lesion size and stability. Therefore we believe that selectively targeting and altering SMC phenotypic modulation can result in novel and effective therapeutic treatments of atherosclerosis. However, the mechanisms by which OCT4 and KLF4 function *in vivo* to affect SMC phenotype and how those changes significantly alter plaque size and stability are not fully understood, and need to be elucidated in order to consider future treatment options.

Future Directions

While the scope of these experiments exemplify a comprehensive study of SMC phenotypic switching in both mouse and human lesions several important and interesting questions remain. Experiments are described below in decreasing order of priority which can answer some key additional questions associated with this project.

Do macrophages from SMC origins possess different functions than macrophages of hematopoietic origins?

The only way to directly assess the functional differences between macrophages of hematopoietic origins versus SMC origins is to observe them *in vivo*, in particular, their ability to phagocytize. Recently, *in vivo* imaging using 2-photon microscopy has made leaps and bounds in the ability to capture the interaction of multiple cell types in live animal models. For example, Kreisel *et al.*^{182, 183} developed a model where neutrophil extravasation into the lung in response to inflammatory stimuli could be visualized using time-lapse 2-photon microscopy. This technology is also being perfected in mouse models of atherosclerosis. Break throughs in extracting data from motion artifacts over the past ten years have made the use of 2-photon microscopy possible both *ex vivo* and *in vivo*^{184, 185}, and more recently has allowed for the study of immune cell interactions within the intima¹⁸⁶.

In order to determine the functional differences between SMC derived macrophages and hematopoietic derived macrophages using 2-photon microscopy, a new mouse model will need to be employed. First, the *Myh11-CreER^{T2} Apoe^{-/-}* mice would be crossed to a ROSA floxed Stop tomato red reporter line in order to be compatible with commercially available GFP transgenic mouse lines, such as *LysM-GFP* and *Arg1-YFP*. Next, the SMC-tomato red lineage tracing mouse would be crossed to the commercially available *LysM-GFP* mice (in order to label maturing macrophages). This mouse

line could then be treated with tamoxifen from 6-8 weeks of age to label SMCs red before the start of Western diet, and visualize the newly differentiating macrophages with green from the *LysM-GFP*, as Western diet treatment continues and lesions progress. Using 2-photon microscopy YFP+/tomato red+ cells (SMC derived macrophages) could be distinguished from YFP-/tomato red+ cells (hematopoietic derived macrophages). Through the use of this system, functional responses to external stimuli can be assessed without the fear of an *in vitro* artifact that would arise from attempting to isolate these cells and study them in culture.

In addition to future 2-photon experiments, we are currently working to isolate mRNA from sorted eYFP+/LGALS3+ and eYFP-/LGALS3+ cells to assess changes in mRNA expression between SMC derived and hematopoietic derived macrophages. However, aortas that are digested to a single cell suspension for flow cytometry have low yields of cells ranging from 50,000-500,000 events per mouse depending on the amount of atherosclerosis present in each animal. Given that the average of eYFP positive population in a young healthy mouse is ~60%, only 30,000 to 300,000 of those cells are YFP+. Further calculating the average population of SMC derived macrophages seen by flow cytometry, which is diluted by large segments of the aorta that do not possess advanced atherosclerosis, we would be left with a maximum of 15,000 cells per mouse analyzed. In fact, this is very close to the actual numbers of cells that we have retrieved per animal thus far (2,000-5,000 eYFP+/LGALS3+ cells/mouse).

However, even if at the maximum 15,000 cells per mouse, a minimum of ten animals would need to be pooled to ensure sufficient mRNA for a microarray or RNAseq experiment. Our next avenue of inquiry will be to sort YFP+/LGALS3+ and YFP-/LGALS3+ cells for nano-ChIPseq in order to assess changes in histone modifications in SMC derived macrophages compared to hematopoietic derived macrophages.

How does KLF4 regulate the phenotypic modulation of SMCs to a macrophage-like state, and how might this transition effect plaque size/stability?

In vitro assays showed KLF4 to be necessary for cholesterol treatment induced *Lgals3* mRNA expression (Figure 12), and greatly reduced the number of SMC derived macrophages within the atherosclerotic lesion (Figure 10), but more studies are necessary to determine **how** KLF4 regulates this transition. One theory is that KLF4, already known to down-regulate a cohort of SMC marker genes^{90, 95}, simultaneously functions through the activation of monocytes to macrophages through binding to genes such as iNOS¹⁵². In order to test this hypothesis the lab has been gathering samples of KLF4 WT and KO SMCs treated with cholesterol to determine by ChIP analysis if KLF4 is binding to iNOS or other macrophage associated genes within the macrophage-like SMCs.

The loss of SMC derived macrophages was correlated to increased plaque stability and decreased lesion size. One hypothesis that could explain these results is that SMC derived macrophages are not efficient phagocytes and

impair the ability of the “professional phagocytes” from functioning within the lesion. KLF4 is not only indicated in monocyte differentiation to macrophages, but is also important in polarization of macrophages to an M2 state¹⁵³. Macrophages are similar to SMCs in their ability to modulate into a plethora of phenotypes that each have unique contributions to the development of atherosclerosis. Most commonly referred to are the M1 and M2 macrophage phenotypes. M1 macrophages are most frequently seen in early stage atherosclerotic lesions and where they release high levels of pro-inflammatory mediators such as IL-1 β , whereas M2 macrophages are associated with wound healing and will secrete anti-inflammatory mediators (reviewed by Fernandez-Velasco *et al.*¹⁸⁷ and Koltsova *et al.*¹⁸⁸). In addition, a third type of macrophages, Mox macrophages, can be stimulated by treating either M1 or M2 macrophages with oxidized phospholipids¹⁸⁹. This macrophage subtype also expresses IL-1 β , but not to the same extent as M1 macrophages¹⁸⁹.

Of major interest, recent studies in our lab indicate that genetic loss of IL-1 β signaling is detrimental to lesion stability in advanced atherosclerosis¹⁴⁷. Therefore, the increase in indices of plaque stability within SMC specific KLF4 KO mice may be due to the depletion of M2 state macrophages. Further immunofluorescent staining of YFP+/LGALS3+ cells in conjunction with M2 macrophage markers such as ARG1 and CD206 need to be completed in order to confirm that the decrease SMC derived macrophages represents a decrease in the M2 macrophage population. Also, cytokine arrays on KLF4 WT and KO

cholesterol loaded SMCs could confirm if IL-1 β or other M1/M2 secreted factors are altered with KLF4 KO.

A second hypothesis, as was touched on earlier, is that the loss of KLF4 within SMCs pushed phenotypically modulated SMCs away from a macrophage-like state and into a more synthetic or contractile state. Synthetic state SMCs produce extracellular matrix proteins that can help stabilize plaques. While there were no changes in collagen content in the lesions of SMC YFP^{+/+} *Klf4* ^{Δ/Δ} *ApoE*^{-/-} versus SMC YFP^{+/+} *Klf4*^{wt/wt} *ApoE*^{-/-} mice, there was an increase in ACTA2 staining, especially proximal to the lumen, which has been long associated with differentiated SMCs and increased plaque stability.

Studies revealed that 86% of SMCs within atherosclerotic lesions of 18 week Western diet fed animals are undetectable by ACTA2, but only 23% of these cells were identified as macrophage-like. What is phenotypic state of the other ~60% and how are they affecting atherosclerotic plaque stability?

As outlined in the Introduction, SMCs are remarkably plastic and capable of modulating into at least five different phenotypic states: 1) contractile state, 2) synthetic state, 3) inflammatory state, 4) chondrocyte-like state, and 5) macrophage-like state, as assessed by *in vitro* studies. In our studies we show conclusive evidence of contractile state SMCs and macrophage-like SMCs (eYFP+/LGALS3+ cells in the intima), we have not yet investigated other

phenotypic states of SMCs in our SMC lineage tracing mouse model. Speer *et al.*⁴³ have previously shown evidence of SMC derived chondrocytes within atherosclerotic lesions using a *Tagln*-Cre ROSA26 lacZ mouse model. While this mouse model may label, non-SMCs that up-regulate *Tagln* during the development of atherosclerosis, the morphology and location of the labeled cells leads us to believe that some of our phenotypically modulated SMCs are indeed becoming chondrocyte-like. In order to confirm that a sub-population of these cells are taking on properties of chondrocytes careful co-staining for chondrocyte markers, including Osteopontin, Runx2/Cbfa1 and ALP will need to be analyzed in parallel with the SMC lineage tracer eYFP. Of interest, we also have data showing that POVPC treated cultured SMCs induce osteopontin on both the mRNA and protein level (Supplemental Figure 39).

Based on the work previously done by Alexander *et al.*³⁶, there may also exist distinct inflammatory state SMCs, separate from synthetic state SMCs within the atherosclerotic lesions. Results from microarray screens of SMCs treated with PDGF-DD versus IL-1 β identified two factors, RGS17 and CCL20, that theoretically separate the phenotypically modulated SMCs into synthetic and inflammatory phenotypic states³⁶. In order to identify whether or not these markers label two distinct populations of phenotypically modulated SMCs we would need to stain atherosclerotic lesions from the SMC lineage tracing mice and ascertain that RGS17 and CCL20 do not label the same SMCs. In addition, cell sorting and microarray analysis of YFP+/RGS17+ and YFP+/CCL20+ cells

would confirm that the gene expression profiles are similar to the PDGF-DD and IL-1 β treated SMCs from which the original observation was made. While unclear if these represent yet another type of phenotypically modulated SMC or a subset of one of the states previously listed, it is important to note that a subpopulation of YFP+ cells also express ITGAX (CD11c), a commonly used marker for dendritic cells (Figure 8c).

The plasticity of the phenotypically modulated SMC raises questions about whether or not these cells might represent a mesenchymal stem cell (MSC) population within the lesion. Indeed, Tang *et al.*¹⁸ raised the idea of an MSC (which they labeled MVSC) in injured vessels, but concluded that the source of their multipotent cell arose from cells other than SMCs within the media. Due to inconsistencies between the Tang paper and other findings in the field, we believe that the MVSC cells discovered in their research may actually be phenotypically modulated SMCs¹⁸. In support of this claim, we have completed flow cytometry studies showing a subpopulation of eYFP+ cells (phenotypically modulated SMCs) in 18 week Western diet fed SMC lineage tracing mice that co-express MSC markers ENG+ (CD105) and ATXN1+ (Sca-1) (Figure 19). Our working hypothesis is that SMCs sense environmental cues from the atherosclerotic lesion causing them to de-differentiate and take on characteristics of other cell types in part through the up-regulation of pluripotency factors KLF4 and OCT4.

Other cells in the intima (Figure 13) also expressed OCT4 after Western diet treatment (in the SMC Oct4 KO mouse). What are those cells and how are they contributing to lesion development?

An exciting result from investigating OCT4 expression in SMCs was that a hypercholesterolemic state appears to induce OCT4 expression in multiple cell types (Figure 13). While we are uncertain at the moment what cells these are, we suspect that a subset of the OCT4 expressing cells are macrophages based on morphology. We are currently in the process of generating *LysM^{Cre/Cre} Oct4^{fl/fl} ROSA Stop floxed eYFP^{+/+} ApoE^{-/-}* mice to ascertain how OCT4 up-regulation in macrophages affects atherosclerotic lesion development. We believe that OCT4 functions in SMCs through its ability to promote a de-differentiated state. Since LYSM is up-regulated during monocyte to macrophage differentiation (and has already committed to a macrophage lineage), we may not see the same magnitude of change in the infiltrating macrophages into the lesion as we do for OCT4 KO in SMCs. When analyzing the results of the *LysM^{Cre/Cre}* model we will need to keep this in mind and may decide to utilize the *Itgam-cre* mouse¹⁹⁰ to selectively KO *Oct4^{fl/fl}* in hematopoietic cell lineages in order to assess OCT4's role in the differentiation of hematopoietic cell lineages during the development of atherosclerosis.

Earlier loss of KLF4 was shown to dramatically reduce the instance of SMC derived macrophages (Figure 10). What is the role of OCT4 in SMC phenotypic switching to a macrophage-like state?

We are still in the process of determining the effect of OCT4 on SMC derived macrophages. Currently it appears that there is a reduction in the number of macrophage-like SMCs within the lesions of *Oct4^{Δ/Δ}/ApoE^{-/-} SMC eYFP^{+/+}* mice, however we are uncertain whether or not this is solely a function of the reduced overall numbers of phenotypically modulated SMCs within the lesion, or if OCT4 plays a direct role in SMC to macrophage-like SMC transition. Interestingly, analysis of ACTA2, eYFP, and LGALS3 staining in *Oct4^{WT/WT}/ApoE^{-/-} SMC eYFP^{+/+}* versus *Oct4^{Δ/Δ}/ApoE^{-/-} SMC eYFP^{+/+}* mice revealed that SMC specific OCT4 KO resulted in increased YFP+LGALS3+ cells within the media but no change in the numbers of SMCs (Figure 20a,b). *In vitro* studies also demonstrate increased Lgals3 mRNA expression when OCT4 KO cells are treated with POVPC (Figure 20c). OCT4 KO cells were also more phagocytic of red blood cells when exposed to cholesterol (Figure 20d). Taken together, these results suggest that the putative decrease in macrophage-like SMCs within the atherosclerotic lesion is not due to an inhibitory effect of OCT4 on SMC transition to a macrophage-like state, but instead, an inhibitory effect of OCT4 on SMCs entering the atherosclerotic lesion. While these preliminary data are exciting, there is still a lot of work necessary to flush out the mechanisms behind both

KLF4 and OCT4 regulation of SMC phenotypic switching. Earlier we mentioned submitting KLF4 WT vs KO cholesterol loaded samples out for KLF4 ChIP-sequencing (ChIP-seq). Here I would also recommend preparing similar samples using OCT WT vs KO cells for both ChIP-seq and RNA-seq in order to compare regulatory mechanisms of macrophage gene expression between KLF4 and OCT4 to determine what pathways are most important in the phenotypic transition from SMC to macrophage-like SMC.

How frequent are SMC derived macrophages within human lesions? Are SMC derived macrophages more common in human lesions that have high indices of plaque instability?

While ISH-PLA is a useful method to identify the presence of the H3K4dime mark within SMCs, quantification of phenotypically modulated SMCs using this method is ill advised. Gomez *et al.*¹⁴⁴ reported the estimated efficiency of H3K4dime around 66%, or roughly two-thirds of phenotypically modulated cells are labeled. Another limitation to ISH-PLA is the magnification necessary to evaluate a positive signal inhibits the ability to analyze large regions at once. Our final concern with this approach is the variability present within human atherosclerotic lesions. Even lesions designated in the same risk category have a wide range of features that may alter the microenvironment present in the plaque and bias cells toward one phenotype or another. While these limitations make quantitative assessment of SMC derived macrophages in human atherosclerotic

lesions challenging, we can use the different microenvironments within the lesion to assess how different environmental stimuli can effect SMC phenotypic switching. For instance, we can analyze markers present on phenotypically modulated SMCs near necrotic cores and compare them to SMCs that are proximal to large calcified regions of the plaque.

Does acute pharmacological treatment inhibiting KLF4 also result in reduced lesion? What about overexpression of OCT4?

The experiments described in this dissertation utilized a highly specific mouse model to genetically knockout KLF4 and OCT4 expression in SMCs. One major drawback to our rigorous SMC lineage tracing model system is the requirement that genes of interest be inhibited at an early age (8 weeks old) and therefore can only answer the question what is the effect of KLF4/OCT4 KO in SMCs throughout the ENTIRE course of atherosclerosis development. In order to answer the question what is the effect of KLF4/OCT4 SMC specific inhibition on advanced atherosclerosis, a sophisticated drug treatment would need to be developed. Several major limitations arise when developing cell specific therapeutic agents against transcriptions factors. 1) Traditional drug treatments normally localize in high concentrations to the liver. In order to successfully target SMCs a microvessel coated with a targeting ligand would need to be developed to hone into SMCs. 2) Phenotypically modulated SMCs do not express the same repertoire of genes as contractile state SMCs, and therefore are difficult, if not

impossible, to target. 3) Transcription factors are active in the nucleus of the cell and are difficult to target *in vivo* in complex organisms. While KLF4 and OCT4 may not be ideal targets for therapeutic treatment of atherosclerosis, they demonstrate how subtle manipulations in SMC phenotype can have a profound effect on lesion size and stability.

Therefore, we hope to identify other methods of manipulating SMC phenotypic state *in vivo* as an alternative treatment plan for individuals with pre-existing cardiovascular disease.

One such method would be to systemically treat mice with MircoRNAs (miR) targeted to SMC function. Indeed, it was discovered that miR-145 functions to inhibit KLF4¹⁹¹ and Oct4¹⁹² function and maintain a more contractile state SMC. Moreover, it was also shown that promoter of miR-145 was repressed by Oct4, indicating that miR145 is involved into the Oct4-miR145-Klf4 regulating feedback loop¹⁹². Another potent modulator of SMC phenotypic state is miR-21. Inhibition of miR-21 has been demonstrated to reduce SMC proliferation after balloon injury in rats, but expression of miR-21 is critical to maintaining SMC marker gene expression^{193, 194}. miR-21 has been shown to be up-regulated by TGF β expression in response to SMC differentiation stimuli, whereas miR-24 is up-regulated by PDGF-BB in a de-differentiation response¹⁹⁵. Manipulation of these and other miRs¹⁹⁶ indicated in SMC phenotypic state may represent a feasible method for altering SMC phenotypic state *in vivo*.

Another possibility is to identify KLF4 and OCT4 downstream target genes to find potential molecular pathways that can be used to increase plaque stability. In order to maintain an unbiased approach, we plan to collect several large data sets and perform genome wide analysis of KLF4 and OCT4 targets. First, we are in the process of collecting *in vivo* atherosclerotic samples from KLF4 WT vs KO and OCT4 WT vs KO 18 week Western diet fed animals. These samples are being processed for CHIP-seq and RNA-seq. From these results, we will perform subtractive analysis on the WT vs KO groups to determine what genes were affected by the loss of KLF4 or OCT4. From there, the affected pathways will be compared between KLF4 and OCT4 to determine if there are common mechanisms controlling the various aspects of SMC phenotypic modulation. In order to help rule out changes in gene expression of non-SMCs in these experiments, we are planning to also treat KLF4 WT vs KO and OCT4 WT vs KO cultured SMCs and analyze the samples by CHIP-seq and RNA-seq.

Does the H3K4dime mark on the Myh11 promoter confer SMC lineage memory? If so, can removal of the H3K4dime mark on the Myh11 promoter make SMCs “forget” to re-differentiate? Can addition of the H3K4dime mark on the Myh11 promoter of other cell types cause them to differentiate into SMCs?

Combinations of histone modifications that help promote gene expression or repression comprise what is often referred to as the histone code¹¹⁰. While

most methylation marks cause gene silencing, and acetylation marks confer activation, the location and combination of markers is critical to determining gene regulation¹⁹⁷. During phenotypic modulation, a cohort of epigenetic changes occur on SMC promoters, however H3K4dime remains unchanged¹⁰⁸. In fact, we have been unable to detect changes in the H3K4dime mark after treatment with several factors that induce SMC phenotypic switching (Figure 9 and Supplemental Figure 18), and have shown in Chapter 2 that H3K4dime on the *Myh11* promoter can be used as a SMC lineage tracing method. Interestingly, Pekowska et al. found that when analyzing T-cells, H3K4dime marks were found clustered around T-cell specific genes regardless of actual gene expression¹⁹⁸. When they analyzed brain tissue as an independent control, H3K4dime enrichment patterns were localized to regulatory genes of brain function^{198, 199}. Similar data has been reported in hematopoietic cell lineages²⁰⁰, and more recently in retina development²⁰¹. Therefore, the working hypothesis in the lab is that H3K4dime mark on SMC marker gene promoters confers the cells with lineage identity.

Testing this hypothesis proves to be a difficult task. In order to determine if H3K4dime on the *Myh11* promoter confers lineage memory we need to be able to 1) remove the H3K4dime mark specifically from SMC marker gene promoters to establish whether or not they “forget” to be SMCs; and 2) add the H3K4dime mark specially on SMC marker gene promoters in other cell lineages to determine if the H3K4dime can promote SMC differentiation. Here I will describe a method initiated in the lab by post-doc, Qiong Gan, and how it can be utilized to

accomplish the first objective, and why I believe the second objective is unattainable with our current knowledge of the field and tools at hand.

LSD1 was discovered to be an H3K4 specific demethylase capable of reducing H3K4me and H3K4dime, but unable to reduce H3K4trime to an unmodified state²⁰². While LSD1 has higher specificity to H3K4, it is important to note that it can also target lysine residues on H3K9²⁰². Since demethylases can act on a wide range of targets, we plan to utilize the specificity of SRF-myocardin gene activation in SMCs in order to remove the dimethylation mark from H3K4 specifically from SMC marker gene promoters. Our lab has previously shown that myocardin is both necessary and sufficient for SMC marker gene expression, and that loss of myocardin did not negatively affect other tissues, such as the heart^{92, 93}. Myocardin was therefore determined to be an excellent SMC specific honing mechanism for LSD1 action.

Currently in development in the lab is a fusion protein that combines the binding region of myocardin with the demethylase LSD1 (Myocd-LSD1). Preliminary data demonstrate that H3K4dime enrichment on the *Acta2* and *Myh11* promoters was reduced when cultured rat SMCs were treated with the fusion protein containing the functional LSD1 gene, but not one with a point mutation in the catalytic domain (Figure 21). The Myocd-LSD1 construct is currently being regenerated to optimize our understanding of experimental results including: the addition of an RFP lineage tag so that transfection can be monitored in individual cells, insertion into a Tet On retroviral delivery system to

temporarily examine the loss of H3K4dime in cell culture experiments, and insertion of the fusion protein into a lentiviral vector in order to test our hypothesis *in vivo*.

Our preliminary results using the Myocd-LSD1 fusion protein are the result of constitutive expression of the fusion protein. One of our first experiments will utilize the newly developed Tet On retroviral Myocd-LSD1 to determine if removal of H3K4dime on SMC promoters 1) causes SMC dedifferentiation or 2) prevents SMC redifferentiation after POVPC or PDGF-BB stimulated phenotypic modulation. However, the real test of H3K4dime function in SMC differentiation arises will come from *in vivo* models of injury-repair.

In particular, we plan to test the lentiviral fusion protein in the wire injury model of vascular injury. We have previously published that SMCs proliferate and migrate into the neointima 7 days post wire injury (Figure 1a). Unlike chronic inflammatory diseases such as atherosclerosis where injury and inflammation are ongoing, preliminary results from carotid wire injury models demonstrate that the injury will fully resolve within a few weeks. In order to assess the role of H3K4dime of SMC gene promoters, we plan to treat SMC lineage tracing mice with the lentiviral fusion protein post wire injury to determine whether or not SMCs are capable of redifferentiating in the absence of the H3K4dime mark on SMC gene promoters. We plan to use H3K4dime *Myh11* ISH-PLA to confirm that cells transfected with the fusion protein did in fact get demethylated.

While several methyltransferases have been indicated as H3K4 specific²⁰³, we cannot ascertain whether non-SMC lineages assume a SMC phenotype by using a fusion protein for myocardin and an H3K4 methyltransferase. Lysine 4 on histone 3 is capable of three unique states of methylation, mono-, di-, and tri-methylation. Only the H3K4dime mark has been indicated as a potential SM lineage mark, but constitutive binding of a methyltransferase to the SMC gene promoters would likely result in continued methylation of H3K4. In addition, based on recent literature that H3K4dime may infer lineage determination in other cell types, it is likely that non-SMCs would contain H3K4dime on other gene loci that would confound our results. While determining whether or not addition of H3K4dime on SMC gene loci can cause other committed cell types to become SMCs, if the previous limitations can be overcome, this method may be useful in determining whether or not addition of H3K4dime on SMC loci can push an embryonic stem cell to become a SMC.

At what point in development do SMCs acquire the H3K4dime mark?

In fact, preliminary research suggests that H3K4dime precedes SMC differentiation, and may be a method of committing cells to a SMC lineage. In A404 cells, a multipotential cell line that when treated with retinoic acid (RA) will differentiate into SMCs, the H3K4dime mark was enriched on the *Myh11* promoter after 24 hours of RA treatment, whereas mRNA expression of *Myh11* did not begin until 48 hours (Figure 22a, b). In addition, the *Myh11* H3K4dime

mark was seen in the proximal regions of the developing dorsal aorta at day 10.5 by ISH-PLA (Figure 22c). Future experiments utilizing the LSD1-fusion protein will help determine whether or not this epigenetic mark is necessary for SMC differentiation or just happens to correlate with SMC lineage. In correlate, these results will help us further understand why macrophages can upregulate markers of SMC lineages, but do not acquire the H3K4dime mark on the *Myh11* promoter (as determined by the in vitro conditions tested thusfar). With the emergence of single cell mRNA analysis tools and nano-ChIP technology, we hope to one day laser capture cells that express SMC markers such as ACTA2, but are negative for H3K4dime and compare them to ACTA2 H3K4dime positive cells to determine what, if any differences there are between the two types of cells.

Figure 17. Schematic of KLF4 and OCT4 function in SMC phenotypic switching in response to vascular injury and atherosclerosis.

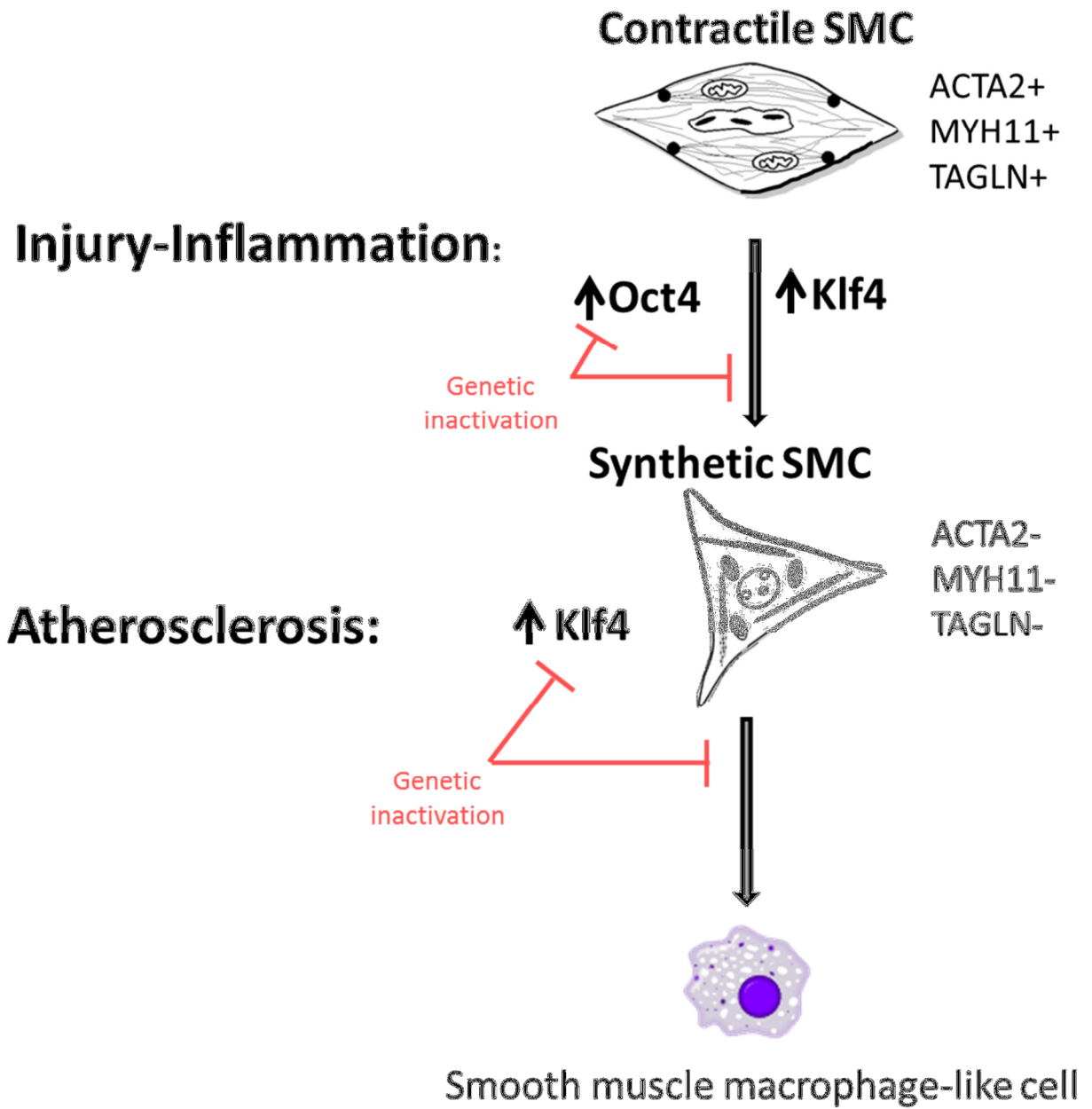


Figure 18. Oct4 is up-regulated in SMCs in the context of Western diet feeding.

Data acquired by Laura Shankman to be submitted with the results of Chapter 4 to *Nature*. 18 week WD fed *SMC eYFP^{+/+} ApoE^{-/-}* mice were stained for ACTA2 (red), eYFP (green), OCT4 (magenta), or DAPI (blue).

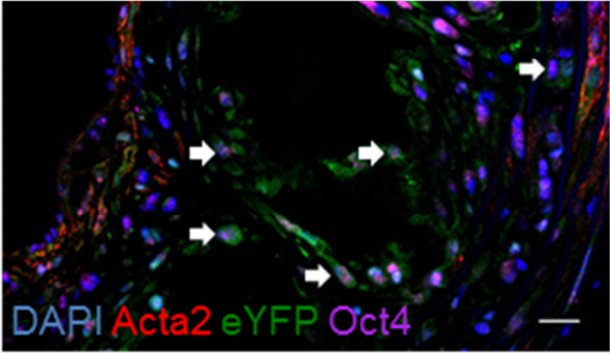
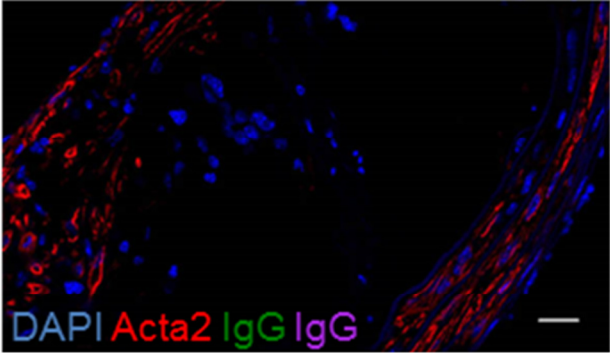


Figure 19. YFP+ cells from aortas of 18 week western diet fed SMC lineage tracing mice express multiple markers of mesenchymal stem cells (MSC).

Preliminary results by Laura Shankman. Vessels from the iliac bifurcation to the aortic root and including both carotids were harvested from 18-week WD fed SMC *eYFP^{+/+} ApoE^{-/-}* animals and carefully dissected as to remove fat contamination. The vessels were then flayed and minced to assist with enzymatic digestion before stained with antibodies of interest. Cells were gated CD45-, CD34-, CD144-, prior to analysis of the eYFP+ population. Students one way t-test was used to compare the eYFP+ subpopulation of CD44+, ENG+ (CD105), ATXN1+ (Sca-1), and ENG+ ATXN1+ to determine whether or not a significant population of potential MSC-like cells existed within the lesion.

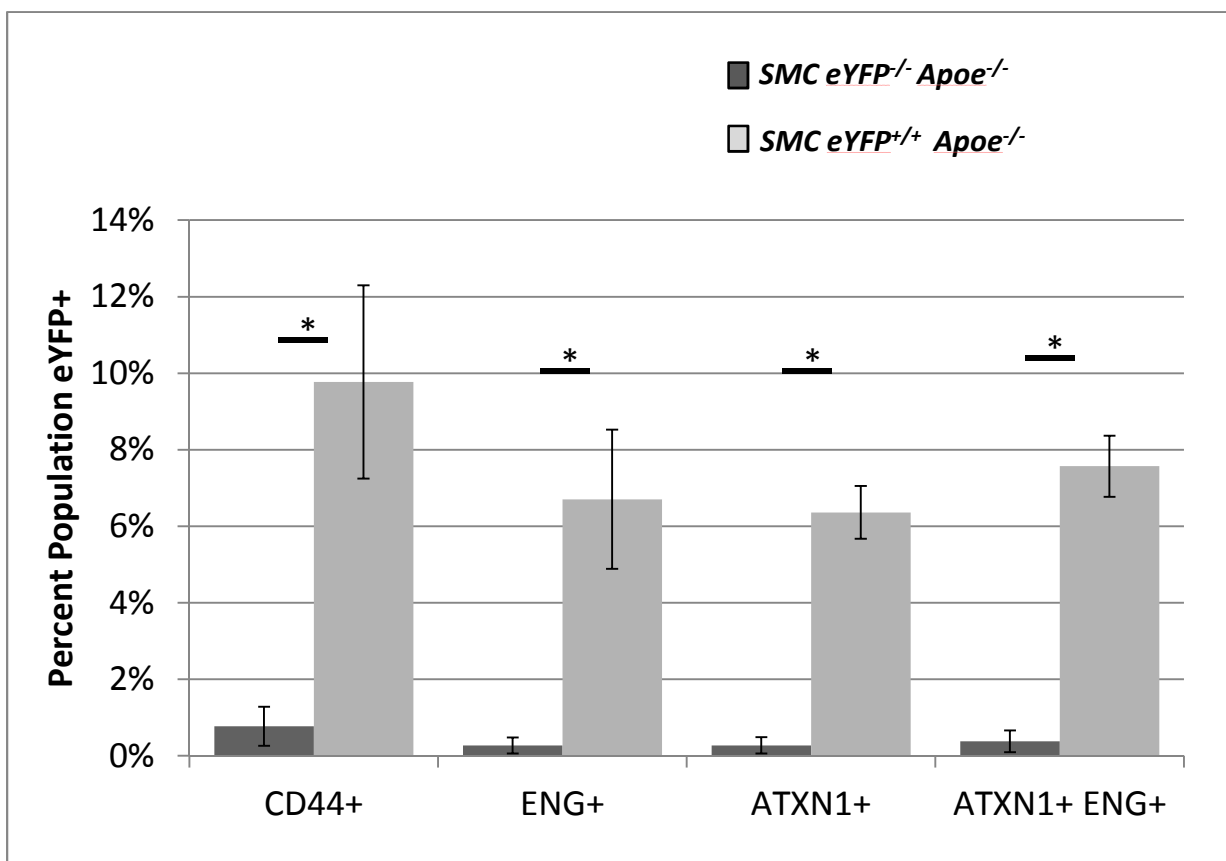


Figure 20. OCT4 activates Lgals3 in response to POVPC treatment and exhibits increased phagocytosis of red blood cells in response to cholesterol loading treatment.

Preliminary results by Olga Cherepanova. Analysis of 10 μm thick sections of BCAs from 18 week WD fed $Oct4^{WT/WT}/Apoe^{-/-}$ SMC $eYFP^{+/+}$ and $Oct4^{\Delta/\Delta}/Apoe^{-/-}$ SMC $eYFP^{+/+}$ mice. (a) Quantification of YFP+, ACTA2+ and YFP+/ACTA2+ cells within the media. (b) Analysis of LGALS3+ and LGALS3+/YFP+ staining within the media region. (c) Treatment of OCT4 WT and KO cells with vehicle or POVPC results in increased Lgals3 mRNA expression in OCT4 KO cells. (d) Phagocytosis of RBCs by OCT4 WT and KO cells treated with M β CD-cholesterol for 72 hours (n=2).

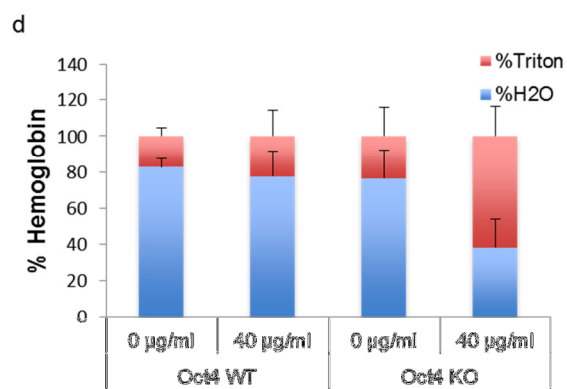
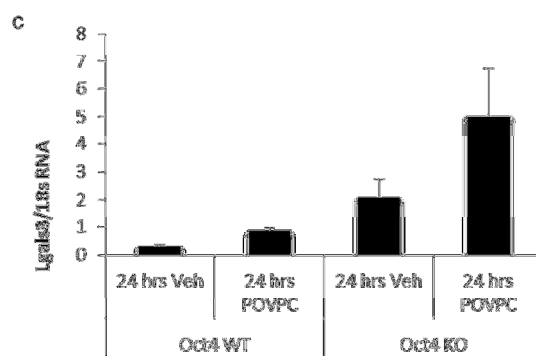
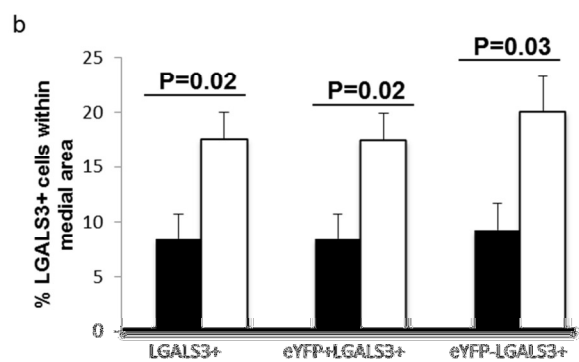
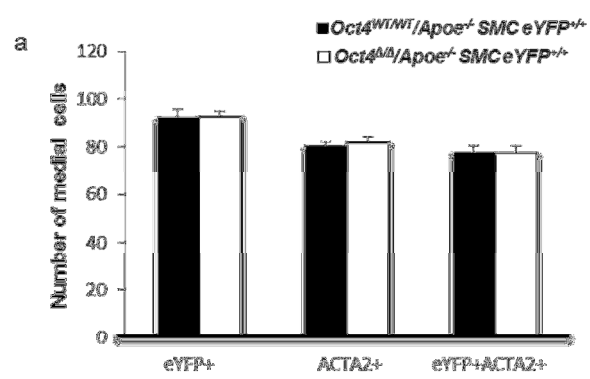


Figure 21. A Novel Myocardin-LSD1 fusion protein selectively demethylates H3K4me2 at SMC specific gene promoters.

Preliminary results by Qiong Gan. A) The two fusion protein consists of the Flag-tagged SRF binding domain of Myocardin fused to either full length (WT) LSD1 or an LSD1 containing a point mutation rendering it catalytically inactive (Mut). B) Global H3K4me2 levels in cultured SMCs remain unchanged in response to stable transfection with the fusion protein. C) H3K4me2 levels are decreased in 518 cell lines stably transfected with the WT fusion protein but remain unchanged in cell lines stably transfected with the mutant. The WT fusion protein selectively demethylates H3K4me2 at SMC (Myocardin-SRF dependent) promoters but not CArG-SRF dependent promoters (c-Fos). 518-Cultured SMC. NT-LSD1 WT- Cells stably transfected with the WT fusion protein. NT-LSD1 Mut- Cells stably transfected with a catalytically inactive mutant fusion protein

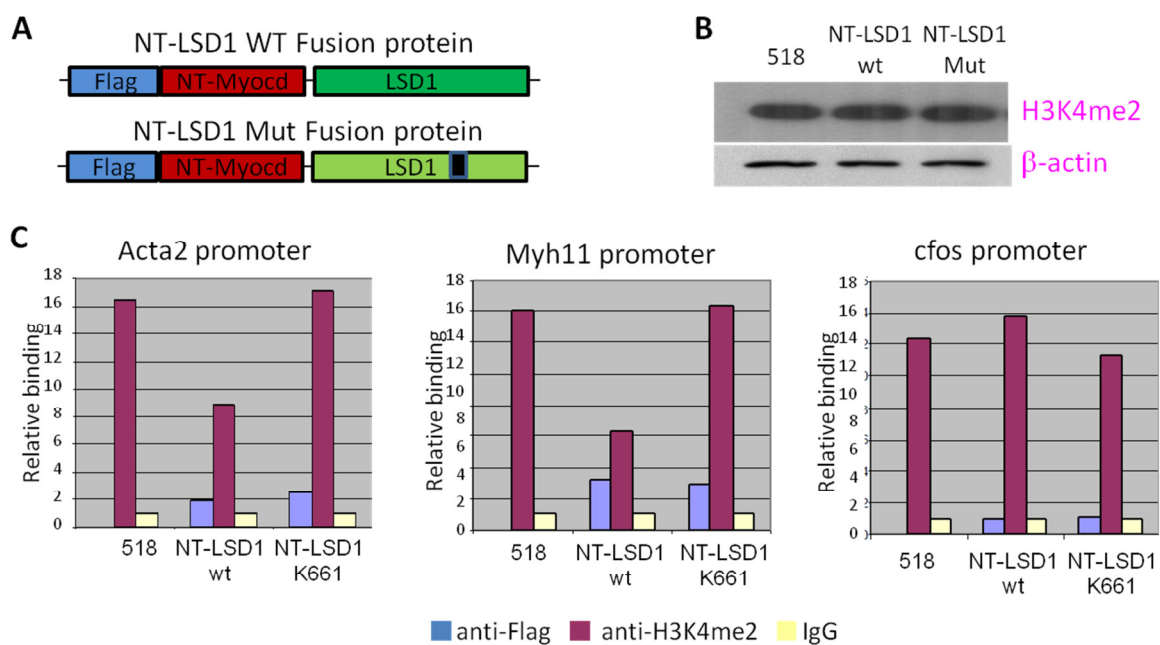
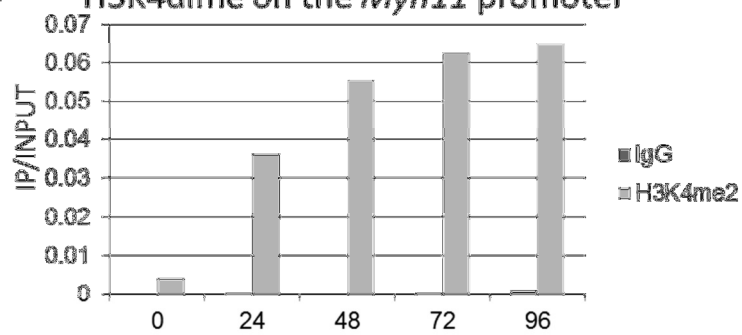
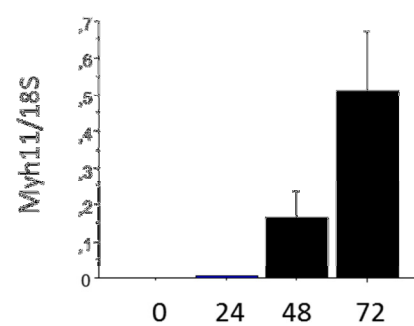
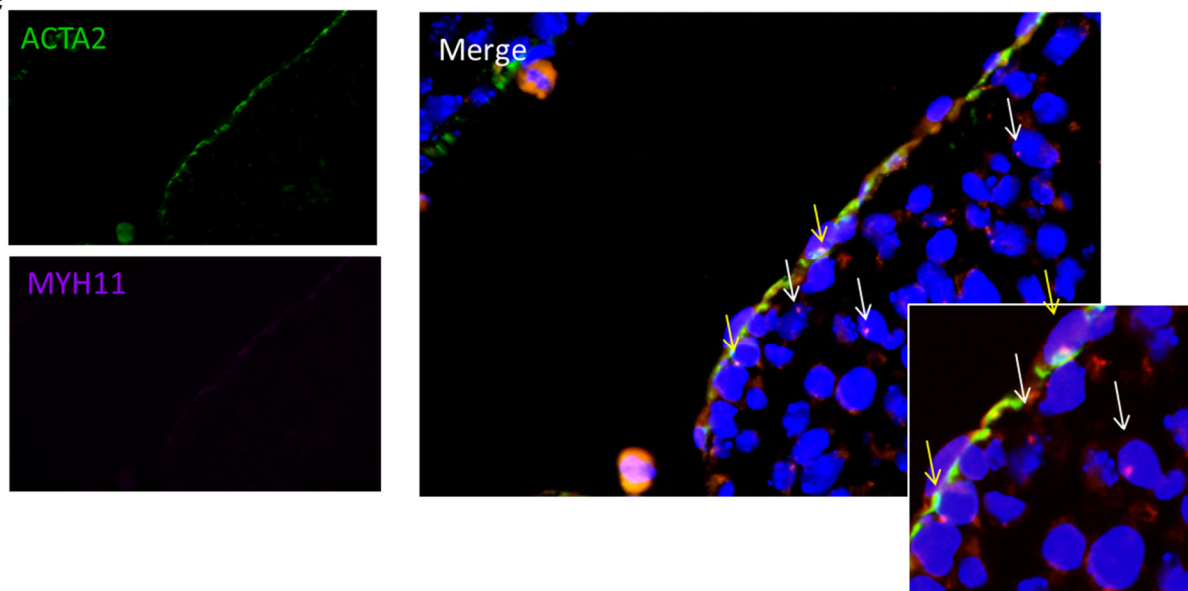


Figure 22. H3K4dime is acquired on the MYH11 promoter before the expression of SMC marker genes.

Preliminary results by Delphine Gomez. A404 cells, a totipotent culture cells, were treated with retinoic acid (RA) to induce SMC lineage. (a) Cells begin to acquire the H3K4dime mark on the *Myh11* promoter after 24 hours of RA treatment. (b) *Myh11* mRNA expression appears after 48 hours of RA treatment. (c) 10.5 day embryos reveal cells positive for *Myh11* H3K4dime in regions directly adjacent to the forming dorsal aorta.

a H3K4dime on the *Myh11* promoter**b****c**

Chapter 6:

References

Reference List

1. Libby,P., Ridker,P.M., & Hansson,G.K. Progress and challenges in translating the biology of atherosclerosis. *Nature* 473, 317-325 (2011).
2. Lusis,A.J. Atherosclerosis. *Nature* 407, 233-241 (2000).
3. Go,A.S. *et al.* Executive summary: heart disease and stroke statistics--2014 update: a report from the american heart association. *Circulation* 129, 399-410 (2014).
4. Bonow,R.O., Smaha,L.A., Smith,S.C., Jr., Mensah,G.A., & Lenfant,C. World Heart Day 2002: the international burden of cardiovascular disease: responding to the emerging global epidemic. *Circulation* 106, 1602-1605 (2002).
5. Owens,G.K., Kumar,M.S., & Wamhoff,B.R. Molecular regulation of vascular smooth muscle cell differentiation in development and disease. *Physiol Rev.* 84, 767-801 (2004).
6. Stary,H.C. *et al.* A definition of initial, fatty streak, and intermediate lesions of atherosclerosis. A report from the Committee on Vascular Lesions of the Council on Arteriosclerosis, American Heart Association. *Circulation* 89, 2462-2478 (1994).
7. Kuro-o M *et al.* Developmentally regulated expression of vascular smooth muscle myosin heavy chain isoforms. *J. Biol. Chem.* 264, 18272-18275 (1989).
8. Duband,J.L., Gimona,M., Scatena,M., Sartore,S., & Small,J.V. Calponin and SM 22 as differentiation markers of smooth muscle: spatiotemporal distribution during avian embryonic development. *Differentiation* 55, 1-11 (1993).
9. Gabbiani,G. *et al.* Vascular smooth muscle cells differ from other smooth muscle cells: predominance of vimentin filaments and a specific alpha-type actin. *Proc. Natl. Acad. Sci. U. S. A* 78, 298-302 (1981).
10. Mack,C.P. & Owens,G.K. Regulation of smooth muscle alpha-actin expression in vivo is dependent on CArG elements within the 5' and first intron promoter regions. *Circ. Res.* 84, 852-861 (1999).

11. Regan,C.P., Adam,P.J., Madsen,C.S., & Owens,G.K. Molecular mechanisms of decreased smooth muscle differentiation marker expression after vascular injury. *J. Clin. Invest* 106, 1139-1147 (2000).
12. Zhang,J. *et al.* Generation of an adult smooth muscle cell-targeted Cre recombinase mouse model. *Arterioscler. Thromb. Vasc. Biol.* 26, e23-e24 (2006).
13. Li,L., Miano,J.M., Cserjesi,P., & Olson,E.N. SM22 alpha, a marker of adult smooth muscle, is expressed in multiple myogenic lineages during embryogenesis. *Circ. Res.* 78, 188-195 (1996).
14. Wamhoff,B.R. *et al.* A G/C element mediates repression of the SM22alpha promoter within phenotypically modulated smooth muscle cells in experimental atherosclerosis. *Circ. Res.* 95, 981-988 (2004).
15. Shen,Z. *et al.* Smooth muscle protein 22 alpha-Cre is expressed in myeloid cells in mice. *Biochem. Biophys. Res. Commun.* 422, 639-642 (2012).
16. Iwata,H. *et al.* Bone marrow-derived cells contribute to vascular inflammation but do not differentiate into smooth muscle cell lineages. *Circulation* 122, 2048-2057 (2010).
17. Weiss,D.J., Liggitt,D., & Clark,J.G. Histochemical discrimination of endogenous mammalian beta-galactosidase activity from that resulting from lac-Z gene expression. *Histochem. J.* 31, 231-236 (1999).
18. Tang,Z. *et al.* Differentiation of multipotent vascular stem cells contributes to vascular diseases. *Nat. Commun.* 3, 875 (2012).
19. Nguyen,A.T. *et al.* Smooth muscle cell plasticity: fact or fiction? *Circ. Res.* 112, 17-22 (2013).
20. Nemenoff,R.A. *et al.* SDF-1alpha induction in mature smooth muscle cells by inactivation of PTEN is a critical mediator of exacerbated injury-induced neointima formation. *Arterioscler. Thromb. Vasc. Biol.* 31, 1300-1308 (2011).
21. Wirth,A. *et al.* G12-G13-LARG-mediated signaling in vascular smooth muscle is required for salt-induced hypertension. *Nat. Med.* 14, 64-68 (2008).
22. Bentzon,J.F., Sondergaard,C.S., Kassem,M., & Falk,E. Smooth muscle cells healing atherosclerotic plaque disruptions are of local, not blood, origin in apolipoprotein E knockout mice. *Circulation* 116, 2053-2061 (2007).

23. Sata, M. *et al.* Hematopoietic stem cells differentiate into vascular cells that participate in the pathogenesis of atherosclerosis. *Nat. Med.* 8, 403-409 (2002).
24. Caplice, N.M. *et al.* Smooth muscle cells in human coronary atherosclerosis can originate from cells administered at marrow transplantation. *Proc. Natl. Acad. Sci. U. S. A* 100, 4754-4759 (2003).
25. Stewart, H.J., Guildford, A.L., Lawrence-Watt, D.J., & Santin, M. Substrate-induced phenotypical change of monocytes/macrophages into myofibroblast-like cells: A new insight into the mechanism of in-stent restenosis. *J. Biomed. Mater. Res. A* (2008).
26. Desmouliere, A., Geinoz, A., Gabbiani, F., & Gabbiani, G. Transforming growth factor-beta 1 induces alpha-smooth muscle actin expression in granulation tissue myofibroblasts and in quiescent and growing cultured fibroblasts. *J. Cell Biol.* 122, 103-111 (1993).
27. Ronnov-Jessen, L. & Petersen, O.W. Induction of alpha-smooth muscle actin by transforming growth factor-beta 1 in quiescent human breast gland fibroblasts. Implications for myofibroblast generation in breast neoplasia. *Lab Invest* 68, 696-707 (1993).
28. Adam, P.J., Regan, C.P., Hautmann, M.B., & Owens, G.K. Positive- and negative-acting Kruppel-like transcription factors bind a transforming growth factor beta control element required for expression of the smooth muscle cell differentiation marker SM22alpha in vivo. *J. Biol. Chem.* 275, 37798-37806 (2000).
29. Hautmann, M.B., Madsen, C.S., & Owens, G.K. A transforming growth factor beta (TGFbeta) control element drives TGFbeta-induced stimulation of smooth muscle alpha-actin gene expression in concert with two CARG elements. *J. Biol. Chem.* 272, 10948-10956 (1997).
30. Gomez, D. & Owens, G.K. Smooth muscle cell phenotypic switching in atherosclerosis. *Cardiovasc. Res.* 95, 156-164 (2012).
31. Sima Allahverdian, Ali Cyrus Chehroudi, Bruce M. McManus, Thomas Abraham, & Gordan A. Francis. Contribution of Intimal Smooth Muscle Cells to Cholesterol Accumulation and Macrophage-Like Cells in Human Atherosclerosis. *Circulation* . 14 A.D.

Ref Type: Thesis/Dissertation

32. Rekhter, M.D. Collagen synthesis in atherosclerosis: too much and not enough. *Cardiovasc. Res.* 41, 376-384 (1999).

33. Clarke,M.C. *et al.* Apoptosis of vascular smooth muscle cells induces features of plaque vulnerability in atherosclerosis. *Nat. Med.* 12, 1075-1080 (2006).
34. Blank,R.S. & Owens,G.K. Platelet-derived growth factor regulates actin isoform expression and growth state in cultured rat aortic smooth muscle cells. *J. Cell Physiol* 142, 635-642 (1990).
35. Holycross,B.J., Blank,R.S., Thompson,M.M., Peach,M.J., & Owens,G.K. Platelet-derived growth factor-BB-induced suppression of smooth muscle cell differentiation. *Circ. Res.* 71, 1525-1532 (1992).
36. Alexander,M.R., Murgai,M., Moehle,C.W., & Owens,G.K. Interleukin-1beta modulates smooth muscle cell phenotype to a distinct inflammatory state relative to PDGF-DD via NF-kappaB-dependent mechanisms. *Physiol Genomics* 44, 417-429 (2012).
37. Thomas,J.A. *et al.* PDGF-DD, a novel mediator of smooth muscle cell phenotypic modulation, is upregulated in endothelial cells exposed to atherosclerosis-prone flow patterns. *Am. J. Physiol Heart Circ. Physiol* 296, H442-H452 (2009).
38. Hayashi,K. *et al.* Differentiated phenotype of smooth muscle cells depends on signaling pathways through insulin-like growth factors and phosphatidylinositol 3-kinase. *J. Biol. Chem.* 273, 28860-28867 (1998).
39. Hayashi,K. *et al.* Phenotypic modulation of vascular smooth muscle cells induced by unsaturated lysophosphatidic acids. *Circ. Res.* 89, 251-258 (2001).
40. Pidkovka,N.A. *et al.* Oxidized phospholipids induce phenotypic switching of vascular smooth muscle cells in vivo and in vitro. *Circ. Res.* 101, 792-801 (2007).
41. Rong,J.X., Shapiro,M., Trogan,E., & Fisher,E.A. Transdifferentiation of mouse aortic smooth muscle cells to a macrophage-like state after cholesterol loading. *Proc. Natl. Acad. Sci. U. S. A* 100, 13531-13536 (2003).
42. Clement,N. *et al.* Notch3 and IL-1beta exert opposing effects on a vascular smooth muscle cell inflammatory pathway in which NF-kappaB drives crosstalk. *J. Cell Sci.* 120, 3352-3361 (2007).
43. Speer,M.Y. *et al.* Smooth muscle cells give rise to osteochondrogenic precursors and chondrocytes in calcifying arteries. *Circ. Res.* 104, 733-741 (2009).

44. Steitz,S.A. *et al.* Smooth muscle cell phenotypic transition associated with calcification: upregulation of Cbfa1 and downregulation of smooth muscle lineage markers. *Circ. Res.* 89, 1147-1154 (2001).
45. Owens,G.K. Regulation of differentiation of vascular smooth muscle cells. *Physiol Rev.* 75, 487-517 (1995).
46. Frid,M.G., Moiseeva,E.P., & Stenmark,K.R. Multiple phenotypically distinct smooth muscle cell populations exist in the adult and developing bovine pulmonary arterial media in vivo. *Circ. Res.* 75, 669-681 (1994).
47. Frid,M.G., Aldashev,A.A., Dempsey,E.C., & Stenmark,K.R. Smooth muscle cells isolated from discrete compartments of the mature vascular media exhibit unique phenotypes and distinct growth capabilities. *Circ. Res.* 81, 940-952 (1997).
48. Couffinhal,T., Duplaa,C., Moreau,C., Lamaziere,J.M., & Bonnet,J. Regulation of vascular cell adhesion molecule-1 and intercellular adhesion molecule-1 in human vascular smooth muscle cells. *Circ. Res.* 74, 225-234 (1994).
49. Jiang,B. *et al.* Temporal control of NF-kappaB activation by ERK differentially regulates interleukin-1beta-induced gene expression. *J. Biol. Chem.* 279, 1323-1329 (2004).
50. Libby,P., Warner,S.J., & Friedman,G.B. Interleukin 1: a mitogen for human vascular smooth muscle cells that induces the release of growth-inhibitory prostanoids. *J. Clin. Invest* 81, 487-498 (1988).
51. Massberg,S. *et al.* Activated platelets trigger an inflammatory response and enhance migration of aortic smooth muscle cells. *Thromb. Res.* 110, 187-194 (2003).
52. Andreeva,E. Subendothelial smooth muscle cells of human aorta express macrophage antigen in situ and in vitro. *Atherosclerosis*(1997).
53. Argmann,C.A. *et al.* Human smooth muscle cell subpopulations differentially accumulate cholesteryl ester when exposed to native and oxidized lipoproteins. *Arterioscler. Thromb. Vasc. Biol.* 24, 1290-1296 (2004).
54. Cecchi,E. *et al.* Role of hemodynamic shear stress in cardiovascular disease. *Atherosclerosis* 214, 249-256 (2011).
55. Ross,R. Atherosclerosis--an inflammatory disease. *N. Engl. J. Med.* 340, 115-126 (1999).

56. Gijzen,F., van der Giessen,A., van der Steen,A., & Wentzel,J. Shear stress and advanced atherosclerosis in human coronary arteries. *J. Biomech.* 46, 240-247 (2013).
57. Glass,C.K. & Witztum,J.L. Atherosclerosis. the road ahead. *Cell* 104, 503-516 (2001).
58. Stary,H.C. *et al.* A definition of advanced types of atherosclerotic lesions and a histological classification of atherosclerosis. A report from the Committee on Vascular Lesions of the Council on Arteriosclerosis, American Heart Association. *Arterioscler. Thromb. Vasc. Biol.* 15, 1512-1531 (1995).
59. Libby,P. & Theroux,P. Pathophysiology of coronary artery disease. *Circulation* 111, 3481-3488 (2005).
60. Moreno,P.R. *et al.* Macrophage infiltration in acute coronary syndromes. Implications for plaque rupture. *Circulation* 90, 775-778 (1994).
61. Shah,P.K. Mechanisms of plaque vulnerability and rupture. *J. Am. Coll. Cardiol.* 41, 15S-22S (2003).
62. Fernandez-Ortiz,A. *et al.* Characterization of the relative thrombogenicity of atherosclerotic plaque components: implications for consequences of plaque rupture. *J. Am. Coll. Cardiol.* 23, 1562-1569 (1994).
63. Falk,E. Plaque rupture with severe pre-existing stenosis precipitating coronary thrombosis. Characteristics of coronary atherosclerotic plaques underlying fatal occlusive thrombi. *Br. Heart J.* 50, 127-134 (1983).
64. Davies,M.J. & Thomas,A.C. Plaque fissuring--the cause of acute myocardial infarction, sudden ischaemic death, and crescendo angina. *Br. Heart J.* 53, 363-373 (1985).
65. Davies,M.J. Thrombosis in acute myocardial infarction and sudden death. *Cardiovasc. Clin.* 18, 151-159 (1987).
66. Davies,M.J. Stability and instability: two faces of coronary atherosclerosis. The Paul Dudley White Lecture 1995. *Circulation* 94, 2013-2020 (1996).
67. Davies,M.J., Richardson,P.D., Woolf,N., Katz,D.R., & Mann,J. Risk of thrombosis in human atherosclerotic plaques: role of extracellular lipid, macrophage, and smooth muscle cell content. *Br. Heart J.* 69, 377-381 (1993).

68. Davies,M.J., Bland,J.M., Hangartner,J.R., Angelini,A., & Thomas,A.C. Factors influencing the presence or absence of acute coronary artery thrombi in sudden ischaemic death. *Eur. Heart J.* 10, 203-208 (1989).
69. Falk,E., Nakano,M., Benton,J.F., Finn,A.V., & Virmani,R. Update on acute coronary syndromes: the pathologists' view. *Eur. Heart J.*(2012).
70. Falk,E., Shah,P.K., & Fuster,V. Coronary plaque disruption. *Circulation* 92, 657-671 (1995).
71. Hodgson,J.M. *et al.* Intracoronary ultrasound imaging: correlation of plaque morphology with angiography, clinical syndrome and procedural results in patients undergoing coronary angioplasty. *J. Am. Coll. Cardiol.* 21, 35-44 (1993).
72. Otsuka,F., Sakakura,K., Yahagi,K., Joner,M., & Virmani,R. Has Our Understanding of Calcification in Human Coronary Atherosclerosis Progressed? *Arterioscler. Thromb. Vasc. Biol.*(2014).
73. Huang,H. *et al.* The impact of calcification on the biomechanical stability of atherosclerotic plaques. *Circulation* 103, 1051-1056 (2001).
74. Proudfoot,D. *et al.* Apoptosis regulates human vascular calcification in vitro: evidence for initiation of vascular calcification by apoptotic bodies. *Circ. Res.* 87, 1055-1062 (2000).
75. Burleigh,M.C. *et al.* Collagen types I and III, collagen content, GAGs and mechanical strength of human atherosclerotic plaque caps: span-wise variations. *Atherosclerosis* 96, 71-81 (1992).
76. Neumeister,V., Scheibe,M., Lattke,P., & Jaross,W. Determination of the cholesterol-collagen ratio of arterial atherosclerotic plaques using near infrared spectroscopy as a possible measure of plaque stability. *Atherosclerosis* 165, 251-257 (2002).
77. Crisby,M. *et al.* Pravastatin treatment increases collagen content and decreases lipid content, inflammation, metalloproteinases, and cell death in human carotid plaques: implications for plaque stabilization. *Circulation* 103, 926-933 (2001).
78. Kolodgie,F.D. *et al.* The thin-cap fibroatheroma: a type of vulnerable plaque: the major precursor lesion to acute coronary syndromes. *Curr. Opin. Cardiol.* 16, 285-292 (2001).

79. Meir, K.S. & Leitersdorf, E. Atherosclerosis in the apolipoprotein-E-deficient mouse: a decade of progress. *Arterioscler. Thromb. Vasc. Biol.* 24, 1006-1014 (2004).
80. Rosenfeld, M.E. *et al.* Advanced atherosclerotic lesions in the innominate artery of the ApoE knockout mouse. *Arterioscler. Thromb. Vasc. Biol.* 20, 2587-2592 (2000).
81. Getz, G.S. & Reardon, C.A. Animal models of atherosclerosis. *Arterioscler. Thromb. Vasc. Biol.* 32, 1104-1115 (2012).
82. Jackson, C.L., Bennett, M.R., Biessen, E.A., Johnson, J.L., & Krams, R. Assessment of unstable atherosclerosis in mice. *Arterioscler. Thromb. Vasc. Biol.* 27, 714-720 (2007).
83. Bentzon, J.F. & Falk, E. Atherosclerotic lesions in mouse and man: is it the same disease? *Curr. Opin. Lipidol.* 21, 434-440 (2010).
84. Alexander, M.R. Smooth Muscle Cell Phenotypic Modulation. 2011.
Ref Type: Thesis/Dissertation
85. Moses, H.L., Yang, E.Y., & Pietenpol, J.A. TGF-beta stimulation and inhibition of cell proliferation: new mechanistic insights. *Cell* 63, 245-247 (1990).
86. Deaton, R.A., Gan, Q., & Owens, G.K. Sp1-dependent activation of KLF4 is required for PDGF-BB-induced phenotypic modulation of smooth muscle. *Am. J. Physiol Heart Circ. Physiol* 296, H1027-H1037 (2009).
87. Salmon, M., Gomez, D., Greene, E., Shankman, L., & Owens, G.K. Cooperative binding of KLF4, pELK-1, and HDAC2 to a G/C repressor element in the SM22alpha promoter mediates transcriptional silencing during SMC phenotypic switching in vivo. *Circ. Res.* 111, 685-696 (2012).
88. Cherepanova, O.A. *et al.* Oxidized phospholipids induce type VIII collagen expression and vascular smooth muscle cell migration. *Circ. Res.* 104, 609-618 (2009).
89. Yoshida, T., Kaestner, K.H., & Owens, G.K. Conditional deletion of Kruppel-like factor 4 delays downregulation of smooth muscle cell differentiation markers but accelerates neointimal formation following vascular injury. *Circ. Res.* 102, 1548-1557 (2008).
90. Liu, Y. *et al.* Kruppel-like factor 4 abrogates myocardin-induced activation of smooth muscle gene expression. *J. Biol. Chem.* 280, 9719-9727 (2005).

91. Chen,J., Kitchen,C.M., Streb,J.W., & Miano,J.M. Myocardin: a component of a molecular switch for smooth muscle differentiation. *J. Mol. Cell Cardiol.* 34, 1345-1356 (2002).
92. Du,K.L. *et al.* Myocardin is a critical serum response factor cofactor in the transcriptional program regulating smooth muscle cell differentiation. *Mol. Cell Biol.* 23, 2425-2437 (2003).
93. Li,S., Wang,D.Z., Wang,Z., Richardson,J.A., & Olson,E.N. The serum response factor coactivator myocardin is required for vascular smooth muscle development. *Proc. Natl. Acad. Sci. U. S. A* 100, 9366-9370 (2003).
94. Yoshida,T. *et al.* Myocardin is a key regulator of CArG-dependent transcription of multiple smooth muscle marker genes. *Circ. Res.* 92, 856-864 (2003).
95. Yoshida,T., Gan,Q., & Owens,G.K. Kruppel-like factor 4, Elk-1, and histone deacetylases cooperatively suppress smooth muscle cell differentiation markers in response to oxidized phospholipids. *Am. J. Physiol Cell Physiol* 295, C1175-C1182 (2008).
96. Wernig,M. *et al.* In vitro reprogramming of fibroblasts into a pluripotent ES-cell-like state. *Nature* 448, (0 AD).
97. Takahashi,K. *et al.* Induction of pluripotent stem cells from adult human fibroblasts by defined factors. *Cell* 131, 861-872 (2007).
98. Kim,J.B. *et al.* Oct4-induced pluripotency in adult neural stem cells. *Cell* 136, (0 AD).
99. Lengner,C.J. *et al.* *< i>* Oct4 Expression Is Not Required for Mouse Somatic Stem Cell Self-Renewal. *Cell Stem Cell* 1, (0 AD).
100. Kim,S., Ip,H.S., Lu,M.M., Clendenin,C., & Parmacek,M.S. A serum response factor-dependent transcriptional regulatory program identifies distinct smooth muscle cell sublineages. *Mol. Cell Biol.* 17, 2266-2278 (1997).
101. Madsen,C.S. *et al.* Smooth muscle-specific expression of the smooth muscle myosin heavy chain gene in transgenic mice requires 5'-flanking and first intronic DNA sequence. *Circ. Res.* 82, 908-917 (1998).
102. Hungerford,J.E., Owens,G.K., Argraves,W.S., & Little,C.D. Development of the aortic vessel wall as defined by vascular smooth muscle and extracellular matrix markers. *Dev. Biol.* 178, 375-392 (1996).

103. Arimura,C. *et al.* Primary structure of chicken skeletal muscle and fibroblast alpha-actinins deduced from cDNA sequences. *Eur. J. Biochem.* 177, 649-655 (1988).
104. Babij,P., Kelly,C., & Periasamy,M. Characterization of a mammalian smooth muscle myosin heavy-chain gene: complete nucleotide and protein coding sequence and analysis of the 5' end of the gene. *Proc. Natl. Acad. Sci. U. S. A* 88, 10676-10680 (1991).
105. Miano,J.M., Carlson,M.J., Spencer,J.A., & Misra,R.P. Serum response factor-dependent regulation of the smooth muscle calponin gene. *J. Biol. Chem.* 275, 9814-9822 (2000).
106. Miano,J.M., Cserjesi,P., Ligon,K.L., Periasamy,M., & Olson,E.N. Smooth muscle myosin heavy chain exclusively marks the smooth muscle lineage during mouse embryogenesis. *Circ. Res.* 75, 803-812 (1994).
107. van der Loop,F.T., Schaart,G., Timmer,E.D., Ramaekers,F.C., & van Eys,G.J. Smoothelin, a novel cytoskeletal protein specific for smooth muscle cells. *J. Cell Biol.* 134, 401-411 (1996).
108. McDonald,O.G., Wamhoff,B.R., Hoofnagle,M.H., & Owens,G.K. Control of SRF binding to CARG box chromatin regulates smooth muscle gene expression in vivo. *J. Clin. Invest* 116, 36-48 (2006).
109. Kim,J.B. *et al.* Oct4-induced pluripotency in adult neural stem cells. *Cell* 136, 411-419 (2009).
110. Jenuwein,T. & Allis,C.D. Translating the histone code. *Science* 293, 1074-1080 (2001).
111. Kouzarides,T. Chromatin modifications and their function. *Cell* 128, 693-705 (2007).
112. Law,J.A. & Jacobsen,S.E. Establishing, maintaining and modifying DNA methylation patterns in plants and animals. *Nat. Rev. Genet.* 11, 204-220 (2010).
113. Azuara,V. *et al.* Chromatin signatures of pluripotent cell lines. *Nat. Cell Biol.* 8, 532-538 (2006).
114. Bernstein,B.E. *et al.* A bivalent chromatin structure marks key developmental genes in embryonic stem cells. *Cell* 125, 315-326 (2006).
115. Cedar,H. & Bergman,Y. Epigenetics of haematopoietic cell development. *Nat. Rev. Immunol.* 11, 478-488 (2011).

116. Litt,M.D., Simpson,M., Gaszner,M., Allis,C.D., & Felsenfeld,G. Correlation between histone lysine methylation and developmental changes at the chicken beta-globin locus. *Science* 293, 2453-2455 (2001).
117. Rada-Iglesias,A. *et al.* A unique chromatin signature uncovers early developmental enhancers in humans. *Nature* 470, 279-283 (2011).
118. Shechter,D. *et al.* Analysis of histones in *Xenopus laevis*. I. A distinct index of enriched variants and modifications exists in each cell type and is remodeled during developmental transitions. *J. Biol. Chem.* 284, 1064-1074 (2009).
119. Manabe,I. & Owens,G.K. Recruitment of serum response factor and hyperacetylation of histones at smooth muscle-specific regulatory regions during differentiation of a novel P19-derived in vitro smooth muscle differentiation system. *Circ. Res.* 88, 1127-1134 (2001).
120. Alexander,M.R. & Owens,G.K. Epigenetic Control of Smooth Muscle Cell Differentiation and Phenotypic Switching in Vascular Development and Disease. *Annu. Rev. Physiol*(2011).
121. Dahl,J.A. & Collas,P. A rapid micro chromatin immunoprecipitation assay (microChIP). *Nat. Protoc.* 3, 1032-1045 (2008).
122. Roh,T.Y. & Zhao,K. High-resolution, genome-wide mapping of chromatin modifications by GMAT. *Methods Mol. Biol.* 387, 95-108 (2008).
123. Lievens,S. & Tavernier,J. Single protein complex visualization: seeing is believing. *Nat. Methods* 3, 971-972 (2006).
124. Rantala,J.K. *et al.* SHARPIN is an endogenous inhibitor of beta1-integrin activation. *Nat. Cell Biol.* 13, 1315-1324 (2011).
125. Soderberg,O. *et al.* Direct observation of individual endogenous protein complexes in situ by proximity ligation. *Nat. Methods* 3, 995-1000 (2006).
126. Brobeil,A. *et al.* PTP1B is phosphorylated by Lyn and c-Src kinases lacking dephosphorylation by PTP1B in acute myeloid leukemia. *Leuk. Res.* 35, 1367-1375 (2011).
127. Lampugnani,M.G. *et al.* A novel endothelial-specific membrane protein is a marker of cell-cell contacts. *J. Cell Biol.* 118, 1511-1522 (1992).
128. Carmeliet,P. Mechanisms of angiogenesis and arteriogenesis. *Nat. Med.* 6, 389-395 (2000).

129. Hanahan,D. Signaling vascular morphogenesis and maintenance. *Science* 277, 48-50 (1997).
130. Weibrecht,I. *et al.* Visualising individual sequence-specific protein-DNA interactions in situ. *N. Biotechnol.* 29, 589-598 (2012).
131. Gustafsdottir,S.M. *et al.* In vitro analysis of DNA-protein interactions by proximity ligation. *Proc. Natl. Acad. Sci. U. S. A* 104, 3067-3072 (2007).
132. You,J.S. & Jones,P.A. Cancer genetics and epigenetics: two sides of the same coin? *Cancer Cell* 22, 9-20 (2012).
133. Cui,K. *et al.* Chromatin signatures in multipotent human hematopoietic stem cells indicate the fate of bivalent genes during differentiation. *Cell Stem Cell* 4, 80-93 (2009).
134. Nguyen,A.T., Taranova,O., He,J., & Zhang,Y. DOT1L, the H3K79 methyltransferase, is required for MLL-AF9-mediated leukemogenesis. *Blood* 117, 6912-6922 (2011).
135. Ng,R.K. & Gurdon,J.B. Epigenetic inheritance of cell differentiation status. *Cell Cycle* 7, 1173-1177 (2008).
136. Ng,R.K. & Gurdon,J.B. Epigenetic memory of an active gene state depends on histone H3.3 incorporation into chromatin in the absence of transcription. *Nat. Cell Biol.* 10, 102-109 (2008).
137. Christova,R. & Oelgeschlager,T. Association of human TFIIID-promoter complexes with silenced mitotic chromatin in vivo. *Nat. Cell Biol.* 4, 79-82 (2002).
138. Saffitz,J.E. & Schwartz,C.J. Coronary atherosclerosis and thrombosis underlying acute myocardial infarction. *Cardiol. Clin.* 5, 21-30 (1987).
139. Libby,P. & Aikawa,M. Stabilization of atherosclerotic plaques: new mechanisms and clinical targets. *Nat. Med.* 8, 1257-1262 (2002).
140. Virmani,R., Kolodgie,F.D., Burke,A.P., Farb,A., & Schwartz,S.M. Lessons from sudden coronary death: a comprehensive morphological classification scheme for atherosclerotic lesions. *Arterioscler. Thromb. Vasc. Biol.* 20, 1262-1275 (2000).
141. Lee,R.T. & Libby,P. The unstable atheroma. *Arterioscler. Thromb. Vasc. Biol.* 17, 1859-1867 (1997).

142. Libby,P. Inflammation in atherosclerosis. *Arterioscler. Thromb. Vasc. Biol.* 32, 2045-2051 (2012).
143. Martin,K. *et al.* Thrombin stimulates smooth muscle cell differentiation from peripheral blood mononuclear cells via protease-activated receptor-1, RhoA, and myocardin. *Circ. Res.* 105, 214-218 (2009).
144. Gomez,D., Shankman,L.S., Nguyen,A.T., & Owens,G.K. Detection of histone modifications at specific gene loci in single cells in histological sections. *Nat. Methods* 10, 171-177 (2013).
145. Katz,J.P. *et al.* The zinc-finger transcription factor Klf4 is required for terminal differentiation of goblet cells in the colon. *Development* 129, 2619-2628 (2002).
146. Vooijs,M., Jonkers,J., & Berns,A. A highly efficient ligand-regulated Cre recombinase mouse line shows that LoxP recombination is position dependent. *EMBO Rep.* 2, 292-297 (2001).
147. Alexander,M.R. *et al.* Genetic inactivation of IL-1 signaling enhances atherosclerotic plaque instability and reduces outward vessel remodeling in advanced atherosclerosis in mice. *J. Clin. Invest* 122, 70-79 (2012).
148. McDonald,O.G. & Owens,G.K. Programming smooth muscle plasticity with chromatin dynamics. *Circ. Res.* 100, 1428-1441 (2007).
149. Geisterfer,A.A., Peach,M.J., & Owens,G.K. Angiotensin II induces hypertrophy, not hyperplasia, of cultured rat aortic smooth muscle cells. *Circ. Res.* 62, 749-756 (1988).
150. Vladykovskaya,E. *et al.* Reductive metabolism increases the proinflammatory activity of aldehyde phospholipids. *J. Lipid Res.* 52, 2209-2225 (2011).
151. Pegorier,S., Stengel,D., Durand,H., Croset,M., & Ninio,E. Oxidized phospholipid: POVPC binds to platelet-activating-factor receptor on human macrophages. Implications in atherosclerosis. *Atherosclerosis* 188, 433-443 (2006).
152. Feinberg,M.W. *et al.* The Kruppel-like factor KLF4 is a critical regulator of monocyte differentiation. *EMBO J.* 26, 4138-4148 (2007).
153. Liao,X. *et al.* Kruppel-like factor 4 regulates macrophage polarization. *J. Clin. Invest* 121, 2736-2749 (2011).

154. Alaiti,M.A., Orasanu,G., Tugal,D., Lu,Y., & Jain,M.K. Kruppel-like factors and vascular inflammation: implications for atherosclerosis. *Curr. Atheroscler. Rep.* 14, 438-449 (2012).
155. Sharma,N. *et al.* Myeloid Kruppel-like factor 4 deficiency augments atherogenesis in ApoE^{-/-} mice--brief report. *Arterioscler. Thromb. Vasc. Biol.* 32, 2836-2838 (2012).
156. Zhou,G. *et al.* Endothelial Kruppel-like factor 4 protects against atherothrombosis in mice. *J. Clin. Invest* 122, 4727-4731 (2012).
157. Dandre,F. & Owens,G.K. Platelet-derived growth factor-BB and Ets-1 transcription factor negatively regulate transcription of multiple smooth muscle cell differentiation marker genes. *Am. J. Physiol Heart Circ. Physiol* 286, H2042-H2051 (2004).
158. Clarke,M. & Bennett,M. The emerging role of vascular smooth muscle cell apoptosis in atherosclerosis and plaque stability. *Am. J. Nephrol.* 26, 531-535 (2006).
159. Clarke,M.C. *et al.* Chronic apoptosis of vascular smooth muscle cells accelerates atherosclerosis and promotes calcification and medial degeneration. *Circ. Res.* 102, 1529-1538 (2008).
160. Stemme,S., Fager,G., & Hansson,G.K. MHC class II antigen expression in human vascular smooth muscle cells is induced by interferon-gamma and modulated by tumour necrosis factor and lymphotoxin. *Immunology* 69, 243-249 (1990).
161. Cordes,K.R. *et al.* miR-145 and miR-143 regulate smooth muscle cell fate and plasticity. *Nature* 460, 705-710 (2009).
162. Kehler,J. *et al.* Oct4 is required for primordial germ cell survival. *EMBO Rep* 5, (0 AD).
163. Nichols,J. *et al.* Formation of pluripotent stem cells in the mammalian embryo depends on the POU transcription factor Oct4. *Cell* 95, (0 AD).
164. Lengner,C.J., Welstead,G.G., & Jaenisch,R. The pluripotency regulator Oct4. *Cell Cycle* 7, (0 AD).
165. Firth,A.L., Yao,W., Remillard,C.V., Ogawa,A., & Yuan,J.X.-J. Upregulation of Oct-4 isoforms in pulmonary artery smooth muscle cells from patients with pulmonary arterial hypertension. *Am J Physiol Lung Cell Mol Physiol* 298, (0 AD).

166. He,W., Li,K., Wang,F., Qin,Y.-R., & Fan,Q.-X. Expression of OCT4 in human esophageal squamous cell carcinoma is significantly associated with poorer prognosis. *World J Gastroenterol* 18, (0 AD).
167. Holmberg,J. *et al.* Activation of neural and pluripotent stem cell signatures correlates with increased malignancy in human glioma. *PLoS One* 6, (0 AD).
168. Atlasi,Y., Mowla,S.J., Ziaee,S.A.M., Gokhale,P.J., & Andrews,P.W. OCT4 spliced variants are differentially expressed in human pluripotent and nonpluripotent cells. *Stem Cells* 26, (0 AD).
169. Takeda,J., Seino,S., & Bell,G.I. Human Oct3 gene family: cDNA sequences, alternative splicing, gene organization, chromosomal location, and expression at low levels in adult tissues. *Nucleic Acids Res* 20, (0 AD).
170. Cantz,T. *et al.* Absence of OCT4 expression in somatic tumor cell lines. *Stem Cells* 26, (0 AD).
171. Libby,P. Molecular bases of the acute coronary syndromes. *Circulation* 91, (0 AD).
172. Kumar,A. & Lindner,V. Remodeling with neointima formation in the mouse carotid artery after cessation of blood flow. *Arterioscler Thromb Vasc Biol* 17, (0 AD).
173. Piedrahita,J.A., Zhang,S.H., Hageman,J.R., Oliver,P.M., & Maeda,N. Generation of mice carrying a mutant apolipoprotein E gene inactivated by gene targeting in embryonic stem cells. *Proc Natl Acad Sci U S A* 89, (0 AD).
174. Newby,A.C. Molecular and cell biology of native coronary and vein-graft atherosclerosis: regulation of plaque stability and vessel-wall remodelling by growth factors and cell-extracellular matrix interactions. *Coron Artery Dis* 8, (0 AD).
175. Bennett,M., Yu,H., & Clarke,M. Signalling from dead cells drives inflammation and vessel remodelling. *Vascul Pharmacol* 56, (0 AD).
176. Fukui,R. *et al.* Increased migration in late G(1) phase in cultured smooth muscle cells. *Am J Physiol Cell Physiol* 279, (0 AD).
177. Feldman,N. *et al.* G9a-mediated irreversible epigenetic inactivation of Oct-3/4 during early embryogenesis. *Nat Cell Biol* 8, (0 AD).
178. Lambert,C.M., Roy,M., Robitaille,G.A., Richard,D.E., & Bonnet,S. HIF-1 inhibition decreases systemic vascular remodelling diseases by

- promoting apoptosis through a hexokinase 2-dependent mechanism. *Cardiovascular research* 88, (0 AD).
179. Shatrov,V.A., Sumbayev,V.V., Zhou,J., & Brüne,B. Oxidized low-density lipoprotein (oxLDL) triggers hypoxia-inducible factor-1alpha (HIF-1alpha) accumulation via redox-dependent mechanisms. *Blood* 101, (0 AD).
 180. Mathieu,J. *et al.* HIF induces human embryonic stem cell markers in cancer cells. *Cancer Res* 71, (0 AD).
 181. Botquin,V. *et al.* New POU dimer configuration mediates antagonistic control of an osteopontin preimplantation enhancer by Oct-4 and Sox-2. *Genes Dev* 12, (0 AD).
 182. Kreisel,D. *et al.* In vivo two-photon imaging reveals monocyte-dependent neutrophil extravasation during pulmonary inflammation. *Proc. Natl. Acad. Sci. U. S. A* 107, 18073-18078 (2010).
 183. Nava,R.G. *et al.* Two-photon microscopy in pulmonary research. *Semin. Immunopathol.* 32, 297-304 (2010).
 184. Megens,R.T. *et al.* In vivo high-resolution structural imaging of large arteries in small rodents using two-photon laser scanning microscopy. *J. Biomed. Opt.* 15, 011108 (2010).
 185. van,Z.M. *et al.* Two-photon microscopy for imaging of the (atherosclerotic) vascular wall: a proof of concept study. *J. Vasc. Res.* 41, 54-63 (2004).
 186. Koltsova,E.K. *et al.* Dynamic T cell-APC interactions sustain chronic inflammation in atherosclerosis. *J. Clin. Invest* 122, 3114-3126 (2012).
 187. Fernandez-Velasco,M., Gonzalez-Ramos,S., & Bosca,L. Involvement of monocytes/macrophages as key factors in the development and progression of cardiovascular diseases. *Biochem. J.* 458, 187-193 (2014).
 188. Koltsova,E.K., Hedrick,C.C., & Ley,K. Myeloid cells in atherosclerosis: a delicate balance of anti-inflammatory and proinflammatory mechanisms. *Curr. Opin. Lipidol.* 24, 371-380 (2013).
 189. Kadl,A. *et al.* Identification of a novel macrophage phenotype that develops in response to atherogenic phospholipids via Nrf2. *Circ. Res.* 107, 737-746 (2010).

190. Yang, J. *et al.* Transgenic tools for analysis of the haematopoietic system: knock-in CD45 reporter and deleter mice. *J. Immunol. Methods* 337, 81-87 (2008).
191. Davis-Dusenbery, B.N. *et al.* down-regulation of Kruppel-like factor-4 (KLF4) by microRNA-143/145 is critical for modulation of vascular smooth muscle cell phenotype by transforming growth factor-beta and bone morphogenetic protein 4. *J. Biol. Chem.* 286, 28097-28110 (2011).
192. Xu, N., Papagiannakopoulos, T., Pan, G., Thomson, J.A., & Kosik, K.S. MicroRNA-145 regulates OCT4, SOX2, and KLF4 and represses pluripotency in human embryonic stem cells. *Cell* 137, 647-658 (2009).
193. Davis, B.N., Hilyard, A.C., Lagna, G., & Hata, A. SMAD proteins control DROSHA-mediated microRNA maturation. *Nature* 454, 56-61 (2008).
194. Ji, R. *et al.* MicroRNA expression signature and antisense-mediated depletion reveal an essential role of MicroRNA in vascular neointimal lesion formation. *Circ. Res.* 100, 1579-1588 (2007).
195. Chan, M.C. *et al.* Molecular basis for antagonism between PDGF and the TGFbeta family of signalling pathways by control of miR-24 expression. *EMBO J.* 29, 559-573 (2010).
196. Torella, D. *et al.* MicroRNA-133 controls vascular smooth muscle cell phenotypic switch in vitro and vascular remodeling in vivo. *Circ. Res.* 109, 880-893 (2011).
197. Nightingale, K.P., O'Neill, L.P., & Turner, B.M. Histone modifications: signalling receptors and potential elements of a heritable epigenetic code. *Curr. Opin. Genet. Dev.* 16, 125-136 (2006).
198. Pekowska, A., Benoukraf, T., Ferrier, P., & Spicuglia, S. A unique H3K4me2 profile marks tissue-specific gene regulation. *Genome Res.* 20, 1493-1502 (2010).
199. Zhang, J., Parvin, J., & Huang, K. Redistribution of H3K4me2 on neural tissue specific genes during mouse brain development. *BMC. Genomics* 13 Suppl 8, S5 (2012).
200. Orford, K. *et al.* Differential H3K4 methylation identifies developmentally poised hematopoietic genes. *Dev. Cell* 14, 798-809 (2008).

201. Popova,E.Y. *et al.* Stage and gene specific signatures defined by histones H3K4me2 and H3K27me3 accompany mammalian retina maturation in vivo. *PLoS. One.* 7, e46867 (2012).
202. Shi,Y. *et al.* Histone demethylation mediated by the nuclear amine oxidase homolog LSD1. *Cell* 119, 941-953 (2004).
203. Shilatifard,A. Molecular implementation and physiological roles for histone H3 lysine 4 (H3K4) methylation. *Curr. Opin. Cell Biol.* 20, 341-348 (2008).